Physical Rev
Wallis
Copy 1

THE
PHYSICAL REVIEW

A Journal of Experimental and Theoretical Physics Established by E. L. Nichols in 1893

VOL. 55, No. 1 JANUARY 1, 1939 SECOND SERIES

Galactic Rotation and the Intensity of Cosmic Radiation at the Geomagnetic Equator

M. S. VALLARTA, C. GRAEF* AND S. KUSAKA†
Massachusetts Institute of Technology, Cambridge, Massachusetts

(Received June 10, 1938)

The angle of deflection experienced by a primary cosmic particle moving in the plane of the geomagnetic equator is calculated for different energies and the result used to find the diurnal variation in the intensity of cosmic rays arriving vertically at the geomagnetic equator. If it is assumed that the number of primaries varies inversely as the cube of their energy, the calculation shows that there should be a diurnal variation in the vertical intensity of 0.17 percent, if all primaries are positive, with a maximum at 13 hr. 20 min. sidereal time. With a ratio of three positive to one negative primary, and the same distribution law, the amplitude of the diurnal variation should be 0.1 percent with a maximum at 12 hr. 30 min. sidereal time, while if the primary radiation as a whole is neutral (one positive particle to each negative) the amplitude should be 0.06 percent with maximum at 8 hr. 40 min. sidereal time. If the number of primaries is an exponentially decreasing function of their energy, the amplitude of the diurnal variation should be 0.24 percent with maximum at 18 hr. sidereal time, assuming all primaries are positive; if the primary radiation is neutral the amplitude should be 0.19 percent and the maximum should occur at 20 hr. 40 min. sidereal time. The expected diurnal variations for several values of the lower limiting energy are also discussed.

1.

A FUNDAMENTAL question in the theory of cosmic radiation is whether the radiation comes from outside our own galaxy. A possible way of answering this problem was first suggested in 1935 by Compton and Getting.[1] They pointed out that, as a consequence of the motion of rotation of our galaxy as a whole, there should be a small diurnal variation of the intensity depending on sidereal time. Since then they, and a number of others, have assiduously sought to establish experimentally the existence of this effect, as yet with results which are in part contradictory and largely inconclusive.

Compton and Getting developed the theory of the galactic rotation effect without regard to the deflection of charged primary particles by the earth's magnetic field. They then made a rough estimate of the error introduced by neglecting this deflection, and pointed out that it should result in still further decreasing the small expected diurnal variation in the absence of a magnetic field. In view of the importance of the question at issue, it appeared desirable to develop the exact theory of the galactic rotation effect even if at present the calculations can be carried out rigorously only for the particularly simple case of particles moving in the plane of the geomagnetic equator. A calculation due to van Wijk[2] already showed that, under the assumption that the number of primary particles varies as an exponentially decreasing function of their energy,

* Fellow of the John Simon Guggenheim Memorial Foundation.
† At present graduate student at the University of California, Berkeley, California.

[1] A. H. Compton and I. A. Getting, Phys. Rev. 47, 817 (1935).

[2] L. A. van Wijk, Physica 3, 769 (1936).

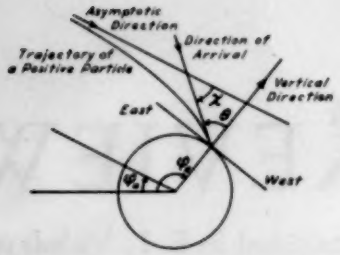

FIG. 1. The figure is drawn for an observer looking down on the equatorial plane from the north pole.

the maximum value of the diurnal variation for particles coming vertically at the geomagnetic equator should be about 0.25 percent, instead of 0.3 percent which would be expected if the earth's magnetic field were absent. He did not attempt to calculate the phase of the diurnal variation.

In the present paper we calculate the deflection of cosmic particles moving in the equatorial plane and then, by taking into account the motion of the earth due to the galactic rotation, we find the diurnal variation in the intensity of cosmic rays arriving vertically at a point in the geomagnetic equator. Methods similar to those used here yield the diurnal variation in any direction in the east-west plane at the geomagnetic equator. The results are similar to those reported here.

2.

The angle of deflection of a primary cosmic-ray particle reaching the earth from infinity can be easily calculated in the case we are now considering. We shall confine our attention to positive particles; the deflection of negative particles will be equal in magnitude but in the opposite direction to that of positive particles with the same absolute charge, mass, and energy. From Fig. 1 we see that the angle of deflection χ is given by

$$\chi=\varphi_e-\varphi_a-\theta, \tag{1}$$

where φ_e and φ_a are the polar angles of the trajectory for $r=r_e$, the radius of the earth, and for $r=\infty$, respectively, and θ is the direction of arrival of the particle at the earth. We are using Störmer's normalized coordinates so that r_e is the ratio of the radius of the earth to the radius of the circular periodic orbit of the particle, and it is a measure of the energy of the particle. For the angles we have adopted the following conventions: φ is measured positive westward from the polar axis to the radius vector; θ is measured positive eastward from the vertical to the reversed direction of arrival; χ is measured positive clockwise from the asymptotic direction to the direction of arrival (Fig. 1).

The angles φ_e and φ_a are obtained by putting $r=r_e$ and $r=\infty$, respectively, in the polar equation of the trajectory.[3] For $\gamma_1<1$ ($2\gamma_1$ is the moment of momentum of the particle, in the equatorial plane, at infinity and is a constant of the motion) we have

$$\begin{aligned}\varphi_e&=\sin^{-1}(k\sin\psi_e)+(\gamma_1/\sqrt{2})F(\alpha,\psi_e),\\ \varphi_a&=\sin^{-1}(k\sin\psi_a)+(\gamma_1/\sqrt{2})F(\alpha,\psi_a),\end{aligned} \tag{2}$$

where

$$\begin{aligned}\psi_e&=\cos^{-1}(r_e\gamma_1^{-1})/(r_e(1+\gamma_1^2)^{\frac{1}{2}}),\\ \psi_a&=\cos^{-1}\gamma_1(1+\gamma_1^2)^{-\frac{1}{2}},\\ k&=\sin\alpha=[\tfrac{1}{2}(1+\gamma_1^2)]^{\frac{1}{2}},\end{aligned}$$

and $F(\alpha,\psi)$ is the elliptic integral of the first kind. For $\gamma_1>1$ we have

$$\begin{aligned}\varphi_e&=\psi_e+\gamma_1(1+\gamma_1^2)^{-\frac{1}{2}}F(\alpha,\psi_e),\\ \varphi_a&=\pi/4+\gamma_1(1+\gamma_1^2)^{-\frac{1}{2}}F(\alpha,\pi/4),\end{aligned} \tag{3}$$

where $\psi_e=\sin^{-1}[(2r_e\gamma_1+r_e^2-1)/2r_e^2]^{\frac{1}{2}}$,

and $\sin\alpha=[2/(1+\gamma_1^2)]^{\frac{1}{2}}$.

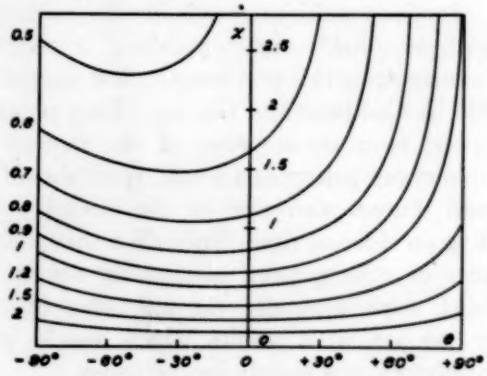

FIG. 2. The angle of deflection as a function of the angle of arrival, for different energies (expressed in störmers). $r_e=0.5$ for $\theta=0$ corresponds to an asymptotic orbit for which $\chi\to\infty$.

[3] C. Graef and S. Kusaka, J. Math. Phys. **17**, 43 (1938). See also, L. A. van Wijk and H. Zanstra, Physica **3**, 75 (1936).

Now θ and γ_1 are related by Störmer's equation[4]

$$\sin\theta = 2\gamma_1/r_e - 1/r_e^2, \tag{4}$$

so that for any given value of r_e, χ is a function of θ alone.

We have calculated χ for all possible values of θ ($-90°$ to $+90°$) and for several values of r_e. The result is plotted in Fig. 2 where χ is given in radians and θ in degrees.

3.

We shall define the intensity of cosmic radiation, I, as the number of particles received per second per unit area. Then if $f(E)$ is the energy distribution function at infinity, the intensity of cosmic rays arriving in the vertical direction at the earth when it is considered to be at rest with respect to the distribution of cosmic rays is, by Liouville's theorem,

$$I = \int_{E_0}^{\infty} f(E)dE, \tag{5}$$

where E_0 is the lowest energy the particle can have to arrive at the given point of the earth in this direction. When the motion of the earth is taken into account the intensity is given by[5]

$$I' = \int_{E_0}^{\infty} \frac{f(E)dE}{(1-\beta\cos\omega')^3} \tag{6}$$

where β is the ratio of the velocity of the earth to the velocity of light, ω' is the angle between the velocity of the earth and the reversed tangent to the trajectory at infinity. From Fig. 3 it is seen that

$$\omega' = \chi + \omega, \tag{7}$$

where ω is the angle between the velocity of the earth and the vertical at the point of observation. From the analysis[6] of Swann, Heitler, Nordheim

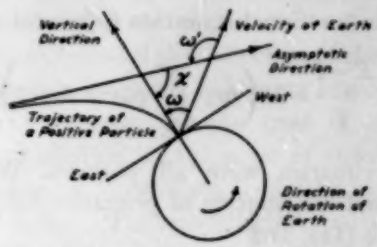

FIG. 3. Diagram of the angles used in the text.

and others, a likely distribution function of the primaries is

$$f(E) = c/E^3. \tag{8}$$

Now the energy in störmers written in terms of the energy of the particle in electron volts is[7]

$$r_e = R\left(\frac{E}{300MceZ}\right)^1\left(1+\frac{600m_0c^2}{E}\right)^1, \tag{9}$$

which for very high energies ($E \gg m_0c^2$) reduces to

$$r_e = KE^1, \tag{10}$$

where K is a constant. Hence

$$f(E) = K^6/r_e^6 \tag{11}$$

and so

$$I = 2K^4\int_{r_0}^{\infty} dr/r^5, \tag{12}$$

and, from (6),

$$I' = 2K^4\int_{r_0}^{\infty} (1+3\beta\cos\omega')dr/r^5, \tag{13}$$

where r_0 is the value of r_e corresponding to E_0. Thus r_0 is the least energy for vertical arrival at the equator, that is, 500 millistörmers.[8] Now

[4] C. Störmer, Zeits. f. Astrophys. **1**, 237 (1930). This paper contains references to his previous work.

[5] A. H. Compton and I. A. Getting, reference 1. The lower limit of the integral (6), according to W. F. G. Swann (Phys. Rev. **51**, 718 (1937)), should be $E_0/(1+\beta\cos\omega_0')$, obtained by applying a Lorentz transformation to the energy E_0 of the particle at infinity. We are unable to agree with this line of reasoning. With respect to the terrestrial observer the limiting energy in the earth's magnetic field is E_0 and the distribution at infinity is anisotropic, as given by the denominator in (6). With respect to the extragalactic observer the limiting energy is not E_0 because the particle moves with respect to him in a combined electric and magnetic field, and its kinetic energy is neither E_0 nor is it conserved, but the distribution of particles with respect to him is of course isotropic. If Swann's suggestion were correct, I', and therefore $\Delta I/I$ (Eq. 15), would be indeterminate by the amount 2β, since the limiting angle ω_0' corresponding to the limiting energy E_0 is infinite because the limiting trajectory described by this particle is asymptotic to the circular (periodic) orbit. We are indebted to Professor G. Lemaitre for illuminating conversations on the correct approach to this problem.

[6] W. F. G. Swann, Phys. Rev. **50**, 1103 (1936); W. Heitler, Proc. Roy. Soc. **A161**, 261 (1937); L. W. Nordheim, Phys. Rev. **51**, 1110 (1937); **53**, 694 (1938).

[7] G. Lemaitre and M. S. Vallarta, Phys. Rev. **43**, 87 (1933).

[8] G. Lemaitre and M. S. Vallarta, Phys. Rev. **50**, 530 (1936), Fig. 10.

according to Oort,[9] β is of the order of 0.001 so that we may neglect, as we have done in (13), squares and higher powers of β. From (12) and (13) we get

$$I'-I=2K^4\int_{r_0}^{\infty}3\beta\cos\omega'\,dr/r^5. \qquad (14)$$

Hence the fractional variation in intensity is

$$\frac{\Delta I}{I}=\frac{I'-I}{I}=2\beta\left(6r_0^4\int_{r_0}^{\infty}\cos\omega'\,dr/r^5\right). \qquad (15)$$

if the primaries were all positive. With an exponential distribution of primaries $f(E)=e^{-KE}$ instead of (11), and

$$\frac{\Delta I}{I}=6\beta e^{r_0^2}\int_{r_0}^{\infty}re^{-r^2}\cos\omega'\,dr \qquad (16)$$

under the assumption that all particles are positive. In the actual computation the integrals (15), (16) were found graphically for several values of ω with $r_0=0.5$.

4.

For a mixture of positive and negative particles, we must treat the two components separately. As we have stated earlier, changing the sign of the particle merely changes the sign of χ. Hence, if we assume the same distribution law for negative as for positive particles, our result obtained for positive particle holds for negative particles if the sign of θ is reversed. This follows from Eq. (7) and the fact that ω' enters only as $\cos\omega'$ in Eqs. (15), (16). Now if we use the subscripts + and − to denote quantities referring to positive and negative components of the primary radiation, respectively, then what we want to find is

$$\Delta(I_+ + I_-)/(I_+ + I_-)$$

and we know $\Delta I_+/I_+$ and $\Delta I_-/I_-$. Now if there are n times as many positives as negatives in any energy band, then, since the intensity is proportional to the number of particles

$$\frac{1}{n+1}\left[n\frac{\Delta I_+}{I_+}+\frac{\Delta I_-}{I_-}\right]=\frac{\Delta(I_+ + I_-)}{(I_+ + I_-)}=\frac{\Delta I}{I}. \qquad (17)$$

[9] J. H. Oort, Bull. Astr. Inst. of the Netherlands **6**, 155 (1931).

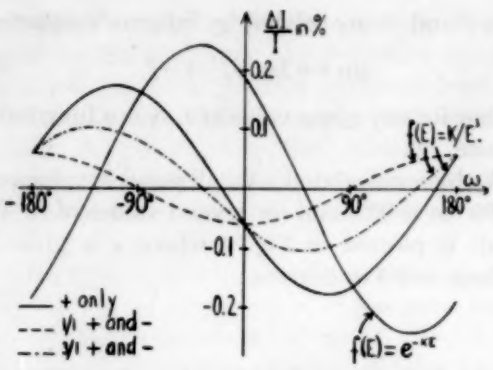

FIG. 4. The galactic diurnal variation of Compton and Getting.

Thus the effect of a mixture of positive and negative primaries is easily found if the ratio of the two components is known.

From Johnson's measurements[10] of the east-west and the north-south asymmetries in Mexico ($\lambda=29°$), the ratio of the positive to the negative primaries in the energy band between 400 and 450 millistörmers has been estimated by Vallarta to be about 3 to 1. It is clear that an established ratio of positives to negatives in any energy interval is not in any way to be interpreted as meaning that the same ratio holds throughout the whole energy spectrum. Assuming, however, that the same ratio holds throughout the primary distribution, we may calculate the variation in the intensity. We simply put $n=3$ in Eq. (17).

5.

Figure 4 gives the result of this calculation. The variation in the vertical intensity is plotted as a function of ω. This is just the sidereal time expressed in angular measure plus a constant which is determined from the fact that the velocity of the earth according to Oort[9] is in the direction 20 hr. 55 min. right ascension and 47° N declination. It is found that the zero of ω corresponds to 20 hr. 40 min. The full curves show the percentage variation for positive particles alone; the amplitude is 0.17 percent and the maximum occurs at 13 hr. 20 min. sidereal time, assuming an inverse cube distribution, and 0.24 percent, in agreement with van Wijk's result,[2] with maximum at 18 hr. sidereal time, assuming

[10] T. H. Johnson, Phys. Rev. **47**, 91 (1935); **48**, 287 (1935).

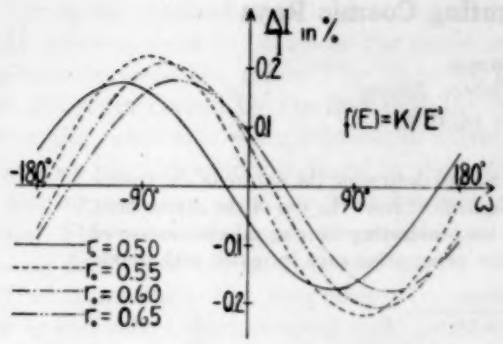

FIG. 5. The galactic diurnal variation for different values of the low energy limit. Inverse cube distribution of positive primaries.

an exponentially decreasing distribution. The other two curves show the expected diurnal variation if there are three positive primaries to each negative, and if there is an equal number of positives and negatives (primary radiation as a whole neutral), assuming in each case an inverse cube distribution. It may be pointed out that if the primary radiation as a whole is neutral, the amplitude of the expected diurnal variation is less than 0.1 percent, for an inverse cube distribution, and consequently its detection, or alternately the proof of its nonexistence, requires a very careful experimental investigation.[11] It is also plain that a knowledge of the experimental diurnal variation as a function of sidereal time would lead to valuable conclusions as to the ratio of positive to negative primaries and as to their distribution law.

It should also be emphasized that, as already indicated by Compton and Getting, the magnitude of the diurnal variation is smaller than would be expected if the deflection of the particles in the earth's magnetic field were neglected, and the phase, except for the case of a neutral primary radiation, in the sense of equal number of positives and negatives, is shifted by a rather large amount. For undeflected particles, the amplitude of the diurnal variation should be 3β or 0.3 percent and the maximum should always occur at 20 hr. 40 min. sidereal time.

The effect of filtering off low energy particles above the magnetic cut-off is exhibited in Fig. 5. It is seen that the effect depends rather considerably as regards both magnitude and phase on the lower limit of the energy if the distribution law goes according to the inverse cube. Such is not the case for an exponentially decreasing distribution, which is rather insensitive to the lower cut-off. The possibility of enhancing the expected effect by filtering off low energy particles, however, should not be overlooked, nor that of obliterating it (for $r_0 = 0.54$) if the number of positive and negative primaries is the same.

The calculation of the galactic rotation effect for trajectories not lying wholly in the equatorial plane and for latitudes other than the equator is rendered considerably more difficult by the fact that the equations of motion are then no longer integrable. This investigation is being undertaken and the results will be presented in a future paper.

[11] Whether a diurnal variation depending on sidereal time exists or not is a question which does not seem to be decided at the time of writing. Forbush's careful statistical analysis of the intensity measurements made with a Compton-Bennett automatic recording meter at Huancayo, Peru, reported at the University of Chicago's symposium on cosmic rays (June 30, 1938), which are comparable to a good approximation with the theoretical results reported here, would not seem to rule out the existence of an effect such as would be expected for a primary radiation consisting of equal number of positive and negative particles having an inverse cube distribution. The requirement of a neutral radiation, necessary on other grounds, is thus seen to be consistent with present experimental evidence. Forbush's result, however, does seem to rule out an exponentially decreasing distribution of primaries, provided they satisfy the condition of being as a whole neutral. Cf. S. E. Forbush, Phys. Rev. **52**, 1254 (1937).

The Nature of the Penetrating Cosmic Rays

VOLNEY C. WILSON
University of Chicago, Chicago, Illinois
(Received November 18, 1938)

Geiger-Müller tube experiments have been performed to determine the nature of the cosmic rays present at depths of 30 and 300 meters water equivalent from the top of the atmosphere. At both of these depths, the observable cosmic rays are penetrating ionizing rays accompanied by soft showers. The ratio of the soft showers to the penetrating rays increases with depth.

IN A previous experiment,[1] cosmic-ray intensities were measured at various depths into the earth's crust. When the logarithm of the intensity was plotted against the logarithm of the depth, one straight line from 20 m to 250 m[2] and another from 250 m to 1420 m seemed to represent the data very well. This appeared to indicate that there are two types of very penetrating cosmic rays; one with a maximum range of about 250 m, and one with a much greater range. It was suggested that the first of these consists of "heavy electrons" and the second of "neutrinos."[3]

The present paper is a report of experiments which were performed: first, at a moderate depth (30 m) to determine the nature of the first group; and second, at a depth greater than 250 m (300 m) to determine the nature of the second group. The G-M (Geiger-Müller) tubes used for these experiments have copper cathodes nine cm in diameter and 71 cm long. A complete description of these tubes and the coincidence circuit used is given in a previous report.[1]

EXPERIMENT AT 30 m DEPTH

The first experiment was performed in a tunnel of the Chicago Tunnel Company at a depth of 30 m. Two absorption curves were obtained; one with lead placed between the second and third G-M tubes (See *D* of Fig. 3), and another with lead above all four G-M tubes (See *E* of Fig. 3).

If all the penetrating rays at any particular depth are ionizing rays, then, after correcting for small effects caused by showers and scattering, the absorption curve with the lead between the G-M tubes should be the same as the curve with the lead above all four tubes. If all the penetrating rays are non-ionizing rays and are detectable only by the ionizing secondaries produced, then the absorption curve with the lead above all four tubes should depend upon the absorption coefficient of the primary and secondary rays; whereas, the absorption curve with the lead between the tubes should depend only upon the absorption coefficient of the secondaries entering the first G-M tube. (The non-ionizing primaries and the secondaries produced in the lead will not be detected by the two upper tubes and so will not be recorded.) Evidently, then, the ionizing rays will show the same absorption curve whether the lead is above or between the tubes; whereas the non-ionizing secondary producing ray will show much more absorption when the lead is placed between the tubes.

The data obtained are represented in Fig. 1. Each point has a probable error ($0.67\sqrt{N}$) of about 1.5 percent. Except for the point at the extreme left, 2.54 cm of lead (not shown in diagram) was kept around the two lower tubes to shield them from weak shower particles. To measure the showers, the second tube from the top was moved down 50 cm and to the right 20 cm. The shower counting rate with only the 2.5-cm lead shield was about three percent of the vertical coincidence rate, and without the shield, about four percent.

[1] V. C. Wilson, Phys. Rev. **53**, 337 (1938).
[2] All depths in this report are given in meters water equivalent from the top of the atmosphere.
[3] Further encouragement for this hypothesis was given by the experiment of P. Auger and A. Rosenberg, Comptes rendus **201**, 1116 (1935), in which they observed only a 3 percent decrease by 10 cm of lead at a depth of 70 m; thus suggesting that the first group consists of penetrating ionizing rays; and by the experiment of J. Barnóthy and M. Farró, Zeits. f. Physik **104**, 744 (1937), who say: "At great depths, about 800 m, the ionizing part of the cosmic radiation consists only of shower particles produced by a nonionizing radiation." They conclude that this non-ionizing radiation consists of "neutrinos."

The curve obtained with lead above all four G-M tubes appears to be below the curve with the lead between the tubes. This is probably a real difference caused by the fact that the lead above the tubes was more efficient in shielding the tubes from showers produced in the ceiling of the tunnel than was the lead between the tubes. This effect is more noticeable at the greater depth and will be discussed later.

The broken line in Fig. 1 represents the absorption in equivalent thicknesses of rock[1] assuming a mass absorption. The agreement between the two curves is good considering the different absorbing materials used and the different solid angles subtended by the G-M tubes in the two cases.

Therefore we see that within the probable errors, the two absorption curves, one with lead above all four tubes and another with lead between the tubes, agree up to 29 cm of lead. Furthermore, the absorption with 11.3 meters water equivalent of rock above the tubes is about the same as the absorption with 11.3 meters water equivalent of lead between the tubes. One is led to conclude that at 30 meters water equivalent from the top of the atmosphere there are some showers present,[4] but that the large majority of the cosmic rays are penetrating ionizing rays—probably barytrons.

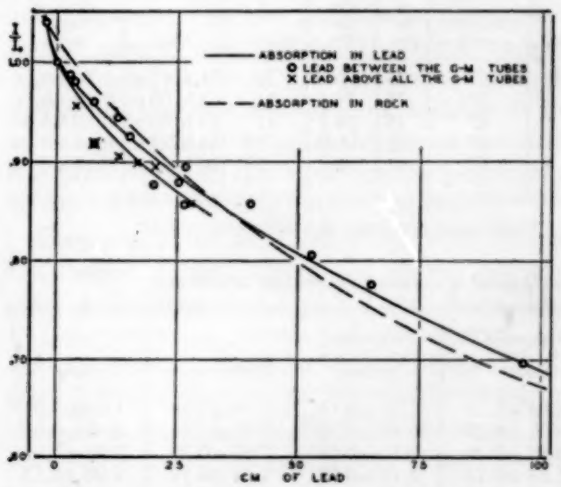

FIG. 1. Absorption of the vertical component of the cosmic rays present at 30 m. See reference 2.

[4] P. Auger and A. Rosenberg have shown that these are soft showers. Comptes rendus **202**, 1923 (1936).

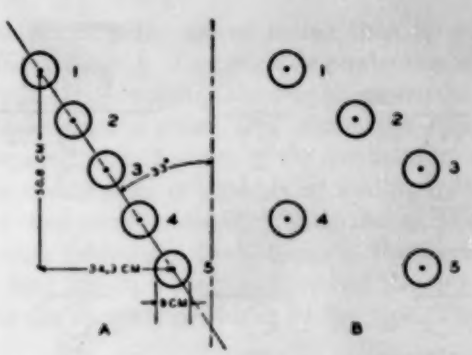

FIG. 2. Arrangements of the G-M tubes to test the relative abundance of showers to single ionizing cosmic rays.

EXPERIMENT AT 300 m DEPTH

The second experiment was performed in the Snow Hill Coal Mine at Terre Haute, Indiana, at a depth of 300±10 meters water equivalent from the top of the atmosphere. This experiment was divided into several parts. First, to test the conclusion of Barnóthy and Farró,[3] that all ionizing rays at great depths are shower particles, five G-M tubes were arranged in line and tipped to 33° from the vertical according to *A* Fig. 2; and this counting rate was then compared with that obtained with the three central tubes moved out of line as in *B* Fig. 2. Showers produced in the ceiling, 12 feet above the center of the apparatus, had about the same probability of being recorded with one arrangement as with the other. The data are shown in Table I. From twofold and threefold horizontal coincidence rates, it was calculated that the chance counts were about one in 17 days. Arrangement *A* gave 13 times as many coincidences as *B*. Therefore, one may conclude that at 300 m there are showers present, but that the majority of the coincidences are caused by single ionizing particles.

TABLE I. *The relative abundance of the single ionizing cosmic rays to the cosmic-ray showers at 300 m.**

ARRANGEMENT	COUNTS	TIME	COUNTS PER HOUR
A	107	17 h 10 m	6.23±0.42
B	9	24 h 10 m	0.37±0.08
B	13	23 h 20 m	0.56±0.11
A	154	26 h 25 m	5.83±0.32

Average $A = 6.03 \pm 0.25$ ratio $A/B = 13.1 \pm 2.0$
Average $B = 0.46 \pm 0.07$

* See reference 2.

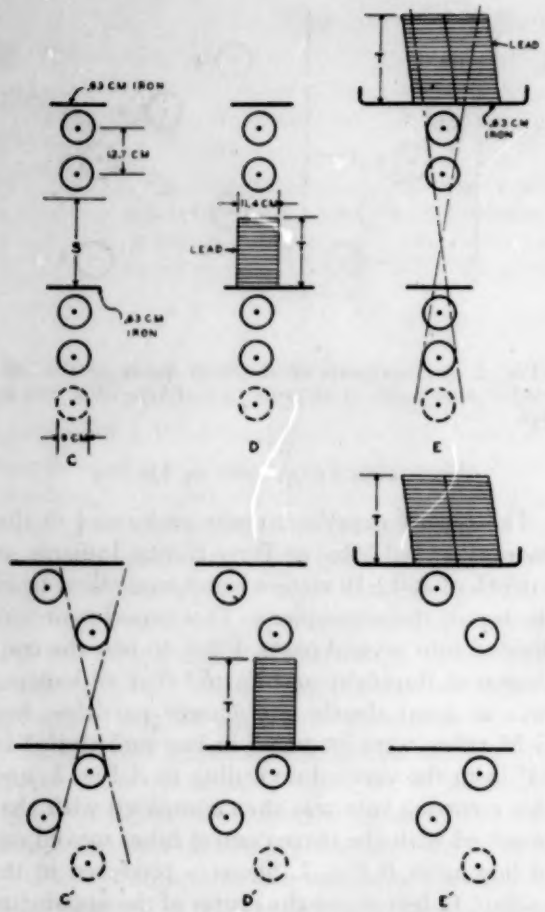

FIG. 3. Arrangements of the G-M tubes to measure the absorption of the vertical component of the cosmic rays.

To determine the penetration of these particles, an experiment similar to that at 30 m was performed. The arrangements of the tubes are shown in Fig. 3, and the data are given in Tables II and III. It was found that not all of the coincidences were caused by single rays going through all the tubes, but that showers produced in the surrounding rock could cause coincidences without the individual particles penetrating the lead between or above the tubes. To correct for this, the tubes were moved out of line as is illustrated in *C'*, *D'* and *E'* of Fig. 3, and the coincidence rate thus obtained (Table III) was subtracted from the vertical coincidence rate (Table II) to give the true coincidence rate caused by single ionizing particles.

The data are represented graphically in Fig. 4. At this depth the absorption curve in lead is so nearly linear over this short range that it was drawn as a straight line. Statistical weights, inversely proportional to the squares of the probable errors, were assigned to these points, and the position and slope of the line were determined by the method of least squares. The absorption of the vertical rays in rock at this depth[1] is included for comparison. Since the curve with lead between the G-M tubes agrees so well with the curve with rock above the tubes, it is quite certain that the single ionizing rays are penetrating rays, and probably they are the rays which carry the cosmic-ray energy down to this depth. In the

TABLE III. *Showers and chance counts for corrections to Table II.*

No.	Arrangement	S in cm	Cm of Pb	Counts	Time	Counts per hour
1	*C'*	25	0.0	26	21 h 45 m	1.20±0.16
2	*D'*	25	24.1	14	24 h 00 m	0.58±0.10
3	*E'*	25	24.1	17	33 h 50 m	0.50±0.08
4	*C'*	101	0.0	8*	44 h 22 m	0.18±0.04
5	*D'*	101	100.3	2*	20 h 30 m	0.10±0.05

* These counts were made with fivefold coincidence.

TABLE II. *The absorption in lead of the vertical component of cosmic rays present at 300 m.**

No.	Arrangement	S in cm	Cm of Pb	Counts	Time	Counts per hour	Showers and chance counts	Difference	I/I_0
1	*C*	25	0.0	863	95 h 20 m	9.05±0.21	1.20±0.16	7.85±0.26	1.00±0.05
2	*D*	25	24.1	378	45 h 29 m	8.31±0.29	0.58±0.10	7.73±0.31	0.98±0.05
3	*E*	25	24.1	364	45 h 20 m	8.03±0.29	0.50±0.08	7.53±0.29	0.96±0.05
4	*C*	101	0.0	132**	78 h 05 m	1.69±0.13	0.18±0.04	1.51±0.14	1.00±0.13
5	*D*	101	100.3	75**	57 h 40 m	1.30±0.09	0.10±0.05	1.20±0.10	0.80±0.10
6	*D*	101	10.1	13**	11 h 20 m	1.15±0.21	0.10±0.05	1.05±0.22	0.70±0.16
7	*D*	101	50.8	19**	13 h 20 m	1.43±0.23	0.10±0.05	1.33±0.24	0.88±0.18

* See reference 2.
** These counts were made with fivefold coincidence.

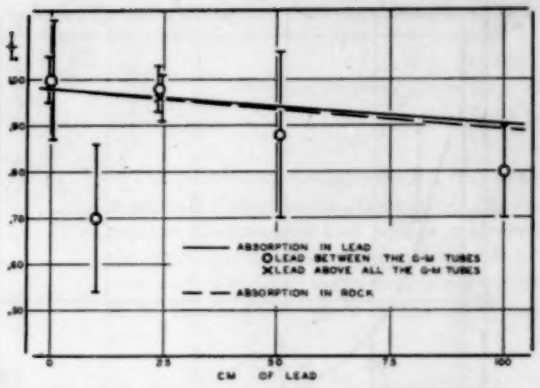

FIG. 4. Absorption of the vertical component of the cosmic rays present at 300 m. See reference 2.

light of the new theories[5] and experiments[6] on the production and penetration of barytrons, it seems probable that the majority of the rays at 300 m are barytrons which are produced in the upper atmosphere.

As was shown in Table I, there are also some showers present. In order to determine the penetration of the individual shower particles, the tubes were arranged according to *F* of Fig. 5. The lead between the two bottom tubes was not altered, and only the thickness *X* of the horizontal piece of lead was varied. At least one ray from each shower would have to penetrate the thickness of lead *X* in order that the shower could be recorded. The results are shown in Fig. 6. It is apparent that the particles in the showers are not penetrating, and that the showers are so-called "soft" showers. The 11.4 cm of lead absorbed all the shower rays, but because of the large separation of the tubes this does not exclude the possibility of the existence of penetrating showers with very small angular spread.

Counting rates were obtained with various thicknesses of lead above the shower arrangement as is shown in *G* Fig. 5. These data (Table IV) also show the presence of soft showers. The lead appeared to be either more effective in absorbing the showers or less effective in producing them than was the rock. Probably, however, this apparently large absorption was caused by the geometrical arrangement rather than by a true difference in the absorption or production of the rays in the two materials. For example, the lead covered such a small area above the tubes as compared with the area of the surrounding rock, that the number of showers emanating from the lead was small compared with the number of showers emanating from the rock. Furthermore, the lead was in a position to shield the top tube from the showers produced in the rock. The apparent rise in the shower rate from 20 cm to 50 cm may be a false rise which can be explained as caused by statistical errors.

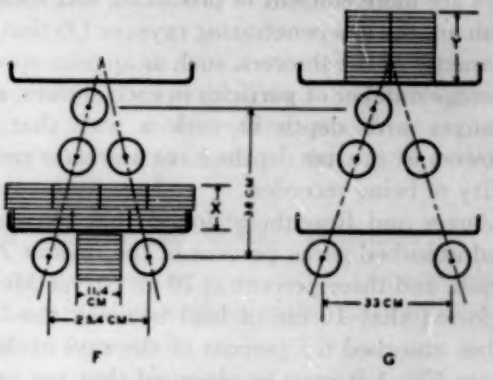

FIG. 5. Arrangements of the G-M tubes to measure the absorption of the cosmic-ray showers.

In order to compare shower intensities with vertical ray intensities at different depths, the arrangement of the tubes and surrounding material must be the same at each depth. Reading No. 4 of Table III compared with reading No. 4 of Table II gives a shower intensity at 300 m of 12 percent of the vertical intensity as compared with four percent for the same arrangement at 30 m. At 300 m, in the coal mine, the apparatus was set up inside a room with a hemispherical ceiling which was about 9 ft. above the apparatus; whereas the walls and ceiling of the tunnel at 30 m were only about 2 ft. from the top of the apparatus. Considering the different surrounding conditions, this change agrees well with the change in the relative intensities of showers to vertical rays shown in the copper mine experiment.[1] There the shower intensity was four percent of the vertical intensity at 30 m, and 8 percent at 300 m.

No quantitative conclusions can be made from these comparisons, but it is significant that the

[5] *a*. A. H. Compton, Proc. Phys. Soc. London **47**, 747 (1935). *b*. T. S. Bowen, R. A. Millikan and H. V. Neher, Phys. Rev. **53**, 217 (1938). *c*. W. Heitler, Proc. Roy. Soc. **A166**, 529 (1938). *d*. H. Euler, Zeits. f. Physik, **110**, 692 (1938).

[6] M. Schein and V. C. Wilson, Phys. Rev. **54**, 304 (1938).

shower intensity decreases less rapidly with depth than does the vertical intensity.

Heitler predicts that barytrons can produce soft showers indirectly through intermediate photons.[6c] If one assumes that the soft showers are produced by the penetrating ionizing rays, then to explain the relative increase of shower intensity with depth one may assume: (1) that there is a non-ionizing agent also producing soft showers; (2) that the more penetrating ionizing rays are more efficient in producing soft showers than are the less penetrating rays; or (3) that the character of the showers, such as angular spread, average number of particles in each shower, etc., changes with depth in such a way that the showers at greater depths have a greater probability of being recorded.

Auger and Rosenberg[8] found that ten cm of lead absorbed seven percent of the rays at 29 m depth, and three percent at 70 m. Grivet-Meyer[7] reported that 10 cm of lead between the G-M tubes absorbed 6.5 percent of the rays at 30 m. From Fig. 1 it may be observed that ten cm of lead between the tubes absorbs 7.4 percent of the rays at 30 m. All of the above values are in good agreement. The absorption by ten cm of lead at 60 m as taken from Nielson and Morgan's[8] curve is about 23 percent. This unusually high absorption by the first ten cm of lead is inconsistent with the above-mentioned data, but since the latter experiment was done with only twofold coincidence, it is probable, as Neilson and Morgan suggest, that many showers were counted as vertical rays, and so the first part of the curve is actually an absorption measurement of the shower particles at 60 m depth. To the writer's knowledge no similar experiments have been performed at 300 m.

TABLE IV. *Cosmic-ray showers under lead at 300 m.*[*]

ARRANGEMENT	CM OF PB	COUNTS	TIME	COUNTS PER HOUR
G	0.0	13	21h 30 m	0.60±0.11
G	2.54	12	23h 43 m	0.51±0.10
G	20.3	7	24h 10 m	0.29±0.07
G	50.8	9	23h 00 m	0.39±0.09

[*] See reference 2.

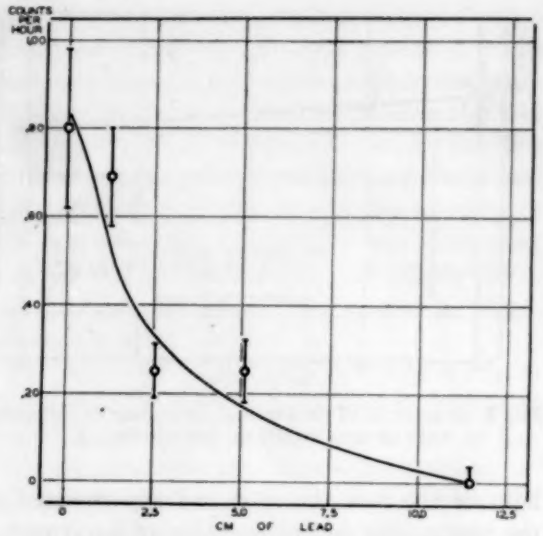

FIG. 6. Absorption of the cosmic-ray showers present at 300 m. See reference 2.

CONCLUSION

The experiments of the present report indicate that there is not a marked difference in the type of rays present at 30 m and 300 m, and that the plot of the logarithm of the intensity against the logarithm of the depth would be better represented by a smooth curve with a gradually changing slope than by two straight lines with a sudden change at 250 m depth.[1]

At both 30 m and 300 m the observable cosmic rays are penetrating ionizing rays accompanied by soft showers, which are relatively more abundant at the greater depth.

In conclusion, the writer wishes to express his sincere appreciation to Professor A. H. Compton, not only for suggesting this problem but also for his generous assistance and valuable discussions. The writer is indebted to Mr. J. F. Peterson and Mr. James Healy of the Chicago Tunnel Company; and to Messrs. James Hyslop, A. K. Hert, Harold Lowry, Fred Bieler, Andrew Hyslop and Andrew Hyslop, Jr. of the Snow Hill Coal Company for their kind interest and excellent cooperation; and to Dr. Marcel Schein for his helpful discussions.

[7] T. Grivet-Meyer, Comptes rendus **206**, 833 (1938).
[8] W. M. Nielson and K. Z. Morgan, Phys. Rev. **54**, 245 (1938).

A Critical Analysis for Sidereal Time Variations of Cosmic Rays on the Pacific

JULIAN L. THOMPSON
Ryerson Physical Laboratory, University of Chicago, Chicago, Illinois
(Received November 7, 1938)

The problem of distinguishing a true sidereal diurnal variation in cosmic-ray intensity from a seasonal change in the amplitude of the solar diurnal variation is approached from the standpoint of the harmonic dial type of analysis. It is shown that the regular cyclic arrangement of the datum points taken in chronological order serves as a criterion for the presence of the sidereal time variation. Cosmic-ray data taken on the Pacific Ocean during 1936 by A. H. Compton and R. N. Turner are shown to contain no sidereal diurnal component larger than the experimental error.

THE search for evidence as to the reality of a periodic change of intensity of cosmic rays according to sidereal time is made difficult by the presence of the much larger solar diurnal variation. The appearance of a sidereal diurnal variation upon formal analysis of a series of data by no means assures one of its reality. As has been pointed out by Messerschmidt,[1] if there is a seasonal variation in the amplitude of the solar diurnal wave, then when averaged over a period of a year according to sidereal time there will appear a residual variation from this cause having no connection with a true sidereal time period. In discussing this problem at the 1938 Chicago Cosmic-Ray Symposium, however, S. E. Forbush indicated that it should be possible, by the use of the harmonic dial type of analysis, to detect the presence of a true sidereal variation if it is greater than the experimental error.[2]

THE IDEAL HARMONIC DIAL

In this type of analysis, considering only the first harmonic or 24-hour wave, one determines from the data of one day or a small group of days the amplitude and phase of the variation by the usual Fourier analysis. The tip of an imaginary hand on a 24-hour clock dial, pointing to the hour of maximum and having its length proportional to the amplitude, serves to locate a point on the dial which represents these data. This is done for each day or group of days and these points then form a cloud whose mass center will indicate the mean time of maximum and the mean amplitude.[3]

Solar component of constant amplitude

Consider now the type of dial to be expected from an ideal case of solar diurnal variation of constant amplitude

$$c \sin\left(\frac{2\pi t}{T_1}+\alpha\right),$$

where t is the time in solar days and α is the phase angle. T_1, the period in solar days, is, of course, unity. In this case, by use of a solar time dial, all of the points will be found to be coincident and the cloud will consist of but one point which lies at a distance c and angle $\pi/2-\alpha$ from the origin. On the other hand, if there is present only a sidereal diurnal variation of constant amplitude represented by

$$h \sin\left(\frac{2\pi t}{T_2}+\beta\right),$$

where T_2 is the sidereal period in solar days, t has the same significance as before, and β is the phase angle, the points will fall on a circle of radius h concentric with the dial. Combining these two variations and expressing in terms of frequency rather than period we have

$$f(t)=c \sin(2\pi\nu_1 t+\alpha)+h \sin(2\pi\nu_2 t+\beta),$$

where ν_1 and ν_2 are the frequencies in periods per

[1] W. Messerschmidt, Zeits. f. Physik **78**, 682 (1932).
[2] A. H. Compton and I. A. Getting [Phys. Rev. **47**, 817 (1935)] note that a distinction can be made between a sidereal period and a seasonal variation of the solar period by comparing the phase of the apparent sidereal effect in the northern and southern hemispheres. The method here used has the advantage that it does not require data from more than one station.
[3] For a comprehensive discussion of the harmonic dial as used in geophysical and cosmical problems see J. Bartels (a) Terr. Mag. **40**, 1 (1935); (b) Terr. Mag. **37**, 291 (1932).

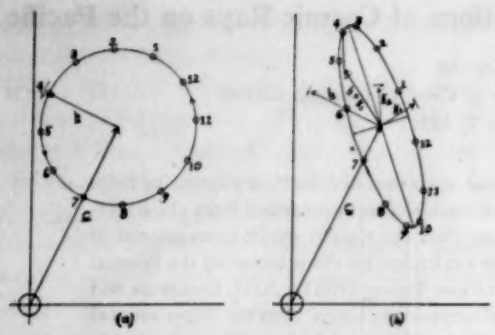

FIG. 1. Periodicities plotted on solar time dial. (a) Combination of solar diurnal and sidereal diurnal variations each of constant amplitude. (b) Combination of solar diurnal variation of harmonically varying amplitude with sidereal diurnal variation of constant amplitude.

solar day corresponding to the periods T_1 and T_2. Since these frequencies are nearly equal we may write $\nu_2=\nu_1+\mu$ so that the expression for the total variation becomes

$$f(t)=c\sin(2\pi\nu_1 t+\alpha)+h\sin(2\pi\nu_1 t+2\pi\mu t+\beta).$$

μ is small compared to ν_1 and to a first approximation what is represented is the sum of two sine curves of equal frequency but with their relative phases varying slowly with the period $1/\mu$. If an arbitrary time origin is chosen, the amplitude of the resultant diurnal variation will be a maximum and equal to $c+h$ when $\alpha=2\pi\mu t+\beta$. When $\alpha+\pi=2\pi\mu t+\beta$ the amplitude will have a minimum value of $c-h$. This will appear on the harmonic dial as a vector of amplitude h revolving with a period of $1/\mu$ solar days about the end point of **c**, as shown in Fig. 1(a). As $\mu=1/365$ this rotating vector will complete one revolution in a solar year. The resultant vector representing the combination of the two variations will therefore show a seasonal phase shift as well as a seasonal change in amplitude. The maximum shift of phase will be $\pm\arcsin h/c$. If data representing this type of variation are plotted on a solar time dial the points will progress regularly around the circle in a counter-clockwise direction. This regular cyclic order of the plotted points is an important characteristic.

Solar component with seasonal amplitude variation

To investigate the effect of a seasonal variation in the amplitude of the solar component let

$$\left(c+2k\cos\frac{2\pi t}{T_3}\right)\sin\left(\frac{2\pi t}{T_1}+\alpha\right)$$

represent a harmonic variation of period T_1 with an amplitude varying with a period T_3. Bartels[4] has pointed out in a similar connection that this is equivalent to three harmonic variations of slightly different periods,

$$\left(c+2k\cos\frac{2\pi t}{T_3}\right)\sin\left(\frac{2\pi t}{T_1}+\alpha\right)$$
$$=c\sin\left(\frac{2\pi t}{T_1}+\alpha\right)+k\sin\left(\frac{2\pi t}{T_1}-\frac{2\pi t}{T_3}+\alpha\right)$$
$$+k\sin\left(\frac{2\pi t}{T_1}+\frac{2\pi t}{T_3}+\alpha\right).$$

If $T_3=nT_1$ this simplifies as follows:

$$\frac{2\pi t}{T_1}-\frac{2\pi t}{nT_1}+\alpha=\frac{2\pi nt-2\pi t}{nT_1}+\alpha=\frac{2\pi t}{nT_1/(n-1)}+\alpha,$$

and similarly

$$\frac{2\pi t}{T_1}+\frac{2\pi t}{nT_1}+\alpha=\frac{2\pi t}{nT_1/(n+1)}+\alpha.$$

Thus there appear variations of three different periodicities, T_1, $(n/n-1)T_1$ and $(n/n+1)T_1$. In the particular case under discussion $n=365$, so that periods appear of 1 solar day, 365/364 solar days and 365/366 solar days. This latter period is one sidereal day which thus in a purely formal manner appears from the analysis of a seasonally varying solar component. On the harmonic dial these two extra periodicities appear as vectors of amplitude k revolving in opposite directions with the period T_3 (one solar year) around the end-point of the solar amplitude vector. It should be noted that there is no seasonal variation of phase introduced thereby, only variation in amplitude.

If the seasonal amplitude variation of the solar component and the sidereal component are both

[4] Cf. paragraph A8 of reference 3(a). The discussion by A. G. McNish [J. Frank. Inst. **215**, 697 (1933)] suggests an analysis somewhat similar to that here described.

present the resulting variation could be expressed by

$$f(t)=c\sin\left(\frac{2\pi t}{T_1}+\alpha\right)+k\sin\left(\frac{2\pi t}{nT_1/(n-1)}+\alpha\right)+k\sin\left(\frac{2\pi t}{nT_1/(n+1)}+\alpha\right)+h\sin\left(\frac{2\pi t}{nT_1/(n+1)}+\beta\right).$$

Since the period of the sidereal wave will be the same as the period of one of the components of the seasonal variation, these may be added together to give a single harmonic component of the total variation. The discussion from this point is considerably clarified by following it in terms of rotating vectors on the harmonic dial.

Let the tip of the constant vector **c** in Fig. 1(b) be the pole, with the polar axis in the direction of **c**, and let k be the common amplitude of the oppositely rotating vectors $\mathbf{k}_1$ and $\mathbf{k}_2$ with position angles of ϕ and $-\phi$ together representing the seasonal amplitude variation of the solar diurnal wave. The sidereal diurnal wave is represented by a vector of amplitude h and position angle $\phi+\delta$. The periods are all one solar year and the time origin is chosen so that $\phi=0$ on the date of the maximum amplitude of the solar diurnal variation.

The sidereal diurnal vector **h** and the vector $\mathbf{k}_1$ rotate in the same direction at a constant angle δ with each other, and may be combined into one vector **r** of amplitude $r=(h^2+k^2+2hk\cos\delta)^{\frac{1}{2}}$ at an angle $\theta=\arctan(h\sin\delta)/(k+h\cos\delta)$ with $\mathbf{k}_1$. We have then two vectors $\mathbf{h}+\mathbf{k}_1$ and $\mathbf{k}_2$ rotating in opposite directions with the same period, having unequal amplitudes and being at an angle θ when $\phi=0$.[5] When $\phi=-\frac{1}{2}\theta$ or $\phi=\pi-\frac{1}{2}\theta$ these two vectors will be parallel and give a maximum displacement from the fixed end-point of **c**. When $\phi=\pi/2-\frac{1}{2}\theta$ or $\phi=3\pi/2-\frac{1}{2}\theta$ the rotating vectors are antiparallel and the displacement from the end-point of **c** is a minimum. This fixes the positions and magnitudes of the major and minor axes of the ellipse traced out by the resultant of both rotating vectors, semi-major axis

$$(h^2+k^2+2hk\cos\delta)^{\frac{1}{2}}+k,$$

semi-minor axis

$$(h^2+k^2+2hk\cos\delta)^{\frac{1}{2}}-k,$$

angle between major axis and **c**

$$\tfrac{1}{2}\arctan(h\sin\delta)/(k+h\cos\delta).$$

A straight line locus will be obtained when the minor axis is zero, that is, when $(h^2+k^2+2hk\cos\delta)^{\frac{1}{2}}=k$. Solving this expression for δ gives $\delta=\arccos(-h/2k)$. This is possible only for $\pi/2<\delta<3\pi/2$ since h and $2k$ are the amplitudes of the sidereal diurnal wave and the seasonal wave, respectively, and essentially positive. If $\delta=0$ the major axis of the resultant ellipse will be parallel with **c**. The semi-major axis will then have a length $h+2k$ and the semi-minor axis h. In any case there will be a seasonal variation in phase as well as in amplitude, and when datum points are plotted they will lie in chronological order around the ellipse or along the straight line. Except when $(h^2+k^2+2hk\cos\delta)^{\frac{1}{2}}<k$ the ellipse will be described in the counter-clockwise direction.

Distinction between real and spurious sidereal diurnal variation

We see from the foregoing that in the case of a simple seasonal variation in the amplitude of the solar diurnal vector, there is no variation in phase, only variation in amplitude on the harmonic dial despite the appearance of two extra periodicities in the analysis. If a sidereal diurnal variation is present, alone or in conjunction with a seasonal variation in the solar amplitude, variation in phase is always introduced, and the plotted points taken in order will always have a cyclic arrangement. Formal analysis in this case will show two extra periodicities which will in general be of different amplitude.

This form of analysis should give definite evidence as to the presence of a true sidereal diurnal component even in the presence of a seasonal variation of the amplitude of the solar component, a case which the familiar method fails to distinguish clearly. With seasonal and sidereal diurnal variations of exactly equal

[5] A discussion of the case of two oppositely rotating vectors of unequal amplitudes will be found in Karl Stumpff, *Grundlagen und Methoden der Periodenforschung* (Springer, 1937), pp. 129–132.

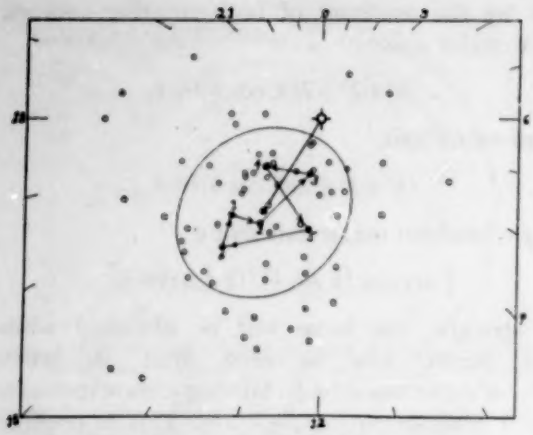

FIG. 2. Solar time dial for 1936 cosmic-ray data from the Pacific Ocean. Light circles, 3–4 day means: heavy circles, all data combined to show chronological order. (Data from Compton and Turner.)

amplitude and opposite phase (i.e., the date on which solar and sidereal diurnal maxima occur together is the date for the minimum in the seasonal variation) we would find, not a canceling of the two effects, but a straight line perpendicular to **c** the mean amplitude vector of the solar diurnal variation. The orderly progression of the datum points along this line would distinguish it from a mere statistical scatter in phase.

THE ACTUAL HARMONIC DIAL

Passing from these ideal cases in which we have assumed no statistical fluctuations to the actual case, we can expect that the larger the relative importance of the statistical fluctuations, the more ill defined the cyclic figures will become. When they reach such magnitude that the figure becomes a random pattern, we can be sure that no sidereal diurnal variation exists which can be distinguished reliably from a seasonal variation in the amplitude of the solar component. In this case, if the computed probable ellipse for the cloud shows a pronounced eccentricity with its major axis approximately in the direction of the solar amplitude vector we can say that a seasonal variation in the amplitude of the solar component is indicated, but can draw no conclusion regarding the reality of a sidereal diurnal variation except that it must be smaller than the probable error of the solar variation.

APPLICATION

The method of analysis outlined above has been applied to data gathered on the Pacific Ocean by Compton and Turner over a period of about 11 months. In view of the fact than an analysis of these data shows no significant change in the solar diurnal variation of intensity with geomagnetic latitude,[6] the data from various latitudes have been combined and examined as a whole for possible evidence of a sidereal time variation.

That portion of the data covering the trips between Vancouver and Auckland was used to compute the constants of the first harmonics of 63 diurnal variation curves; each combined data from three or four days. When plotted on a solar time dial as shown in Fig. 2, a mean amplitude of 0.23 percent is found, with the maximum occurring at about 14 hours. The major axis of the probable ellipse lies within 23° of the mean amplitude vector. Since, however, the ratio of the axes is but 1.17, no predominant variation in either amplitude or phase is conclusively demonstrated. To examine the cloud for cyclic arrangement of the points, time averages are so taken that all the data are represented by six points. These six points when plotted show an irregular figure-eight pattern in which the phase variations are random but the variations in amplitude follow a consecutive order. To be sure that combining data from various latitudes has not masked the effect sought, dials are shown in Fig. 3 for three latitude zones and in each case the random arrangement of the points is evident.[7]

The probable error in phase of these points is

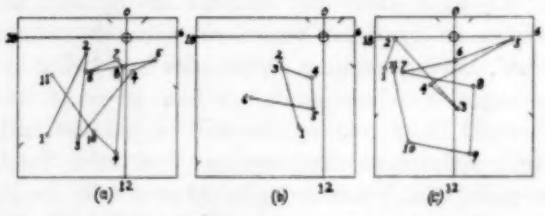

FIG. 3. Pacific Ocean data (1936) by latitude zones. (a) 10°–40°N, (b) 10°N–10°S, (c) 10°–40°S, geomagnetic latitude.

[6] J. L. Thompson, Phys. Rev. **54**, 93 (1938).

[7] It will be noted that the data from the equatorial zone describe a rough figure eight. If real, this would mean a sidereal 12-hour period. The statistical variations of the points are however so great as to make this indication of doubtful significance.

roughly one hour and phase shifts of about this magnitude would be necessary in order to restore the points to a cyclic arrangement. The estimated probable error of phase of one hour corresponds to a probable error in amplitude of 0.06 percent. Within such a probable error, therefore, the present data indicate no significant sidereal diurnal variation. There is however, in the consecutive order of the points according to amplitude, a rather strong indication of an annual change in the amplitude of the solar diurnal variation.

The most specific theory which would predict a sidereal time variation of cosmic rays is that of Compton and Getting,[2] according to which the motion of the earth with the rotation of the galaxy results in a slight excess of cosmic rays from the direction of motion. According to a new calculation by Vallarta, Graef and Kusaka (in this issue, page 1), the amplitude of the sidereal time variation from this cause should be about 0.15 to 0.2 percent, roughly twice as great as estimated by Compton and Getting. The present analysis thus gives significant, though not conclusive, evidence that the sidereal diurnal variation is less than demanded by this theory.

The writer wishes to acknowledge his indebtedness to Professor A. H. Compton for calling this problem to his attention and for his very helpful criticisms of the discussion presented.

JANUARY 1, 1939 PHYSICAL REVIEW VOLUME 55

On the Penumbra of Cosmic Radiation

R. ALBAGLI HUTNER
Massachusetts Institute of Technology, Cambridge, Massachusetts

(Received April 18, 1938)

The development of the theory of the penumbra is given, and a few examples of penumbral trajectories are shown. Pairs of values of the energy and latitude having penumbral regions are indicated. Two methods of analyzing the data obtained by means of Bush's Differential Analyzer are given; the first yielding the allowed directions for just one type of penumbral orbit over all latitudes and for one energy; the second giving the whole penumbra for one energy and one latitude. The energy chosen in each case was $r=0.425$ störmer (1.08×10^{10} ev for electrons). By means of the second method, the almost complete allowed cone is obtained for this energy and for a geomagnetic latitude of 20°.

I. DEVELOPMENT OF THE THEORY

WE ARE concerned in this paper with the general problem of the motion of a charged, primary, cosmic particle in the field of the earth's magnetic dipole, and, in particular, with the determination of allowed and forbidden directions in the "penumbra," i.e., the region between the Störmer cone and the main cone, in the terminology adopted by Lemaitre and Vallarta.[1, 2]

Since, according to Lemaitre and Vallarta, the immediate problem is reduced to that of determining the allowed incident directions at a given point, two angles, η and θ, are used for the presentation of the final results.[2] If the intersection of the ray with a unit hemisphere erected at that point be projected on the horizontal plane, the coordinates of the point of projection will be $\sin\theta$ and $\cos\theta\sin\eta$. This horizontal projection affords a two-dimensional picture of all the spatial directions permitted at a point and is the method adopted by Lemaitre and Vallarta for presenting their analyses. It is the one used in this paper, and will be referred to as the cone diagram or cone projection.

By means of the equation

$$\tan\eta = d\lambda/dx \qquad (1)$$

the angle[3] η can be determined from the solutions

[1] G. Lemaitre, M. S. Vallarta and L. Bouckaert, Phys. Rev. **47**, 435 (1935).
[2] G. Lemaitre and M. S Vallarta, Phys. Rev. **49**, 719 (1936).
[3] For the necessary definitions see reference 2.

of the differential equations[2] of motion in the meridian plane obtained directly from Bush's Differential Analyzer.[4]

The angle θ is obtained from Störmer's[5] formula:

$$\pm\sin\theta=\frac{2\gamma_1 r-\cos^2\lambda}{r^2\cos\lambda}, \qquad (2)$$

where the positive sign is to be used for positive particles, and the negative for negative particles.[3]

FIG. 1. The size and position of the cone diagram varies with r and λ.

From Eq. (2) it is seen that for a given r and λ the angle θ varies with γ_1; thus by using this equation one can regard η and γ_1 instead of η and θ as the two variables concerned for constructing the cone diagram. Since $\sin\theta$ can only have values from $+1$ to -1, there is just a limited range of γ_1's of significance in defining the cones for a given (r, λ), as shown in Fig. 1. Since the ordinate of the cone projection varies with η and the abscissa with γ_1, each pertinent value of γ_1 and all η directions must be investigated in order to find allowed and forbidden directions.

For $\gamma_1 \geq 1$, Störmer[5] showed that, for energies below $r=1$ störmer[3] (5.96×10^{10} ev for electrons), all values of η are forbidden directions. These directions are all outside a circular cone with axis along the east-west line, which cone is referred to as the Störmer cone.

For values of γ_1 between 0.78856[6] and 1, Störmer's allowed and forbidden regions in the meridian plane are so shaped that the part in the vicinity of the earth is joined to infinity by a pass, narrow for γ_1 just less than one, and wider as γ_1 decreases. Störmer[5] has shown that there exists a family of periodic orbits guarding this pass. Later Lemaitre[7] proved that these orbits are unstable. Somewhat earlier Lemaitre and Vallarta[8] had shown that the family disappears for $\gamma_1<0.783$, a result which was later refined by Lemaitre[9] to $\gamma_1<0.78856$. Each member (one for each γ_1) of this family of unstable periodic orbits admits a family of orbits asymptotic to it, which has been discussed by Lemaitre and Vallarta,[2] and Schremp[10] in connection with the main cone. For Lemaitre and Vallarta have shown that not only is there a Störmer circular cone *outside* of which *no* directions are allowed, but contained within this cone there is an irregular one, called the main cone, *inside* of which *all* directions are allowed. All of the directions contained within this main cone represent angles of incidence for dynamic paths coming directly from infinity (i.e., each path does not loop on itself in the meridian plane before hitting the earth; these are the nonreëntrant orbits referred to by Schremp[10]). It is the family of asymptotic orbits mentioned above that determine part of the boundary of the main cone.

FIG. 2. A few types of reëntrant (penumbral) orbits. The earth would be represented by a straight, vertical line, whose position with respect to each orbit would be determined by the energy considered.

[4] V. Bush, J. Frank. Inst. 212, 447 (1931).
[5] C. Störmer, Zeits. f. Astrophys. 1, 237 (1930); Oslo Univ. Observatory, Publication No. 10, 1934. References to his previous work are given in each of these.
[6] The recent paper by O. Godart, Ann. Soc. Sci. de Bruxelles 58, 27 (1938), indicates that this value of γ_1 should be 0.788541.
[7] G. Lemaitre, Ann. Soc. Sci. de Bruxelles 54, 162 (1934).
[8] G. Lemaitre, M. S. Vallarta, Phys. Rev. 43, 87 (1933). The sign of the magnetic field should be changed.
[9] G. Lemaitre, Ann. Soc. Sci. de Bruxelles 54, 194 (1934).
[10] E. J. Schremp, Phys. Rev. 54, 153 (1938).

However, if the orbit coming from infinity loops on itself one or more times (is reëntrant[10] one or more times) before reaching a given point on the earth, its direction of incidence will fall between the main cone and the Störmer cone in the region called "penumbra" by Lemaitre and Vallarta.[2]

The first trajectory in Fig. 2 illustrates the simplest type of penumbral orbit possible, i.e., having just one loop or reëntrant section.[10] A few examples of relatively simple orbits, having two reëntrant sections, are also shown in Fig. 2; more involved trajectories have more and more loops, their number increasing to infinity. Such examples are not easy to exhibit. Because the nonasymptotic orbits follow the pattern of the asymptotic ones, it is possible to build types of permitted penumbral orbits without the direct use of the Differential Analyzer, once the general outline of the system of envelopes of the asymptotic orbits is known. This system of envelopes was obtained by Lemaitre and Vallarta[2] and qualitatively extended by Schremp a few years ago, and the predictions made on this basis were in all cases verified by the runs of the machine. Although the actual quantitative results, such as the values of η and θ, must be

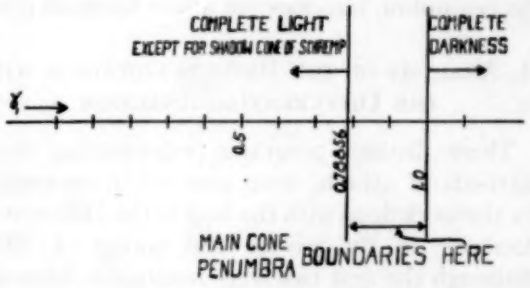

FIG. 3. The dependence of the allowed cone boundaries on γ_1.

obtained from the Differential Analyzer, the understanding enabling one to make these predictions is necessary both for the efficient use of the Differential Analyzer, and for gleaning quantitative results from the machine curves.

Besides the principal periodic orbit guarding the pass, called the "outer periodic orbit," there is, closer to the dipole, another one called the "inner periodic orbit," whose existence was first shown by Störmer.[5] Led by inspection of

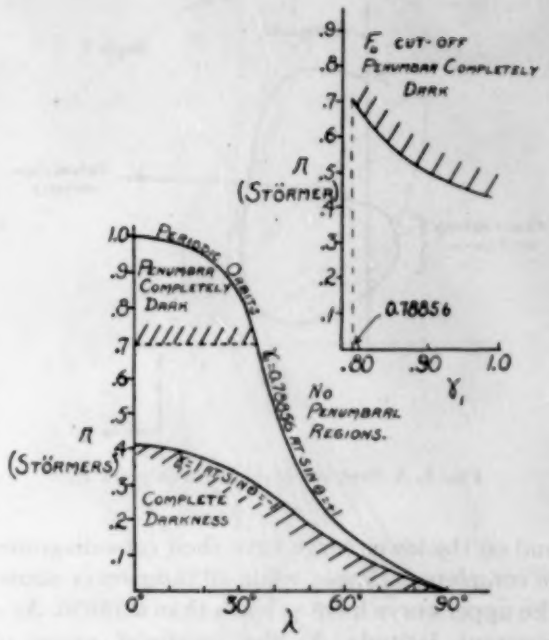

FIG. 4. Energy limits for the existence of penumbra.

Störmer's results Schremp[10] proved that all reëntrant sections, which constitute the distinctive feature of penumbral orbits, must cross the equator between the inner and outer periodic orbits. It has been proved that as the value of γ_1 decreases from 1, these two orbits approach each other (the outer moving in faster than the inner moves out), until they coalesce for $\gamma_1 = 0.78856$ and then disappear for all smaller values of γ_1. It follows (Schremp) that the asymptotic and all the penumbral orbits occur only in the range $0.78856 < \gamma_1 < 1$, (Fig. 3). For values of γ_1 below this range particles reach the earth for all values of η within the shadow cone obtained by Schremp[11] which extends to values of $\gamma_1 < 0.78856$.

It should be remembered that for each pair of values (r, λ) there is a limited range of pertinent values of γ_1 (Fig. 1). In fact for each latitude there is but a limited range of energies for which γ_1 lies in the range where irregularities exist in the allowed directions of incidence. It is in this limited range of energies that the north-south and the east-west asymmetries occur. In the lower graph of Fig. 4 all of the (r, λ) combinations having this property lie between the two solid curves; all the pairs of values of (r, λ) below

[11] E. J. Schremp, Phys. Rev. 54, 158 (1938).

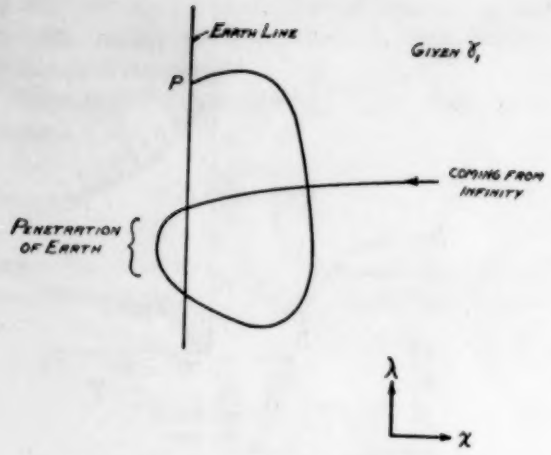

FIG. 5. A direction of darkness at point P.

and on the lower curve have their cone diagrams in complete darkness, while all those on or above the upper curve have γ_1's less than 0.78856. At a constant latitude, λ, the pertinent range of energies can be read from this diagram.

As pointed out by Schremp,[10] the impenetrability of the earth is an important factor for determining the penumbral bands. In the (x, λ) plane (conformal map of the meridian plane) it will be recalled that the earth is represented by vertical straight lines; hence whenever there are minima and maxima of x along a trajectory there is a possibility of blocking it out by the earth. Fig. 5 illustrates this for the simplest type of penumbral orbit. Because of the continuity with respect to the initial conditions, and of the consequent gradual deformation of the shapes of the trajectories, whole sections of a given type of orbit will be cut out by the earth's line (see also Fig. 8). This means a banded structure of the penumbral regions.

Experience with the solutions indicates that each orbit coming from infinity and having one or more loops or reëntrant sections, must have a minimum of x somewhere behind the F_0 envelope of the asymptotic orbits. (This envelope has been described by Lemaitre and Vallarta;[2] its position varies with γ_1. An example is shown in Fig. 7.) The conclusion to be drawn from this, first pointed out by Schremp[10] (Theorem 7), is that all the values of x, and therefore r, greater than that of the highest value of x on this envelope must have the penumbra completely dark for that and higher values of γ_1. This γ_1, above which the penumbra is dark, is called the F_0 cut-off. The upper diagram of Fig. 4 shows the F_0 cut-off for all values of r, as obtained from a study of the trajectories traced by the Differential Analyzer. This indicates that at least all the energies above $r=0.7$ störmer will have the entire penumbra dark, as carried over into the lower graph. For energies between 0.7 and 0.414 störmer the indicated values of γ_1 are the highest

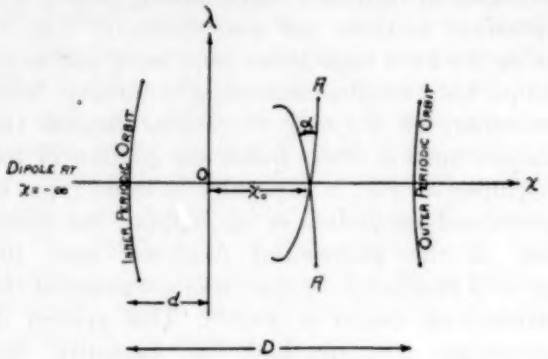

FIG. 6. The pencil of reëntrant orbits at a point on the equator.

ones for which there can be any "light" in the penumbra. It amounts to an extension of the region of complete darkness to γ_1's less than 1 for the penumbra, but does not affect the main cone.

II. Analysis of the Results Obtained with the Differential Analyzer

Three distinct programs, representing three methods of attack, were planned in succession for the work done with the help of the Differential Analyzer in the winter and spring of 1937. Although the first two were invaluable from the standpoint of gaining familiarity with the trajectories, it was the third approach which yielded the numerical results reported here.[12] This depended on the application of Schremp's result that all reëntrant sections must cross the equator between the inner and outer periodic orbits.

Description of the third program

Passing through each point along the equator between the inner and outer periodic orbits there

[12] More details can be obtained from the author's Ph.D. thesis, R. Albagli, Massachusetts Institute of Technology, December, 1937.

are two self-reversing (at the points A of Fig. 6) orbits, the consequence of which is that trajectories to the right of A will turn out toward the pass, while those to the left will turn in toward the dipole. Thus any section of an orbit passing through the point x_0, within the angle α, will turn in at both ends and be a reëntrant section. The angle α is zero at the equatorial points of both periodic orbits, and has a maximum near the middle of the interval D.

All reëntrant orbits can be generated by starting at different points along the equator, for each γ_1, and varying the initial angle, η', through the angle α at that point, making it theoretically possible to get a complete picture of the penumbra. The angle between the tangent to the trajectory at the equator and a parallel to the λ-axis is called η'. In practice, intervals of the distance along the equator, intervals of the angle α, and intervals of the values of γ_1 had to be chosen, so that the completeness of the results

TABLE I. *Values of $\alpha/2$ in radians.*

y_0	$\gamma_1 = 0.99$	0.97	0.93	0.89	0.85	0.82
0.07	0.430					0.027
.12					0.108	
.13	.575	0.500				
.14			0.354	0.220		
.23						.070
.39						.090
.47					.180	
.52	.800					
.54		.630				
.55						.085
.60			.400			
.68				.231		
.71						.062
.87						.029
.93					.033	
.95		.125		.047		
.97	.154					
.98			.025			

TABLE II. *Values of $\alpha/2$ in radians.*

y_0	$\gamma_1 = 0.99$	0.97	0.95	0.93	0.91	0.90	0.89	0.88
0.05		0.285		0.173	0.130			
.10		.430	0.355	.293	.230		0.188	
.20	0.638	.550	.480	.413	.321		.270	
.30	.710	.622	.522	.447	.370	0.329	.307	0.264
.35							.310	.267
.40		.638	.533	.454	.375	.333	.310	.274
.45				.447	.368		.304	.267
.50		.634	.525	.437	.337		.291	
.60		.593	.480		.319		.259	
.70		.525		.340	.266			
.80		.405	.304	.240	.190		.148	
.82				.212				
.90		.234	.158	.123	.099		.078	
.925				.095				

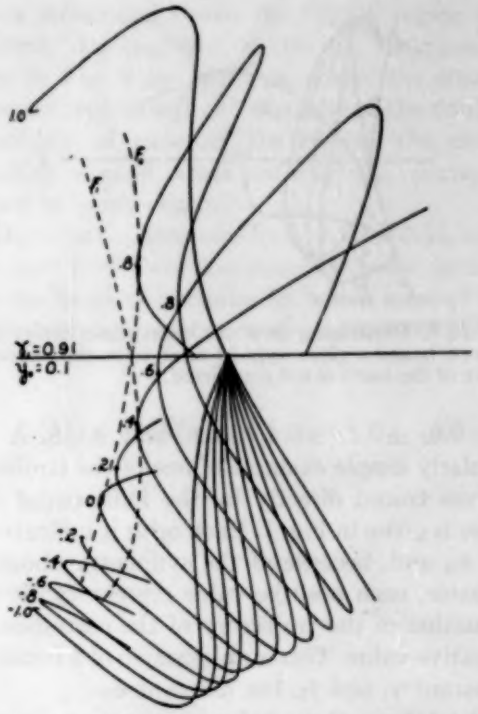

FIG. 7. A family of trajectories as obtained directly from the Differential Analyzer. The number beside each curve is the value of ϕ_0.

depended on the ability to interpolate between the machine curves for each of these variables.

The quantity y_0, where

$$y_0 = (|x_0| + |d|)/D,$$

was used to specify the starting point, i.e., y_0 is the fraction of the distance D (Fig. 6) that the starting point is away from the inner periodic orbit. For each y_0, curves were run at different initial angles η'; however, instead of designating the orbit by η', the quantity ϕ_0 was used,

$$\phi_0 = \eta'/\tfrac{1}{2}\alpha,$$

where $\alpha/2$ is the angle of the self-reversing orbit with a parallel to the λ-axis. When the program was begun the first orbit traced at a point, y_0, was the one for which $\eta' = 0°$. Then η' was increased till the self-reversing orbit was obtained. This determined the angle $\alpha/2$, after which orbits were generated over this range of η', but for negative values of the angle. Later when good estimates could be made of the value of $\alpha/2$, this was first determined at the given y_0, and the other trajectories developed were those for which

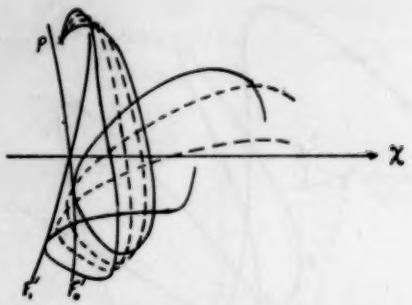

FIG. 8. Illustrating how the asymptotic orbits (solid curves) bound a given type of orbit when the impenetrability of the earth is not considered.

$\phi_0 = 0.0, \pm 0.2, \pm 0.4, \pm 0.6$, and ± 0.8. A particularly simple example of one of the families of curves traced directly by the Differential Analyzer is given in Fig. 7. Each orbit is indicated by its ϕ_0, and, because of the symmetry about the equator, each positive value represents the continuation of the trajectory of the corresponding negative value. This is an example of a family for constant γ_1 and y_0, but different ϕ_0.

By taking these same curves and grouping them into families of constant γ_1 and ϕ_0, but varying y_0 the same types of envelopes are obtained, permitting interpolations as above. Still a third group of families is formed by varying γ_1 while keeping y_0 and ϕ_0 fixed.

Since there are three ways of interpolating, starting points were taken rather far apart (for considering the extreme complexity of the curves, the rapidity with which they vary for points close to the outer periodic orbits, and the total number of γ_1's involved) in the hope that all the necessary data could be assembled within a reasonable time. Tables I and II indicate all of the data on which the final numerical results presented here depend. The γ_1's are listed across the top, and the y_0's in the first vertical column. The numbers in the other columns represent the values of $\alpha/2$ in radians. At least ten runs were made at each chosen point.

To analyze the data it is important to realize that the region over which a given type of orbit (characterized by the number of reëntrant sections) extends is bordered on all sides by asymptotic orbits; a typical example is shown in Fig. 8. The lines marked F_0' and F_1' are the envelopes of the asymptotic orbits. The two orbits drawn in full lines emanating from the point P are asymptotic orbits since they are tangent to F_0' and F_1'. The nonasymptotic orbits between them, two of which are drawn in dotted lines, bounce in the region between the asymptotic envelopes, and all go directly to infinity; any nonasymptotic orbits not included between the asymptotic ones will have at least one more reëntrant section.

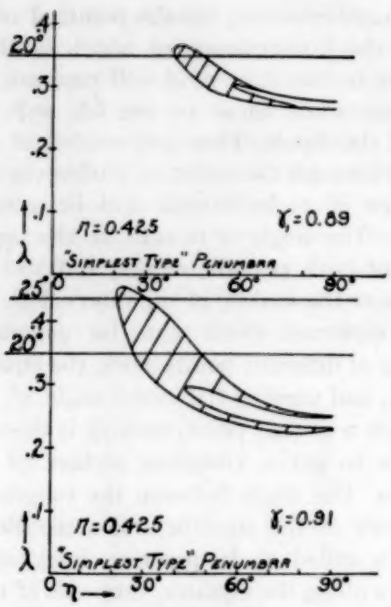

FIG. 9. Penumbra regions obtained by means of the first method of analysis.

However, if the energy is such that the earth line through the starting point P intersects the region between F_0' and F_1' it is obvious that all orbits bouncing to the left of this line will be blocked by the earth. Thus in this case the regions of "light" will be bounded on one side by asymptotic orbits, and on the other by nonasymptotic trajectories of the second kind.

First method of analyzing machine data

The first program led to the conjecture that the simplest type of penumbral orbit (first one of Fig. 2) would contribute the most "light;" therefore it was decided to try to outline these regions first, by determining the appropriate asymptotic orbits and orbits of the second kind, as already discussed.

Altogether there were six variables to be considered: r, λ, η, γ_1, ϕ_0 and y_0. After some consideration the energy chosen was $r = 0.425$ (1.08×10^{10} ev for electrons). The simultaneous

values of η and λ for all of the pertinent orbits were plotted, after which those (η, λ) combinations for allowed directions on the earth had to be determined. In order to find the limits of this patch of "light" by means of the continuity with γ_1, ϕ_0 and y_0, the (η, λ) diagrams were graphed in two distinct ways: (1) C_{γ_1}, wherein γ_1 was constant, and the lines of equal ϕ_0 and of equal y_0 were drawn; (2) C_{ϕ_0}, wherein ϕ_0 was constant, and the lines of equal γ_1 and y_0 were drawn. With the aid of the three ways of grouping the curves mentioned above, the "light" region was outlined. An example of the C_{γ_1} diagrams is given in Fig. 9 for two γ_1's, where the shaded areas are regions of light. Because of the double-valuedness of parts of the region, the corresponding shaded areas on the C_{ϕ_0} diagrams cannot be easily shown.

When the C_{γ_1} diagrams for $\gamma_1 = 0.89, 0.91, 0.93, 0.95$, and 0.97 were completed, it could be seen that the range of latitudes for which most of the simplest type penumbra occurs is from 10° to 30°

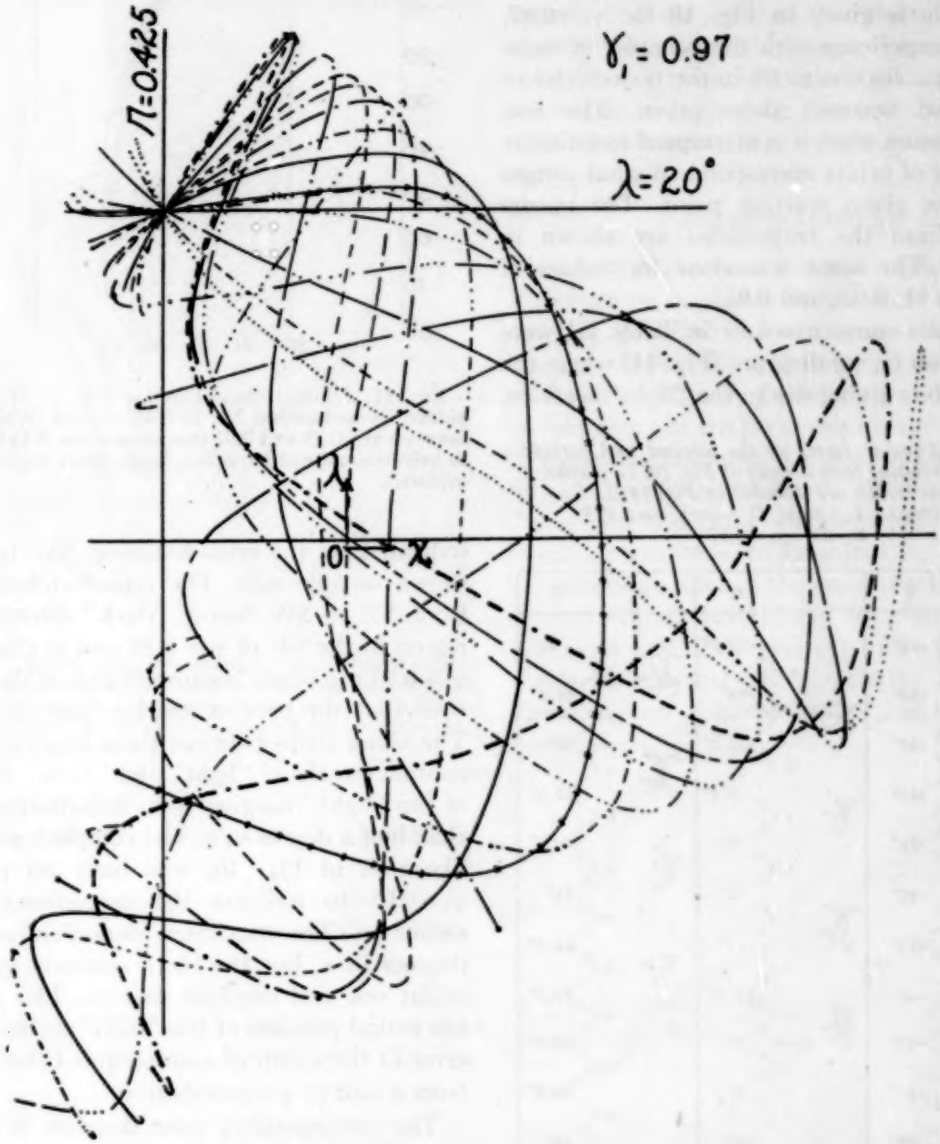

FIG. 10. To form this example of an η-diagram, the curves emanating from a point were obtained by interpolating between the machine curves.

for $r=0.425$. But it is to be remembered that this refers to just one region of "light" in the whole penumbra at a given latitude.

Second method of analyzing the machine data

Efforts were next turned to the task of getting the complete picture of the penumbra for at least one energy and one latitude. The most direct method was to try to build up the complete η-diagram for the point $r=0.425$, $\lambda=20°$ for each γ_1, by interpolating between the curves obtained directly from the Differential Analyzer. An example is given in Fig. 10 for $\gamma_1=0.97$. Extensive experience with the behavior of these solutions enables one to fill in the trajectories to be expected between those given. The real difficulty comes when it is attempted to estimate what types of orbits correspond to what ranges of η at the given starting point. The results obtained from the trajectories are shown in Table III. The same was done for values of $\gamma_1=0.89$, 0.91, 0.93, and 0.95.

The results summarized as in Table III were plotted on an (η, γ_1) diagram (Fig. 11) where the types of orbits giving rise to the "light" sections,

TABLE III. *Tabular forms of the allowed and forbidden directions resulting from a study of Fig. 10. In graphical form, these results are included in Fig. 11. L. S.—light streaks, L.—light, D.—dark, $r=0.425$. $\lambda=20°$. $\gamma_1=0.97$.*

η	η	η
-90°	-38.5°	46°
-69°	-38°	46.5°
-63°	-35.5°	49°
-57°	-5.5°	49.5°
-52°	-4°	50.5°
-48°	-2°	51°
-47°	-1°	56.5°
-46°	+1.5°	57.5°
-43°	2°	58.5°
-42°	5°	60.5°
-39°	44°	64°
-38.5°	46°	

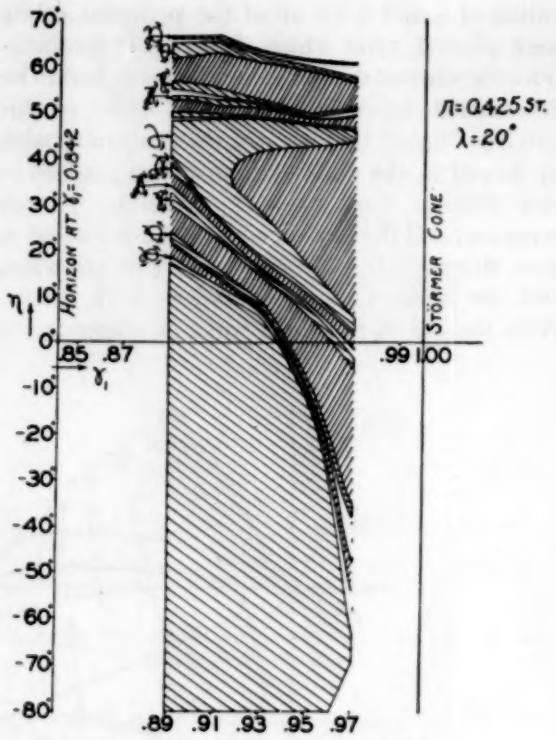

FIG. 11. Allowed (cross-hatched NW to SE) and forbidden (cross-hatched NE to SW) regions. White regions between $\gamma_1=0.89$ and 0.97 contain streaks of light of small to infinitesimal widths; other, large, white regions not yet explored.

indicated by the cross-hatching NW to SE are shown on one side. The cross-hatched regions from NE to SW denote "dark" directions; the region to the left of $\gamma_1=0.89$ and to the right of $\gamma_1=0.97$ are blank because of lack of data at the time that the present analysis was carried out. The blank strips between these two values of γ_1 contain streaks of "light" and "dark," the width of the "light" ranging from infinitesimal to less than half a degree in η. The complete η-diagram, like that of Fig. 10, was built up twice for $\gamma_1=0.95$ to indicate the consistency of the estimates. The maximum deviation was three degrees in η, but the more common value was about one and one-half degrees. This refers to the actual position of the "light" strips, but the error in the width of each strip is believed to be from a half to a whole degree.

The corresponding cone diagram is given in Fig. 12, where the largest "light" area is the main cone. The vertical cross-hatched strip to

the left of the line $\gamma_1 = 1$ is caused by the F_0 cut-off; the narrow half-crescent-shaped, cross-hatched space along the northern horizon is the shadow cone of Schremp.

III. Conclusions

The penumbral bands are bounded by orbits asymptotic to the outer principal periodic orbit and by orbits of the second kind. It has been possible to determine almost completely the cone diagram for one energy and latitude, i.e., $r = 0.425$ störmer (1.08×10^{10} ev for electrons) and $\lambda = 20°$ geomagnetic latitude. On the basis of the experience gained from the present work it is surmised that smaller energies will have penumbral regions containing much larger "light" areas, while higher energies will have much smaller "light" bands. To be able to determine cosmic-ray asymmetries it is desirable to have at least the complete allowed cone for *all the energies* having penumbra *at a given latitude*. No reasonable predictions can be made just from the work already done, for, although the allowed cone and penumbra will vary continuously with the energy, it is conjectured that the rate of change is very great over the range of energies appertaining to a given latitude. This work is being continued with the help of a grant voted by the American Association for the Advancement of Science.

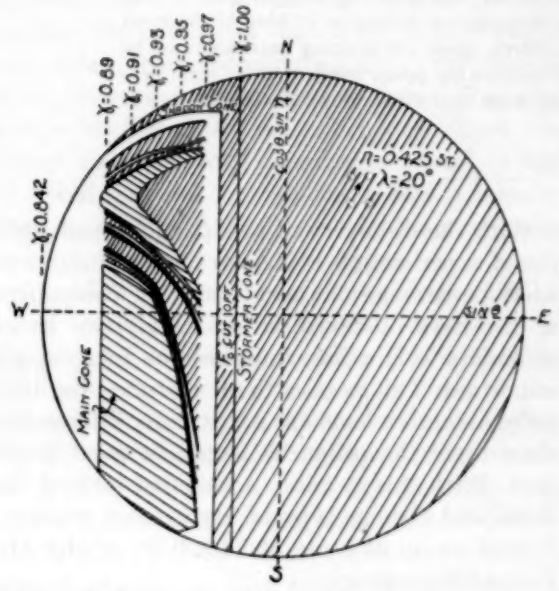

Fig. 12. Almost complete allowed cone. Allowed regions black or cross-hatched NW to SE, forbidden regions cross-hatched NE to SW, white regions between $\gamma_1 = 0.89$ and 0.97 contain streaks of small to infinitesimal widths; other, large, white regions not yet explored.

Acknowledgments

It is with pleasure that the author takes this opportunity to thank Professor M. S. Vallarta for his guidance, keen interest and constant encouragement. Long discussions with Professor Vallarta and Dr. E. J. Schremp were invaluable in mapping out the programs for the work on the Differential Analyzer. Talks with Dr. A. Banos, Jr. are deeply appreciated. Thanks are due to Dean V. Bush for making the Differential Analyzer available; to President K. T. Compton for supplying some of the necessary funds; to the United States Government for contributing by means of a W.P.A. project; to Professor S. H. Caldwell, Colonel R. C. Eddy, Mr. C. E. Shannon and their assistants for their willing cooperation.

New Evidence for the Existence of Penetrating Neutral Particles

FRANCIS R. SHONKA
University of Chicago,[1] Chicago, Illinois

(Received November 14, 1938)

An experiment of the Rossi-Hsiung type was performed at an altitude of 14,200 ft. with a fourfold coincidence array of Geiger-Müller tubes in a vertical position. Thicknesses of 12.7 to 17.3 cm of lead served as absorber between the counters. Additional varying thicknesses were placed alternately above and between the counters, i.e., in positions A and B. For small thicknesses the ratio of the counting rates with the lead in position A to that for position B was very little greater than unity. This means very slight production of barytrons by photons at this altitude. For greater thicknesses (19 to 23 cm), however, the ratio A/B becomes 1.06 ± 0.02. Working at sea level, and having the bottom tube shielded with 25 mm of lead, Hsiung obtained the same results. Maass, using no shield for the tubes, found the ratio A/B equal to 1.2. The most reasonable interpretation of the fact that this ratio is greater than unity seems to be the production of barytrons by non-ionizing primaries. In view of the great thickness of lead required to give the maximum effect, these non-ionizing particles must be much more penetrating than photons. This high penetrating power suggests their identification with the neutrettos (neutral particles having mass and other properties similar to the barytron) postulated by Heitler.

INTRODUCTION

ONE of the major conclusions of Bowen, Millikan and Neher[2] from their recent high altitude cosmic-ray measurements was that the number of primary ionizing particles entering the atmosphere is too small to justify the hypothesis that the large number of penetrating cosmic-ray particles found at sea level comes from outside the atmosphere. They accordingly suggested that these penetrating rays may be produced in the atmosphere as secondaries from high energy primaries which are themselves absorbed before they reach the earth. A similar suggestion had been made by Compton[3] as an alternative interpretation of Hsiung's[4] experiment. This experiment, as other similar ones performed by Rossi[5] and Maass,[6] showed that at sea level no significant part of the penetrating radiation is being produced as secondaries from non-ionizing rays. It was apparent, however, that higher in the atmosphere such production of penetrating secondaries might nevertheless occur if the primary rays were quickly absorbed by the air.

With the discovery of new particles and additional experimental evidence, the question as to what percentage of the penetrating component of the rays observed at sea level may be of secondary origin has thus become increasingly important. This applies to all altitudes, but altitudes above sea level are particularly interesting, since there the primaries would be most abundant. With this in mind, a modified form of the Rossi and Hsiung type of experiment was performed at an altitude of 14,200 ft. at the Mt. Evans Observatory.

APPARATUS

The apparatus consisted of a fourfold coincidence array of Geiger-Müller tubes. These tubes were made of a copper cylinder 4.1 cm in diameter, 38 cm in length, and 0.05 mm wall thickness, sealed in glass. The central electrode was a 0.075-mm tungsten wire. The assembly of these tubes has been previously described.[7] The tubes had exceptionally good characteristics, including plateaus of over 1000 volts, obtained by a special cleansing and baking technique.

Each Geiger-Müller tube was surrounded by four plates of lead, 1.6 cm thick. These four plates formed the sides only of a rigid box, 5.71 cm×8.9

[1] Present address: Department of Physics, De Paul University, Chicago, Illinois.
[2] I. S. Bowen, R. A. Millikan and H. V. Neher, Phys. Rev. **53**, 217 (1938).
[3] A. H. Compton, Proc. Phys. Soc. London **47**, 747 (1935).
[4] D. S. Hsiung, Phys. Rev. **46**, 653 (1934).
[5] B. Rossi, Zeits. f. Physik **82**, 151 (1933).
[6] H. Maass, Ann. d. Physik **27**, 507 (1936).
[7] J. B. Hoag, *Electron and Nuclear Physics* (D. Van Nostrand Company, 1938), p. 432.

cm×55.9 cm, having no top or bottom. The lead boxes containing the tubes were then stacked on two channel iron shelves, separated by 47 cm, as shown diagrammatically in Fig. 1. The two channel iron shelves were supported one above the other by a framework of angle iron. For vertical fourfold coincidences, two of the lead boxes containing the Geiger-Müller tubes were placed on the lower platform of channel iron, and two on the upper one. Any desired separation of the counting tubes was obtained by placing plates of lead underneath the bottom-most tube. Additional plates of lead absorber were inserted between the boxes containing the tubes. When smaller thicknesses of lead were used between the tubes, correspondingly larger thicknesses were placed below the bottom tube. Thus the Geiger-Müller tubes were brought closer together and the rate of counting increased. It will be noted that the lead is piled in such a manner that all rays producing coincidences must pass through the same vertical thickness.

The high voltage source for the Geiger-Müller tubes was essentially the circuit described by Gingrich,[8] a modification of the Evans[9] circuit. The counting circuits[10] employed were of the Neher-Pickering[11] type. For the relay circuit a No. 57 tube was used. For the recording circuit an 885 Thyratron activated a circuit-breaking magnetic relay; the pulses were registered on a Veeder-Root counter. This recording system was capable of counting fifty evenly spaced impulses per second. By means of switches in the screen grids of the No. 57 tubes in the recording circuits, any desired combination of n-fold coincidences could be recorded. All of the circuits were built to operate on 110-volt 60-cycle current. This was obtained at the top of Mt. Evans from a 500-watt gasoline engine generator set.

With the tubes in a horizontal plane and shielded heavily with lead, the individual counting rates N_i, and the double and triple accidental coincidence rates A_{ij} and A_{ijk}, were recorded. Then by means of the Eckart-Shonka[10] formula the values of the time constants (τ_i) were calculated to be as follows: $\tau_1=2.38\times10^{-5}$, $\tau_2=2.17\times10^{-5}$, $\tau_3=1.85\times10^{-5}$, and $\tau_4=2.04\times10^{-5}$ minute. With these values of τ_i and the individual counting rates N_i, the accidental fourfold counting rate A_{1234} was found to be 0.004 counts per minute.

The efficiencies of the tubes for cosmic-ray particles were obtained by the method of Street and Woodward.[12] The resulting efficiencies were:

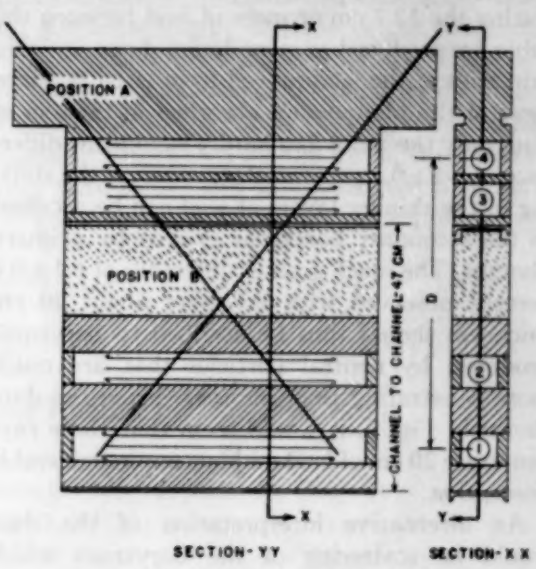

FIG. 1. Arrangement of tubes and absorbers.

tube I, 97.5 percent, tube II, 97 percent, tube III, 98 percent and tube IV, 98 percent.

RESULTS AND INTERPRETATION

Readings were taken with the tubes in a vertical position, with the thickness of lead between the tubes varying from 12.7 to 17.3 cm. This lead served as the absorber for the soft secondary particles. In addition to this, various thicknesses of lead were placed alternately above and between the counting tubes, i.e., positions A and B (Fig. 1). In order to increase the rate of counting, larger solid angles were used with the smaller thicknesses of lead. Table I shows the results of these experiments. The tabulated values are corrected for accidental counts and efficiencies. The errors given are probable errors.

[8] N. S. Gingrich, Rev. Sci. Inst. **7**, 207 (1936).
[9] R. D. Evans, Rev. Sci. Inst. **5**, 371 (1934).
[10] C. Eckart and F. R. Shonka, Phys. Rev. **53**, 752 (1938).
[11] H. V. Neher and W. H. Pickering, Phys. Rev. **53**, 316 (1938).
[12] J. C. Street and R. H. Woodward, Phys. Rev. **46**, 1029 (1934).

In Fig. 2 the ratio of the counting rate with the lead in position A to that for position B is plotted against the thickness of the lead that is moved from A to B. The open circles are a graphical representation of Table I, and the full circles are the averages of the first five and last four points, respectively.

The most evident interpretation of the fact that A/B is greater than unity is that ionizing rays (presumably barytrons) capable of penetrating the 12.7 cm or more of lead between the tubes are produced as secondaries of non-ionizing primaries in the lead moved from A to B. Since most of the photons are absorbed in two cm of lead, only the small and hardly significant difference of 1.5 ± 0.5 percent observed with the shifting of the thinner layers of lead can be ascribed to the secondary barytrons excited by primary photons. The much greater difference of 6.1 ± 0.6 percent observed with layers of about 20 cm thickness should thus be ascribed to barytrons produced by neutral particles that are much more penetrating than photons. From the data shown in Fig. 2, it would seem that these rays penetrate 20 cm of lead without any considerable absorption.

An alternative interpretation of the data would be scattering of the barytrons which traverse the lead. When the lead is in position B, scattering of barytrons would reduce the counts by a larger factor than would scattering in position A. Though it appears unlikely that this effect is large enough to account for the difference observed in the two positions, the data on scattering are inadequate definitely to rule out this possibility.

Working at sea level with a threefold cosmic-ray telescope, and having the bottom tube shielded with 2.5 cm of lead, Hsiung[4] found the ratio A/B to be 1.06 when alternating 20 cm of lead between positions A and B. Under similar conditions, Maass,[6] using unshielded tubes, alternated various thicknesses of iron between positions A and B and found the ratio A/B greater than unity with a maximum at about 30 cm of iron for which thickness this ratio was 1.2. It is possible, especially in the work of Maass, that some of the excess counts were caused by showers and scattering.

TABLE I. *Number of counts per minute for various thicknesses of lead at A or B.*

D IN CM (SEE FIG. 1)	CM OF PB BETWEEN TUBES	CM OF PB AT A OR B	COUNTS PER MINUTE		RATIO $\frac{A}{B}$
			POSITION A	POSITION B	
38.4	17.5	0.32	5.97 ± 0.05	5.90 ± 0.05	1.012 ± 0.012
38.4	17.5	0.95	5.99 ± 0.05	5.94 ± 0.05	1.008 ± 0.008
38.4	17.5	1.59	6.04 ± 0.05	6.08 ± 0.05	0.993 ± 0.012
38.4	17.5	1.91	6.01 ± 0.05	5.83 ± 0.05	1.031 ± 0.012
38.4	17.5	2.22	5.98 ± 0.06	5.91 ± 0.06	1.012 ± 0.012
38.4	17.5	5.71	5.69 ± 0.07	5.60 ± 0.07	1.016 ± 0.017
51.1	17.5	12.7	3.83 ± 0.07	3.67 ± 0.07	1.035 ± 0.024
54.5	15.9	19.68	3.48 ± 0.03	3.28 ± 0.03	1.061 ± 0.013
54.5	15.9	20.00	3.47 ± 0.04	3.23 ± 0.03	1.074 ± 0.013
54.5	14.3	20.32	3.41 ± 0.03	3.23 ± 0.03	1.056 ± 0.013
54.5	12.7	23.18	3.42 ± 0.03	3.23 ± 0.03	1.059 ± 0.013

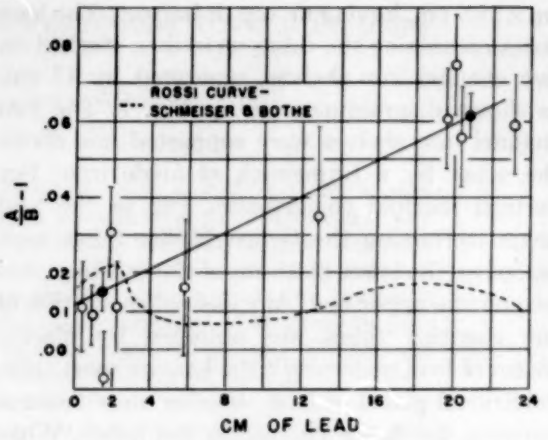

FIG. 2. Ratio of the counting rates with lead in positions A and B as a function of thickness of lead.

While the experiment on Mt. Evans was in progress, Schein and Wilson[13] took similar equipment in an aeroplane to an altitude of 25,000 feet. They alternated 2.2 cm of lead between the second and third tubes of a fourfold system (position B) and above all four tubes (position A). At 25,000 feet, they find the ratio A/B equal to 2.1 ± 0.44. This increase is probably due to barytrons produced by photons. Heitler[14] calculates that about one in 40 photons will be spen+ by producing a barytron. This would be adequate to account for their observed increase of counts in position A.

The small magnitude of the increase in the counting rate in position A for small thicknesses of lead is to be expected on the basis of Heitler's[14] calculations, since, if the production of soft shower particles by photons is 40 times as frequent as the production of penetrating second-

[13] M. Schein and V. C. Wilson, Phys. Rev. **54**, 304 (1938).
[14] W. Heitler, Proc. Roy. Soc. **166**, 529 (1938).

aries, the effect would be too small to be detected at lower altitudes. Thus the effect observed by Schein and Wilson[13] with 2.2 cm of lead at 25,000 feet altitude is different from the effect observed with ten times greater thickness in the experiments, such as the present ones, made at lower altitudes.

On the basis of the results of Maass,[6] Heitler[15] postulates the existence of a neutretto (a neutral particle having mass and other properties similar to the barytron) which could be transformed into a negative barytron by colliding with a neutron or into a positive barytron by colliding with a proton. Because of the great thickness of lead absorber used in this experiment, the probability of registering soft secondary and scattered rays was less than in the work of Hsiung[4] and Maass.[6] Thus the results presented in this paper offer more definite evidence for the existence of a penetrating neutral ray than do the results of previous experiments.

[15] N. Arley and W. Heitler, Nature **142**, 158 (1938).

ACKNOWLEDGMENT

The author wishes to express his appreciation to Professor A. H. Compton for suggesting this problem and for his continued assistance. Grateful acknowledgment is made to the Massachusetts Institute of Technology and the University of Denver for the use of the facilities of the Mt. Evans Observatory; to Dr. J. C. Stearns, through whom arrangements for the use of the Observatory were made; and to the Denver City Parks for the transportation of the fuel supplies.

JANUARY 1, 1939 PHYSICAL REVIEW VOLUME 55

The Gamma-Radiation from Boron Bombarded by Deuterons

E. R. GAERTTNER,* W. A. FOWLER AND C. C. LAURITSEN
Kellogg Radiation Laboratory, California Institute of Technology, Pasadena, California

(Received November 7, 1938)

By a method already described, the gamma-ray spectrum from B+D has been obtained by observing the positron-electron pairs ejected from a thin lead lamina (0.033 cm) and the recoil electrons from a carbon lamina (0.12 cm). Gamma-ray components with quantum energies 1.5 ± 0.2, 2.2 ± 0.3, 4.4 ± 0.3, 6.9 ± 0.4 and 9.1 ± 0.4 Mev are indicated with relative intensities $>2.5 : 2.5 : 1.0 : 0.3 : 0.1$. An attempt is made to correlate the energies and relative intensities of the observed gamma-ray components with those of the proton and neutron groups.

INTRODUCTION

THE recoil electrons ejected from the thick glass wall of a cloud chamber by the gamma-radiation from boron bombarded with deuterons were studied by Crane, Delsasso, Fowler and Lauritsen,[1] and indicated two lines at about 2.4 and 4.2 Mev and a number of weak components of higher energy. An improved method for determining gamma-ray energies from the secondary electrons and pairs ejected from thin laminae has already been described in detail in earlier publications.[2,3] This method has been extended to the study of this radiation, and if due allowance is made for the lower resolving power of the earlier experiments, the original results are not in contradiction with those reported here.

Except for a few minor changes the experimental procedure employed was essentially the same as that described in reference 2. In order to select those recoil electrons which were ejected nearly in the forward direction by the gamma-rays the distance from the target to the scatterer

* Horace H. Rackham Post-Doctoral Fellow. This work was completed during the tenure of his National Research Fellowship.

[1] Crane, Delsasso, Fowler and Lauritsen, Phys. Rev. **46**, 1109 (1934).

[2] Delsasso, Fowler and Lauritsen, Phys. Rev. **51**, 391 (1937).

[3] Fowler, Gaerttner and Lauritsen, Phys. Rev. **53**, 628 (1938).

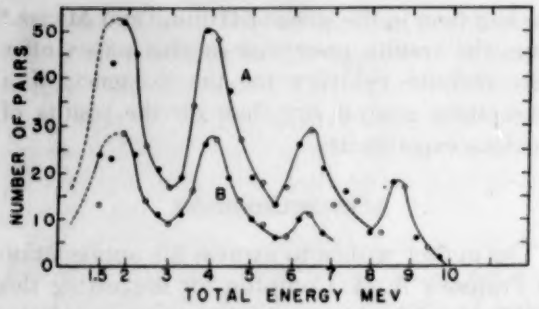

FIG. 1. Curve *A*, the distribution in total energy of 300 positron-electron pairs ejected from 0.033 cm lead foil by the radiation from B+D measured in fields of 1700 and 1000 gauss, and plotted in overlapping intervals of 0.57 Mev. Curve *B* contains that portion of the pairs measured in the 1000 gauss field. The dotted portions indicate by how much the low energy component has been broadened to account for those low energy pairs which have been lost in the measuring process.

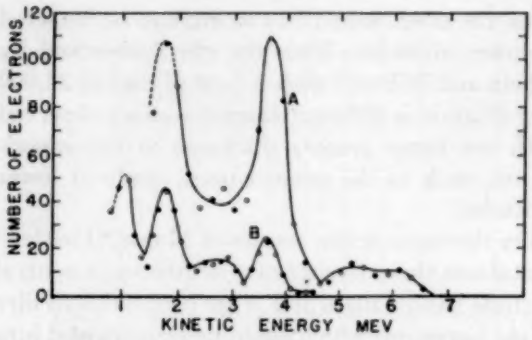

FIG. 2. Curve *A*, the distribution in kinetic energy of 450 electrons ejected from a carbon lamina 0.12 cm thick within an angle of 20° with the forward direction of the radiation, measured in fields of 1500 and 1000 gauss, and plotted in overlapping intervals of 0.46 Mev. Curve *B* contains that portion of the electrons measured in the 1000 gauss field. The curves have been broken in the regions of low resolving power.

was increased to 20 cm. This made it possible to select those electrons which made an angle less than 20° with the forward direction of the radiation. Also, in order to have a clear view of both sides of the scatterer so that only those tracks originating in the carbon lamina could be selected, the scatterer was placed two cm from the center of the chamber. In the experiments with pairs where the origin of the tracks was more certain, the lead foil was placed five cm from the center of the chamber to allow more space for measuring the energy of the pair members. The thickness of the carbon scatterer was 1.2 mm (0.5 Mev) and that of the lead 0.033 cm (0.4 Mev).

The accelerating tube was operated at 550 to 850 kilovolts peak voltage while the total ion current was about twenty microamperes during the chamber expansion. The ion beam was not magnetically separated during the cloud chamber observations but previous magnetic analysis indicated that the proton contamination was less than five percent. Light hydrogen, except for one percent in the heavy hydrogen employed, was not introduced into the tube in the period intervening between the magnetic analysis and the cloud chamber observations. That none of the observed radiation can be attributed to boron bombarded by protons is further substantiated by the fact that no evidence was found for a gamma-ray line near 11.8 Mev, the energy of the most intense component of the radiation from B+H.[3] Targets of pure amorphous boron (Eimer and Amend) were used and were frequently replaced, consequently very little of the radiation can be attributed to other reactions involving deuterium.

THE ENERGY OF THE GAMMA-RADIATION

Curve *A* (Fig. 1) shows the distribution in total energy (kinetic energy $+2\ mc^2$) of 300 positron-electron pairs ejected from the lead lamina, plotted in overlapping 0.57-Mev intervals. These pairs were measured in magnetic fields of 1000 and 1700 gauss. Curve *B* shows that portion of the pairs (209) measured in the lower field. The relative intensities of the high energy pairs (groups at 4, 6.5 and 8.7 Mev) are best secured from the higher field measurements. On the other hand, those of the lower energy pairs (groups at two and four Mev) are best secured from the lower field measurements because there is a tendency in the measuring process to discriminate against tracks of small radius of curvature. Consequently the relative intensities of the two- and the four-Mev groups given by curve *B* have been assumed correct and those of curve *A* have been made to conform with this. Also, because low energy pairs are lost, the apparent width of the two-Mev group is less than that of the four-Mev group. Therefore, in the determination of the energy of the lowest group, the average energy taken from a curve which has been broadened to agree roughly with that of the

four-Mev group has been used. The corrected part of the curve is indicated by the dotted line. The quantum energies of the four groups indicated in curve *A* are determined by adding 0.4 Mev (thickness of the lead) to the average energies of the groups. This procedure gives 2.2 ± 0.3, 4.4 ± 0.3, 6.9 ± 0.4 and 9.1 ± 0.4 Mev for the average energies with their estimated probable errors. The half-widths of the groups can be reasonably attributed entirely to errors inherent in this method of measurement.

Curve *A* (Fig. 2) shows the distribution in kinetic energy of 450 electrons ejected from a carbon lamina (0.12 cm) within an angle of 20° with the forward direction of the gamma-radiation, and plotted in overlapping intervals of 0.46 Mev. These electrons were measured in magnetic fields of 1000 and 1500 gauss. Curve *B* shows only those electrons measured in the lower field. Again the relative intensities are best represented by the lower field measurements of curve *B*, and curve *A* has been dotted in the region where it is considered untrustworthy. The data of Fig. 2 reveal two prominent groups at approximately two and four Mev in addition to a group of 1.3 Mev which is evident only in the lower field measurements. Adding 0.25 Mev to the extrapolated recoil electron energies gives the most probable quantum energies, with their estimated probable errors, as 1.5 ± 0.2, 2.3 ± 0.3 and 4.3 ± 0.3 Mev. Because of the decrease of Klein-Nishina scattering with energy the data at higher energy are too meager to check those high energy groups indicated by the pair distribution although there is some indication of the group at 6.9 Mev. Because of the low efficiency of pair production just above one Mev, the line at 1.5 Mev was not indicated by the pair data.

The Relative Intensities of the Gamma-Ray Components

Estimates of the relative intensities of the gamma-rays from both the pair and recoil distributions are given in Table I. In estimates from the pair curves the relative intensities have been corrected for the variation in pair formation cross section with energy. In computing the relative pair intensities of the 2.2- and 4.4-Mev components the corrected curve of the low energy pair distribution has been employed. In estimates from the recoil curves the relative intensities have been corrected for the total Klein-Nishina cross section. Since only those electrons enter into the distribution which are scattered within an angle of 20° with the forward direction of the quanta, little error is introduced by using the total cross section for all components except the one at 1.5 Mev. A lower limit of the intensity of this component is given.

Origin of the Radiation

The reactions which have been suggested to account for the emission of protons, neutrons, and β-particles when boron is bombarded with deuterons are as follows:

$$B^{10}+H^2\rightarrow C^{11}+n^1+6.34\text{ Mev} \qquad (1)$$
$$\downarrow$$
$$B^{11}+\beta^+ \qquad (1')$$

$$B^{11}+H^2\rightarrow C^{12}+n^1+13.68\text{ Mev} \qquad (2)$$

$$B^{10}+H^2\rightarrow B^{11}+H^1+9.30\text{ Mev} \qquad (3)$$

$$B^{11}+H^2\rightarrow B^{12}+H^1+\sim 0\text{ Mev} \qquad (4)$$
$$\downarrow$$
$$C^{12}+\beta^- \qquad (4')$$

The Q values of the above reactions are those

TABLE I. *Relative intensities of five main components of the gamma-radiation from* $B+H^2$.

Gamma-Ray Energy	Relative Pair Intensities	Relative π*	Int. from Pairs	Relative Recoil Intensities	Relative σ**	Int. from Recoils	Weighted Intensities
1.5	—	—	—	>4.0	1.73	>2.5	>2.5
2.2	1.0	0.28	3.5	2.5	1.57	1.6	~2.5
4.4	1.0	1.00	1.0	1.0	1.00	1.0	1.0
6.9	0.5	1.73	0.3	0.2	0.72	0.3	0.3
9.1	0.25	2.26	0.1	—	—	—	0.1

* π = pair-formation cross section.
** σ = Klein-Nishina cross section.

calculated from the atomic masses by Livingston and Bethe.

The neutrons emitted when boron is bombarded with deuterons have been investigated by Bonner and Brubaker[4] who observed four homogeneous groups with Q values 13.4, 9.0, 6.0 and 3.9 Mev and relative intensities 0.36 : 0.38 : 0.07 : 0.19[5] Of these four groups the first two must be attributed to reaction (2) because it alone is exothermic enough to produce them. If the last two groups are also caused by this reaction, then three excited states of C^{12} at 9.5, 7.4 and 4.4 Mev are indicated and the quantum energies of the possible optical transitions are 9.5, 7.4, 5.1, 4.4, 3.0 and 2.1 Mev. The existence of gamma-ray components at 9.1 ± 0.4 and 6.9 ± 0.4 shows that the higher states of C^{12} are produced in the disintegration. That they do not couple readily with the state at 4.4 Mev is the simplest explanation of the nonexistence of components at 5.1 or 3.0 Mev. If the last two neutron groups are also partly caused by reaction (1) then the ground state of C^{11} and an excited state at 2.1 Mev enter.

The protons from B+D have been attributed to reaction (3) by Cockcroft and Lewis[6] who found three homogeneous groups of protons with Q values 9.11, 6.99 and 4.62 Mev and relative intensities 0.40 : 0.13 : 0.47. The over-all intensity was given as one-half that of reaction (1). Excited states of B^{11} at 4.5 and 2.1 are indicated, the quantum energies of the possible optical transitions being 4.5, 2.4 and 2.1 Mev. No proton group of intensity comparable to the yield of β-rays (20 times the 9.11-Mev proton group), reported by Crane, Delsasso, Fowler and Lauritsen[7] was found down to a range of 1 cm. The state of B^{12} is thus at least 13.7 Mev above the ground state of C^{12}, and as the observed β-rays extend only to 12 Mev the β-transition may be to an excited state of C^{12}. Another, but improbable, alternative is that an excited state of B^{12} is always produced in reaction (4).

The reactions producing alpha-particles when boron is bombarded by deuterons do not, in general, result in excited states of the nuclei Be^9 or Be^8 which emit gamma-radiation. The observed gamma-ray components agree well with the majority of the optical transitions among states of C^{12} and B^{11} discussed above. It is comparatively simple to devise a set of linear equations which the intensities of these transitions must obey employing the proton and neutron group intensities given above. Unfortunately, the equations do not give the intensities of each transition uniquely. We find, however, that the observed intensities satisfy the required relationships derived assuming only reactions (1), (2) and (3) as long as the strong component at 1.5 Mev is excluded. It is well to note that the observed intensities of the 9.1 and 6.9 Mev components require that the over-all neutron yield of reaction (2) be at least ten times that of (1). Correction for the abundance ratio of the isotopes of boron reduces this factor to 2.5. We are tempted to ascribe the strong 1.5-Mev component to reaction (4) which is comparable in intensity to (2). If an excited state of C^{12} is involved the gamma-emission should be radioactive and we are now attempting to observe this.

[4] Bonner and Brubaker, Phys. Rev. **50**, 308 (1936).

[5] Dr. W. E. Stephens has kindly computed the relative intensities of the neutron groups by correcting Bonner and Brubaker's data for geometrical factors of cloud chamber observation and for the change of neutron-proton collision cross section with energy (Wigner).

[6] Cockcroft and Lewis, Proc. Roy. Soc. **154**, 246 (1936).

[7] Crane, Delsasso, Fowler and Lauritsen, Phys. Rev. **47**, 887 (1935).

Radioactive Isotopes of Cu, Zn, Ga and Ge

R. SAGANE*
Radiation Laboratory, University of California, Berkeley, California
(Received October 3, 1938)

A study has been made of the radioactive isotopes produced in Cu, Zn, Ga and Ge by bombardment with both fast and slow neutrons. Some of the isotopes were also produced by deuteron bombardment. The results may be summarized in the following table of decay periods.

Element	*Mass No.*	*Sign*	*Half-life*	*β-Ray Energy*	*γ-Ray*
Nickel	63	e^-	2.5±0.3 hr.	medium	—
Copper	62	e^+	10 ±0.5 min.	hard	γ
Copper	64	e^-	12.8±0.3 hr.	soft	γ
Copper	66	e^-	5 ±1 min.	medium	—
Zinc	63	e^+	35 ±3 min.	hard	γ
Zinc	65	e^+	210 ±30 min.	very soft	γ
Zinc	69	e^-	57 ±3 min.	hard	—
Gallium	68	e^+	66 ±2 min.	hard	γ
Gallium	70	e^-	20 ±1 min.	hard	—
Gallium	72	e^-	14.1±0.2 hr.	hard	γ
(Gallium	74?	e^-	6 ±1 day	—	—)
Germanium	69	e^+	30 ±3 min.	hard	—
Germanium	71	e^+	26 ±3 hr.	medium	γ
Germanium	75	e^-	81 ±3 min	medium	—
Germanium	77	e^-	8 ±1 hr.	—	—
Arsenic	71	e^+	50 ±3 hr.	soft	γ
Arsenic	73	e^+	88 ±2 min.	medium	γ
Arsenic	74	e^-	16 ±2 days	medium	γ
Arsenic	77	e^-	55 ±5 days	very soft	γ

The writer failed to find the Cu^{61} (e^- $T=3.5h$) suggested by the Michigan group in fast neutron bombardments of copper. No trace of the 23-hr. period reported by Fermi and his collaborators was found in neutron bombardments of gallium.

INTRODUCTION

IN CONTINUATION of work[1] at the Cavendish Laboratory on nuclear reactions involving a loss of a neutron from a nucleus, the writer started a more detailed study of the "neutron loss" periods. He soon noticed that in the many investigations[2] of the radioactivity induced in Cu, Zn and Ga but few of the isotopes produced had been identified. There still remain many discrepancies in the experimental data. As for germanium very little has been reported so far.

It is the purpose of the present paper to report the results of the study[3] of the radioactivity induced in these elements by fast and slow neutrons and by deuteron bombardments which have been carried out in the Radiation Laboratory of the University of California.

APPARATUS

The cyclotron in the Radiation Laboratory was used as a source of deuterons and neutrons. At the time of the bombardments it was adjusted to furnish currents of 20 to 150 μa of deuterons of energy from 5.5 Mev to 7.6 Mev.

Ordinary copper plates which are usually of sufficient purity were used as copper targets. The

* Now at the Tokyo Imperial University.
[1] Chang, Goldhaber and Sagane, Nature **139**, 962 (1937).
[2] Amaldi, D'Agostino, Fermi, Pontecorvo, Rasetti and Segrè, Proc. Roy. Soc. **149**, 522 (1935). Livingood, Phys. Rev. **50**, 425 (1935). McLennan, Grimmet and Read, Nature **135**, 505 (1935). Van Voorhis, Phys. Rev. **50**, 895 (1936). Heyn, Nature **138**, 723 (1936); Physica **4**, 160 (1936). Pool, Cork and Thornton, Phys. Rev. **52**, 212 (1938).
[3] Most of the results except those of Ge+D were reported at the Stanford meeting held on Dec. 17, 1937. Sagane, Phys. Rev. **53**, 212 (1938).

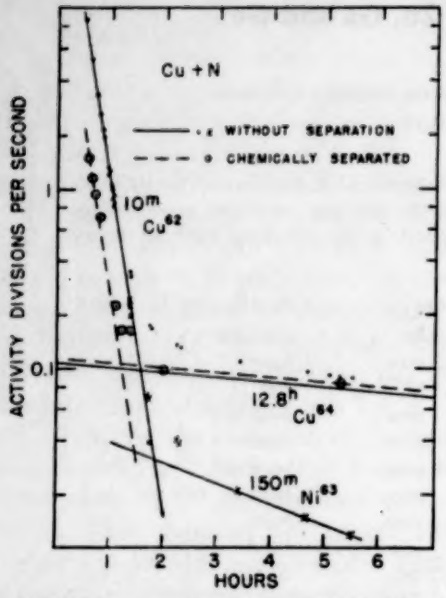

FIG. 1A. Decay curves for copper when bombarded by fast neutrons. The curve taken without chemistry can be analyzed in three periods, while the curve taken after chemical separation consists from two periods showing that the 150-min. period is not caused by a copper isotope.

zinc, gallium and germanium targets were also in metallic form and were of high purity, claimed to be 99.9 percent.

For bombardments with fast neutrons, both lithium and beryllium targets were bombarded and the samples were placed inside a small box made of cadmium sheets one to two millimeters in thickness, filled with boric acid. The box was generally put in the forward direction of the beam. For bombardments with slow neutrons, the samples were placed inside a paraffin block which was generally put at right angles to the beam.

All the measurements of activity were carried out with Lauritsen-type quartz fiber electroscopes[4] with aluminum windows of 1/10,000" thickness. Absorption measurements were made by placing aluminum or lead sheets between the source and the window.

COPPER

This element has been reported by many authors[2] to give the well-known 5-min. and 12.8-hr. periods with slow neutrons. With fast neutrons from Li+D, Heyn reported first that six-min. and 10.5-min. periods were produced.

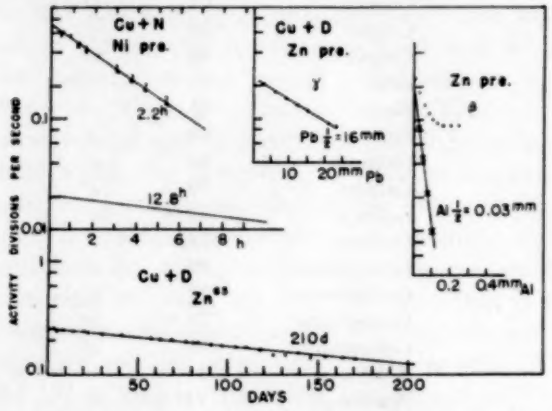

FIG. 1B. A decay curve for a nickel precipitate from a copper sample bombarded by neutrons, and a decay curve for a long lived zinc isotope obtained when copper was bombarded by deuterons. Absorption curves for the zinc isotope are also shown.

On the other hand, Pool, Cork and Thornton[5] suggested the formation of Cu^{61} (3.5 hr.) when bombarded with fast neutrons.

Bombardment with slow neutrons on Cu resulted in the formation of two periods, 5 min. and 12.8 hr. as was predicted. With fast neutrons, three periods 10 min., 2.5 hr. and 12.8 hr. were noticed as shown in Fig. 1A. Chemical separations showed that the 10-min. and the 12.8-hr. periods were caused by Cu isotopes and the one of 2.5 hr. was caused by a nickel isotope. With a

[4] I am indebted to Dr. A. H. Snell for the use of one of his electroscopes.

[5] Pool, Cork and Thornton, Phys. Rev. 52, 41 (1937).

TABLE I. *Summary of results obtained in the bombardment of copper.*

Isotopes	Cu^{65}	Cu^{62}	Ni^{63}	Cu^{64}	Co	Co	Zn^{65}
Bombardment							
Slow neutrons	5 min. (n, γ)		2.5 hr. (n, p)	12.8 hr. (n, γ)			
Fast neutrons (Li)		10 min. $(n, 2n)$	2.5 hr. (n, p)	12.8 hr. (n, γ) $(n, 2n)$			
Fast neutrons (Be)			2.5 hr. (n, p)	12.8 hr. (n, γ)			
Deuterons	5 min. (d, p)			12.8 hr. (d, p)	(30 days?)*	(215 days?)*	210 days (d, γ)
γ-rays		10 min. (γ, n)					

* Segrè and others.

simple magnet close to the electroscope[6] the signs of the β-rays were determined and it was found that the 10-min. period was caused by a positron emitter and the others were caused by negative electron emitters. When copper samples were bombarded with deuterons, the 12.8-hr. period was very strongly activated and a rather weak 5-min. period was also obtained.

In addition to these two, some very long periods have been reported by Segrè and his collaborators[7] who find a zinc isotope with a half-life of 245 days and cobalt isotopes with half-lives of about a month and 215 days.

This long lived zinc isotope was studied carefully by separating zinc isotope from the copper filings scraped from the copper deflecting plate of the cyclotron. The decay curve and the absorption curve which are shown in Fig. 1B shows that this isotope has a half-life of about 210 days. It was found that this isotope emits low energy positrons[8] and hard γ-rays of about 2.5 Mev in energy. The results are summarized in Table I.

There is no doubt that the 5-min. and the 12.8-hr. periods are caused by Cu^{66} and Cu^{64}, respectively. The 10-min. period is found when copper samples are bombarded by neutrons of more than 12 Mev in energy[9] and is also obtained by photodisintegration.[1, 10] Moreover, it emits positrons. These three facts rather definitely determine the assignment of this isotope to be Cu^{62}.

The 2.5-hr. period must be either Ni^{63} or Ni^{65}. If the relative abundance of Cu^{63} and Cu^{65} and that of Ni^{62} and Ni^{64} is taken into account it is most likely to be Ni^{63}. The three-hour period found in nickel with slow neutron bombardments[11] may be caused by the same isotope.[12]

As for the long life zinc isotope, it should be Zn^{65} which must be formed as the result of a rare process of deuteron capture. Discussions for the assignment are given in the next section. Nothing has been done for the investigation of Co isotopes reported by Segrè.

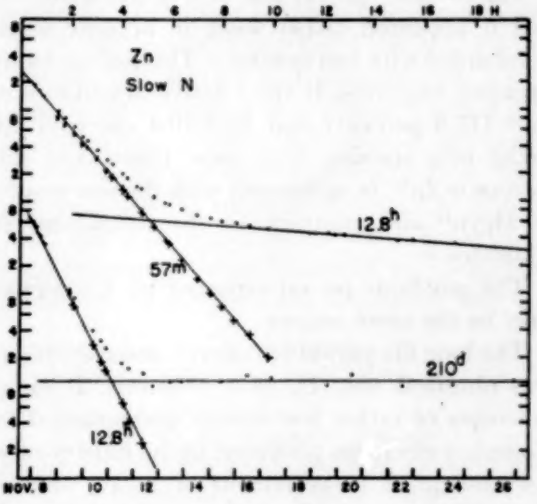

FIG. 2A. A decay curve for zinc when bombarded by slow neutrons. This is analyzed in three periods, 57-min. 12.8-hr. and 210 day.

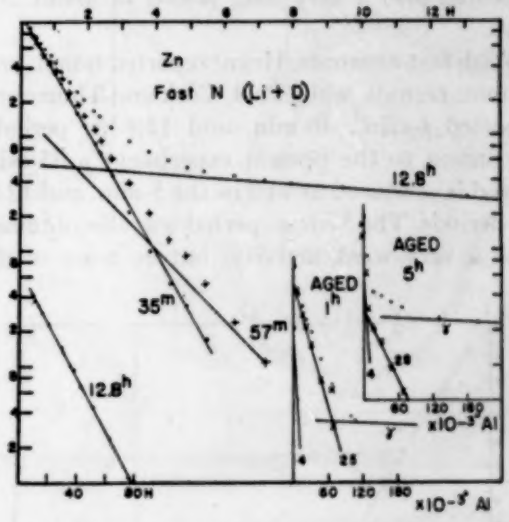

FIG. 2B. A decay curve for zinc when bombarded by fast neutrons. This is analyzed in three periods, 35 min., 57 min. and 12.8 hr. Note that the 57-min. period appears very weak compared with Fig. 2A and no trace of the 210-day period is found.

ZINC

With slow neutrons, a 57-min. period was produced very strongly. In addition to this, a

[6] I am indebted to Dr. A. H. Snell for the use of his device.

[7] Perrier, Santangelo and Segrè, Phys. Rev. **53**, 104 (1938).

[8] A study of β-rays with a cloud chamber has been done in Tokyo and the results will be published soon.

[9] Sagane, Phys. Rev. **53**, 492 (1938).

[10] Bothe and Gentner, Nature, pp. 25, 90, 126, 191, 284 (1937).

[11] Naidu, Nature **137**, 578 (1936). Rotbalt, Nature **136**, 515 (1935). Oeser and Tuck, Nature **139**, 1110 (1937).

[12] Simultaneously with my publication at the Stanford meeting, Heyn reported (Physica **4**, 1224 (1937)) his recent results which are in good agreement with mine except a slight discrepancy of a numerical value for half-value periods.

TABLE II. *Summary of results obtained in the bombardment of zinc.*

ISOTOPES	Cu^{65}	Zn^{63}	Zn^{69}	Ni^{63}	Cu^{64}	Zn^{65}
Bombardment						
Slow neutrons			57 min. (n, γ)		12.8 hr. (n, p)	210 days (n, γ)
Fast neutrons Li	5 min. (n, p) (6 min.)	35 min. $(n, 2n)$ (40 min.)	w57 min. (n, γ)	(2.5 hr.) (n, γ)	12.8 hr. (n, p) (12.5 hr.)*	
Fast neutrons Be	5 min. (n, p)	35 min. $(n, 2n)$	w57 min. (n, γ) (1 hr.)		12.8 hr. (n, p) 12 hr., 25 hr., 97 hr.†	
Deuterons						
γ-rays	38 min.‡					

* Heyn.
† Livingood.
‡ Bothe, Gentner, Chang, Goldhaber, Sagane.

5-min. and a 12.8-hr. period were also activated, as had been reported by Fermi and others.[2] There appeared also a very long period of about 200 days.

With fast neutrons, Heyn[2] reported 6-min. and 60-min. periods, while Pool, Cork and Thornton[13] reported 6-min., 40-min. and 12.8-hr. periods. According to the present experiment a 35-min. period is produced as well as the 5-min. and 12.8-hr. periods. The 57-min. period was also obtained with a very weak activity, but no trace of the

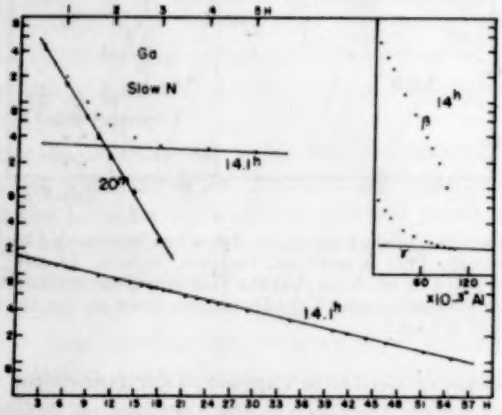

FIG. 3A. Decay curves obtained when gallium samples were bombarded by slow neutrons. No trace of the 23-hr. period was found.

210-day period was found. Examples of the decay curves obtained are shown in Figs. 2, A and B.

Chemical separations showed that the 35-min., 57-min. and 210-day periods were all zinc isotopes and the 12.8-hr. period was a copper isotope.

No trial was made for deuteron bombardment, as Dr. Livingood has already bombarded zinc samples with deuterons, and intends to repeat it to check his previous results. According to him, four periods, 1 hr., 12 hr., 25 hr. and 97 hr. were reported.

By hard γ-ray bombardments,[1, 10] it has been reported that a 38-min. period was obtained in zinc. The results are summarized in Table II.

The 35-min. period was only activated appreciably with fast neutrons of energy higher than 9 Mev[3] and it emits positrons. These facts suggest that this period is produced by the neutron loss process, i.e., the $(n, 2n)$ reaction. So this must be Zn^{63}. The 38-min. period reported by γ-ray bombardments and the 34-min. period reported by Ridenour and Henderson[14] on the α-particle bombardments of nickel, the 40-min. period reported by Pool, Cork and Thornton[13] must be the same.

The 57-min.[8] period was very water-sensitive, and it appeared rather weak in activity when bombarded with fast neutrons. This isotope emits negative electrons. If the relative abundance of Zn^{68} (17.8 percent) and Zn^{70} (0.4 percent) are taken into account, it is most likely that this isotope is Zn^{69}, in agreement with the new results of Heyn[12] and contrary to the assignment of Thornton.[15]

The one-hour period reported by Livingood[2] may be the same isotope.

The long life period of order of about 210 days was obtained only by slow neutrons. It emits positrons of rather low energy accompanied by Compton electrons produced by its hard γ-rays. An absorption measurement of γ-rays showed that this isotope emits very hard γ-rays ($Pb\frac{1}{2}$ ~15 mm) which is in good agreement with the results obtained on the zinc isotope produced by Cu+D. There remains only one possibility for a positron emitting zinc isotope which can be

[13] Pool, Cork and Thornton, Phys. Rev. **52**, 239 (1937).

[14] Ridenour and Henderson, Phys. Rev. **52**, 889 (1937).
[15] Thornton, Phys. Rev. **53**, 326 (1938).

produced by Cu+D and Zn+n, so this isotope must be Zn^{65}.

GALLIUM

With slow neutrons, two periods, 20 min. and 23 hr. were reported first by Fermi and his collaborators.[2] When bombarded with fast neutrons. Pool, Cork and Thornton[9] reported that they observed 20 min. (e^-), 55 min. (e^+), 1.7 hr. (e^+) and 22 hr. (e^-).

As shown in Fig. 3A the decay curves obtained with slow neutron bombardments gave only two periods; the well-known 20-min. period and a new 14-hr. period. No trace of the 23-hr. period reported by Fermi and others or by the Michigan group was found. With fast neutrons only three periods, 20 min., 66 min. and 14 hr. were found. Not even a trace of the 1.7-hr. period or the 23-hr. period was found. Chemical separations showed that all three periods were due to gallium isotopes.

As this sample has a very low melting point, no attempt has as yet been made at deuteron bombardment. The results are summarized in Table III.

Ga^{70} and Ga^{72} are the only two possible isotopes for a radioactive gallium which emits negative electrons. If the fact is taken into account that the 20-min. period is activated not only by slow neutrons but also by fast neutrons and γ-rays, it is quite certain that this 20-min.[16] period must be caused by Ga^{70}. The 18.2-min. period reported by DuBridge and his collaborators[17] in $Zn+p$ may be caused by the same isotope. On the other hand, the other 14-hr. period which is a negative electron emitter is not produced by γ-ray bombardments. These two points support very well the conclusion that this 14-hr. period should be caused by Ga^{72}. The 66-min.[8] period can only be obtained when the energy of the bombarding neutrons is higher than 6 Mev.[3] This isotope emits positrons and is produced also by hard γ-ray bombardments. These facts afford good evidence that this isotope is Ga^{66}, which is most probably a positron-emitting a Ga isotope.

The author must add a line about a negative result in attempting to check the reaction Ga^{69} (n, α) Cu^{66} which we have reported in *Nature*.[1] Although several very short exposures to fast neutrons, less than one minute, were made, no trace of the five-min. period was found.

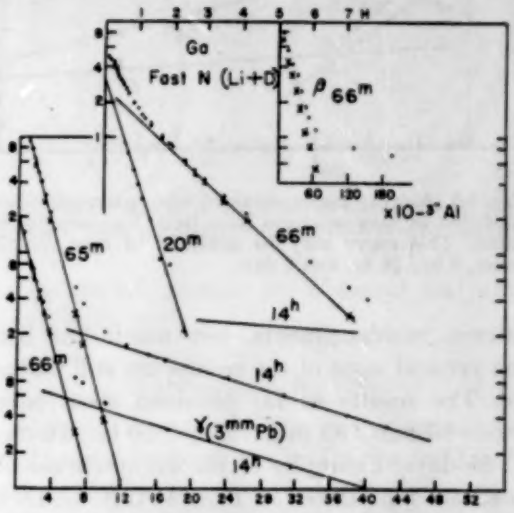

FIG. 3B. Decay curves obtained when gallium samples were bombarded by fast neutrons.

GERMANIUM

Germanium with slow neutrons gives four periods, 81 min., 8 hr., 26 hr. and six days. With fast neutrons 29-min., 81-min., very weak 8-hr., 26-hr. and six-day periods were produced. As for

[16] Mann, Phys. Rev. **52**, 405 (1937).
[17] DuBridge, Barnes and Buck, Phys. Rev. **51**, 995 (1937).

TABLE III. *Summary of results obtained in the bombardment of gallium.*

ISOTOPE		Ga^{70}	Ga^{66}	Ga^{72}
Bombardment				
Slow neutrons		20 min. (n, γ)		14 hr. (n, γ)
Fast neutrons	Li	20 min. (n, γ) $(n, 2n)$	66 min. $(n, 2n)$	14 hr. (n, γ)
	Be	20 min. (n, γ) $(n, 2n)$	66 min. $(n, 2n)$	14 hr. (n, γ)
γ-rays		20 min. (γ, n)	66 min. (γ, n)*	

* Bothe, Gentner, Chang, Goldhaber, Sagane.

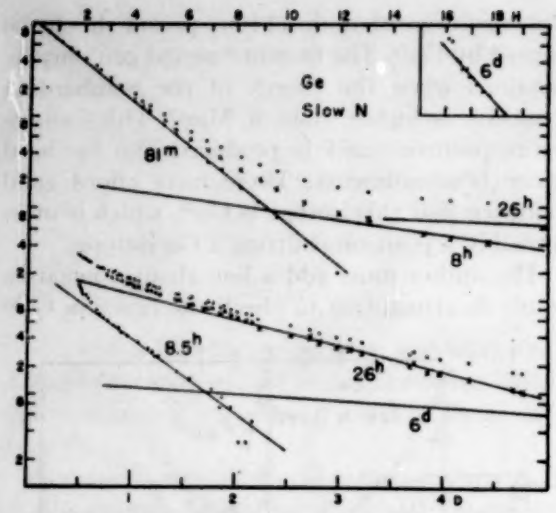

FIG. 4A. A decay curve obtained when germanium was bombarded by slow neutrons from Be+D surrounded by paraffin. This curve may be analyzed in four periods, 81 min., 8 hr., 26 hr. and 6 day.

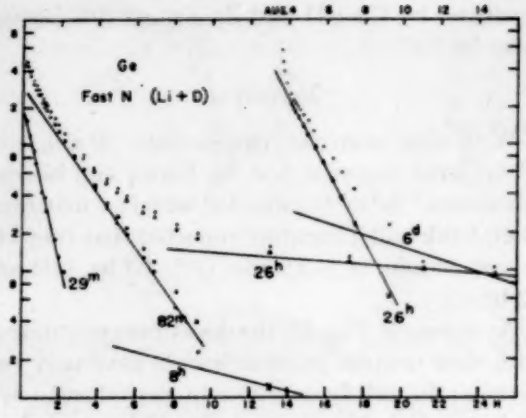

FIG. 4B. A decay curve obtained when germanium was bombarded by fast neutrons from Li+D. This curve may be analyzed in five periods, 29 min., 82 min., 8 hr., 26 hr. and 6 day. Note that the 81-min. and 8-hr. periods appear rather weak compared with Fig. 4A.

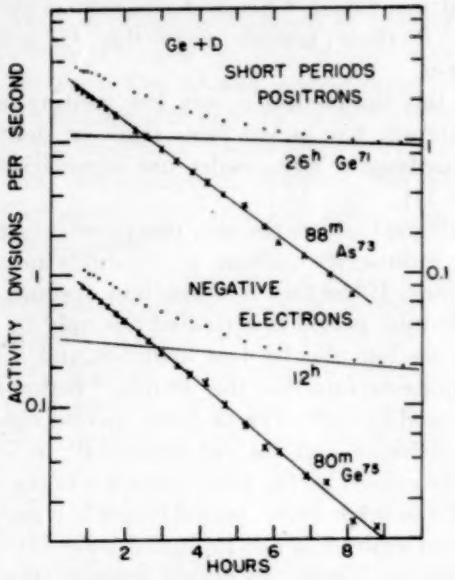

FIG. 4C. Parts of decay curves showing short periods obtained when germanium was bombarded by deuterons. These curves were taken by measuring only positrons or negative electrons with a simple magnet close to the electroscope.

deuteron bombardments, not much has been done yet and some of the results are still inaccurate. The results so far obtained show seven periods 80 min., 88 min., 12 hr., 50 hr., 16 days and 55 days. Examples of the decay curves obtained are reproduced in Figs. 4-A, B, C, D, E. The results are summarized in Table IV.

Since the positron-active 29-min. period was produced in appreciable intensity when the energy of the bombarding neutrons is higher than 5.5 Mev,[3] it is most likely caused by Ge^{69}. The 81-min.[8] period was formed in strong intensity in each bombardment. This isotope emits negative electrons and is sensitive to slow neutrons. Because of the relative abundance of Ge^{74} (37 percent) and Ge^{76} (6.5 percent), the isotope in question is probably Ge^{75}.

The 88-min. period obtained in deuteron bombardments is positron active and decay curves were followed by measuring only the positron activity. Although no chemical separation has as yet been carried out this period may be caused by As^{73}.

The 8-hr. period was obtained appreciably only in slow neutron bombardments. With fast neutrons only a trace of this period was noticed, indicating very clearly that this period is very sensitive to slow neutrons. There remains only one possibility for this kind of negative electron active period, that is Ge^{77}.

The 26-hr. period is positron active and can be obtained with both fast and slow neutrons. These points are good enough to assign this period to Ge^{71}.

The 50-hr. period found in deuteron bombardments is expected to be caused by an arsenic

isotope, probably As^{71}, because it emits positrons. The positrons emitted are of very low energy and are accompanied by strong γ-rays.

The 6-hr. period is rather too weak in activity to check the sign of the β-particles emitted. Thus not much can be said about this period, but I suspect that it may be caused by a gallium isotope, probably Ga^{74}.

The 12-hr. period found in Ge+D may be identical to Ge^{77} (8 hr.) or might be Na^{24} contamination.

The 16-day period was obtained by deuteron bombardments only. This isotope emits both positive and negative electrons and was proved to be an arsenic isotope by chemical separations. These points allow one to ascribe this period to As^{74}, as has been reported recently.[18]

In addition to these periods a very soft negative β-ray emitter was noticed, the half-life of which is about 55 days. This was also proved to be an arsenic isotope by chemical test and is most likely As^{77}.

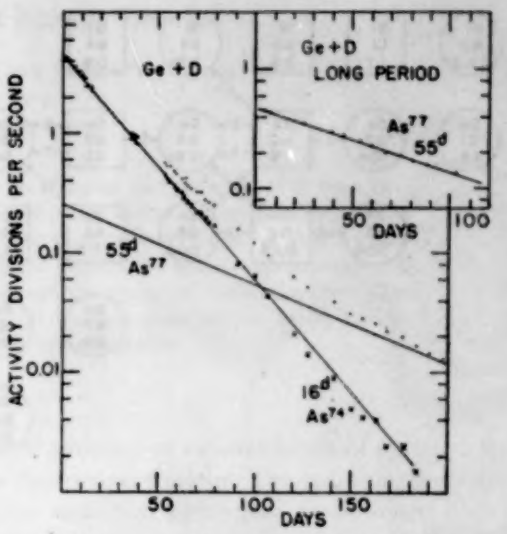

FIG. 4E. Parts of a decay curve showing long periods obtained when germanium was bombarded by deuterons.

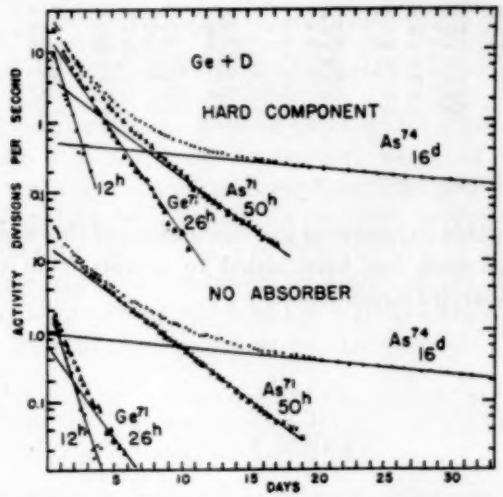

FIG. 4D. Parts of decay curves showing 26-hr. and 50-hr. periods obtained when germanium was bombarded by deuterons. A decay curve obtained by measuring the activity with an aluminum absorber 0.024'' thick is mentioned as hard component.

[18] Sagane, Kojima and Ikawa, Phys. Rev. **54**, 149 (1938).

SUMMARY OF REACTIONS

Figure 5 shows a portion of the periodic table in the neighborhood of Cu, Zn, Ga and Ge. The radioactive isotopes are shown in circles and the arrows indicate the reactions studied in this article. In some of these samples, existence of K radiation was found. But to get definite conclusions, further work must be done, because internal conversion of γ-rays must be taken into account.

The values of half-value thickness or maximum range of β-rays are not given intentionally, because they depend too much on the geometry of the measuring apparatus; on the other hand, the study of the β-rays of those isotopes discussed has been started in Tokyo and some of the results are expected to be published soon.

ACKNOWLEDGMENT

The author is very greatly indebted to Professor E. O. Lawrence for the opportunity of using

TABLE IV. *Summary of results obtained in the bombardment of germanium.*

ISOTOPES	Ge^{69}	Ge^{75}	As^{73}	Ge^{77}	Ge^{77}	As^{81}	Ga?	As^{74}	As^{77}
Bombardment									
Slow neutrons		81 min. (n, γ)		8 hr. (n, γ)	26 hr. (n, γ)		6 days (n, p)		
Fast neutrons (Li)	29 min. $(n, 2n)$	81 min. (n, γ)		w 8 hr. (n, γ)	26 hr. (n, γ)		6 days (n, p)		
Fast neutrons (Be)	29 min. $(n, 2n)$	81 min. (n, γ)		w 8 hr. (n, γ)	26 hr. (n, γ)		6 days (n, p)		
Deuterons		80 min. (d, p)	88 min. (d, n)	12 hr.?	26 hr. (d, p)	50 hr. (d, n)		16 days (d, n)	55 days (d, n)

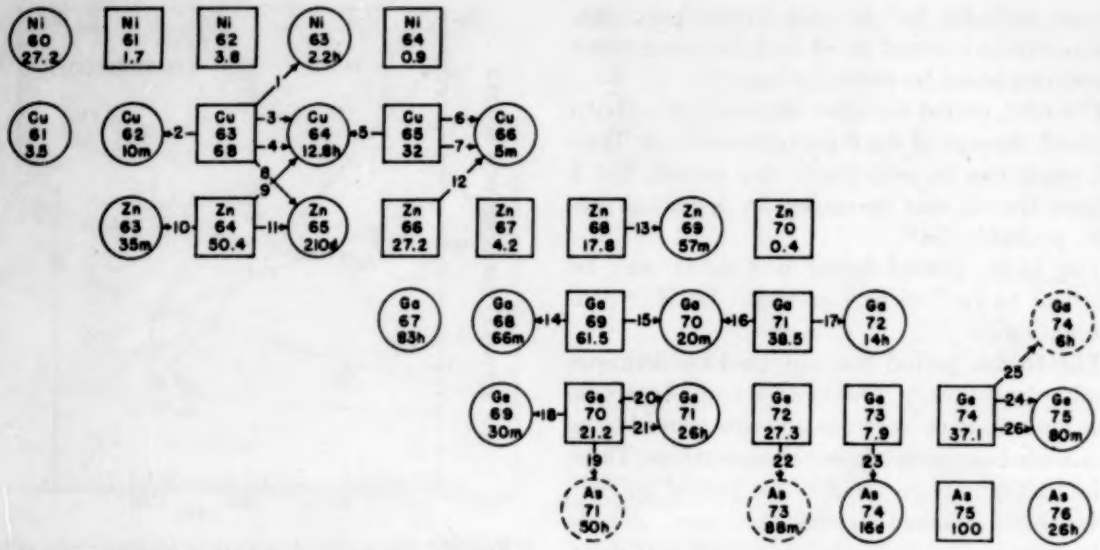

FIG. 5. This diagram gives a summary of all the transmutations described in this paper. The stable isotopes (squares) are given with their percentage abundance in small figures. Radioactive isotopes are given in circles, which are dotted when there is still some ambiguity as to their exact identification. The numbered arrows indicate transmutations which have been observed, and the reactions describing them are as follows:

‡1	$Cu^{63}(n,p)$	Ni^{63}	9	$Zn^{64}(n,p)$	Cu^{64}	16	$Ga^{71}(n,2n)$	Ga^{70}	*23	$Ge^{73}(d,n)$	As^{74}
2	$Cu^{63}(n,2n)$	Cu^{62}	10	$Zn^{64}(n,2n)$	Zn^{63}	*17	$Ga^{71}(n,\gamma)$	Ga^{72}	*24	$Ge^{74}(n,\gamma)$	Ge^{76}
3	$Cu^{63}(n,\gamma)$	Cu^{64}	*11	$Zn^{64}(n,\gamma)$	Zn^{65}	*18	$Ge^{70}(n,2n)$	Ge^{69}	†*25	$Ge^{74}(n,p)$	Ga^{74}
4	$Cu^{63}(d,p)$	Cu^{64}	12	$Zn^{66}(n,p)$	Cu^{66}	†*19	$Ge^{70}(d,n)$	As^{71}	*26	$Ge^{74}(d,p)$	Ge^{75}
5	$Cu^{65}(n,2n)$	Cu^{64}	‡13	$Zn^{68}(n,\gamma)$	Zn^{69}	*20	$Ge^{70}(n,\gamma)$	Ge^{71}	*27	$Ge^{76}(d,n)$	As^{77}
6	$Cu^{65}(n,\gamma)$	Cu^{66}	14	$Ga^{69}(n,2n)$	Ga^{68}	*21	$Ge^{70}(d,p)$	Ge^{71}	*28	$Ge^{76}(n,\gamma)$	Ge^{77}
7	$Cu^{65}(d,p)$	Cu^{66}	15	$Ga^{69}(n,\gamma)$	Ga^{70}	†*22	$Ge^{72}(d,n)$	As^{73}	*29	$Ge^{76}(d,p)$	Ge^{77}
‡8	$Cu^{65}(d,\gamma)$	Zn^{65}									

* Reactions which are newly reported in this paper.
† Reactions which were observed but not yet checked carefully enough.
‡ Reactions which have not been established well, but are proved in this paper to exist.

the cyclotron and for his helpful discussion and encouragement. He is also very greatful to the staff of the Radiation Laboratory for their valuable suggestions and discussions of this work. This work has been aided by grants from the Research Corporation.

The Widths of Nuclear Energy Levels†

J. H. MANLEY,* H. H. GOLDSMITH AND JULIAN SCHWINGER‡
Columbia University, New York, New York

(Received November 7, 1938)

Neutron absorption measurements with Rh both as absorber and detector have been performed, in order to obtain information about the levels of the compound nucleus responsible for the 44″ period of Rh. The absorption curves have been analyzed by assuming a single sharp resonance and taking into consideration the angular distribution of the neutrons emerging from the source and the absorption of the neutrons and the electrons in the detector. This analysis yields the values: (a) 6100×10^{-24} cm² for the capture cross section at resonance; (b) 0.17 ev for the total width; (c) 1.6×10^{-3} ev for the neutron width.

THE selective capture of slow neutrons has been explained by a resonance process in which the neutron is captured in a virtual state of the compound system formed by the capturing nucleus and the incident neutron. According to this explanation, the cross section for the radiative capture of a neutron with kinetic energy E is

$$\sigma(E)=\left(\frac{E_0}{E}\right)^{\frac{1}{2}}\frac{\sigma_0(\Gamma/2)^2}{(E-E_0)^2+(\Gamma/2)^2}, \qquad (1)$$

provided only one level is effective for capture. Here Γ is the total (radiation) width of the virtual state of the compound nucleus, and σ_0 is the capture cross section for neutrons having the resonance energy E_0. The cross section at resonance may be expressed in terms of Γ_n, the partial (neutron) width of the virtual state arising from neutron emission, by the relation

$$\sigma_0=\pi\frac{2J+1}{2I+1}\frac{\hbar^2}{ME_0}\frac{\Gamma_n}{\Gamma}, \qquad (2)$$

where I is the angular momentum of the capturing nucleus, and J is the angular momentum of the virtual state. Since there appears to be no method of determining this latter quantity, we shall incorporate the unknown factor $(2J+1)/(2I+1)$ into the neutron width.

The neutron and radiation widths deduced from slow neutron data are of great importance for nuclear theory since they provide the only available information concerning the probabilities of emission of various kinds of particles from the compound nucleus. The ratio of the neutron to the radiation width may be obtained directly from the cross section at resonance, if the energy of resonance is known. If the total width is then determined by some method, such as the thermal and resonance activation method of Amaldi and Fermi, the neutron width may be calculated.

A direct method of obtaining the cross section at resonance is an absorption measurement in which the substance under investigation is used both as an absorber and as a detector of the resonance neutrons. The characteristic feature of this process is the "self-reversal" of the resonance line in the case of narrow resonances ($\Gamma/E_0\ll1$). Neutrons in the immediate neighborhood of the resonance are almost completely removed by a small thickness of absorber. Additional thicknesses are then much less effective in reducing the intensity of the beam since only the more penetrating neutrons in the "wings" of the resonance line remain. As a result, the apparent absorption coefficient will be a function of absorber thickness, which decreases rapidly with increasing thickness of absorber.

It is the purpose of this paper to obtain the neutron and radiation widths of the level responsible for the activation of the rhodium 44-sec. period by a theoretical analysis of such "self-reversal" absorption curves.

Experimental Procedure and Results

The irradiations were carried out on the top surface (30×22 cm) of a paraffin block 15 cm high. A radon-beryllium source of about 600 mC initial strength was symmetrically located 3 cm

† Publication assisted by the Ernest Kempton Adams Fund for Physical Research of Columbia University.
* Now at the University of Illinois.
‡ Tyndall Fellow of Columbia University.

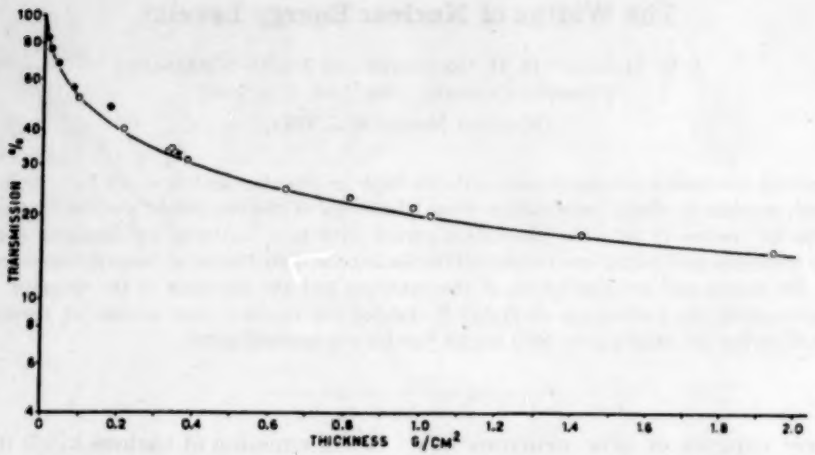

FIG. 1. Self-absorption in Rh as indicated by a 0.35 g/cm² detector. ● = Data of Preiswerk and v. Halban, × = Amaldi-Fermi, ○ = Present data, — = Calculated curve for $n\sigma_0/\rho = 36$ cm²/g.

below this surface. Cadmium sheet 0.45 mm thick covered the entire surface with the exception of a 9×9 cm opening at the center. For all measurements with D neutrons this square was covered with a plane sheet of cadmium 0.1×10×10 cm. The absorbers were placed on this cadmium sheet. The detectors were in contact with the upper surface of the absorber in order to provide a calculable geometry. Activation of the detector by stray thermal neutrons was prevented by a cadmium cover. Since the detector height was a function of the absorber thickness, it was necessary to correct for the variation of neutron intensity above the surface. This variation was measured and found to be closely linear with height in the range used. This correction, applied to all measurements, amounts to a maximum of 12 percent at 6 mm.

For the absorption curves we have used rhodium detectors of two different thicknesses. One, 0.35 g/cm² by 4×5 cm, was made of Rh powder in a paper packet which was slightly paraffined to prevent distortion. Since the paraffin might possibly alter the energy distribution of the neutrons, another type was constructed in which the Rh powder was bound to a thin nickel sheet by the minimum amount of lacquer. This type was 0.11 g/cm² by 5×5 cm.

The thick Rh absorbers consisted of powdered metal placed in containers of four-mil nickel sheet with the aid of a template to secure uniform thickness. Thinner absorbers were made to a convenient thickness by diluting with talc. The thinnest absorber was obtained by electroplating Rh on nickel. All absorbers were approximately 6×7 cm.

The activities of the detectors were measured with an ionization chamber similar to that described by Amaldi and Fermi.[1] This chamber was connected to an FP54 amplifier, and the current measured by the rate-of-drift method. The apparatus was very linear in the range used, and, at frequent intervals, care was taken to measure the chamber sensitivity with a uranium standard and the amplifier sensitivity by applying a known potential to the grid.

For the activity measurements a standard procedure of one-minute irradiation and one-half-minute interval followed by a one-minute ionization measurement was used. The results, therefore, while applying to the 44-sec. period, are independent of exact knowledge of the period, and the contribution of the longer period is sufficiently small to be neglected. Any data used for calculation of transmission values were the average of at least nine such activity measurements. From the individual measurements and their deviations it follows that no transmission value has a probable error greater than 3 percent.

The transmission of various thicknesses of Rh as determined by the "thick" Rh detector is given in Fig. 1 (open circles). Fig. 2 shows the

[1] Amaldi and Fermi, Phys. Rev. **50**, 899 (1936).

results for the "thin" detector. The calculated curves are shown in each case, and the "thick" detector calculated curve is shown in Fig. 2 to illustrate the effect of detector thickness which has so often been overlooked in previous work.

Analysis of Absorption Curves

The fundamental assumption which we shall make is that the resonance absorption arises from a single, narrow resonance level of the compound nucleus. By virtue of the assumption that only one resonance level is effective for capture, the simple one-level formula (1) is applicable. Furthermore, the assumption of a narrow resonance ($\Gamma/E_0 \ll 1$) enables us to neglect the variation of the term $(E_0/E)^{\frac{1}{2}}$ over the resonance region. We may thus write the capture cross section in the more simple form

$$\sigma(E)=\sigma_0/\left[1+\left(\frac{E-E_0}{\Gamma/2}\right)^2\right]. \tag{3}$$

The observed transmission curves are essentially measurements of the activity of a detector (defined as the number of β-rays emitted per second immediately after an infinite time of irradiation) with various thicknesses of absorber interposed between the paraffin and the detector. The essential elements involved in the determination of the detector activity are the distribution in angle and energy of the neutrons emerging from the paraffin, the reduction of neutron intensity in the absorber, the neutron absorption in the detector, and the absorption in the detector of the β-rays created by the capture process. Fermi has shown that the number of neutrons emitted per unit solid angle at an angle ϑ with the normal to a paraffin surface is approximately proportional to $\cos\vartheta+3^{\frac{1}{2}}\cos^2\vartheta$. For resonance neutrons, however, the assumption of spherically symmetric scattering used in deriving this distribution is no longer valid, and one would expect an approach to a cosine distribution. For this reason and for simplicity[2] we shall assume that the angular distribution of the resonance neutrons is proportional to $\cos\vartheta$, that is, we assume that the number of neutrons emitted per second per unit area of the paraffin with energies in the range between E and $E+dE$, and with angles to the normal of the surface between ϑ and $\vartheta+d\vartheta$, is equal to

$$2N(E)dE\cos\vartheta\sin\vartheta d\vartheta. \tag{4}$$

A detailed knowledge of the energy distribution function $N(E)$ is unnecessary since we may neglect the variation of the neutron intensity over the narrow resonance region.

It is essential that the absorption of the β-rays in the detector be included in the evaluation of the detector activity, for most measurements are performed with detectors which are thick with respect to electronic absorption. We shall make the questionable, though convenient assumption that the β-rays are absorbed exponentially, with an absorption coefficient μ_e.

From these assumptions and approximations, it immediately follows that the activity of a detector of thickness δ_2, with an absorber of thickness δ_1 interposed between it and the paraffin, is proportional to

$$\begin{aligned} A_{\delta_1,\delta_2} &= 2N(E_0)\int_0^{\delta_2}dx\int_0^{\pi/2}\sin\vartheta d\vartheta\int_{-\infty}^{\infty}dE n\sigma(E) \\ &\quad\times e^{-n\sigma(E)(\delta_1+x)/\cos\vartheta}e^{-\mu_e x} \\ &= \Gamma N(E_0)\int_0^{\delta_2}dx\int_0^{\pi/2}\sin\vartheta d\vartheta\int_{-\infty}^{\infty}d\xi\frac{n\sigma_0}{1+\xi^2} \\ &\quad\times e^{-n\sigma_0/(1+\xi^2)(\delta_1+x)/\cos\vartheta}e^{-\mu_e x}, \end{aligned} \tag{5}$$

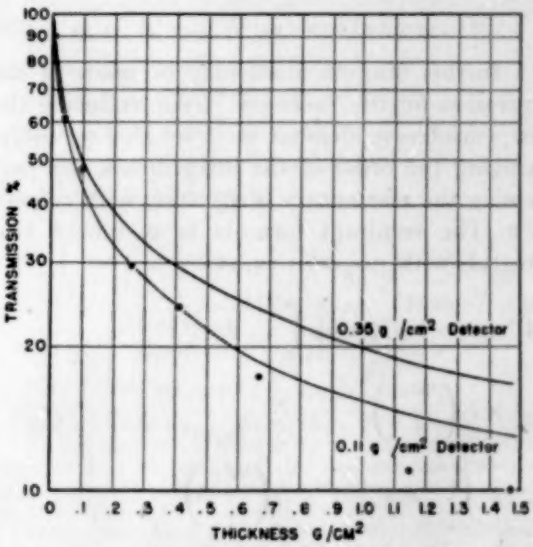

FIG. 2. Self-absorption in Rh as indicated by a 0.11-g/cm² detector (⊙). Solid curves are calculated for the detector thicknesses assuming $n\sigma_0/\rho=36$ cm²/g.

[2] Additional support for this simplification is provided by a calculation performed by Mr. M. Hamermesh which shows that the transmission at an absorber thickness of 0.1 g/cm² is inappreciably affected by replacing the cosine distribution with the Fermi distribution (cosine −49.9 percent, Fermi −49.6 percent).

where n represents the number of nuclei per cm³ which are effective for capture, and $\xi=(E-E_0)/\frac{1}{2}\Gamma$. The integration with respect to ξ may be performed with the aid of the formula

$$\int_{-\infty}^{\infty}\frac{d\xi}{1+\xi^2}e^{-\zeta/(1+\xi^2)}=\pi e^{-\zeta/2}I_0\left(\frac{\zeta}{2}\right). \quad (6)$$

Hence,

$$A_{\delta_1,\delta_2}=\pi\Gamma n\sigma_0 N(E_0)\int_0^{\delta_2}dx\int_0^1 dz \times e^{-(n\sigma_0/2)(\delta_1+x)/z}I_0\left(\frac{n\sigma_0}{2}\frac{\delta_1+x}{z}\right)e^{-\mu_e x}, \quad (7)$$

in which $\cos\delta$ is designated by z.

For the purpose of numerical calculation, it is convenient to introduce a new quantity, which we shall term the "activity," defined by

$$\text{"}A\text{"}_{\delta_1,\delta_2}=\tfrac{2}{3}(\mu_e n\sigma_0)^{\frac{1}{2}}\int_0^{\delta_2}dx\int_0^1 dz \times e^{-(n\sigma_0)/2(\delta_2+x)/z}I_0\left(\frac{n\sigma_0}{2}\frac{\delta_1+x}{z}\right)e^{-\mu_e x}. \quad (8)$$

The convenience of this definition lies in the fact that the "activity" of a detector, with zero thickness of absorber, is always less than one, and becomes equal to one only in the special case of an infinite cross section at resonance and an infinite detector thickness. It is evident from (7) and (8) that the relation between the activity A_{δ_1,δ_2} and the "activity" $\text{"}A\text{"}_{\delta_1,\delta_2}$ is:

$$A_{\delta_1,\delta_2}=\tfrac{2}{3}\pi\Gamma(n\sigma_0/\mu_e)^{\frac{1}{2}}N(E_0)\text{"}A\text{"}_{\delta_1,\delta_2}. \quad (9)$$

A further simplification may be made in the expression for the "activity" by introducing the new variable η, defined by $x=-\delta_1+z\eta$, interchanging the order of the integrations and performing the elementary integration with respect to z. The resultant formula is a sum of two integrals with respect to η, *viz:*

$$\text{"}A\text{"}_{\delta_1,\delta_2}=\tfrac{2}{3}(\mu_e n\sigma_0)^{\frac{1}{2}}\left\{\int_{\delta_1}^{\delta_1+\delta_2}d\eta e^{-(n\sigma_0/2)\eta} \times I_0\left(\frac{n\sigma_0}{2}\eta\right)\frac{1+\mu_e\delta_1-(1+\mu_e\eta)e^{-\mu_e(\eta-\delta_1)}}{(\mu_e\eta)^2} + \int_{\delta_1+\delta_2}^{\infty}d\eta e^{-(n\sigma_0/2)\eta}I_0\left(\frac{n\sigma_0}{2}\eta\right) \times\frac{1+\mu_e\delta_1-(1+\mu_e\delta_1+\mu_e\delta_2)e^{-\mu_e\delta_2}}{(\mu_e\eta)^2}\right\}. \quad (10)$$

In general, this final integration must be carried out numerically. However, for large absorber thicknesses we may use the asymptotic form of $I_0(x)$, i.e.,

$$I_0(x)\sim\frac{e^x}{(2\pi x)^{\frac{1}{2}}} \quad (11)$$

which gives a result accurate to within 2 percent for values of x as small as 6. Inserting this expression for $I_0(x)$ into Eq. (8) we find that, for large absorber thicknesses ($n\sigma_0\delta_1\gtrsim 12$), $\text{"}A\text{"}_{\delta_1,\delta_2}$ is given to within ~ 1 percent by

$$\text{"}A\text{"}_{\delta_1,\delta_2}=\frac{1}{\pi^{\frac{1}{2}}}\int_0^{\mu_e\delta_2}\frac{e^{-x}}{(\mu_e\delta_1+x)^{\frac{1}{2}}} =e^{\mu_e\delta_1}\{\Phi(\mu_e(\delta_1+\delta_2)^{\frac{1}{2}})-\Phi((\mu_e\delta_1)^{\frac{1}{2}})\}, \quad (12)$$

where $\Phi(x)$ denotes the error integral, defined by

$$\Phi(x)=\frac{2}{\pi^{\frac{1}{2}}}\int_0^x e^{-t^2}dt. \quad (13)$$

The neutron transmission through an absorber of thickness δ_1 is defined to be the fraction by which the activity of the detector is reduced when the absorber is interposed between the detector and the paraffin. The transmission, therefore, can be written

$$P_{\delta_2}(\delta_1)=\frac{A_{\delta_1,\delta_2}}{A_{0,\delta_2}}=\frac{\text{"}A\text{"}_{\delta_1,\delta_2}}{\text{"}A\text{"}_{0,\delta_2}}, \quad (14)$$

which involves only the cross section at resonance and not the resonance energy and the total width. It is perhaps not entirely superfluous to point out that the transmission thus defined is not the fraction of the incident number of neutrons which penetrate the absorber. The transmission at large thicknesses assumes a particularly simple form in two special cases: (a) $n\sigma_0\delta_1\gg 1$, $n\sigma_0\delta_2\ll 1$, $\mu_e\delta_2\ll 1$; (b) $\delta_1\gg\delta_2$, $\mu_e\delta_2\gg 1$, $n\sigma_0\gg\mu_e$, which correspond, respectively, to a thin detector and to a thick detector whose electronic absorption coefficient is small compared with the cross section at resonance. It is easily shown that the transmissions in these two cases are $P=2/3(\pi n\sigma_0\delta_1)^{\frac{1}{2}}$ and $P=1/(\pi\mu_e\delta_1)^{\frac{1}{2}}$, respectively.

Since the transmission curves involve only a single adjustable parameter, the cross section at resonance, an attempt to bring the calculated curves into coincidence with the observed curves

by suitably choosing the resonance cross section is a severe test of the assumed dependence of the capture cross section on the energy of the neutron. We shall now describe calculations of this nature for rhodium.

Rhodium

Experimental transmission curves have been obtained for the two detector thicknesses $\rho\delta_2=0.11$ g/cm² and $\rho\delta_2=0.35$ g/cm². The cross section at resonance is most conveniently calculated from the data obtained with the thicker detector. Anticipating that $n\sigma_0\delta_2>12$ for $\rho\delta_2=0.35$ g/cm², we may calculate the "activity" "A"$_{0,\delta_2}$ from Eq. (8) by integrating with respect to x from zero to infinity, subtracting the integral from δ_2 to infinity and utilizing the asymptotic expansion of $I_0(x)$ in the latter integral. Thus,

$$\text{"}A\text{"}_{0,\delta_2}=\tfrac{2}{3}(\mu_c n\sigma_0)^{\frac{1}{2}}\int_0^\infty dx\int_0^1 dz e^{-(\mu_c+n\sigma_0/2z)x}\, I_0\left(\frac{n\sigma_0}{2}\frac{x}{z}\right)-\tfrac{2}{3}\left(\frac{\mu_c}{\pi}\right)^{\frac{1}{2}}\int_{\delta_2}^\infty dx\frac{e^{-\mu_c x}}{x^{\frac{1}{2}}}\int_0^1 z^{\frac{1}{2}}dz$$

$$=\tfrac{2}{3}\int_0^1 dz\left(\frac{z}{1+(\mu_c/n\sigma_0)z}\right)^{\frac{1}{2}}-(1-\Phi(\mu_c\delta_2)^{\frac{1}{2}}), \quad (15)$$

since $$\int_0^\infty e^{-ax}I_0(bx)dx=\frac{1}{(a^2-b^2)^{\frac{1}{2}}}, \quad a>b. \quad (16)$$

Performing the integration with respect to z we obtain, finally:

$$\text{"}A\text{"}_{0,\delta_2}=\tfrac{2}{3}\frac{n\sigma_0}{\mu_c}\left(1+\frac{\mu_c}{n\sigma_0}\right)^{\frac{1}{2}}+\tfrac{2}{3}\left(\frac{n\sigma_0}{\mu_c}\right)^{\frac{1}{2}}\times\log\left(\left(1+\frac{\mu_c}{n\sigma_0}\right)^{\frac{1}{2}}-\left(\frac{\mu_c}{n\sigma_0}\right)^{\frac{1}{2}}\right)-(1-\Phi(\mu_c\delta_2)^{\frac{1}{2}}). \quad (17)$$

Using the asymptotic expansion of $I_0(x)$ in the second integral of the expression (10) for the "activity" "A"$_{\delta_1,\delta_2}$ we obtain

$$\text{"}A\text{"}_{\delta_1,\delta_2}=\tfrac{2}{3}(\mu_c n\sigma_0)^{\frac{1}{2}}\int_{\delta_1}^{\delta_1+\delta_2}d\eta e^{-(n\sigma_0/2)\eta}\times I_0\left(\frac{n\sigma_0}{2}\eta\right)\frac{1+\mu_c\delta_1-(1+\mu_c\eta)e^{-\mu_c(\eta-\delta_1)}}{(\mu_c\eta)^2}+\frac{1}{\pi^{\frac{1}{2}}}\frac{1+\mu_c\delta_1-(1+\mu_c\delta_1+\mu_c\delta_2)e^{-\mu_c\delta_2}}{(\mu_c\delta_1+\mu_c\delta_2)^{\frac{1}{2}}}. \quad (18)$$

We may now calculate the resonance cross section by fitting the experimental transmission at some value of the absorber thickness. Taking $\rho\delta_1=0.10$ g/cm², and using the experimental value of the electronic absorption coefficient, $\mu_e/\rho=7.3$ cm²/g,[3] we find that the observed transmission of 50 percent is obtained with $n\sigma_0/\rho=36$ cm²/g.[4] This value of the absorption coefficient, which corresponds to a cross section at resonance of $6{,}100\times10^{-24}$ cm²,[5] justifies the assumption that $n\sigma_0\delta_2>12$. With the value of the resonance cross section thus obtained, we may now calculate the complete absorption curve for comparison with experiment. The results of this calculation, which are in good agreement with the experimental points, are given as the solid line of Fig. 1.

Despite the good agreement, it seemed advisable to check the results with a thinner detector (0.11 g/cm²). The calculated curve ($n\sigma_0/\rho=36$) and the experimental points are shown in Fig. 2. The agreement is good for transmissions greater than 20 percent, but for lower values the observed transmissions are definitely less than those calculated. Agreement is hardly to be expected at large absorber thicknesses in view of the neglect of the factor $(E_0/E)^{\frac{1}{2}}$ which may well be of considerable importance in this region where only the wings of the line contribute to the activity of the detector. For the thick detector, the agreement at large thicknesses of absorber must be attributed to the effect of the paper container in increasing the number of neutrons in the center of the line where the capture probability is large. This effect increases the transmission. Such a process was demonstrated by a simple experiment.

Another check of the value of $n\sigma_0/\rho$ can be obtained very simply by measuring the activity of both faces of a rhodium detector. The ratio of the activities is given by

$$\frac{\int_0^\delta dx\int_0^1 dz e^{-(n\sigma_0 x)/2z}I_0\left(\frac{n\sigma_0 x}{2z}\right)e^{-\mu_e x}}{\int_0^\delta dx\int_0^1 dz e^{-(n\sigma_0 x)/2z}I_0\left(\frac{n\sigma_0 x}{2z}\right)e^{-\mu_e(\delta-x)}}. \quad (19)$$

[3] Amaldi, Hafstad and Tuve, Phys. Rev. **51**, 896 (1937).

[4] An estimate of the sensitivity of this method may be obtained from the following: (a) An assumed absorption coefficient of 52 cm²/g yields a transmission of 45 percent. (b) 29 cm²/g gives a transmission of 55 percent.

[5] Bethe (Rev. Mod. Phys. **9**, 146 (1937)) has mentioned our reported result (Phys. Rev. **51**, 1022 (1937)), but has incorrectly given the absorption coefficient at resonance as 19 cm²/g instead of 36 cm²/g, although the cross section given in his Table XXVII, p. 151, is correct.

For a detector thickness $\rho\delta=0.36$ g/cm² and $n\sigma_0/\rho=36$ Eq. (19) gives the value 2.1. Amaldi and Fermi have observed a ratio of two for this thickness of detector. We have measured the ratio for a Rh sheet 0.18 g/cm² (kindly loaned us by Professor E. O. Salant) and found it to be 1.43 ± 0.01. The calculated value is identical.

The total width of the rhodium resonance level may be obtained from Amaldi and Fermi's measurements of the resonance and thermal activity of a detector, averaged over all positions and orientations inside a large block of paraffin. The average over-all directions may be replaced by an average with respect to two opposite orientations of the detector, whence it may be shown that the mean resonance activity of the detector is proportional to

$$\int A_{res}d\tau=\tfrac{1}{2}\pi n\sigma_0 Q\lambda_0\frac{\Gamma}{E_0}\int_0^\delta dx\int_0^1 dz \times\exp\left[-\frac{n\sigma_0 x}{2z}\right]I_0\left(\frac{n\sigma_0}{2z}x\right)\cdot\tfrac{1}{2}(e^{-\mu_e x}+e^{-\mu_e(\delta-x)}), \quad (20)$$

where Q is the number of neutrons emitted per second from the source, λ_0 is the mean free path in paraffin of the resonance neutrons, and δ denotes the thickness of the detector. The average thermal activity, which is most conveniently measured by subtracting the activity obtained with a Cd filter on both sides of the detector from the activity measured with the detector screened by Cd on only one side, is similarly proportional to

$$\int A_{therm}d\tau=\frac{2}{2+(3)^{\frac{1}{2}}}n\sigma_c Q\lambda_c N^{\frac{1}{2}}\int_0^\delta dx\int_0^1 dz \times e^{-(n\sigma_c x)/z}(1+(3)^{\frac{1}{2}}z)e^{-\mu_e x}. \quad (21)$$

In deriving this expression, the dependence of the thermal cross section σ_c on energy has been neglected. Here λ_c represents the mean free path in paraffin of the thermal neutrons and N symbolizes the average number of mean free paths traversed by a thermal neutron before capture.

From these two expressions, Γ/E_0 may be calculated in terms of the experimentally determined ratio of the resonance and thermal activities, *viz;*

$$\frac{\Gamma}{E_0}=\frac{4}{\pi}\frac{\sigma_c}{\sigma_0}\frac{\lambda_c N^{\frac{1}{2}}}{\lambda_0}\frac{\int A_{res}d\tau}{\int A_{therm}d\tau}\frac{\frac{1}{1+\frac{1}{2}(3)^{\frac{1}{2}}}\int_0^\delta dx\int_0^1 dz e^{-(n\sigma_c/z)x}(1+(3)^{\frac{1}{2}}z)e^{-\mu_e x}}{\int_0^\delta dx\int_0^1 dz e^{-(n\sigma_0/2z)x}I_0\left(\frac{n\sigma_0}{2z}x\right)(e^{-\mu_e x}+e^{-\mu_e(\delta-x)})}. \quad (22)$$

According to Amaldi and Fermi, the experimental value of this activity ratio, obtained with a detector thickness of $\rho\delta=0.36$ g/cm², is

$$\frac{\int A_{res}d\tau}{\int A_{therm}d\tau}=\frac{4.58\cdot10^5}{1.5\cdot10^6}=0.30. \quad (23)$$

The other experimental quantities involved in Eq. (22) have also been determined. The thermal cross section of Rh has the value $\sigma_c=120\times10^{-24}$ cm², corresponding to an absorption coefficient of 0.7 cm²/g. The mean free path in paraffin of the thermal neutrons is $\lambda_c=0.30$ cm. The mean free path of the resonance neutrons has not been measured accurately. It may, however, be obtained from the thermal mean free path, using the theoretically calculated effect of molecular binding. Assuming the protons in a paraffin molecule to be isotropically bound, Fermi has shown that $\lambda_0/\lambda_c=3.3$. Bethe, however, has lowered this value to $\lambda_0/\lambda_c=2.8$ by taking into consideration the anisotropic binding of the protons. The mean free path of the resonance neutrons is, therefore, equal to $\lambda_0=0.85$ cm. The last experimental quantity we shall require is $N^{\frac{1}{2}}$. Experiments on the "albedo" of thermal neutrons in paraffin yield the result that $N^{\frac{1}{2}}=14$.

Combining these experimental values with the calculated values of the integrals, we obtain $\Gamma/E_0=0.072$. This result for Γ/E_0 with a reso-

nance energy $E_0=2.0$,[6] leads to a total width of the Rh resonance of $\Gamma=0.14$ ev. The value of the width thus obtained from relative activity measurements may be compared with the width calculated from the thermal and resonance cross sections by assuming the one-level formula (1) to be applicable. Taking the average energy of the thermal neutrons as $kT=0.026$ ev, we obtain

$$\sigma_c=\left(\frac{E_0}{kT}\right)^{\frac{1}{2}}\left(\frac{\Gamma}{2E_0}\right)^2\sigma_0, \qquad (24)$$

since the resonance energy is large compared to both kT and the natural width. Inserting the values of σ_c and σ_0, namely $\sigma_c=120\times10^{-24}$ cm^2 and $\sigma_0=6{,}100\times10^{-24}$ cm^2, we find that $\Gamma=0.19$ ev, which is in substantial agreement with the value of the width deduced from activity measurements in view of the uncertainty in the experimental values of many of the quantities involved.[7] If the total width be taken as 0.17 ev, a weighted mean, the value of the neutron width is $\Gamma_n=1.6\times10^{-3}$ ev.

In their early experiments on resonance neutrons Amaldi and Fermi measured the self-absorption of rhodium for a single absorber thickness (0.36 g/cm^2). Their detector thickness and geometry were the same as in the present "thick" detector case, and their value which is included in Fig. 1 is in excellent agreement with our data for this absorber thickness. Unfortunately the importance of self-reversal was not realized at the time of their measurements, and their effective absorption coefficient $n\sigma_0/\rho=2.0$ at 0.36 g/cm^2 is almost twenty times smaller than the absorption coefficient at the resonance energy.

Preiswerk and von Halban[8] discovered the dependence of absorption coefficient on absorber thickness and correctly attributed it to self-reversal. Their data is also included in Fig. 1, although, since their geometry and detector thickness have not been stated, complete agreement cannot be expected.

Since this work was completed, Jaeckel[9] has applied a similar method to the case of rhodium obtaining an absorption coefficient at resonance of 25 cm^2/g. The use of an old value of the electronic absorption coefficient (6 instead of 7.3), however, should make his value too low.

Discussion

The experimental transmission curve decreases more rapidly with absorber thickness than $\delta_1^{-\frac{1}{2}}$, which is the shape of the absorption curve deduced from (12) when the absorber thickness is large compared with the detector thickness. This discrepancy between observed and calculated transmissions at large absorber thicknesses indicates that one or more of the approximations which have been made in the preceding analysis are invalid under these conditions. Approximations have been introduced concerning the neutron intensity variation with energy and angle, the energy dependence of the capture cross section, and the law of electronic absorption. The discrepancy is necessarily to be attributed to an inadequacy of the approximate formula (3) representing the cross section, and to the neglected variation of the neutron intensity with energy, for it may be shown that with our previous assumptions concerning these quantities the calculated transmission varies at large thicknesses as $\delta_1^{-\frac{1}{2}}$, quite independently of the laws governing electronic absorption and neutron angular distribution.

Equation (3) presupposes a single resonance which is sufficiently narrow to permit the neglect of the factor $(E_0/E)^{\frac{1}{2}}$ in the resonance region. Furthermore, we have implicitly neglected the effect of the thermal motion of the capturing nuclei, i.e., the Doppler effect. That the Doppler effect is of no great importance may be seen by comparing the Doppler width[10], [11]

[6] Data of Goldsmith-Rasetti corrected for boron scattering and electronic absorption in the detector.

[7] The agreement is somewhat improved by utilizing recent mean free path measurements. The thermal neutron mean free path deduced from the measurements of H. Carroll and J. R. Dunning is $\lambda_c=0.25$ cm. According to unpublished measurements of V. W. Cohen, H. H. Goldsmith, and J. Schwinger (see Letter to the Editor, this issue), the mean free path in paraffin of resonance neutrons is $\lambda_0=0.6$ cm. The experimental ratio λ_0/λ_c is therefore 2.4 which must replace the calculated ratio of 2.8. The value of the total width is altered to 0.17 ev which compares more favorably with the value of 0.19 ev deduced from the thermal cross section of Rh.

[8] Preiswerk and von Halban, Nature **138**, 163 (1936).

[9] Jaeckel, Zeits. f. Physik **107**, 669 (1937).

[10] Bethe, Rev. Mod. Phys. **9**, 140 (1937).

[11] The quoted formula for the Doppler width is deduced by neglecting the binding of the capturing nuclei. Recent calculations by W. E. Lamb, Jr. (in press) have shown that

$$\Delta = 2((mE_0kT)/M)^{\frac{1}{2}} = 0.045 \text{ ev}$$

with the total width $\Gamma = 0.17$ ev. In consequence of the small value of Δ/Γ, the Doppler effect alters the capture cross section only in the immediate vicinity of the resonance, a region which contributes but little to the activity at large absorber thicknesses. Therefore the Doppler effect exerts no influence on the shape of the theoretical transmission curve in the region where disagreement with experiment exists.

Under the conditions obtaining at large absorber thicknesses, appreciable absorption is not confined to the immediate neighborhood of the resonance energy, thus invalidating the neglect of the variation of the neutron intensity $N(E)$. In the absence of experimental knowledge concerning this variation, it is reasonable to assume that the neutron intensity varies approximately as $1/E$.

In order to determine whether the removal of the approximations made in connection with the single resonance formula is sufficient *per se* to explain the discrepancy, thus obviating the necessity of invoking additional resonances, we have calculated the shape of the transmission curve at large thicknesses, using the complete formula (1) for the cross section, and $N(E) = 1/E$. Although these refinements do not suffice to reconcile theory and experiment, a somewhat slower variation of neutron intensity, *viz:* $1/E^{\frac{1}{2}}$, was found quite sufficient to reproduce the shape of the experimental transmission curves. It would therefore appear that the activity arising from the resonance level at two volts is competent of accounting for the observed transmission curves.

It is of some interest to note that Rh 3.9 min. has a resonance level at approximately the same energy as the two-volt resonance of Rh 44 sec.[12] The possibility of an effect of the resonance associated with the longer period should be considered, for although we are measuring the activity of the 44-sec. period, the absorption process involves the excitation of both periods. However, the approximate equality of the measured resonance energies of the two periods, coupled with the fact that the concentration of the isotope Rh^{103} is about 1000 times that of the isotope Rh^{101} proves almost conclusively that both periods arise from the same resonance level of the radioactive isotope Rh^{104}; i.e., Rh 44 sec. and Rh 3.9 min. are isomeric forms of the nucleus Rh^{104}. Inasmuch as the branching-ratio for the two periods is presumably independent of the energy of the captured neutron, the cross section for the formation of Rh 44-sec. differs from the total cross section by a constant factor, which obviously changes all the activities by a constant factor, and thus leaves the calculated transmissions unaffected.

In conclusion, the authors wish to express appreciation to the American Platinum Company for the rhodium which it so kindly loaned to the Columbia Department of Physics; and to Mr. M. Hamermesh for aid in some of the calculations.

the effect of crystal binding is to replace kT by the average vibrational energy per degree of freedom in the case of large natural width. This would lead to an effective temperature about 20 percent higher than T, which has no material effect on our conclusions. We are indebted to Dr. Lamb for the privilege of quoting his results before publication.

[12] Goldsmith and Rasetti, Phys. Rev. **50**, 328 (1936).

Radioactivity Induced by Nuclear Excitation*

I. Excitation by Neutrons

M. GOLDHABER,† R. D. HILL,‡ *Cavendish Laboratory, Cambridge, England*

AND

LEO SZILARD, *Clarendon Laboratory, Oxford, England*

(Received November 5, 1938)

It is shown that the 4.1-hr. period of indium can be produced by nuclear excitation of indium and is to be attributed to an excited metastable state, $In^{115,*}$ of the stable In^{115}. This result is obtained by studying the radioactivity produced in indium by neutrons of different energy distributions and by studying the chain reactions produced in cadmium by fast neutrons. It is found that In^{115*} can be produced from In^{115} by 2.5-Mev neutrons, but not noticeably by strong sources of photoneutrons which have energies of a few hundred thousand electron volts. A radioactive Cd^{115} of 2.5-day half-life time is found to transform with emission of negative electrons into In^{115*}. Cd^{115} was produced by neutron loss from Cd^{116} and by neutron capture from Cd^{114}.

WHEN indium is bombarded with fast neutrons from a Rn-Be source, a radioactive indium isotope, of 4.1-hr. half-life time, is produced which emits negative electrons.[1] So far, it has been assumed, that when an element is transformed by neutron bombardment into its own radioactive isotope, the radioactive isotope is generated either through neutron capture or through neutron loss from the bombarded element. The present experiments, however, indicate that this radioactive In isotope is generated through a new type of nuclear process—nuclear excitation leading to a metastable isomer of the stable In^{115}. For this metastable isomer we introduce the symbol In^{115*}.

As it was known that more than two radioactive isotopes of indium could be generated by neutron bombardment from the two stable isotopes of indium, a further investigation of their generation appeared to be of interest. Two of these radioactive isotopes, of 13-sec. and 54-min. half-life time, have been assigned to mass number 116. They are isomers produced from In^{115} by radiative capture of the neutron. In order to learn more about the generation of the 4.1-hr. period, which did not appear to be water-sensitive, we made the following experiments.

§1. GENERATION OF In^{115*} FROM INDIUM

A thick indium foil was bombarded with Rn-α-Be neutrons, and showed the 4.1-hr. period more strongly than the 54-min. capture period. A similar indium foil irradiated with photoneutrons from a strong radium-beryllium source (0.5 g Ra-260 g Be) did not show the 4.1-hr. period, though the photoneutron source was so strong that it produced the 54-min. capture period with an initial activity of 1200 impulses per minute recorded by a Geiger-Müller counter. Control experiments showed that this large activity was caused by the primary photoneutrons and not by slower scattered neutrons which would obviously produce a large activity of the 54-min. period by resonance capture. If the 4.1-hr. period, which is strongly produced by the fast Rn-α-Be neutrons, belonged to an isomer of In^{116}, it would be difficult to understand why this period is not appreciably produced from In^{115} by capture of the photoneutrons which have energies of a few hundred thousand electron volts. We conclude therefore that this period must not be attributed to In^{116}.

We made further experiments with neutrons from a radon-boron source. It was found that

* Some of these experiments have been reported at the Washington Meeting of the American Physical Society, April 1938, and at the British Association Meeting in Cambridge, August 1938. (See Nature **142**, 521 (1938)).

† Now at the University of Illinois.

‡ 1851 Exhibition Scholar, now at the University of Illinois.

[1] Szilard and Chalmers, Nature **135**, 99 (1935); Amaldi, d'Agostino, Fermi, Pontecorvo, Rasetti and Segrè, Proc. Roy. Soc. **A149**, 522 (1935); Lawson and Cork, Phys. Rev. **52**, 531 (1937).

these neutrons excite the 4.1-hr. period more strongly than either the 25-min. period of I, or the 54-min. period of In, which are both caused by neutron capture; and also much more strongly than other investigated periods which are known to require fast neutrons for their excitation, such as the 10-min. and 15-hr. periods of Al, the 2.3-min. period of Si, and the 2.3-min. period of P. The 170-min. period of P which does not require very fast neutrons for its excitation is, however, more strongly activated than the 4.1-hr. period of In. These results are in accord with the fact that a radon-boron source is deficient in very fast neutrons compared with a Rn-α-Be source. The strong activation of the 4.1-hr. period in the present experiment cannot be attributed to a neutron loss reaction from either In^{113} or In^{115} for such a reaction requires very fast neutrons.

Nor can the strong activation of this period by radon-boron neutrons be attributed to neutron capture from In^{113}, since the relative abundance of this isotope is only five percent. The capture cross section of In^{113}, corrected for the half-value thickness of the β-rays, would have to be 100 times larger than the capture cross section of iodine. In the absence of slow neutrons we cannot expect such large differences of capture cross sections among the strongly absorbing elements of odd atomic number of such similar atomic weight. This is borne out by an unpublished survey of the relative capture cross sections of elements for Ra+Be photoneutrons which was made by J. H. E. Griffiths, Oxford, in collaboration with one of us.

Finally indium was irradiated with neutrons of about 2.5-Mev energy, produced by bombarding heavy ice with deuterons of 250 kev. The 4.1-hr. period was found to be strongly activated. Obviously this cannot be caused by a neutron loss reaction, since the available energy is certainly less than the binding energy of the neutron in an In isotope.

The experiments described rule out the possibility that this radioactive indium isotope is generated from a stable indium isotope by neutron capture, or neutron loss, and therefore exclude an indium isotope of mass number 112, 114 or 116 as the carrier of the 4.1-hr. period. Moreover, the fact that photoneutrons from a Ra-Be source do not excite the 4.1-hr. period, while neutrons from the D+D reaction do so, suggests that its carrier might arise through a process which has a real or apparent energy threshold.

These results forced us to assume that the 4.1-hr. period is generated by a new type of process. In order to explain this period we assumed that the In^{115} nucleus may be excited by neutron impact and left in a metastable excited state, In^{115*}. This metastable In^{115*} may be radioactive and transform either by β-disintegration into its stable isobar Sn^{115}, or by emission of γ-rays and internal conversion electrons into the stable In^{115}.

If this assumption is correct it should be possible to produce this radioactive indium isotope by other methods of nuclear excitation from indium, e.g. by proton impact. S. W. Barnes and P. W. Aradine, Rochester, will report in the following paper on the nuclear excitation of indium by protons.

It is conceivable that the existence of a metastable state of In^{115} is connected with the high nuclear spin (9/2) of In^{115}. If the metastable In^{115*} has a small spin it will be difficult to reach the metastable state from the ground state by a direct transition. As a rule, a higher excited state of indium will have to be produced, from which the metastable state can be reached by one or more spontaneous transitions. The apparent energy threshold of In^{115*} may therefore be considerably above the level of the metastable state.

TABLE I. *Stable and some radioactive isotopes of cadmium, indium and tin in the mass range 112 to 117. For stable isotopes the relative abundance in percent is given in heavy type. For radioactive isotopes the half-life periods are given in italics.*

M	$_{48}$Cd		$_{49}$In	$_{50}$Sn
117	*4h*	→	*2.3h*	9.1
116	7.3		*13s*	15.5
			54m	
115	*2.5d*	→	*4.1h*	0.4
			95.5	
114	28.0			0.8
113	12.3		4.5	
112	24.2			1.1

§2. Generation of In^{115*} from Cadmium

Other methods of producing In^{115*} can be devised, and we have isolated In^{115*} from cadmium bombarded by neutrons from Li+D,

thus confirming our assignment of the 4.1-hr. period.

As can be seen from Table I, cadmium has an isotope of mass number 116 having a relative abundance of 7.3 percent. By bombarding cadmium with fast neutrons of the Li+D reaction, one could hope to produce a radioactive Cd^{115} by the neutron loss reaction Cd^{116} $(n, 2n)$. Such a radioactive isotope could be expected to emit negative electrons and it might transform partly into the stable In^{115} and partly into the metastable In^{115*}.

We bombarded metallic cadmium for several hours with neutrons from Li+D using deuterons of 950 kev and currents averaging 30μa. The irradiated cadmium was dissolved in nitric acid and a small quantity of indium was added. Indium was precipitated by adding ammonia. The indium which was separated from the cadmium solution two days after the irradiation showed a single activity decaying with a 4.1-hr. period. By successive separations of indium from the cadmium solution it was found that this radioactive indium isotope grew from a parent substance of 2.5-day half-life period. This indium isotope was found to emit negative electrons.

We have compared the half-life period and the electron absorption curve of this radioactive indium isotope with the half-life period and the electron absorption curve of the radioactive indium isotope produced by fast neutrons from indium. The result confirms our assumption that the two are identical and that the carrier of the 4.1-hr. period is In^{115*}. The range of the electrons in Al was found to be 0.15 g/cm^2. This corresponds to an energy of 550±100 kev.

Our experiments show that In^{115*} grows from the parent Cd^{115} which decays with a half-life time of 2.5 days. We find by magnetic analysis that Cd^{115} emits negative electrons, thus transforming into In^{115*} and perhaps also into the stable In^{115}.[2]

To investigate whether Cd^{115} can also be obtained by slow neutrons we irradiated with neutrons a cadmium sheet which was enclosed between two similar cadmium sheets and placed inside a paraffin block. We found that the two outer sheets showed a stronger activity of the 2.5-day period than the inner sheet. This indicates that Cd^{115} is produced by slow neutron capture from Cd^{114}. The activity produced in this way is small compared with the activity produced by the neutron loss reaction from Cd^{116}.

The properties of In^{115*} are of great interest both from the point of view of the nature of isomeric nuclei and of isobaric pairs. A detailed investigation of the radiations emitted by In^{115*} is now being carried out. An account of some preliminary experiments has been given at the British Association Meeting.[3]

We wish to thank all those who have cooperated in this work: Dr. F. M. Brewer, Old Chemistry Laboratory, Oxford, who in the early stages of this work identified the carrier of the 4.1-hr. period as an isotope of indium; Mr. P. I. Dee, Cavendish Laboratory, Cambridge, who made it possible for us to use strong Li+D neutron sources; Drs. E. T. Booth, C. H. Collie and C. Hurst, Clarendon Laboratory, Oxford, who carried out the irradiations with D+D neutrons. Our thanks are also due to Professor F. A. Lindemann, F.R.S. and to Dr. J. D. Cockcroft, F.R.S. for their kind interest in this work. We are much indebted to the Anaconda Wire and Cable Company who very generously enabled us to work with large quantities of indium.

[2] A radioactive Cd isotope of similar half-life time (58 hr.) has been previously reported to exist by Cork and Thornton (Phys. Rev. **51**, 608 (1937)), but assigned by them to mass number 117. They also reported a radioactive isotope of In of 2.3-hr. half-life time which they ascribed to In^{117} and which appeared to grow from a 58-hr. Cd parent. We find this indium isotope only when we precipitate indium from the cadmium solution in a time less than two days after irradiation. By successive separations we find that it grows from a 4-hr. Cd parent, a radioactive isotope which has been previously reported by Cork and Thornton and at the time assumed to be Cd^{115}.

[3] See Nature **142**, 521 (1938).

Radioactivity Induced by Nuclear Excitation*

II. Excitation by Protons

S. W. BARNES, *Department of Physics, University of Rochester, Rochester, New York*

AND

P. W. ARADINE,** *Department of Chemistry, University of Rochester, Rochester, New York*

(Received November 5, 1938)

Radioactive indium resulting from proton bombardment of indium exhibits negative electron emission which decays with a 4.1-hr. half-life. Proton bombardment of cadmium does not produce this activity. It is ascribed to a metastable excited state of In^{115} designated by In^{115*} formed by a new type of proton excitation process. Control experiments exclude the possibility of its being formed by stray neutrons. The cross section for protons of 5.8 Mev is about 10^{-29} cm².

AT THE present time there are known seven radioactive periods assigned to In isotopes. Of these, six periods have been definitely assigned to five mass numbers, i.e., 111, 112, 114, 116, 116 and 117. The assignment of the seventh period, a 4.1-hr. negative electron emitter, has been subject to doubt.

This activity[1] discovered by Szilard and Chalmers has been found by Lawson and Cork both after fast neutron bombardment of indium and after deuteron bombardment of cadmium. Goldhaber, Hill and Szilard have found that a minimum neutron energy is apparently required to produce this activity. They have suggested[2] that In^{115} can be raised to an excited metastable state by inelastic neutron collisions, in which the neutron is captured and then released with lower energy. They have assumed that the 4.1-hr. period is associated with this metastable excited state which they designate by In^{115*}. This view can be tested by proton bombardment of indium. It is obvious that no previously known type of proton reaction could produce any radioactive In isotope by bombardment of In. Thus if the 4.1-hr. activity is found it is conclusive proof that it is produced by a new type of process, In (p-p).

This may be substantiated in another way. No stable isotope Cd^{115} being known, proton bombardment of Cd should not yield isomers of In^{115} by the Cd (p-n) reaction. In^{114}, however, ought to be formed from Cd^{114}.

We have bombarded Cd and In with 6.7-Mev protons in the cyclotron. Our experiments show (a) that proton bombardment of indium produces the 4.1-hr. activity and (b) that proton bombardment of Cd does not, although it does give the 50-day activity characteristic of In^{114}. These results corroborate the assignment of the 4.1-hr. activity to In^{115*} and show that this metastable state can be produced by exciting the indium nucleus by fast protons.

A sample of "pure" indium was selected for use. A chemical microanalysis showed the following impurities to be present—Pb, Sb and Sn in amounts of 1. to 0.1 percent and Al, Fe, Cd, Bi and Zn in amounts of 0.1 to 0.01 percent. One of us then carried the sample through a chemical procedure calculated to reduce the abundance of these impurities by at least a factor of 10. The purified indium, again in metallic form, was rolled into foil six mil (0.006″) in thickness.

Since the cyclotron chamber is a strong source of neutrons when it is producing protons of over six Mev, it was necessary to separate the effects on the indium of the neutrons and protons. For this purpose two indium foils, separated by a ten-mil (0.01″) foil of Pb were mounted in the vacuum bombardment cup. Foil (1) facing the beam received protons and stray neutrons. Foil (2) immediately behind the lead foil received no protons but the same stray neutrons as struck foil (1).

A ninety-minute bombardment with a ½-μa

* Some of these experiments have been reported at the Washington meeting of the American Physical Society, April, 1938.

** Now at Taylor Instrument Company, Rochester, New York.

[1] L. Szilard and B. Chalmers, Nature **135**, 99 (1 35); J. L. Lawson and J. M. Cork, Phys. Rev. **52**, 531 (1937).

[2] See preceding paper.

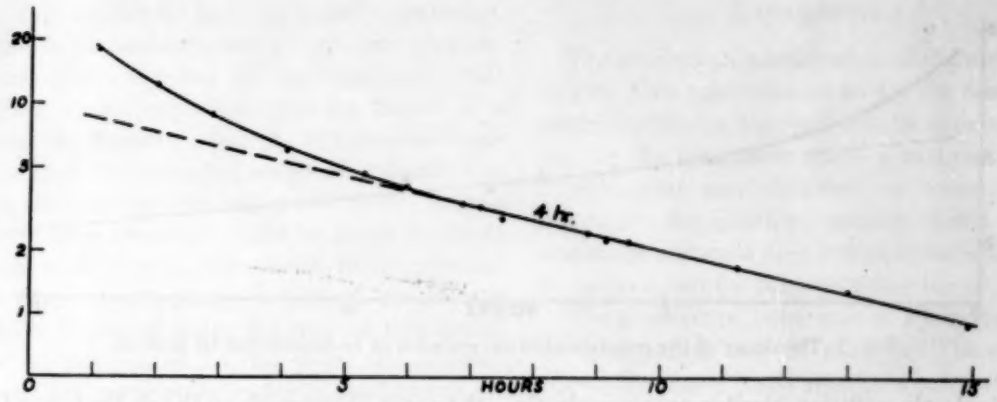

FIG. 1. Decay of indium precipitate from In bombarded by protons. The ordinates when multiplied by 30 give the number of β-particles emitted per sec. in all directions by the sample.

beam of 6.7-Mev protons produced in foil (2) a small activity of the 54-min. period which is caused by neutrons but no activity of a 4.1-hr. period. This latter period did not appear in foil (2) even with much longer exposures.

Samples of In chemically separated from In foil (1) after this foil was exposed to the proton beam showed an activity decaying according to Fig. 1. Six hours after exposure the decay curve shows only a 4-hr. period.

Visual inspection of cloud-chamber tracks from this sample showed that the majority of the emitted electrons were negative, but the activity was too weak for a satisfactory investigation by this method. More definite information as to the sign was obtained in the following way.

A small electromagnet is suspended over the window of the ionization chamber and the active sample placed at the edge of the air gap between the poles in an arrangement which has been described by one of us.[3] A small lead shield between the radioactive sample and the window prevents electrons from entering the chamber in the absence of the magnetic field. Fig. 2 shows the decay curve obtained from a bombarded In foil with a magnetic field which allowed only negative electrons to enter the chamber. It shows the 4.1-hr. period. This period did not appear when the magnetic field was reversed, thus the 4.1-hr. activity does not exhibit an appreciable positive electron emission.

It was not possible to make an accurate determination of the range of the electrons but the values so far obtained are consistent with the value found for the 4.1-hr. period produced from Cd by fast neutrons.[2]

It appears from our results that fast protons can excite the stable In^{115} and produce a metastable In^{115*}. The cross section for the excitation of the In nucleus which leads (not necessarily directly) to In^{115*} is found to be about 10^{-29} cm^2 for 5.8-Mev protons.

This cross section is much smaller than the cross section for p-n reactions in this region of the periodic system. For instance if neighbors of In, Cd and Sn, are bombarded by protons, radioactive isotopes of In and Sb are produced respectively and the cross sections for these reactions are about 10^{-26} cm^2. Radioactivities caused by p-n reactions can therefore easily overshadow radioactivities caused by nuclear excitation. Fortunately the p-n reaction in In^{115}, the more abundant In isotope, apparently leads to a stable isotope Sn^{115}. This pair is one of the three known cases of such stable isobars. In^{113}, however, which has a relative abundance of less than five percent might yield a radioactive Sn^{113} by a p-n reaction. One of the activities observed in a sample of Sn which has been separated from bombarded In may be caused by Sn^{113}. This activity is now being investigated along with other activities produced by proton bombardment of In and Cd.

Weisskopf has pointed out that a proton can excite a nucleus in two different ways, i.e., either

[3] S. W. Barnes, Rev. Sci. Inst. in press.

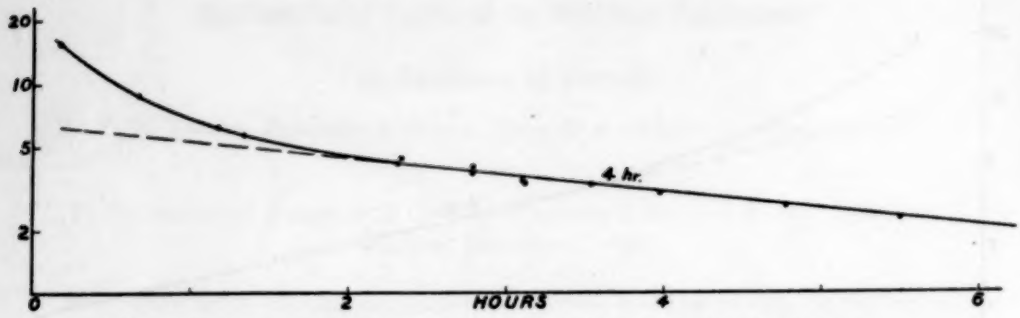

FIG. 2. The decay of the negative electron emission of In bombarded by protons.

by an inelastic collision similar to an inelastic collision of a neutron or through the action of the electric field of the proton.[4]

The authors gratefully acknowledge their indebtedness to Dr. L. Szilard and Dr. M. Goldhaber for suggestions which prompted this study and for valued suggestions made by them and Professor L. A. DuBridge during the course of the work. They wish to thank Professor Line for microanalytical work, Mr. R. Grabenstetter for chemical separations and particularly Mr. T. Enns for much help in connection with cyclotron operation.*

[4] V. F. Weisskopf, Phys. Rev. 53, 1018 (1938).

* *Note added in proof.*—Indium has been bombarded with 0.01 μa of 8.5-Mev alpha-particles. No 4.1-hr. activity was observed. According to this result the cross section for excitation of In^{115} with 8.5-Mev alpha-particles cannot be more than twice the cross section for the excitation of In^{115} by 6.5-Mev protons.

JANUARY 1, 1939 PHYSICAL REVIEW VOLUME 55

The Quadratic Zeeman Effect

F. A. JENKINS AND E. SEGRÈ
University of California, Berkeley, California

(Received November 9, 1938)

The Zeeman effects of the principal series lines of sodium and potassium in the range $n=10$ to 35 are observed in absorption, using the new 60-inch cyclotron magnet. With a field of 27,000 gauss, the lines having n in the neighborhood of ten show a normal triplet representing the complete Paschen-Back effect of the narrow ^2P doublet. From about $n=12$ to 20 all components show an increasing displacement toward short wave-lengths proportional to (n^*),[4] the shift of the π components being half that of the center of the two σ components. This is the quadratic Zeeman effect, varying as H^2, and is here measured and compared quantitatively with theory for the first time. The agreement with the simple theory is excellent as far as $n=20$. Beyond this the lines show an additional displacement in the same direction, increasing as a higher power of n. At the same time the lines are broadened toward the red, with indications of an unresolved component whose intensity increases rapidly with n. The displacement is interpreted as a perturbation by the F states, whose separation from the P states in this region becomes comparable with the magnetic energy. The additional lines causing the broadening represent forbidden transitions $^2S\rightarrow{}^2F$. Beyond $n=28$ the broadening increases suddenly and becomes symmetrical, until the lines are no longer distinguishable at $n=35$. All of these perturbation effects are compared with the theoretical results given in the accompanying paper by Schiff and Snyder. Some features are accounted for quantitatively, while the others are satisfactorily explained qualitatively.

THE quadratic Zeeman effect is a displacement toward short wave-lengths of the Zeeman components of a spectral line, proportional to the square of the magnetic field. It is directly related to the diamagnetic term in the theory of magnetism, which contains the square of the "radius" of the atom. In both classical and quantum mechanical theories of the Zeeman

effect this quadratic term is usually neglected, because it is unobservable under most circumstances. The existence of the quadratic shift was first shown experimentally by Segrè[1] in a study of the Zeeman effect of the last observable members of the principal series of sodium. The shift could only be detected qualitatively, and no accurate measurements could be made for comparison with theory. Hence we have repeated these experiments under improved conditions, and have extended them, for reasons mentioned below, to potassium. In our work the Zeeman patterns are completely resolved, and the shifts are measured rather accurately. For the last members of the series, a new perturbation effect is found, which in sodium appears as an unsymmetrical broadening of all Zeeman components, eventually becoming symmetrical and smearing the lines into an apparent continuum considerably before they reach the series limit. The theory of these effects is discussed in the accompanying paper by Schiff and Snyder.

The simple theory of the quadratic effect[2] gives displacements proportional to the fourth power of n^*, the effective quantum number, and since the coefficient is of the order of magnitude of 10^{-15} cm^{-1}, the shifts become detectable only for rather large values of n^*, exceeding about 12. The Zeeman effects usually studied involve small n, and hence the quadratic term is negligible in these cases. In the study of lines of large n, one is practically restricted to absorption lines, since for emission it is not possible to put a sufficient number of atoms in the initial states to obtain the required intensity. The principal series of the alkalis afford the most favorable case, the sodium series having been observed in absorption[3] as far as $n=59$. To obtain these lines without undue pressure broadening, the length of the absorbing column of vapor cannot be made too small, and therefore a magnetic field of considerable dimensions is required. We were fortunate in having available the new cyclotron magnet of the Crocker Radiation Laboratory, the poles of which have a diameter of 152 cm.

[1] E. Segrè, Nuovo Cimento **11**, 304 (1934).
[2] See for example J. H. Van Vleck, *Theory of Electric and Magnetic Susceptibilities*, p. 178.
[3] R. W. Wood and R. Fortrat, Astrophys. J. **43**, 73 (1916).

Experimental

The original pole separation of the magnet was 56 cm. This was reduced to 4.4 cm by inserting large iron blocks, the final pole faces being 15×63 cm. In the remaining space a magnetic field of 27,000 gauss was obtained, as measured by a fluxmeter. By inserting suitable shims, the field was made constant to ±100 gauss over the region to be occupied by the absorbing vapor.

The absorption tube was of Pyrex tubing 3.5 cm in diameter and 110 cm long. The ends were closed by plane fused quartz windows, and the central portion, 30 cm long, heated by a Nichrome winding. A few lumps of the alkali metal were placed along the heated part, and after the tube had been evacuated and heated until the metal fused, fresh hydrogen was introduced at about ten cm pressure to prevent diffusion to the windows. The temperature required to bring out the high series members of sodium was 500°C. A sensitive criterion for the proper pressure is a characteristic azure blue color of the transmitted light. For potassium it is a light green.

As a source for the continuous spectrum, we used a hydrogen lamp of the conventional design, carrying a current of 180 ma at 7000 volts. With this source, the exposures for the sodium series, which converges at λ2412, varied from 15 to 30 min. For potassium, with a convergence at λ2856, 5 to 10 min. were sufficient. The light was rendered parallel by a quartz-fluorite achromat, and, after traversing the absorption tube, focused on the slit of the spectrograph by a lens of fused quartz. Between this lens and the slit was placed a calcite crystal of such a thickness that the two images of the source, polarized perpendicular and parallel to the magnetic field, almost touched. A diaphragm was used which in one position exposed the two adjacent halves of the images (for the spectra of the π and σ polarizations with field) and in another the two outer halves (for the spectrum without field). A slight artificial shift of about 0.04 mm was introduced between the spectra with and without field, as a result of small mechanical displacements arising from the magnetization of the spectrograph. In the measurements this could be easily determined and corrected for, thanks to the presence of emis-

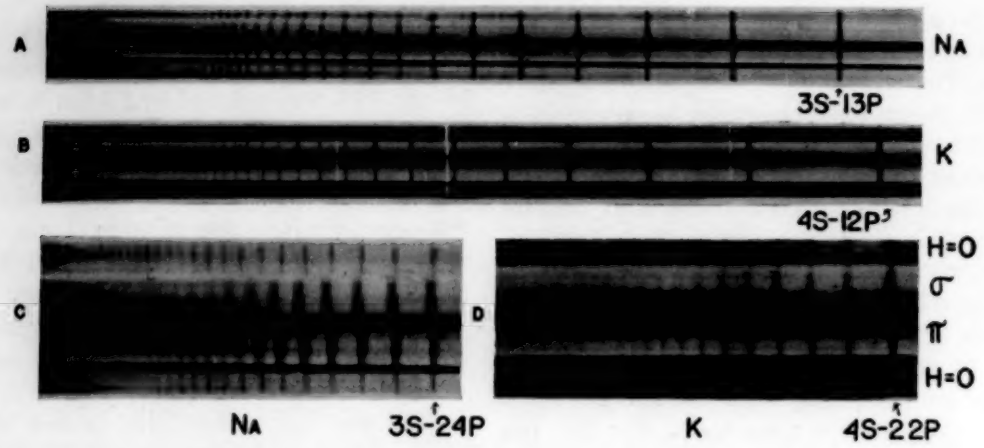

FIG. 1. Zeeman effect of the absorption lines of sodium and potassium. $H=27{,}000$ gauss. (a) Na, low density, (b) K, low density, (c) Detail of the end of the series, Na, higher density, (d) Same for K, higher density.

sion lines coming from a contamination of mercury in the hydrogen lamp.

The spectrograph was a 3-meter Littrow instrument, with a combination of 60° and 30° quartz prisms automatically adjusted for minimum deviation.[4] It gave a dispersion of 0.75A/mm at λ2412, and 1.36A/mm at λ2856. Our best plates of the series without field resolved the sodium lines as far as $n = 51$, and the potassium lines as far as $n=43$.

Several exposures were taken for both sodium and potassium, with different densities of the absorbing vapor. Fig. 1 shows enlargements from two of our plates of each. The fact that the lines with field have a false shift toward the red will be seen from the emission lines on the plates. In the case of potassium, the lines are broader when the vapor is dense enough to produce the high members with any intensity, and only at the lowest densities used were the σ components well resolved. This, combined with the lower dispersion of the spectrograph, made the results for potassium less accurate than those for sodium.

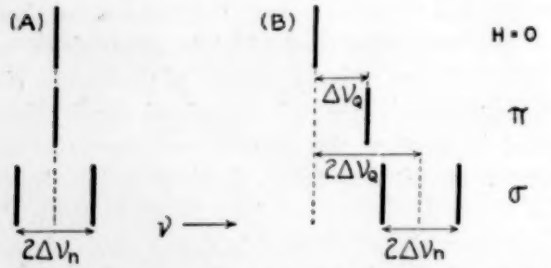

FIG. 2. Zeeman patterns (a) without and (b) with the quadratic effect. The pattern shown in (b) is that predicted for the line $3S-27P$ of Na, with $H=27{,}000$ gauss.

[4] H. E. White, J. Opt. Soc. Am. **25**, 241 (1935).

DATA AND RESULTS

The simple theory of the quadratic effect, outlined in the following section, predicts the Zeeman pattern shown in Fig. 2(b). Both π and σ components are displaced toward higher frequencies, the quadratic shift $\Delta\nu_Q$ of the π component being half of the shift of the center of gravity of the σ components. For comparison, Fig. 2(a) shows the normal pattern to be expected for the lines of fairly low n, i.e., in the neighborhood of $n=10$. This is really a complete Paschen-Back effect of the very narrow doublet $^2S_{\frac{1}{2}}-n\,^2P_{\frac{1}{2},\frac{3}{2}}$.

The lines were measured with a Geneva Society comparator, and a curve of the dispersion in cm^{-1}/mm drawn, by using the known wavelengths of the lines without field. Two different plates were measured for both Na and K. The splitting $\Delta\nu_n$ of the σ components was first used to check the value of the magnetic field by the relation

$$\Delta\nu_n = 4.67\times10^{-5}\,H\ \text{cm}^{-1}.$$

The more accurate measurements for sodium gave values of H varying from 26,700 to 27,300, and therefore we adopt the figure 27,000 obtained with the fluxmeter.

The displacements of the Zeeman components from their no-field positions were then evaluated. The plotted points in Figs. 3 and 4 represent the average displacements obtained from the measurements of lines up to $n=28$. The theory on which the curves are based will be considered in the following section.

As will be seen, especially by inspection of Fig. 1(c), the lines beyond $n=28$ become rapidly broader. In Na this broadening is at first definitely unsymmetrical, shading off toward the longer wave-lengths, and is greater for π than for σ. Fig. 5 shows microphotometer curves of the last few members of these series taken with the Zeiss recording microphotometer. The K lines

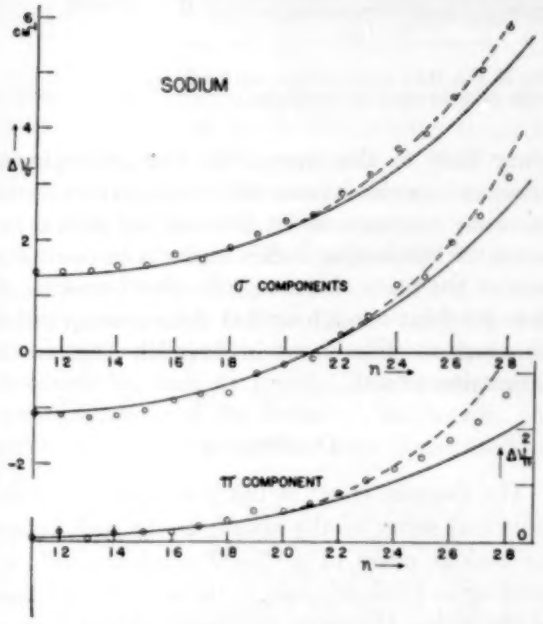

FIG. 3. Displacements of the Zeeman components for sodium. The continuous curves give the theoretical displacements by the simple theory (Eq. (2)), while the broken curves include the perturbation effect (Eq. (9) of Schiff and Snyder).

photometered in Fig. 5(b) were necessarily much weaker than the Na lines, for if the vapor density was further increased to render them stronger, all lines, including those with no field, became rapidly broader.

The microphotometer curves for Na show that the unsymmetrical broadening of the π components is already appreciable for the line $3S-23P$. That it also exists for the σ components is shown by fact that the long wave-length component is

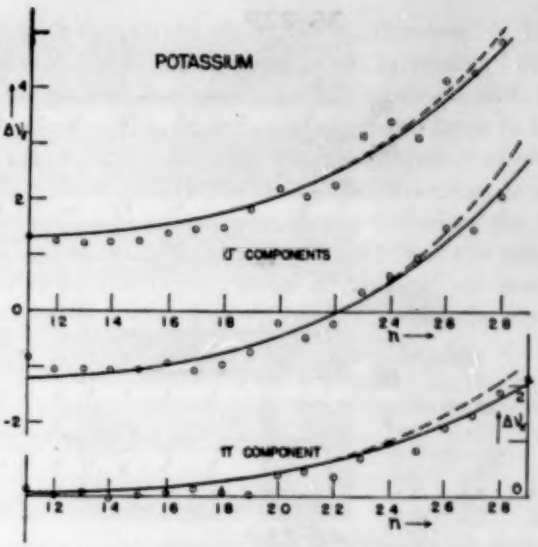

FIG. 4. Displacements of the Zeeman components for potassium. Similar to Fig. 3 for sodium.

consistently stronger, being enhanced by the wing of the adjacent line. Furthermore, there seems to be a definite indication in the curve for the π components that the wing is actually a faint, nearly resolved line that increases in intensity until it is practically equal to the original line at $n=30$. In K the lines are too faint to show such a component even if it existed. It was the anticipation that the broadening effects should be different in K that caused us to try this element. The fact that the unsymmetrical broadening does not appear is in agreement with theoretical expectation, as explained below. One can also conclude that the large difference in broadening between the π and σ components observed for Na is either nonexistent or much less pronounced for K.

We have measured the positions of the intensity maxima of the broadened lines beyond $n=28$. They could be followed as far as $n=35$ in Na and $n=33$ in K. In the case of the π components of Na it is obvious that these maxima do not follow the simple theory of the quadratic effect even approximately. Instead of continuing to increase in proportion to n^4, the displacements reach a maximum at $n=30$, and then decrease rapidly toward zero again. This may be easily seen in Fig. 5(a). Table I gives the results of these measurements. It will be noticed that in K only the last measured π maximum deviates significantly from the simple theory. As pointed out

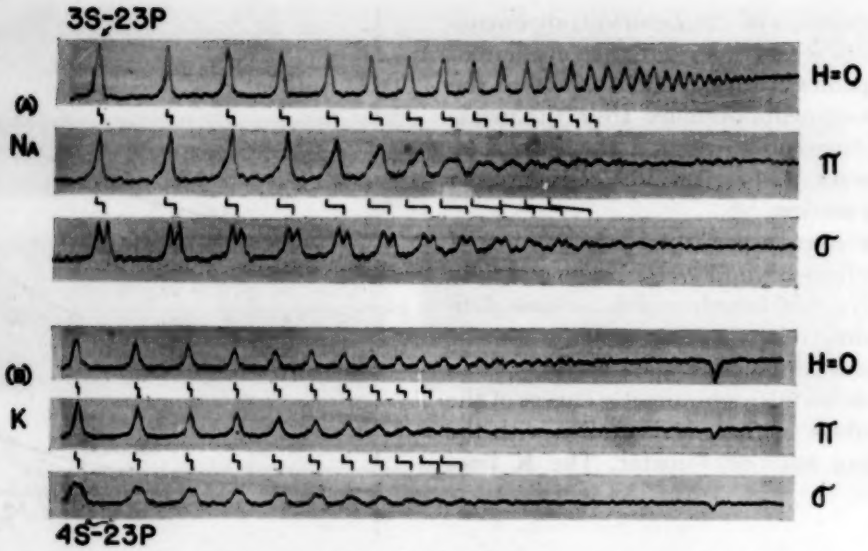

FIG. 5. Microphotometer curves (a) for Na, (b) for K. For the σ components, the displacements of the centers of gravity from the no-field lines are indicated.

below, the first few lines of this table are not expected to agree with the simple theory, but with a more extended theory. (See broken lines in Figs. 3 and 4.)

The displacements of the σ components, on the other hand, go on increasing more or less as expected. In Fig. 1(c) they may be seen to catch up with the no-field lines of next higher n, and on the original plate may be observed to "lap" the no-field lines three times before fading out. This behavior of the π and σ maxima has been verified on microphotometer curves like those of Fig. 5, but taken with a considerably wider slit.

As regards the widths of the lines, it is only possible to obtain qualitative results from our plates. We have measured the widths of the microphotometer peaks at half-maximum for the broadened π and σ components of Na. The curves for the σ doublets can easily be analysed into two identical unsymmetrically broadened curves separated by $\Delta\nu_n$. Table II shows the measured widths of these component peaks, for comparison with those of the π and no-field lines. It must be remembered that the width of these peaks is partly true line width and partly caused by the finite resolution of the spectrograph. The effect of finite resolving power would be to make the observed ratio of the widths of the π to the σ components less than the true ratio, so that it is legitimate to regard the ratio from Table II as a lower limit to the true ratio. The microphotometer curves give a reasonably true picture of the intensity contours of the lines on our plates, because the blackening in this region is on the linear part of the plate characteristic. Furthermore, all lines are faint enough so that there is no question of spurious differences in breadth because of saturation effects.

DISCUSSION

The Zeeman effect of the first few lines of the principal series of the alkalis is the well-known anomalous effect of a $^2S-^2P$ doublet, and, according to Preston's rule, is the same for all lines of the series. However, this holds only as long as the magnetic splitting is small compared to the doublet separation of the ^2P term. For the field we used (27,000 gauss) the first serious departures begin at about $n=6$ in Na. Since the ^2P separation decreases approximately as $1/n^3$, the magnetic splitting rapidly approaches a normal triplet (Paschen-Back effect) because of the uncoupling of the spin and orbit. For $n=10$ the ^2P separation is already small compared to the Larmor frequency $\Delta\nu_n=1.262$ cm^{-1} for the field we used. Therefore, since the lines we studied all have $n>10$, the spin does not need to be considered, and, but for the quadratic effect, we should obtain a normal triplet.

The quadratic Zeeman effect is due to a term in the magnetic energy of the form

$$E=\frac{e^2H^2}{8mc^2}\langle x^2+y^2\rangle_{Av}, \quad (1)$$

in which x and y are the coordinates of the electron, the z direction being that of the magnetic field. From this it is easily seen that the effect is proportional to n^4. We substitute for $\langle x^2+y^2\rangle_{Av}$ its value for hydrogen, and replace n by n^*, as a better measure of the size of the orbit. Neglecting terms in lower powers of n, Eq. (1) then becomes

$$\Delta\nu_Q=\frac{e^2H^2}{8mc^3h}a_0n^{*4}(1+m_l^2)$$
$$=4.98\times10^{-13}n^{*4}H^2(1+m_l^2). \quad (2)$$

Here $a_0=h^2/(4\pi^2e^2m)$ is the radius of the first Bohr orbit, while m_l is the orbital magnetic quantum number in the upper state. Adding the displacement (2) to the normal Zeeman displacement of the P terms, one finds that the two levels with $m_l=\pm1$ preserve their separation $2\Delta\nu_n$, but that their center of gravity is displaced toward the series limit by an amount $H^2e^2a_0n^{*4}/(4mhc^3)$, whereas the level with $m_l=0$ moves in the same direction by half as much. This causes corresponding shifts of the Zeeman components, and gives the pattern which was illustrated in Fig. 2(b).

The continuous curves in Figs. 3 and 4, as well as the calculated values in Table I, were computed from Eq. (2). It is seen that the agreement with experiment is good for $11<n<20$. It is particularly satisfactory that the long wavelength σ component crosses the π component at just the predicted place, $n=26$. However, in Na above $n=20$ there appears an increasing discrepancy in the sense that the observed shift is too large. This deviation is much too large to be caused by an error in the measurement of the field. The qualitative reason for this effect is as follows. The elementary theory considers the P terms alone, and neglects the fact that the magnetic perturbation causes a "mixing" of these states with states of different L, which lie very close to the P terms in this region. Here only the states differing in L by 2 units are to be considered in the first approximation. Thus Eq. (1) is valid only as long as the total magnetic energy is small compared to the energy differences between the P and F terms. When this condition is no longer satisfied, perturbations occur which can be qualitatively described as follows: The eigenfunctions of the F states become mixed with those of the P states of about the same energy, and, in a higher approximation, the same occurs for the H, K, $\cdots$ eigenfunctions. This causes transitions $S\rightarrow F$, $S\rightarrow H$, etc., which are normally forbidden, and at the same time the P and F levels as well as H, K, $\cdots$ are displaced because of a mutual repulsion.

The first of these effects, the occurrence of forbidden lines, is rather clearly seen in the microphotometer curve for the π components of Na in

TABLE II. *Widths of microphotometer peaks for sodium in cm^{-1}.*

	$n=25$	26	27	28	29	30	31
$H=0$	1.6	1.6	1.6	1.6	1.6	1.5	1.6
π	2.3	2.4	2.8	3.9	4.3	4.9	5.7
σ	2.1	2.0	2.0	2.2	2.5	2.7	2.5

TABLE I. *Displacements of broadened components. Measurements represent displacements of maxima in cm^{-1} except where specified. The calculated values are from Eq. (2).*

	Sodium						Potassium			
	π		σ_-		σ_+		π		σ (center of gravity)	
n	OBS	CALC	OBS	CALC	OBS	CALC	OBS	CALC	OBS	CALC
28	2.63	1.97	3.12	2.68	5.84	5.18	1.85	1.73	3.68	3.47
29	3.04	2.28	3.52	3.29	6.44	5.82	2.10	2.01	3.28	4.02
30	3.58	2.62	4.59	4.00	7.19	6.49	2.28	2.33	3.78	4.65
31	3.63	3.00	5.67	4.73	7.91	7.26	2.48	2.67	4.87	5.34
32	1.80	3.41	6.75	5.58	9.06	8.07	1.59	3.06	6.55	6.11
33	0.96	3.88	7.59	6.49	10.08	9.01			6.81	6.96
34	0.83	4.38	8.09	7.51	10.72	10.02				
35	1.00	4.93								

Fig. 5. The nearly resolved wing on the red side of the lines $n=24$ to 30 evidently represents these forbidden lines. This broadening is therefore not a true broadening of the lines, but merely represents the occurrence of new lines not clearly resolved by our spectrograph.

The second effect, namely the displacement of the P terms, is qualitatively in the right direction, as may be seen by reference to Fig. 6, in which a few of the high levels of Na and K are plotted to scale for zero field. In both cases repulsion of the P by the F levels will displace them upward, shifting the line to the violet, but the effect should be much larger in Na because P and F lie closer together. The exact separations of these levels are best seen from the values of the quantum defects, given in Table III. In this table is also included a quantity Δ, the difference between the effective quantum number n^* and the nearest whole number. It is Δ which determines the magnitude of the perturbations. Since the quantum defects $n-n^*$ of the F levels are practically zero for all the alkalis, Δ gives the distance from a P level to the nearest F level, expressed as a fraction of the separation of successive P levels. That the perturbation effect should be smaller in K than in Na is clear from these figures.[5] Furthermore, the intensities of the forbidden lines should be smaller in K, and this accounts for the greater symmetry of the π components in this case (Fig. 5).

The quantitative treatment of these perturbations is given in the accompanying paper by Schiff and Snyder. There it is shown that the displacement of the P states is proportional to n^{11}, and inversely proportional to the separation of the P state and the nearest F state. The broken

TABLE III. *Quantum defects of P states.*

	Li	Na	K	Rb	Cs
$n-n^*$	0.04	0.85	1.71	2.66	3.59
Δ	−0.04	0.15	0.29	0.34	0.41

[5] A similar situation arises in the Stark effect; cf. E. Segrè, Rend. Lincei 19, 395 (1934).

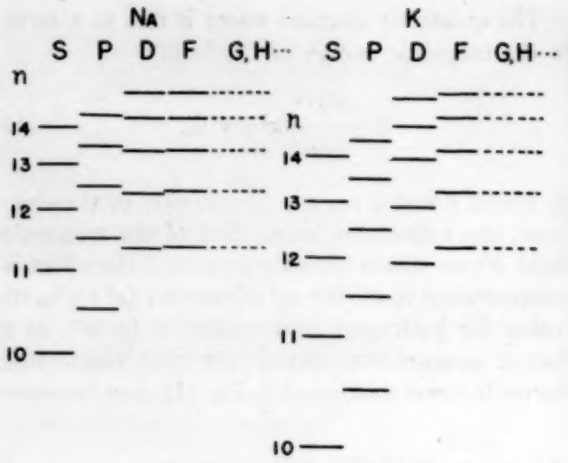

FIG. 6. High terms of Na and K.

curves in Figs. 3 and 4 are plotted from their Eq. (9), and are seen to agree very well up to the point where the lines cease to be relatively sharp, i.e., up to $n=28$ in Na.

For the diffuse maxima above $n=28$ the perturbation by the states of different L is inadequate to account for the observations. In this region the magnetic energy becomes comparable with the separation of states of successive total quantum number n, and thus there occurs a mixing of states differing not only in azimuthal quantum number, but also in total quantum number. This effect is responsible for the large symmetrical broadening of the last observable lines, and also probably for the premature death of the series, which becomes unobservable because of the excessive broadening of its members. The total intensity in this region will, however, remain constant because of the sum rules. For a more quantitative discussion of the effects in this region, and comparison of our measured widths with theory, we again refer to the following paper.

In conclusion, we wish to thank Professor E. O. Lawrence for his cooperation in making the large magnet available. We are also much indebted to Dr. Luis Alvarez, who assisted with the design of apparatus, and to Professor W. F. C. Ferguson, for help with the spectroscopic work.

Theory of the Quadratic Zeeman Effect

L. I. SCHIFF AND H. SNYDER
University of California, Berkeley, California
(Received November 9, 1938)

The experiments of Jenkins and Segrè, reported in the accompanying paper, are considered theoretically. The quadratic Zeeman effect observed in absorption to large orbits in strong magnetic fields is due to the diamagnetic term in the Hamiltonian, which is proportional to the square of the vector potential and hence to the square of the magnetic field. For the alkalis, the problem involves essentially only one electron, and its spin can be ignored. m_l and parity are always exactly defined, while n and l are not. The observed spectrum can be divided up with increasing n into three regions, according as the lines are broadened asymmetrically (region I), broadened further, but nearly symmetrically (region II), and broadened so much as to overlap into a continuum (region III). It is shown that region I corresponds to n being a good quantum number and l a fairly good one; region II to n being a fairly good quantum number and l not good at all; and region III to both n and l breaking down completely as quantum numbers. Good quantitative agreement with the experiments is obtained as long as inter-n perturbations can be neglected. When this can no longer be done (large n), the theory becomes prohibitively complicated, although some qualitative indications can still be obtained from it.

THE quadratic Zeeman effect can arise from two parts of the atomic Hamiltonian. The term linear in the vector potential (and hence in the magnetic field)

$$(e\hbar H/2mc)(m_l+2m_s) \qquad (1)$$

is not a constant of the motion when there is coupling between spin and orbital angular momenta, and therefore gives rise to second-order perturbations proportional to H^2. The diamagnetic term quadratic in the vector potential

$$V=(e^2H^2/8mc^2)r^2\sin^2\theta \qquad (2)$$

gives first-order perturbations that are also proportional to H^2. These two terms are never simultaneously of importance.[1] For (2) is important only for large orbits and strong magnetic fields, in which case the spin and orbital angular momenta are so completely uncoupled that (1) is practically a constant of the motion. This results in a complete Paschen-Back effect, and the electron spin can be ignored entirely. The determination of the atomic level structure under these conditions is reported by Jenkins and Segrè in the accompanying paper (referred to here as JS), and was accomplished by measuring high members of the absorption series from the ground states of sodium and potassium. In this paper, we shall attempt to obtain an understanding of the principal experimental results of JS on the basis of existing atomic theory. For definiteness, we consider sodium, and indicate later how our remarks can be extended to the other alkalis.

It was expected that the experiments of JS would show the well-known quadratic shift of the terms towards higher energies.[1] However, an examination of the microphotometer traces (Fig. 5 of JS) indicates that the situation is more complicated. The observed spectrum can be roughly divided into three regions. In region I ($n<29$), both the $\pi(m_l=0)$ and $\sigma(m_l=\pm1)$ components show an asymmetric broadening; the peaks are on the high energy side of each line. Also, the centers of the lines lie at higher energies than the no-field lines, and the displacements increase with n. As n increases, the lines become broader, and each peak is pushed more to the high energy side of the center of gravity of its line. At the same time the peaks become lower, so that soon the lines become nearly symmetrically broadened (we call this region II, $29<n<33$). Finally the lines become so low and broad that they merge into a continuum showing a weak banded structure (region III, $n>33$). Throughout regions I and II, the centers of both the π and σ lines continue to advance ahead of the no-field lines. In region III, however, this applies only to the σ series. The π series are much more compressed and tend to fall back into step with the no-field series.

[1] Cf. Van Vleck, *Theory of Electric and Magnetic Susceptibilities* (Oxford, 1932), p. 178.

To understand these results, we consider the motion of a single electron in a central field (nucleus plus electron core) and uniform external magnetic field, with neglect of spin. The problem possesses only axial and mirror symmetry, and hence m_l and parity only are exactly defined; the term (2) in the Hamiltonian will prevent n and l from being exact quantum numbers for the terms that interest us. Then the true eigenfunctions can give dipole radiation only by virtue of the amount of $l=1$ state that is mixed into them; moreover, we can restrict our consideration to those upper states for which $m_l=0, \pm 1$. If we choose the usual representation for the unperturbed states in which m_l, n and l are diagonal, then it is readily shown that V has matrix elements between states of all n provided that their l values differ by $0, \pm 2$; since only the $l=1$ part of the perturbed states can radiate, we need consider only the matrix elements of V between states of odd l.

Now according to the Rydberg formula, the P terms in sodium ($l=1$) are depressed by a uniform amount below the corresponding hydrogenic terms (this is due to penetration of the core by the electron when it has low angular momentum), while the $F, H, \cdots$ terms ($l=3, 5, \cdots$) are given quite accurately by the hydrogenic values (see Fig. 6 of JS). The matrix elements of V are proportional to n^4 (see Eq. (3) below), while the separations between successive terms in a series or between corresponding P and F terms are proportional to n^{-3}. Thus, we expect that for small n these separations are large compared to the perturbing energy, and both n and l should be fairly good quantum numbers (region I). Moreover, since the separation between corresponding P and F terms is smaller than the separation between successive terms of a series, we might expect n to be a better quantum number than l, so that we can neglect the inter-n perturbations, and treat the inter-l perturbations as small, in this region. Now the quantum defect for the P series of sodium is 0.85, so that each P term is depressed almost a whole interval below the $F, H, \cdots$ terms of the same n. Thus the important inter-l perturbations will be between a given P term and the $F, H, \cdots$ terms corresponding to an n value that is smaller by one; the P term then lies on the high energy side of the higher l terms with which it combines. This results in a peak on the high energy side of the line, and a smear on the low energy side which is the group of unresolved lines arising from the slightly mixed in terms of higher l. As n increases, l ceases to be a good quantum number before n does. Thus all l terms are thoroughly mixed together, resulting in a nearly symmetric line, while the inter-n perturbations are not yet so large as to seriously affect the regularity of the series (region II). For still higher n values (region III), the inter-n perturbations become so large that n is no longer a good quantum number, and the broadened lines merge together.

Regions I and II

We could hope to deal with regions I and II by neglecting inter-n perturbations, and solving the secular equation obtained from the matrix elements of V between odd l states for a particular m_l and n. But since this matrix has about $n/2$ rows and columns, such a solution would be an extremely tedious matter. However, we can find quite simply the centers of gravity of the broadened lines and their mean square breadths. In region I, we can also find the perturbation of each P state by higher l states consistently to the second order of perturbation theory, and can interpret its perturbed position as the position of the peak of the corresponding broadened line.

To find the matrix of V in these regions, we choose particular values for m_l and n, and label rows and columns according to l values. The angle integrals are readily evaluated, and the only nonvanishing elements that interest us are V_{11}, $V_{13}=V_{31}$, V_{33}, $V_{35}=V_{53}$, etc. In evaluating the radial integrals, we note that because of the r^2 appearing in V, it is important to know the radial functions only for large r, well outside of the inner electronic core. We should thus expect to obtain a good approximation for the radial integrals by using the hydrogenic functions[2] with indices n and l, and putting $n=n^*$ (the effective quantum number) after the integrals are evaluated. For the principal series of sodium ($l=1$), $n^*=n-0.85$, while for the higher series ($l=3, 5, \cdots$), $n^*=n$. As remarked above, however, we expect the mutual perturbations between states

[2] Cf. Condon and Shortley, *Theory of Atomic Spectra* (Cambridge, 1935), p. 114.

of different l to be greatest when their effective quantum numbers (and hence their unperturbed energies) lie closest together. We shall therefore put for the higher l series, $n^*=n-1$. The total energy matrix for a particular m_l and n is:

$$\mathcal{H}_{ll'}(n, m_l)=\mathcal{H}_l^0(n, m_l)\delta_{ll'}+V_{ll'}(n^*, m_l),$$

$$\mathcal{H}_l^0(n, m_l)=-\frac{me^4}{2\hbar^2n^{*2}}+\frac{ehHm_l}{2mc},$$

$$V_{ll}(n, 0)=\frac{\hbar^4H^2}{8m^3c^2e^2}\cdot\frac{n^2[5n^2+1-3l(l+1)](l^2+l-1)}{(2l+3)(2l-1)},$$

$$V_{l,\,l-2}(n, 0)=-\frac{\hbar^4H^2}{8m^3c^2e^2}\cdot\frac{5n^2l(l-1)}{2(2l-1)}\cdot\left\{\frac{(n^2-l^2)[n^2-(l-1)^2]}{(2l+1)(2l-3)}\right\}^{\frac{1}{2}}, \tag{3}$$

$$V_{ll}(n, \pm1)=\frac{\hbar^4H^2}{8m^3c^2e^2}\cdot\frac{n^2[5n^2+1-3l(l+1)]l(l+1)}{(2l+3)(2l-1)},$$

$$V_{l,\,l-2}(n, \pm1)=-\frac{\hbar^4H^2}{8m^3c^2e^2}\cdot\frac{5n^2}{2(2l-1)}\cdot\left\{\frac{(n^2-l^2)[n^2-(l-1)^2](l+1)l(l-1)(l-2)}{(2l+1)(2l-3)}\right\}^{\frac{1}{2}}.$$

To obtain some information from the matrix (3), we assume that it is diagonalized by a normalized real orthogonal matrix S (since $\mathcal{H}$ is real): $\sum_{kl}S_{ik}\mathcal{H}_{kl}S_{jl}=E_i\delta_{ij}$. Then the new eigenfunctions (corresponding to the eigenvalues E_i) are given in terms of the old approximately hydrogenic functions by: $\phi_i=\sum_j S_{ij}\psi_j$. If now we neglect the dependence of the dipole radiation probability on energy over the small range of energies involved in this group of states, this probability will be proportional to the square of the amount of ψ_1 in each ϕ_i, or to S_{i1}^2. The center of gravity of the group of lines is thus given by

$$\bar{E}=\sum_i E_iS_{i1}^2=\mathcal{H}_{11}. \tag{4}$$

The dispersion of the group of lines about their center of gravity, or the mean square breadth of the unresolved broadened line, will similarly be given by:

$$(\Delta E)^2=\sum_i(E_i-\bar{E})^2S_{i1}^2=\sum_i E_i^2S_{i1}^2-\bar{E}^2$$
$$=\sum_j\mathcal{H}_{1j}^2-\bar{E}^2=\mathcal{H}_{13}^2, \tag{5}$$

since $\mathcal{H}_{1j}$ vanishes unless $j=1$ or 3. Neglecting terms of order n^{-2} compared to unity, we thus obtain:

$$\bar{E}(n, 0)=-\frac{me^4}{2\hbar^2n^{*2}}+\frac{\hbar^4H^2n^{*4}}{8m^3c^2e^2},$$
$$\bar{E}(n, \pm1)=-\frac{me^4}{2\hbar^2n^{*2}}\pm\frac{ehH}{2mc}+\frac{\hbar^4H^2n^{*4}}{4m^3c^2e^2}; \tag{6}$$

$$2\Delta E(n, 0)=\left(\frac{3}{7}\right)^{\frac{1}{2}}\cdot\frac{\hbar^4H^2n^{*4}}{4m^3c^2e^2},$$
$$2\Delta E(n, \pm1)=\left(\frac{2}{7}\right)^{\frac{1}{2}}\cdot\frac{\hbar^4H^2n^{*4}}{4m^3c^2e^2}. \tag{7}$$

In Eq. (6), $n^*=n-0.85$; in Eq. (7) we should use a value for n^* approximately halfway between $n-0.85$ and $n-1$, although its precise value is not important. Eq. (6) is well known,[1] and gives the position of the P term if inter-l perturbations are neglected. It is interesting that the center of gravity of the group of lines resulting from these perturbations is still given by the same formula.

Although formulas (6) and (7) apply to both regions I and II, we are, for region I, more interested in the position of the peak E_p of each line than in $\bar{E}$. This can be found by assuming that the inter-l perturbations are not yet strong enough to wipe out the identity of the P state, so that this line will be strongest, and will be shifted towards higher energy by interaction with the other l states. A second-order perturbation calculation gives:

$$E_p=\mathcal{H}_1^0+V_{11}+\sum_{i\neq1}\frac{V_{1i}^2}{\mathcal{H}_1^0-\mathcal{H}_i^0}. \tag{8}$$

Remembering that V_{1i} vanishes unless $i=1$ or 3, and that

$$\mathcal{H}_1^0-\mathcal{H}_3^0=-\frac{me^4}{2\hbar^2}[(n-0.85)^{-2}-(n-1)^{-2}]\approx\frac{me^4\Delta}{\hbar^2n^{*3}},$$

where $\Delta=0.15$, we obtain:

$$E_p(n,0)\approx\bar{E}(n,0)+\frac{3\hbar^{10}H^4n^{*11}}{448m^7c^4e^8\Delta},$$
$$E_p(n,\pm1)\approx\bar{E}(n,\pm1)+\frac{\hbar^{10}H^4n^{*11}}{224m^7c^4e^8\Delta}, \tag{9}$$

where to sufficient approximation, $n^*=n-0.85$. We expect formula (9) to give the position of the peak of the broadened line as long as the peak is well defined and displaced from the center of gravity of the line, that is, throughout region I. In region II, the line is more nearly symmetric, and the peak and center of gravity practically coincide, their position being given by (6).

The transition from region I to region II should take place at such a value n_e of n that the perturbing energy V_{12} and the energy denominator $\mathcal{H}_1^0-\mathcal{H}_2^0$ in (8) are about equal. This gives us the relations:

$$(n_e-0.85)^7\approx\left(\frac{7}{3}\right)^{\frac{1}{2}}\cdot\frac{8m^4c^2e^8\Delta}{\hbar^8H^2},\quad m_l=0,$$
$$\approx\left(\frac{7}{2}\right)^{\frac{1}{2}}\cdot\frac{8m^4c^2e^8\Delta}{\hbar^8H^2},\quad m_l=\pm1. \tag{10}$$

To obtain similar results for the other alkalis, we need only insert into the above formulas (6) to (10) the proper numerical values for n^* and for Δ, which is defined as the effective quantum number for the P series minus the nearest integer; these values are given in Table III of JS.

The measured peaks of the lines are plotted in Figs. 3 and 4 of JS, in which the solid curves are computed from Eq. (6) and the dotted curves are computed from Eq. (9). It will be noted that the experimentally observed peaks follow the dotted curves quite well throughout region I. Towards the end of region I and the beginning of region II, the lines lose their asymmetric character, and the measured peaks begin to give the positions of the centers of gravity of the lines. Thus the experimental points here fall away from the dotted curves and approach the solid curves. This good agreement indicates that the inter-n perturbations in this region do not have an appreciable effect on the positions of the peaks of the lines. On the other hand, the breadths of the lines seem to be given well by Eq. (7), only for rather small values of $n(<25)$. For larger n, the values obtained from Eq. (7) are of the same order of magnitude, but smaller than, the observed values. This seems to indicate that the inter-n perturbations, which were neglected in obtaining (7), do broaden out the lines, and also make the ratio of π to σ breadth larger than the value $(3/2)^{\frac{1}{2}}=1.22$ obtained from (7) (see Table II of JS). The comparison with experiment on this point is complicated by the fact that the mean square breadth defined by (5), and which is most readily calculated, is not simply related to the width at half-maximum, which is most readily measured; however, the two should be of the same order of magnitude.

The value of n at which the transition from region I to region II takes place is given by Eq. (10) as about 29 for the π component, and about 30 for the σ components, in the case of sodium. From Fig. 5a of JS, we see that both these values agree well with experiment. A comparison on this point for potassium is difficult because of the poor definition of the lines.

Region III

In region III, both n and l break down completely as quantum numbers, and we cannot use any of the approximations that made the theory workable in the preceding section. There is a striking experimental observation in this region, however, for which we might hope to get an indication from the theory. This is the compression of the π series relative to the σ series, just before they wash out. One might expect this from the fact that in region II, the π components are much broader than the σ components, thus indicating a greater influence of inter-n perturbations. Then since there are more terms above a given term than below it, and since they get closer together as one goes up the series, the net effect of such perturbations should be to push the terms down and thus compress the series.

Another indication pointing towards the same conclusion can be obtained from an examination of the behavior of the terms near the series limit. Here the electron is controlled mainly by the magnetic field, and it makes many oscillations in this field before it makes one in the Coulomb field. This is the condition for applicability of the adiabatic approximation, which we use here. The solutions of the equations of motion of an elec-

tron in a pure magnetic field are well known,[3] and admit of a continuum of energy levels

$$E=(e\hbar H/2mc)(2\nu+m_l+|m_l|+1)+E_z, \qquad \nu=0, 1, 2, \cdots, E_z\geqq 0, \tag{11}$$

because of the free motion along the field (z direction). We now apply the adiabatic approximation, using the Coulomb field to restrict the motion in the z direction. This gives us a potential for the z motion that is an average of the Coulomb field over the x, y plane for each value of z. We are interested only in the lowest state $\nu=0$, and in $m_l=0$, ± 1; the z potential is then:

$$\begin{aligned} U_0(z)&=-2e^2\beta^{\frac{1}{2}}\exp(\beta z^2)Erfc(|z|\beta^{\frac{1}{2}}), \quad m_l=0,\\ U_1(z)&=-e^2[\beta|z|+\beta^{\frac{1}{2}}\exp(\beta z^2)(1-2\beta z^2)\\ &\quad\times Erfc(|z|\beta^{\frac{1}{2}})], \quad m_l=\pm 1,\\ U_0(0)&=2U_1(0)=-e^2(\pi\beta)^{\frac{1}{2}},\\ U_0\to U_1&\to -e^2/|z|, \quad \text{as} \quad |z|\to\infty; \end{aligned} \tag{12}$$

$$Erfc(x)\equiv\int_x^\infty e^{-t^2}dt;$$

$$\beta\equiv eH/2\hbar c.$$

[3] Cf. Condon and Morse, *Quantum Mechanics* (McGraw-Hill, 1929), p. 79.

Thus U_0 had twice the depth of U_1 at $z=0$ and the same asymptotic form; it can also be shown quite readily that U_0 is less than U_1 for all finite values of z. The total energy is then given approximately by (11), where E_z is now an eigenvalue of the equation:

$$\frac{d^2\chi}{dz^2}+\frac{2m}{\hbar^2}[E_z-U(z)]\chi=0.$$

Then for energies just below the series limit, the eigenvalues for the case $m_l=0$ will be more closely spaced than those for the case $m_l=\pm 1$, since the potential U_0 is considerably deeper than the potential U_1. While this conclusion cannot apply even qualitatively as far from the series limit as the beginning of region III, it serves as another indication that the π component series is expected to be more compressed than the σ component series, as is observed.

It is a pleasure for us to thank Professor J. R. Oppenheimer for several helpful discussions of points that arose in this problem.

JANUARY 1, 1939 PHYSICAL REVIEW VOLUME 55

Surface and Volume Photoelectric Emission from Barium[1]

R. J. CASHMAN AND ELSE BASSOE[2]
Northwestern University, Evanston, Illinois

(Received October 3, 1938)

Spectral sensitivity measurements between 5000 and 2300A have been made on barium surfaces prepared by fractional distillation in a gettered vacuum. The resulting yields are compared with those predicted by Mitchell's square-top barrier theory which is here modified to a form that facilitates comparison with experimental data. From 5000 to 3000A relative values of the observed yields are in good agreement with the modified theory. At 2967A there is an abrupt rise in the experimental curve which continues to the limit of the measurements. This is attributed to the onset of the volume photoelectric effect. The theoretical threshold for the volume effect calculated from the rough formulae of Tamm and Schubin agrees well with the experimental value.

IT is usually assumed in the electron theory of metals that the electrons move independently in a periodic potential field in the metal. The introduction of a metallic surface which is necessary for the photoelectric effect gives rise to a second type of field and complicates the model by destroying the perfect periodicity of the crystal lattice. To avoid this difficulty Tamm and

[1] Presented in part at the Washington meeting of the American Physical Society, April 28–30, 1938.

[2] Now at Leeds and Northrup Company, Philadelphia, Pennsylvania.

Schubin[3] proposed that the photoelectric emission from a metal should be regarded as arising from the superposition of two effects, the surface effect, due to the rapid change in potential at the surface, and the volume effect, due to the internal variations in potential. The argument is based on the fact that an electron in field-free space cannot absorb the energy of a photon and at the same time conserve both energy and momentum. They argue further that the threshold of the volume effect is considerably higher than the threshold for the surface effect since the possible transitions are restricted by a selection rule. The theory of the surface effect can then be simplified by using the Sommerfeld model in which the potential inside the metal is constant.

Experimental tests of the various theories of the surface effect over an extended range of wave-lengths have been confined in the past to observations on the alkali metals. If the theory of Mitchell[4] is taken as the most complete it may be concluded that experimental spectral distributions for the alkalies rise more abruptly and reach a maximum nearer the threshold than is predicted by the theory. In addition the theoretical curves are considerably flatter but the order of magnitude of the photoelectric yields is reasonably good.[5] In view of the rather discordant experimental results for the alkalies both for spectral and energy distributions it seems that more conclusive tests of the theory can be made on metals showing more consistent emission properties. This was the original purpose of the present investigation.

The experimental evidence for the volume effect has been extremely meager. Tamm and Schubin[3] considered the secondary rise which sometimes appears in the spectral distributions of the alkalies as evidence for the volume effect. The ease with which secondary peaks can be produced by contamination of the surface with vapors and gases would lead one to question at least some of these results. Experiments in the far ultraviolet have been carried out on other metals by Kenty,[6] the measurements extending as far as 584A. He found no maximum and subsequent secondary rise as the volume effect predicts. Very recently Baker,[7] working in the Schumann region with cadmium surfaces, has reported a second peak in the emission which he attributes to the volume effect. No attempt was made to work with thoroughly outgassed surfaces.

In the present investigation on spectral distributions, barium was chosen, first, because it possesses the lowest work function of any metal in the pure state with the exception of the alkalies, thereby permitting a wide frequency range, and second, since previous experiments in this laboratory[8] have shown that by using a special vacuum technique its emission properties are extremely stable and reproducible. In order to compare the results obtained with the theory of Mitchell[4] we have made certain simplifications in the theory which seem justifiable and obtain a result for the spectral distribution which may be readily applied to any metal.

Surface Photoelectric Effect

Modified Mitchell theory

The expression obtained by Mitchell (1934 paper, Eq. (83)) for the photoelectric current per unit power of incident radiation contains the frequency, threshold, and angle of incidence as well as the optical constants of the metal. The optical constants appear since the effect of reflection and refraction of the light has been included to prevent the emission from becoming infinite for grazing incidence and zero for normal incidence. The introduction of the optical constants into the theory may yield a more correct dependence of the emission on the angle of incidence but at present makes a critical test of the spectral distribution in this form improbable since very little is known experimentally of the variation of these constants with frequency for

[3] Tamm and Schubin, Zeits. f. Physik **68**, 97 (1931).
[4] K. Mitchell, Proc. Roy. Soc. **A146**, 442 (1934); **A153**, 513 (1936).
[5] The calculations of R. D. Myers, Phys. Rev. **49**, 938 (1936) and of A. G. Hill, Phys. Rev. **53**, 184 (1938) using an image field barrier show a maximum in the spectral sensitivity curve slightly nearer the threshold than the Mitchell theory with the square top barrier. L. I. Schiff and L. H. Thomas, Phys. Rev. **47**, 860 (1935), applied the quantum mechanical theory of the scattering of light by conduction electrons. This refinement also brings the maximum nearer the threshold, though the integral is too complicated for exact evaluation.
[6] Kenty, Phys. Rev. **44**, 891 (1934).
[7] Baker, J. Opt. Soc. Am. **28**, 55 (1938).
[8] Cashman and Huxford, Phys. Rev. **48**, 734 (1935); Jamison and Cashman, Phys. Rev. **50**, 624 (1936).

the desired range. An objection of fundamental importance is the fact that bulk metal optical constants are introduced into the theory of a surface phenomenon. The electrons exist originally in the force field at the surface but the constants of the light wave vary over a distance of the order of a wave-length into the metal. Consequently we consider only the incoming light wave without regard to the perturbation of the electric vector produced by the surface field with the realization that the dependence of the emission on angle of incidence will be incorrect but with the expectation that the form of the spectral distribution curve will be right. With this simplification the Mitchell theory for the square top potential barrier becomes

$$P_z=\frac{e^2\nu_a\sin^2\theta}{16\pi^5m^2c\cos\theta}\int_0^\infty\int_0^\infty\int_{\{\mu(\nu_a-\nu)\}^{\frac{1}{2}},0}^\infty \cdot\frac{4k_z^2\{k_z^2+\mu(\nu-\nu_a)\}^{\frac{1}{2}}}{\nu^4\{(k_z^2+\mu\nu)^{\frac{1}{2}}+[k_z^2+\mu(\nu-\nu_a)]^{\frac{1}{2}}\}^2} \cdot\frac{dk_xdk_ydk_z}{1+\exp h^2(k_x^2+k_y^2+k_z^2-\mu\bar{\nu})/8\pi^2mkT}, \quad (1)$$

where P_z is the emission per unit incident energy (e.s.u./erg), the k's the electron wave numbers associated with the x, y, and z directions, θ the angle of incidence, ν_a the frequency associated with the surface potential step, $\bar{\nu}$ the frequency associated with the width of the Fermi band at absolute zero, and μ a constant equal to $8\pi^2m/h$. In the k_z integration the lower limit is $\{\mu(\nu_a-\nu)\}^{\frac{1}{2}}$ if $\nu<\nu_a$ and 0 if $\nu>\nu_a$.

In order to evaluate (1) we introduce the cylindrical coordinates u, ρ and φ where u is the normal component of velocity. Then $k_z=(2\pi mu/h)$, $k_y=(2\pi m/h)\rho\cos\varphi$, $k_z=(2\pi m/h)\rho\sin\varphi$. Further let $\exp(m\rho^2/2kT)=Z$. Integrating with respect to Z and φ and letting $\frac{1}{2}mu^2+h(\nu-\nu_a)=kTy$, we have

$$P_z=\frac{B(kT)^2}{(h\nu)^4}\int_{0,\ h(\nu-\nu_a)/kT}^\infty \log[1+\exp(\beta-y)] \times\frac{(kTy+W_a-h\nu)^{\frac{1}{2}}(kTy)^{\frac{1}{2}}dy}{[(kTy+W_a)^{\frac{1}{2}}+(kTy)^{\frac{1}{2}}]^2}, \quad (2)$$

where

$$B=8e^2W_a\sin^2\theta/hc\cos\theta, \quad W_a=h\nu_a,$$
$$\beta=h(\nu-\nu_0)/kT, \quad \nu_a-\bar{\nu}=\nu_0,$$

the threshold frequency. Obviously kTy is the normal kinetic energy of the electron outside the metal. We now expand the fractional part of the integrand in powers of $(kTy/W_a)^{\frac{1}{2}}$ and (2) becomes, after converting to amperes per watt

$$P_z=\frac{B(kT)^2}{e(h\nu)^4}\sum X_m\int_0^\infty y^{\frac{1}{2}m}\log[1+\exp(\beta-y)]dy. \qquad m=1,2,3,\cdots. \quad (3)$$

The quantities $h\nu$, W_a and kT are expressed in electron volts. Let $a=1-h\nu/W_a$ and $b=kT/W_a$ then $X_1=(ab)^{\frac{1}{2}}$, $X_2=-2a^{\frac{1}{2}}b$, $X_3=\frac{1}{2}(4a^{\frac{1}{2}}+a^{-\frac{1}{2}})b^{\frac{1}{2}}$, $X_4=-(a^{\frac{1}{2}}+a^{-\frac{1}{2}})b^2$, $X_5=(a^{-\frac{1}{2}}-a^{-\frac{1}{2}}/8)b^{5/2}$.

Integrals of the type represented in Eq. (3)

$$I_m=\int_0^\infty y^{\frac{1}{2}m}\log(1+e^{\beta-y})dy, \qquad m=0,1,2,3,\cdots$$

or its equivalent form

$$I_m=\frac{2}{m+2}\int_0^\infty\frac{y^{\frac{1}{2}m+1}}{e^{y-\beta}+1}dy$$

occur in many applications of the Fermi statistics to the electron theory of metals, and there has been need for a complete solution. Sommerfeld, Nordheim and others have given approximate solutions valid for negative or large positive values of β. Here we give complete solutions for all values of β:

For $\beta\leqq0$:

$$I_m=\Gamma(\tfrac{1}{2}m+1)\sum_{s=1}^\infty\frac{(-1)^{s-1}}{s^{\frac{1}{2}m+1}}e^{s\beta}. \quad (4)$$

For $\beta>0$:

$$I_m=\frac{4\beta^{\frac{1}{2}m+2}}{(4+m)(2+m)} +2\sum_{k=0}^{l}\frac{m!!}{(m-4k)!!2^{2k}}C_{2k+2}\beta^{\frac{1}{2}m-2k}+R(m), \quad (5)$$

where the summation over k is extended to the largest integer l which gives a positive or zero power of β, depending on m. The constant C_{2k+2}

is defined by

$$C_{2k+2}=\sum_{s=1}^{\infty}\frac{(-1)^{s-1}}{s^{2k+2}}=\left(1-\frac{1}{2^{2k+1}}\right)\zeta(2k+2). \quad (6)$$

Values of the zeta function for real variables may be obtained from standard tables.[9] The remainder $R(m)$ is given as follows: if $\frac{1}{2}m$ is an integer,

$$R(m)=\pm(\tfrac{1}{2}m)!\sum_{s=1}^{\infty}\frac{(-1)^{s-1}}{s^{\frac{1}{2}m+2}}e^{-s\beta}, \quad (7)$$

where the + sign is to be used if $\frac{1}{2}m$ is odd, the − sign if $\frac{1}{2}m$ is even. If $\frac{1}{2}m$ is a half-integer:

$$R_m=[\tfrac{1}{2}m(\tfrac{1}{2}m-1)\cdots\tfrac{1}{2}]\sum_{s=1}^{\infty}\frac{(-1)^{s-1}}{s^{\frac{1}{2}m+2}}$$

$$\times\left\{\pi^{\frac{1}{2}}e^{s\beta}[1-\Phi([s\beta]^{\frac{1}{2}})]\pm 2e^{-s\beta}\int_0^{(s\beta)^{\frac{1}{2}}}e^{x^2}dx\right\}, \quad (8)$$

where the + sign is used if $\frac{1}{2}(m+1)$ is an even integer, the − sign if $\frac{1}{2}(m+1)$ is odd. In the latter case the remainder is usually negligible. $\Phi([s\beta]^{\frac{1}{2}})$ is the probability integral with limit $(s\beta)^{\frac{1}{2}}$. Tables of $\int_0^a e^{x^2}dx$ are available to $a=2$ (reference 9), and the integral may be calculated by an asymptotic expansion for large $a(=[s\beta]^{\frac{1}{2}})$ though the remainder $R(m)$ in this case is generally negligible.

The above solution of (1) holds well for the long wave-length side of the maximum of the spectral sensitivity curve (see Fig. 2) but the calculations become rather laborious for the short wave-length side since the convergence of (3) is not rapid for large β. Numerical integration for this region is easily carried out by noting that the integrand in (2) can be written

$$\log[1+e^{\beta-y}]\left(\frac{kT}{W_a}\right)^2\left[\frac{W_i}{kT}-(\beta-y)\right]^{\frac{1}{2}}$$

$$\times y^{\frac{1}{2}}\left[\left(y+\frac{W_a}{kT}\right)^{\frac{1}{2}}-y^{\frac{1}{2}}\right]^2,$$

where $W_i=h\bar{\nu}$. Hence the integrand can be split into two factors $f(y)$ and $F(\beta-y)$ and graphs of $f(y)$ against y and $F(\beta-y)$ against $(\beta-y)$ obtained. From these one gets $F\times f$ for a plot of the integral for any β.

[9] Cf. Jahnke-Emde: *Tables of Functions*.

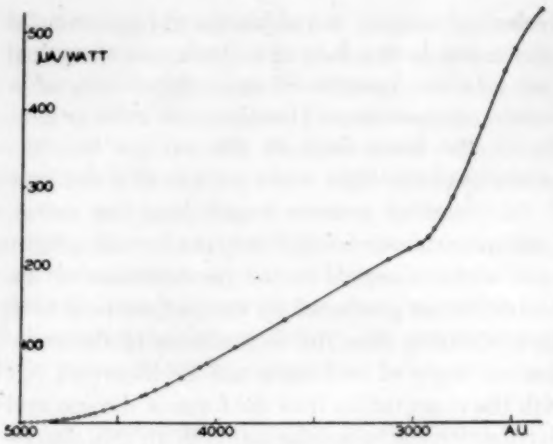

FIG. 1. Photoelectric yield for barium, for unpolarized light at approximately 60° incidence. $\varphi_0=2.49$ ev.

VOLUME PHOTOELECTRIC EFFECT

No calculations have been made to our knowledge of the emission as a function of frequency for the volume effect. Tamm and Schubin,[3] however, have made an estimate of the threshold position using the Bloch eigenfunction for electrons in the periodic field of a metal lattice. If it is assumed that there is one electron per atom, the lattice constant $a=n^{-\frac{1}{3}}$, where n is the number of electrons per unit volume. Their result for the volume threshold at absolute zero becomes

$$\nu_0=2(\nu_1\nu_a)^{\frac{1}{2}}-\nu_1 \quad \text{where} \quad \nu_1=4(\pi/3)^{\frac{1}{2}}\bar{\nu}. \quad (9)$$

EXPERIMENTAL TECHNIQUE

The construction of the phototube and the method of forming the barium surface were similar to that described in previous reports from this laboratory.[8] The envelope was made from a thin Corex D cylindrical blank whose ultraviolet transmission was previously determined. The barium was finally evaporated onto an outgassed movable nickel plate which served as cathode.

Optical system

The light sources employed were a tungsten filament lamp, a 110-volt Uviarc and an H3 high pressure Hg arc with the outer envelope removed. The radiation was focused by means of a quartz-flourite lens onto the entrance slit of a Gaertner monochromator whose exit slit had been removed. The dispersed radiation from this instrument was allowed to fall on a second Gaertner

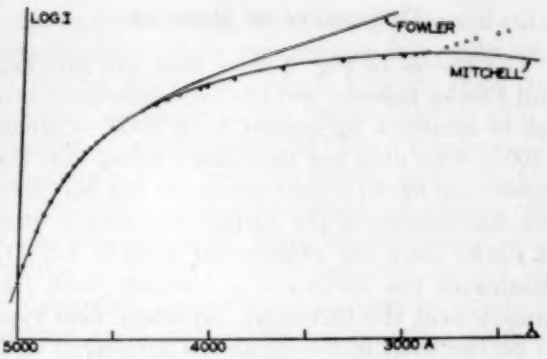

FIG. 2. Comparison of photoelectric yield from barium with theory. Circles are experimental values. Ordinates in arbitrary units. The maximum emission for the Mitchell theory is at 2720A.

monochromator of special design set in such a position that the entrance slit served as exit slit for the first instrument. The construction of the second instrument was such that its optical path was a mirror image of the optical path through the first instrument. The radiation from the exit slit was condensed by a special calibrated achromatic combination consisting of two quartz lenses, fixed to move in opposite directions to or from their optical center. Converging quartz lenses were placed against the entrance and exit slits of the second instrument so that the radiation from near the ends of the slits would not miss the lens which followed. This arrangement was particularly effective in the ultraviolet for increasing the energy output of the system. All slits were set at from 0.1 to 0.2 mm throughout the range of wave-lengths used. No scattered radiation could be detected.

Measurements of the energy of the resolved radiation were made with an improved form of Nichols radiometer[10] and with an evacuated Cartwright thermocouple. For the radiometric measurements an aluminum mirror was fixed about a vertical axis and mounted near the end of the condensing system. Rotation of the mirror through 90° served to expose alternately either the vane of the radiometer or the photoelectric surface to the radiation. With this arrangement the time between observations of photoelectric current and corresponding radiant energy was limited only by the period of the radiometer. For the thermocouple measurements it was found more feasible to mount the phototube beyond the end of the condensing system outside the principal focus and move the thermocouple in or out of the beam of radiation by means of a carriage mounted on a micrometer screw. Slit lengths were reduced to 3 mm so that the final image just covered the thermocouple junction. Measurements of the radiant energy could be made within a few seconds before or after the photocurrent measurement. A Leeds and Northrup galvanometer of sensitivity 5×10^{-8} volt/mm was used with the thermocouple and an FP 54 Pliotron in the circuit of DuBridge and Brown[11] served for the photocurrent measurements.

The thermocouple sensitivity was considerably enhanced by obtaining a low vacuum. To facilitate this the couple was pumped with a diffusion pump for several days and finally sealed off with a side tube containing outgassed barium in a tungsten spiral filament. Slow evaporation of the barium together with an occasional glow discharge in the side tube produced a vacuum which made the thermocouple extremely sensitive. Care must be exercised not to burn out the thermocouple wires during the glow discharge. The radiometer sensitivity was about ten times greater than that of the thermocouple-galvanometer combination but considerably more time was required to get readings due to the long period of the radiometer. This was objectionable when the arcs were unstable.

In obtaining a set of data by either method the monochromators were set at a particular wavelength and several consecutive readings made of the photocurrent and intensity of radiation. This procedure reduced the effect of arc fluctuations to a minimum. The two methods were in agreement within the limit of experimental error.

RESULTS

Measurements taken within an hour after the barium coating was formed and extending over a period of five months showed no observable changes with time in the emission as a function of frequency. The average of several runs is shown in Fig. 1 where the photoelectric yield in microamperes per watt has been plotted against wavelength. The work function for this surface as

[10] B. J. Spence, J. Opt. Soc. Am. **6**, 625 (1922).

[11] DuBridge and Brown, Rev. Sci. Inst. **4**, 532 (1933).

obtained by Fowler plots[12] is 2.49 ev. This value is 0.02 ev lower than that found by one of us[8] for barium deposited on glass. By reversing the electrode connections it was possible to draw electrons from barium deposited on the glass wall of the tube. This surface had the work function 2.51 ev, in agreement with the former value. This evidence together with previous results on the effect of heat treatment of the surface[8] leads us to believe that the small change in work function is attributable to slight differences in surface crystal structure rather than to gas contamination. Surfaces of a composite character or clean surfaces exposed to traces of gas show enhanced "temperature tails" on their spectral distribution curves and give the appearance of a metal emitting photoelectrons at a higher temperature. Fowler plots of the emission from such surfaces show response to wave-lengths several hundred angstroms longer than the threshold. These phenomena were not observed for the surfaces studied. The geometrical arrangement of the various elements of this phototube was such that the nickel plate would be appreciably heated by radiation during the deposition of the barium, whereas the glass wall was kept at room temperature. The coating on the nickel plate has the appearance of a finely etched surface but the coating on the glass is specular. There is considerable evidence in the literature from electron diffraction studies that a metal surface formed by condensation may have a preferential crystal growth depending on the backing surface and its temperature.

In comparing the results with the Mitchell theory (Fig. 2) we have plotted logarithms of the current because of the incorrect factor involving the angle of incidence[13] contained in Eq. (3). A vertical shift of the experimental points should superimpose them on the theoretical curve, log P_s *vs.* λ (Eq. (3)). The following constants were used in the theoretical equation: $kT=0.0259$, $h\nu_0=2.49$, $W_i=3.58$, $W_a=6.07$, all in electron volts. We have also shown in Fig. 2 the variation in theoretical current with wave-length as predicted by the simple Fowler theory.

[12] Fowler, Phys. Rev. **38**, 45 (1931).

[13] It is interesting that for $\theta=60°$ the theoretical current is about one-sixth the experimental current for the wave-length range 5000 to 3000A.

Discussion of Results

The curves of Fig. 2 show that the Mitchell and Fowler theories and the experimental points are in excellent agreement from 5000 to about 4300A. This does not necessarily mean that the square-top model is the correct one but only that the distribution of the surface electrons is that of Fermi since the exponential term in Eq. (1) dominates the variation in emission with frequency near the threshold. An image field type of barrier leads to results also in agreement with Fowler near the threshold.[14]

It is well to mention here that the effect of temperature on the emission at the threshold as predicted by Eq. (3) is no longer a T^2 relation as given by Fowler's[12] and DuBridge's[15] simpler theory but of the form $T^{5/2}(A-BT^{\frac{1}{2}}+CT-\cdots)$ where the work functions are considered constant. This would predict a temperature dependence of Ba slightly under $T^{5/2}$ at the threshold. This is nearer the Young and Frank ($T^{5/2}$) theory,[16] which is based on an approximation valid only near the threshold. The work functions themselves, however, are known to vary with temperature,[17] and this will alter the effective temperature dependence.

From 5000 to about 3000A the experimental data are in good agreement with the Mitchell theory (Fig. 2), a result which might not be expected in view of the rather arbitrary value assigned to the number of electrons per unit volume in calculating W_i. Here we have used 2 electrons per atom. Calculations by Wigner and Seitz[18] on sodium and by Hill[19] on beryllium indicate that for these metals the value is closer to 1. Fortunately the theoretical curve is rather insensitive to small changes in W_i. Fig. 1 shows that near the wave-length 2967A, in the region where the emission is beginning to flatten out, there is an abrupt rise which continues to 2345A, the limit of the measurements. This phenomenon we believe is unquestionably due to the onset of the volume effect. The theoretical curve reaches a peak in this region at 2720A. There are two

[14] K. Mitchell, Proc. Camb. Phil. Soc. **31**, 416 (1935).

[15] DuBridge, *Actualités Scientifiques et Industrielles* No. 268 (Paris).

[16] Young and Frank, Phys. Rev. **38**, 838 (1931).

[17] R. J. Cashman, Phys. Rev. **52**, 512 (1937).

[18] Wigner and Seitz, Phys. Rev. **43**, 804 (1933).

[19] A. G. Hill, Private communication.

reasons for believing that the experimental curve would also reach its maximum in this region were it not for the volume effect. First its slope continually decreases in the region 3129 to 2967A. Second, it will be observed that the slope of the experimental curve below 2600A decreases. One interpretation is that the supply of surface electrons diminishes for wave-lengths below about 2600A so that the total emission (surface and volume electrons) does not increase as rapidly for shorter wave-lengths. We believe, then, that the Mitchell theory with the modifications given above gives an adequate account of the variation in photoelectric yield with wave-length for the surface effect from barium.

In his 1936 paper Mitchell made certain refinements in the theory, designed to take into account surface roughness and lattice structure of the metal. The latter consideration would change the width of the energy band occupied by the conducting electrons at 0°K and hence change $\bar{p}$. Thus two parameters are introduced, ω and ν_0, whose values are adjusted to give the best fit to experimental data. The refined theory compared favorably with the results of Klauer[20] for clean potassium surfaces after an arbitrary choice of parameter values. It appears unnecessary to invoke these quantities in the present work, though an attempt to correlate the theory with the actual yield would undoubtedly require some factor involving the surface roughness.

The theoretical threshold for the volume effect obtained from Eq. (6) is 2950 or 3100A depending on the value assigned to $\bar{p}$ and hence ν_a. Because of the rough assumptions underlying the theory the agreement with the experimental value is satisfactory. The abrupt rise of the emission curve beyond the volume threshold is in marked contrast to the gradual rise after the surface threshold. The latter is dominated by the Fermi probability factor, rather than by the slowly varying excitation and transmission probabilities. The sudden rise in the curve for the volume effect should be explainable in terms of the transition probabilities between discreet energy zones. Another question of interest is the fraction of incident light energy available for the volume effect. Previous experiments[21] on Ba indicate that only $\frac{1}{2}$ percent of the incident light is absorbed by surface electrons. Hence practically all the light is absorbed by internal electrons, and thus one would expect an optimum theoretical yield of almost 50 percent were it not for secondary effects of scattering, re-emission, etc., which are estimated by Sommerfeld[22] to reduce the expected yield from the volume effect to about one percent.

A more complete theory of the spectral and energy distributions for the volume effect should be undertaken. Experiments are now in progress in this laboratory on the normal and total energy distributions for barium from the threshold to 2000A. It would be expected *a priori* that the energy distribution for the volume effect would be considerably different than for the surface effect. If it is possible to separate the two effects considerable information would be obtained about the actual energy states in the metal.

ACKNOWLEDGMENTS

We wish to express our thanks to the Committee on Research Funds of the Graduate School, Northwestern University, for two different grants which have made possible the purchase and construction of most of the equipment described herein. We are indebted also to Professor B. J. Spence of the Physics Department for his cooperation in the construction of the optical system.

[20] Klauer, Ann. d. Physik **20**, 909 (1934).

[21] Cashman and Jamison, Phys. Rev. **50**, 568 (1936).

[22] Sommerfeld, *Handbuch d. Physik* Vol. 24, No. 2, p. 472.

On the Iteration Method and Its Application to the Oxygen Problem*

GABRIEL HORVAY[1]
Columbia University, New York, New York
(Received August 10, 1938)

Past calculations for nuclei heavier than He lead to approximate binding energies considerably less than the experimental values. There are two possible explanations, still in need of clarification: (1) the Hamiltonian is wrong, (2) the convergence of the variation or perturbation methods used is too slow to yield sufficiently accurate results with a reasonable amount of work. A variational method which is essentially equivalent to a perturbation calculation including first-, second-, and third-order contributions to the energy yields strong evidence for believing that in the lowest state of the selected Hamiltonian the oxygen nucleus has a finite radius and the binding energy is greater than that of four α-particles. The Hamiltonian is assumed in the form of "Wigner's first approximation." It is the simplest form which leads to saturation. Methods of extrapolation permit an estimate of its true binding energy, and an approximate value of about 230 mc^2 is obtained. Slowness of convergence is also demonstrated. This paper is concerned with an analysis of the evidence which leads to the above conclusions. The variational method used is the "iteration method" described in Appendix I. It presents many interesting features, notably it permits an estimate of the lowest eigenvalue of the Hamiltonian. The formalism necessary for the calculation of the matrix elements is derived in Appendices II–IV.

INTRODUCTION

CORRELATION of calculations and experiments on binding energies of nuclei in the He shell and on proton and neutron scatterings is the principal source of our present-day knowledge of nuclear forces. Now we have a fair picture of the exchange nature of the forces, their range, their depth, their symmetry properties. Whether the knowledge thus gathered exhausts the most fundamental laws of nuclear processes, or whether some very important links are still missing will come to light when further nuclear properties have been investigated mathematically, and compared with experiments to determine the adjustments which must be made in the present theory. Easily accessible properties for such investigations are the excited levels of very light nuclei, and the binding energies of nuclei in the oxygen shell. Experiments on the latter are very reliable, much new material has recently been obtained concerning the former. But even in these simple problems the theoretical considerations involve extremely laborious calculations.

Nevertheless some headway has been made with excited levels. On the other hand, calculations on binding energies of nuclei beyond the α-particle have not led to any definite conclusions. The principal aim in most of these calculations centered on the accurate determination of the binding energies of oxygen and lithium. Oxygen has been chosen because complete shell configurations permit the use of rather simple approximate wave functions, lithium because it was expected that the small number of particles would give rise to rapid convergence in the mathematical treatment. Nevertheless, the calculated higher approximations gave only small improvement and the question arises whether the eigenvalue to which the process may ultimately converge does not lie considerably higher than the experimental value. And there is even doubt whether a closely bound state is the lowest state of the Hamiltonian.[2]

* Publication assisted by the Ernest Kempton Adams Fund for Physical Research of Columbia University.
[1] University Fellow, 1937–38.

[2] The earliest paper on this subject is that of Heisenberg (Zeits. f. Physik **96**, 473 (1935)). In order to estimate the binding energies of He^4, O^{16}, Ca^{40}, Heisenberg made a variational calculation in which he introduced the use of determinantal wave functions constructed from single particle oscillator functions. Inglis (Phys. Rev. **51**, 531 (1937)) made a second-order perturbation calculation for Li^6 and found, that only by assuming an extreme form of the Hamiltonian with large spin exchange forces, could he account for the stability of Li^6. Carroll and Margenau (Phys. Rev. **53**, 920 (1938)) used a more rigorous variational method for Li^6 with wave functions representing doubly excited configurations and reported a large discrepancy between calculated and experimental results. Only Euler (Zeits. f. Physik **105**, 553 (1937)) found very good convergence. Euler used plane waves in making a second-order perturbation calculation for heavy nuclei and obtained considerable improvement over first-order results. He treated the entire interaction as a perturbation. It is doubtful whether the usual perturbation theory has any meaning if the perturbation is as large as in Euler's calculation.

The primary aim of the present paper was to find a reasonably accurate solution of the oxygen equation,

$$H\varphi = E\varphi. \tag{1a}$$

The Hamiltonian was assumed in the form of "Wigner's first approximation"

$$H = T - T_{c.g.} + W/5 + 4M/5, \tag{1b}$$

where[3]

$$\begin{aligned} T &= -\tfrac{1}{2}\textstyle\sum_1^{16}\Delta_i = \text{kinetic energy},\\ T_{c.g.} &= -(1/32)\Delta_{c.g.} = \text{kinetic energy of the center of gravity},\\ W &= \textstyle\sum\sum_{i<j} J(r_{ij}) = \text{Wigner potential},\\ M &= \textstyle\sum\sum_{i<j} J(r_{ij}) P_{ij} = \text{Majorana potential}, \end{aligned} \tag{1c}$$

$$\begin{aligned} J(r_{ij}) &= (1-g)A \exp\left[-\alpha r_{ij}^2\right],\\ g &= 0.22, \quad A = -72, \quad \alpha = 16. \end{aligned} \tag{1d}$$

Energies are given in mc^2 units, lengths in mean Compton wave-lengths (8.97×10^{-13} cm).

Since a dependable solution could not be obtained, an attempt was made to find an answer to the important question: Is the lowest state of oxygen represented by the Hamiltonian (1b) a closely bound state, or is it a state in which it is dissociated into four noninteracting α-particles? (The latter with an energy of about -220 is certainly a possible state for oxygen, and it is probably the lowest dissociated state if a dissociated state is the lowest.)

The simplest saturation type of Hamiltonian is (1b). Coulomb forces have been neglected. For experimental comparison it is therefore preferable to use the value -270 rather than the value -250, the actual binding, when the Coulomb repulsions are effective. There are two other combinations of the four simple types of exchange forces which lead to saturation.[3] These ought to be added to the above Hamiltonian. In the first approximation their effect cancels out, in higher approximations they will most likely lower the energy.[4] These terms were omitted to make calculations as simple as possible.[5]

The method of approach in this problem will be the same as that used by Feenberg and his coworkers in their successful attack on the He-shell problems.[6] Let Ψ_0 be a trial function. Use the best combination $\Psi_0+\lambda H\Psi_0$ as a new wave function. This method will be called the *iteration method*. It will be of order $n+1$ if a combination of the functions

$$\Psi_0, \Psi_1 = H\Psi_0, \cdots, \Psi_n = H^n\Psi_0 \tag{2}$$

is used as wave function. In general for $n=\infty$ the functions $H^k\Psi_0$ should form a complete set for the representation of the true normal state solution, and the lowest root of the secular equation (3) will tend to the normal state eigenvalue of Eq. (1a) as $n\to\infty$. The secular equation is

$$|E1_{ij}-H_{ij}| = \begin{vmatrix} E-H_1 & EH_1-H_2 & \cdots & EH_n-H_{n+1} \\ EH_1-H_2 & & & \\ \vdots & & & \\ \vdots & & & \\ EH_n-H_{n+1} & \cdots & & EH_{2n}-H_{2n+1} \end{vmatrix} = 0, \tag{3}$$

where

$$H_n \equiv \int \Psi_0^* H^n \Psi_0 d\tau. \tag{4}$$

It is obtained in the usual way from the variational principle.

$$\delta\frac{(\Psi, H\Psi)}{(\Psi, 1\Psi)} = \delta\frac{\sum\lambda_i^*\lambda_j H_{i+j+1}}{\sum\lambda_i^*\lambda_j H_{i+j}} = 0.$$

Ψ_0 is assumed to be normalized. The normalized ground state combination of the first $n+1$

[3] For discussion see Feenberg and Phillips, Phys. Rev. **51**, 597 (1937).

[4] If the first-order perturbation vanishes then the negative second-order term becomes predominant.

[5] An estimate of their contributions will be given at a future time.

[6] Various papers in the Physical Review, 1935–37. For the use of the method compare also Hasse, Proc. Camb. Phil. Soc. **26**, 542 (1930).

functions will be denoted by

$$\Psi(0, 1, \cdots, n) = \lambda_0\Psi_0 + \lambda_1\Psi_1 + \cdots + \lambda_n\Psi_n = \lambda_0\Psi_0 + \lambda_1'\Psi_1' + \cdots + \lambda_n'\Psi_n' \quad (5)$$

A primed function denotes normalization.[7]

Ψ_0 may depend on some parameter σ. To emphasize this fact it may be written as $\Psi_0(\sigma)$. It will be convenient to assume $\Psi_0 \to 0$ as $\sigma \to 0$.

The iteration method has many uses. The most important which concern the present problem are discussed in Appendix I. In Appendices II–IV the method of evaluating matrix elements in terms of a Hartree-Fock determinant Ψ_0 are presented. In the succeeding section the results are analyzed for the special case of oxygen to which the methods of Appendices I–IV give rise.

Binding Energy of O^{16}

With a determinantal wave function (19) constructed from single-particle functions (26), a second-order iteration calculation was performed in an attempt to obtain a fair approximation of the binding energy of oxygen. The calculation of H_1, H_2, H_3 necessitated the evaluation of their components V_{ij} by formulae (30). Table I gives the numerical values of these matrix elements for $\sigma = 0.1, 0.3, 0.5, 0.6, 0.7, 1.0$, where σ is the parameter which determines the spread of the wave function (see Eq. (26)). In computing them the numerical constants given in (1d), namely $A = -72$, $\alpha = 16$, were used. However, multiplication by the proper power of $\rho = -A/72$ and $\kappa = \alpha/16$, as indicated in column 2, permits their

[7] $\psi' = [\int \psi^* \psi d\tau]^{-\frac{1}{2}} \psi$. The average of H^n, $\langle H^n \rangle$, in terms of $\Psi(0, \cdots, n)$ will be denoted by $H_n(0, \cdots, n)$. Actually $H\Psi_0$ is a sum of components Ψ_0, $\Psi_W = W\Psi_0$, $\Psi_M = M\Psi_0$, $\Psi_T = T\Psi_0$. For these quantities a similar notation will be used. For example, the normalized ground state combination of Ψ_M and Ψ_T will be denoted by $\Psi(M, T)$, and the corresponding $\langle H^n \rangle$ by $H_n(M,T)$. $H_1(n) = H_{2n+1}/H_{2n}$, $H_1(W) = H_{WW}/1_{WW}$ are special cases.

Table I. *Components of H_1, H_2, H_3.* ($\rho = -A/72$, $\kappa = \alpha/16$).

Matrix Elements	Multiply Columns by	σ=0.1	0.3	0.5	0.6
1_{OO}	1	1	1	1	1
$1_{WO} = W_{OO}$	$10^2\rho$	−0.79003131	−3.70231452	−7.13327805	−8.8714251
$1_{MO} = M_{OO}$	"	−0.62210195	−1.97825164	−2.81007923	−3.0679716
$1_{TO} = T_{OO}$	$10^2\kappa$	0.57600000	1.72800000	2.88000000	3.4560000
$1_{WW} = W_{WO}$	$10^4\rho^2$	0.79291641	14.8765051	53.8312460	82.6707152
$1_{MW} = W_{MO} = M_{WO}$	"	0.62692515	7.7530280	20.5263081	27.6441960
$1_{MM} = M_{MO}$	"	0.53172595	4.3825813	8.5365413	10.1049301
$1_{WT} = W_{TO} = T_{WO}$	$10^4\rho\kappa$	−0.47341646	−6.6352141	−21.2413169	−31.6550283
$1_{MT} = M_{TO} = T_{MO}$	"	−0.37058263	−3.4968892	−8.2140777	−10.7277746
$1_{TT} = T_{TO}$	$10^4\kappa^2$	0.34099200	3.0689280	8.5248000	12.2757120
W_{WW}	$10^6\rho^3$	−0.95915997	−64.7371148	−429.880403	−809.591924
$W_{MW} = M_{WW}$	"	−0.75620488	−32.6347528	−157.266252	−259.444097
$W_{MM} = M_{MW}$	"	−0.63938896	−18.1471562	−64.210969	−93.221053
M_{MM}	"	−0.55460095	−10.5583551	−27.321176	−34.744447
W_{WT}	$10^6\rho^2\kappa$	0.49007229	27.5710507	165.384629	303.965205
$W_{MT} = M_{WT}$	"	0.38500626	14.1709956	61.926272	99.657446
M_{MT}	"	0.32454263	7.9007577	25.289590	35.715336
T_{WW}	"	0.56659026	28.0441832	166.764140	306.017155
T_{MW}	"	0.44614564	14.3605532	62.149852	99.857979
T_{MM}	"	0.40430964	8.3414451	26.196321	36.853534
W_{TT}	$10^6\rho\kappa^2$	−0.29066536	−12.1856647	−64.827077	−115.773822
M_{TT}	"	−0.22625261	−6.3393488	−24.637078	−38.499607
T_{WT}	"	−0.29184030	−12.2312867	−65.050269	−116.156049
T_{MT}	"	−0.22703673	−6.3544151	−24.675813	−38.547555
T_{TT}	$10^6\kappa^3$	0.20732314	5.5977247	25.915392	44.781797

determination for arbitrary A and α. It was found that $\sigma=0.5$ yields the best solution. For this case the S and P shell components are listed as well. (SP interaction terms are obtained by taking $(V_{ij})_{SP}=V_{ij}-(V_{ij})_S-(V_{ij})_P$.)

Table II gives the fundamental quantities H_1, H_2, H_3, calculated from Table I. The derived results are listed in Table III. The first five lines give the approximate energy when using Ψ_0, Ψ_W, Ψ_M, Ψ_T, Ψ_H individually as approximate wave functions. It is interesting to note that Ψ_W, Ψ_M and Ψ_H are better first approximations than is Ψ_0 while Ψ_T is about equally good. If one plots the curves $H_1(i)$ against σ one finds they are very similar in shape, with the exception of $H_1(1)$ which is steeper. This seems to indicate much similarity between the matrix elements of the functions Ψ_i ($i=0, W, M, T$). But if so, not much improvement can be expected from the use of a combination of these functions rather than one alone; on the other hand, since this similarity suggests a near proportionality for the functions Ψ_0 and $H\Psi_0$ it might appear that Ψ_0 must be a fairly good trial wave function. However it may merely indicate very slow convergence. Nevertheless, $H\Psi_0$ seems to emphasize those features of Ψ_W, Ψ_M, Ψ_T which are missing in Ψ_0, and to give a favorable combination of the Ψ_i. Solution of the fourth-order secular equation with functions $\Psi_0, \cdots, \Psi_T$ for $\sigma=0.5$ gives

$$H_1(0, W, M, T)=-117.7. \qquad (6)$$

The improvement over $H_1(0, 1)$ (line 6 in Table III) is small. A calculation with different σ_i (σ_0, σ_W,σ_M,σ_T) in the Ψ_i also was made[8] but only a very small improvement was obtained over the result in (6).

Figure 1 shows $H_1(0)$, $H_1(1)$, $H_1(0, 1)$ in their dependence on σ. They reach their minima at -93, -105, -117 for $\sigma\backsimeq 0.55$, 0.45, 0.53, re-

[8] Formulae (30) must be modified for such a calculation.

TABLE I.—*Continued.*

MATRIX ELEMENTS	MULTIPLY COLUMNS BY	$\sigma=0.7$	1.0	0.5 "S"	0.5 "P"
1_{00}	1	1	1	1	
$1_{W0}=W_{00}$	$10^2\rho$	−10.5823209	−15.4128772	−0.64847982	−3.45855907
$1_{M0}=M_{00}$	"	−3.2501742	−3.4995422	"	−1.29695964
$1_{T0}=T_{00}$	$10^2\kappa$	4.0320000	5.7600000	0.48000000	2.40000000
$1_{WW}=W_{W0}$	$10^4\rho^2$	116.979360	245.289199	0.5738726	13.0978633
$1_{MW}=W_{M0}=M_{W0}$	"	34.733461	53.931111	"	4.8226217
$1_{MM}=M_{M0}$	"	11.297541	13.070084	"	2.1678046
$1_{WT}=W_{T0}=T_{W0}$	$10^4\rho\kappa$	−43.993590	−91.211471	−0.3631487	−8.6463976
$1_{MT}=M_{T0}=T_{M0}$	"	−13.222727	−20.207995	"	−3.1703458
$1_{TT}=T_{T0}$	$10^4\kappa^2$	16.708608	34.099200	0.2688000	5.9520000
W_{WW}	$10^6\rho^3$	−1351.439478	−4032.58097	−0.630816	−54.099942
$W_{MW}=M_{WW}$	"	−384.454868	−850.684679	"	−19.527407
$W_{MM}=M_{MW}$	"	−123.170967	−204.697756	"	−8.571992
M_{MM}	"	−40.691697	−49.621091	"	−4.060587
W_{WT}	$10^6\rho^2\kappa$	500.510073	1489.135884	0.353101	33.976615
$W_{MT}=M_{WT}$	"	145.523524	319.749094	"	12.237865
M_{MT}	"	46.348242	75.676028	"	5.386820
T_{WW}	"	503.361819	1494.905201	0.438168	34.504220
T_{MW}	"	145.677224	319.657334	"	12.355421
T_{MM}	"	47.706686	77.605747	"	5.757615
W_{TT}	$10^6\rho\kappa^2$	−187.478483	−553.437435	−0.222731	−22.246989
M_{TT}	"	−55.222092	−119.849223	"	−7.990040
T_{WT}	"	−188.072384	−554.994746	−0.239332	−22.357663
T_{MT}	"	−55.274967	−119.881627	"	−8.008486
T_{TT}	$10^6\kappa^3$	71.111836	207.323136	0.172032	15.237120

TABLE II. H_1, H_2, H_3.

	$\sigma=0.1$	0.3	0.5	0.6	0.7	1.0
$10^{-2}H_1$	−0.10368782	−0.66706421	−0.91471899	−0.91666228	−0.85260357	−0.36220918
$10^{-4}H_2$	0.13573154	0.7915741	1.2759363	1.3126506	1.2373673	0.8324580
$10^{-6}H_3$	−0.005951493	−0.7129041	−1.3062780	−1.1984854	−0.8525274	0.8506908

TABLE III. *Results.*

LINE	RESULTS	$\sigma=0.1$	0.3	0.5	0.6	0.7	1.0
1	$H_1(0)$	−10.37	−66.71	−91.47	−91.67	−85.26	−36.22
2	$H_1(W)$	−31.43	−81.22	−95.64	−91.16	−80.48	−20.80
3	$H_1(M)$	−33.85	−92.42	−111.61	−109.27	−100.72	−47.19
4	$H_1(T)$	−11.73	−69.47	−91.29	−89.12	−80.01	−21.78
5	$H_1(1)$	−4.38	−90.06	−102.38	−91.30	−68.90	102.19
6	$H_1(0,1)$	−34.6354	−97.8661	−116.4008	−114.4704	−107.2457	−62.8471
7	λ_0	0.65848	0.35380	0.45005	0.52912	0.60478	0.82193
8	λ_1'	−0.58976	−0.70694	−0.60006	−0.52495	−0.45793	−0.33014
9	$T(0,1)$	78.0	198.8	306.8	359.1	411.3	565.0
10	$W(0,1)$	−123.1	−426.3	−744.5	−901.4	−1054.9	−1478.3
11	$M(0,1)$	−107.0	−255.2	−327.9	−348.6	−363.4	−385.3
12	$R(0)$	0.8209	0.4739	0.3671	0.3351	0.3103	0.2596
13	$R(0,1)$	0.6518	0.4352	0.3544	0.3282	0.3070	0.2621
14	$\rho_{-270}(0)$	4.96	1.873	1.487	1.421	1.390	1.396
15	$\rho_{-270}(0,1)$	2.96	1.570	1.363	1.332	1.320	1.348
16	$\eta_{\lim}$	−151	−204	−192	−183	−174	−144
17	$D_2^{\frac{1}{2}}$	35.4	58.9	66.3	68.7	71.4	83.7

spectively. One would suspect that this shift in σ indicates a shift towards a larger equilibrium radius for the nucleus as the wave function improves. This is not so. The shift towards smaller σ in the minima of H_1, $H_1(0,1)$, ... seems to be characteristic of the iteration method, not of the oxygen problem. The nuclear radius is given by[9]

$$\langle R\rangle \equiv \langle \tfrac{1}{16}\textstyle\sum_1^{16}(\mathbf{r}_i-\mathbf{r}_{c.g.})^2\rangle^{\frac{1}{2}} = \left[\frac{69}{32\alpha\sigma}-\frac{1}{32\alpha^2\sigma^2}(\langle T\rangle-\langle T_{c.g.}\rangle)\right]^{\frac{1}{2}}, \quad (7)$$

an immediate consequence of formulae (28, 29). It is found that for a given σ this quantity decreases as one proceeds from $R(0)$ to $R(0,1)$ (lines 12, 13), approximately offsetting the increase resulting from the decreased σ. For example, H_1 reaches its minimum for $\langle R\rangle \simeq 0.349$ units $=3.12\times10^{-13}$ cm, $H_1(0,1)$ for $\langle R\rangle \simeq 0.345$ units $=3.08\times10^{-13}$ cm. *The approximate constancy of $\langle R\rangle$ constitutes very strong evidence for the existence of a closely bound state.*

It will be shown in Appendix I,c that a good approximation $\Psi(0,\cdots,n)$ must be practically independent of σ. Consequently, *the rate at which the curves H_1, ..., $H_1(0,\cdots,n)$, ... as functions of σ flatten out is an important measure of the rapidity of convergence.* The probable shape of $H_1(0,\cdots,n)$ for n large is shown in Fig. 1. But the curve $H_1(0,1)$ is hardly any flatter than H_1, indicating that the function $\Psi(0,1)$ is not much better than Ψ_0.[10] Therefore, whether or not Ψ_0 is close to the correct eigenfunction, *the convergence is exceedingly slow in this problem.*[11, 11a]

[9] $\langle V\rangle$, the average of V in terms of the function $\Psi(i,\cdots,j)$, is denoted by $V(i,\cdots,j)$.

[10] In the case of He the curve $H_1(0,1)$ is considerably flatter than H_1.

[11] In general one would expect that an nth-order perturbation calculation (n=number of particles) or an iteration calculation of order $n/2$ (n even) or order $(n+1)/2$ (n odd) should yield a fairly close approximation to E_0. But from Fig. 1 it appears that iterations of higher order would be necessary in the present problem.

[11a] *Note added in proof:*—While the curves $H_1(\sigma;0,1,\cdots,n)$ approach the line E_0 monotonically from above, the

Lines 7 and 8 give the coefficients λ_0 and λ_1' of Ψ_0 and Ψ_1' in the ground state combination. In particular, for $\sigma=0.5$ the ground state $\Psi(0, 1)$, $(H_1(0, 1)=-116.40)$ is given by $\Psi(0, 1)=0.450\ \Psi_0-0.600\ \Psi_1'$. It is interesting to note that the function Ψ_1' enters into $\Psi(0, 1)$ with greater weight than does Ψ_0.

The knowledge of λ_0 and λ_1 permits the calculation of

$$V(0, 1)=\lambda_0^2 V_{00}+2\lambda_0\lambda_1 V_{01}+\lambda_1^2 V_{11}, \qquad (8)$$

the average of the potentials in terms of the wave function $\Psi(0, 1)$, listed in lines 9–11. Comparison with the quantities $V(0)$ (given in Table I) shows that the Majorana potential depends more sensitively on the form of the wave function than do the other components of the Hamiltonian.

Lines 14 and 15 give the values $\rho_{-270}(0)$ and $\rho_{-270}(0, 1)$ of $-A/72$ necessary to lower $H_1(0)$ and $H_1(0, 1)$ to -270 (with an accuracy of about 1 mc^2). The smallest such $\rho \backsimeq 1.380$ at $\sigma \backsimeq 0.81$ for H_1, $\rho \backsimeq 1.320$ at $\sigma \backsimeq 0.72$ for $H_1(0, 1)$. The improvement obtained by the use of the more complicated function is quite small.[12] Naturally, H_1 depends linearly on ρ. This is practically true also for $H_1(0, 1)$ in the region $\sigma=0.3$ to 1.0. The values of the potentials obtained for $\sigma=0.70$ with $\rho=1.320$ $(H_1(0, 1)=-269.3$ for this case) are given below: $T(0, 1)=426$, $T_{e.g.}(0, 1)=16.8$, $W(0, 1)=-1432$, $M(0, 1)=-490$.

The results to which solution of the secular equation lead were devoid of much information and to a large extent negative in nature. The numerical values $H_1(0)_{\min}=-93$, $H_1(0, 1)_{\min}=-117$ do not offer any clue as to the approximate location of E_0, especially since the convergence appears to be so slow. The most important information obtained was that $\langle R\rangle$ decreases as one proceeds from Ψ_0 to $\Psi(0, 1)$, and this indicates a most likely existence of a closely bound

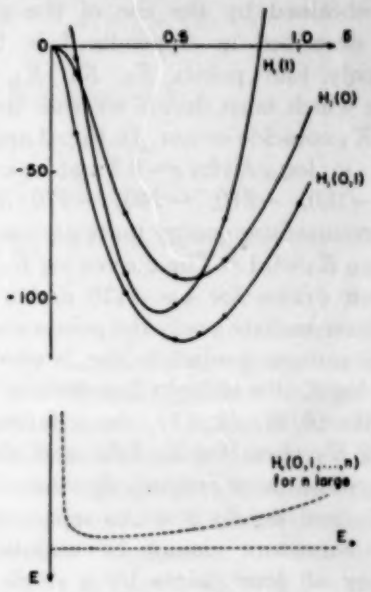

FIG. 1. The approximate binding energy as a function of σ. The rate at which the curves H_1, $H_1(0, 1)$, . . . as functions of σ flatten out is a measure of the rapidity of convergence.

state. Yet, the divergence of $R(0, \cdots, n)$ as $n\to\infty$ is still a possibility, nor does a finite value for $\lim\langle R\rangle$ prove definitely that the state $\lim\Psi(0, \cdots, n)$ lies below -220, the energy represented by four noninteracting α-particles.[13]

curves $\eta_W(\sigma; 0,1, \cdots, n)$ (or $\eta_{\lim}(\sigma; 0, \cdots, n)$, see footnotes 14, 15, 21) must intersect each other for sufficiently high n. For any given σ, $\eta_W(\cdots)$ first decreases, crossing the line E_0. After reaching a minimum, $\eta_W(\cdots)$ increases, approaching E_0 from below. (The points $\sigma=0$ and $\sigma=\infty$ are excluded from all considerations.) *If* $\eta_W(\cdots)$ has only one minimum as a function of n, then the points of intersection of the curves $\eta_W(\sigma; \cdots)$ necessarily lie below the E_0 axis, provided only that the expansion (9) exists with $\epsilon_0 \neq 0$.

[12] This is in contradiction to the findings of Euler. He found $\rho_1=2.36$, $\rho_2=1.40$ for the values of a force ratio, roughly corresponding to the ρ of this paper, to which first- and second-order perturbation calculations lead, respectively, in the case of heavy nuclei. The apparently more rapid convergence in Euler's case is possibly due to the use of a worse initial wave function Ψ_0. Probably it is due to some extent also to the fact that Euler considered only terms up to the second order. It is to be expected that a perturbation calculation including first- second- and third-order contributions to the energy would lead to an improvement of about the same order of magnitude over first-order results as a second-order iteration calculation. This seems to suggest that inclusion of third-order terms in Euler's calculation would have partly offset the improvement obtained in second order. For comparison of the iteration and perturbation methods see Pauling and Wilson, *Introduction to Quantum Mechanics*, Chapter VII.

[13] If four α-particles represented by the selected Hamiltonian are drawn together along the diagonals of a regular tetrahedron one may find: (1) The energy of the system increases continuously. (2) The energy first increases, then a potential hole is reached with a set of metastable states, the lowest of which is above -220. (3) The lowest state in the potential hole is below -220. Here again there are two possibilities: (a) the hole is reached by passing a potential barrier, (b) the energy decreases continuously from -220 to the minimum. Constancy of $\langle R\rangle$ excludes case (1). It also indicates that if case (2) is correct then $H_1(0, \cdots, n)$ will not converge to the -220 eigenvalue of the dissociated state, but to the lowest finite configuration. (Although very unlikely, it is conceivable that the set of functions Ψ_0, Ψ_1, . . . may be incomplete in such a way that some dissociated states of low energy cannot be described in terms of them.) Thus a finite $R(0, \cdots, n)$ for $n\to\infty$ is not a conclusive proof that the lowest state is below -220.

The extrapolation methods of Appendix I will give an indication as to the approximate location of E_0. In order to obtain an estimate of the limitations for E_0, Ansatz (12) has been applied. Line 16 of Table III lists η_{11m}[14] for the various σ. It shows that even on the basis of the rather restricted single-peak distribution function the values $H_1 \leqq -90$ and $E_0 < -200$ are quite possible simultaneously and not unreasonable.[15]

A more accurate estimate for the location of E_0 can be obtained by the use of the graphical method described in Appendix I, b. Unfortunately only four points K_0, K_1, K_2, K_3 are available which must decide whether the curves K_a and K_b coincide or not. In Fig. 2 are plotted $\log_{10} K_0, \cdots, \log_{10} K_3$ for $\sigma = 0.5$ and for $\eta = -120$, -150, -180, -210, -240, -270; for convenient comparison energy units are used which make $\log_{10} K_3 = 0.1$.[16] The curves $\log K_a$, $\log K_b$ have been drawn for $\eta = -120$ and $\eta = -270$. For the intermediate η only the points are plotted in order not to prejudice the reader. When $\eta = -\infty$ $\log K$ is a straight line passing through the points $(0, 0)$, $(2, 0.1)$. As η increases the point $\log K_3$ rises, $\log K_1$ falls and the curve $\log K$ becomes more bulging. By observing that as $\log K_a$ and $\log K_b$ start to separate the increasing curvature cannot be maintained by connecting all four points by a single smooth curve one is lead to believe that -230 ± 20 is a reasonable estimate for the lowest eigenvalue of H.[16a]

Work on this problem was begun during the Summer Session of 1937 at the University of Michigan. The problem and the use of the iteration method as well as the extrapolation method of Appendix I, d were suggested by E. Feenberg. The writer wishes to express his sincere gratitude to Dr. Feenberg for his constant guidance, interest and help. To Professor I. I. Rabi, Professor G. Breit and Professor K. Friedrichs the writer expresses thanks for many interesting and clarifying discussions.

Appendix I. The Iteration Method[17]

(a) An alternate derivation of the secular equation

Let $E_0, E_1, E_2, \cdots$ be the true eigenvalues, $\varphi_0, \varphi_1, \varphi_2, \cdots$ the true orthonormal eigenfunctions[18] of H, ϵ_i the Fourier coefficients of Ψ_0 with respect to them:

$$\Psi_0 = \epsilon_0\varphi_0 + \epsilon_1\varphi_1 + \epsilon_2\varphi_2 + \cdots \quad (\sum_0^\infty \epsilon_i^2 = 1). \tag{9}$$

Then

$$\begin{array}{l|l} 1 = \epsilon_0^2 + \epsilon_1^2 + \cdots + \epsilon_n^2 & + \cdots \\ H_1 = \epsilon_0^2 E_0 + \epsilon_1^2 E_1 + \cdots + \epsilon_n^2 E_n & + \cdots \\ \vdots & \\ H_{2n+1} = \epsilon_0^2 E_0^{2n+1} + \epsilon_1^2 E_1^{2n+1} + \cdots + \epsilon_n^2 E_n^{2n+1} & + \cdots \\ \hline \cdots & \end{array}$$

Discarding all terms outside of the rectangle one is led to Eq. (3) for E_i.

(b) Deviations

Define

$$K_n(\eta) \equiv H_n - \binom{n}{1} H_{n-1}\eta + \cdots + (-1)^n \eta^n$$

$$= \int \Psi_0^*(H-\eta)^n \Psi_0 d\tau = \sum_0^\infty \epsilon_i^2 (E_i - \eta)^n, \tag{10a}$$

$$K_{an}(\eta) \equiv \sum_0^\infty \epsilon_i^2 |E_i - \eta|^n,$$

$$K_{bn}(\eta) \equiv -\sum_0^t \epsilon_i^2 |E_i - \eta|^n + \sum_{t+1}^\infty \epsilon_i^2 |E_i - \eta|^n. \tag{10b}$$

[14] The definition of η_{11m} is given in Appendix I, d.

[15] It is interesting to compare η_{11m} with Weinstein's expression $\eta_W = H_1 - D_2^{\frac{1}{2}}$ which is obtained for η_0 in terms of H_1, H_2 by taking $k = 0$, $p = 1$ in (12b). This cannot be done for any σ. H_3 obtained from expression (13) must be consistent with the calculated H_3. One finds $\sigma \leqq 0.45$ and $\eta_W \leqq -153$.

[16] More exactly: the curve $\log h^n K_n(\eta)$ is plotted *vs.* n. If one uses logarithms, the arbitrariness associated with the choice of the energy unit appears only in the linear $n \log h$ term. h is determined from $2 \log h + \log K_2 = 0.1$.

[16a] *Note added in proof:*—A number of artificial examples have been studied. Those containing a large number of coefficients ϵ_i associated with eigenvalues spread over a large energy range yield results supporting the type of argument used in the text. However there exist examples which show that the method used to locate E_0 is not generally valid. Consequently, the strongest argument for the existence of a stable stationary state remains the fact that the nuclear radius decreases as the wave function is improved.

[17] Kellogg considered the set of functions $\Psi_0, \Psi_{-1} = H^{-1}\Psi_0, \ldots$, and found some very interesting properties, notably that they converge to an eigenfunction of H. (Cf. Courant and Hilbert, Methoden d. Math. Phys. I, 132.)

[18] The system may be supposed to be enclosed in a large box, so that the complete energy spectrum is discrete.

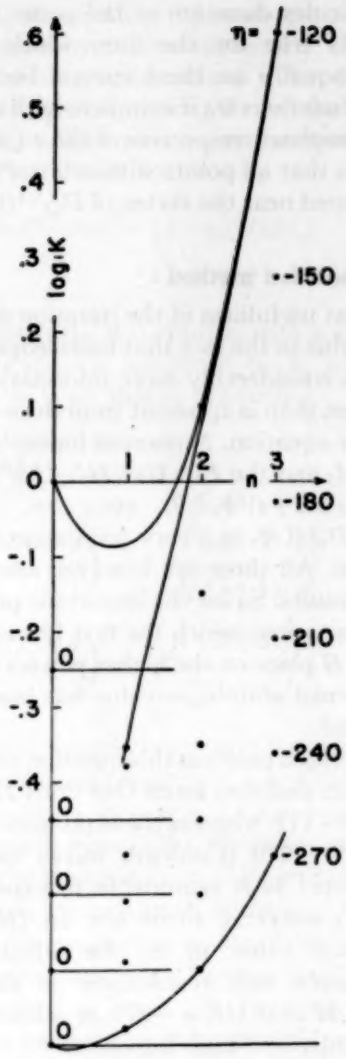

FIG. 2. Determination of E_0 from the coincidence of the curves $\log K_a$ and $\log K_b$ for $\sigma=0.5$. Energy units were used which make $\log_{10} K_2=0.1$.

E_i denotes the highest eigenvalue $\leqslant\eta$. K_n will be called the *nth deviation moment of H with respect to* η, K_{an} *the nth absolute deviation moment of H with respect to* η. Special cases are: the moments with respect to zero, $K_n(0)=H_n$, and the moments with respect to H_1, $K_n(H_1)\equiv D_n$. The latter will be called, simply, *deviations*. The *absolute deviations*, D_{an}, are defined similarly, $D_{an}\equiv K_{an}(H_1)$. The following relations hold:

$$D_n=K_n(\eta)-\binom{n}{1}K_{n-1}(\eta)K_1(\eta)+\cdots+(-1)^nK_1^n(\eta). \quad (11)$$

The deviation moments play a fundamental role, in the theory. For even n $K_{an}=K_n$, for odd n $K_{bn}=K_n$. For $\eta<E_0$ all terms $\epsilon_i^2(E_i-\eta)^n$ are positive and $K_{bn}=K_{an}$. This observation suggests a remarkably simple approximate determination of the eigenvalues of H. Plot K_n *vs.* n. Two separate curves are obtained as long as $\eta>E_0$. The difference between the two, denoted by $2k$, determines

$$k_n=\sum_0^i\epsilon_i^2(E_i-\eta)^n. \quad (10c)$$

Consider in particular k_1:

$$k_1(\eta<E_0)=0,$$
$$k_1(E_0<\eta<E_1)=\epsilon_0^2E_0-\epsilon_0^2\eta,$$
$$k_1(E_1<\eta<E_2)=\epsilon_0^2E_0+\epsilon_1^2E_1-(\epsilon_0^2+\epsilon_1^2)\eta.$$
$$\vdots$$

If the curves K_a and K_b were known exactly and the Fourier coefficients ϵ_i of Ψ_0 with respect to the φ_i were not too small, then the broken line $k_1(\eta)$ would permit determination of the levels E_i and the coefficients ϵ_i. In particular, E_0 would be given by the limiting η for which K_a and K_b coincide.

The question therefore is, to what extent are the curves $K_a(n,\eta)$ and $K_b(n,\eta)$ known? It is easily seen that even when $K(i,\eta)$ is known for only a few values of i, the class of admissible curves is very limited. For $\eta<E_0$ $K(n,\eta)$ is of the type

$$K(x,\eta)=\sum a_iA_i^x=h^x\sum a_iB_i^x \qquad (a_i\geq 0,\ A_i>0;\ h>0,\ B_i>1).$$

(A change in the energy unit manifests itself in a change in the factor h^x.) This curve has at most one minimum, and to the right of this point the curve represents a monotonically increasing function (condition A). If no curve can be drawn through the calculated points which satisfies condition A, then $\eta>E_0$. Thus a system of upper bounds, $\eta_{u.b.}$, is obtained for E_0. The simplest of these, $\eta_{u.b.1}$, is defined as the lowest η for which

$$K_3(\eta)-K_2(\eta)>K_2(\eta)-K_1(\eta)=0.$$

(The minimum of K_n is to the left of $n=2$ if energy units are used for which $K_2(\eta)-K_1(\eta)\gtrsim 0$.) For example in the oxygen problem

one finds $\eta_{a.b.1}=-116.401$ (for $\sigma=0.5$). This compares with $H_1=-91.471$ and $H_1(0,1)=-116.401$.[19] The converse is by no means true. The curves which can be drawn through the calculated points $K(i)$ are not unique. Moreover for very small values of ϵ_0^2 large values of $E_0-\eta$ are needed to make $\epsilon_0^2(E_0-\eta)^n$ appreciable. Thus, when condition A is satisfied, no definite conclusions can be drawn. An estimate of E_0 may be obtained from a study of the approximate shape of the curves K_a, K_b for values of η which are definitely below E_0, and values of η which are definitely above.

(c) Quality of Ψ_0

It is customary to consider Ψ_0 as a good approximation to φ_0 if H_1 is close to E_0, a bad approximation if H_1 and E_0 are rather far apart. This is true insofar as $H_1=E_0$ implies that Ψ_0 is exact. But much better information is obtained about the approximation when all the deviations D_{ak} are considered.

The curves $D_{ak}^{1/k}$ plotted against $\langle H(\sigma)\rangle(=H_1)$ illustrate this point for the special case of oxygen. One such curve, $D_2^{\frac{1}{2}}$, has been calculated, and the values are given in line 17, Table III. The ordinate $\langle H\rangle=-91.5$ intersects these curves in two points, the lower represents $\sigma\backsimeq 0.5$, the upper $\sigma\backsimeq 0.6$. Thus $\Psi_0(0.5)$ is a better wave function than $\Psi_0(0.6)$ even though both yield approximately the same $\langle H\rangle$. These considerations can be extended to include the curves $D_{ak}^{1/k}(0,1)$, $\cdots$, $D_{ak}^{1/k}(0,\cdots,n)$, $\cdots$ plotted against $\langle H(\sigma)\rangle(=H_1(0,1),\cdots,H_1(0,\cdots,n),\cdots$, respectively). The limiting ordinate $\langle H\rangle=-93$ is the common tangent to the vertices of the curves $D_{ak}^{1/k}$. $\langle H\rangle=-117$ is the limiting ordinate of the curves $D_{ak}^{1/k}(0,1)$. As one proceeds to higher n the vertices of these curves tend to the point E_0 on the $\langle H\rangle$ axis.

The envelope of the curves $D_{ak}^{1/k}$, $D_{ak}^{1/k}(0,1)$, $\cdots$, convex if Ψ_0 is good, reaches the $\langle H\rangle$ axis in a perpendicular direction at the point E_0.[20] The same holds true for the lines which connect points of equal σ on these curves, because the system of functions Ψ_i, if complete with reference to φ_0, is complete irrespective of the σ (>0) used. This shows that all points with arbitrary σ (>0) will be located near the vertex of $D_{ak}^{1/k}(0,\cdots,n)$ as $n\to\infty$.

(d) Extrapolation method

The great usefulness of the iteration method is primarily due to the fact that knowledge of a few H_i implies considerably more information about the problem than is apparent from the solution of the secular equation. Numerous inequalities connect the H_i and the E_i : $H_2\geqslant H_1^2$, $H_4\geqslant H_2^2$, $\cdots$, $\int\Psi_0(aH^2+bH+c)^2\Psi_0\geqslant 0$, etc.; or, $E_0<H_1$; $E_0>H_1-D_2^{\frac{1}{2}}$ if Ψ_0 is a very good approximation to φ_0,[21] etc. All these are however merely fragmentary results. So far the important problem of finding limitations which the first few calculated powers of H place on the higher powers of H and on the normal state eigenvalue has been barely investigated.

In the oxygen problem this question turns up in a somewhat modified form. One finds $H_1=-93$, $H_1(0,1)=-117$, whereas the experimental result gives $\langle H\rangle\backsimeq -270$ (Coulomb forces neglected). One inquires: Is it reasonable to expect $H_1(0,\cdots,k)$ to converge to as low an $\langle H\rangle$ as the experimental value, or do the calculated H_1, H_2, H_3 imply such restrictions on the higher powers of H that $\langle H\rangle=-270$ as a limit is very unreasonable, well-nigh impossible?

For the study of these questions Feenberg suggested the following method: replace expression (9) by

$$\Psi_0=N^{-\frac{1}{2}}\int_{\eta_0}^{\infty}\rho_\eta\varphi_\eta d\eta \qquad (12a)$$

where

$$H\varphi_\eta=\eta\varphi_\eta,\quad \int\varphi_\eta\varphi_{\eta'}d\tau=\delta_{\eta\eta'},\quad N=\int_{\eta_0}^{\infty}\rho_\eta^2 d\eta;$$

[19] *Note added in proof:*—These upper bound relations were brought to the writer's attention by Professor Breit who also pointed out a set which is independent of the energy unit, and therefore preferable to the one used above. The simplest of these expressions is $G(\eta)=K_1K_3-K_2^2$. G vanishes at $\eta=H_1(0,1)$, and $G<0$ implies $\eta>E_0$. Thus the condition $G>0$ reduces to the condition of monotonic increase, $\log K_3-\log K_2>\log K_2-\log K_1$, for the logarithmic plot. Expressions analogous to G and involving higher deviations can also easily be set up.

[20] If the approximation is very good, a small improvement in $\langle H\rangle$ will necessitate a large improvement in the wave function, that is, a large drop in D_{ak}. This method therefore yields a convenient estimate of E_0 provided a sufficient number of curves $D_{ak}^{1/k}(0,\cdots,n)$ $(n=0,1,2,\cdots)$ is available so that the convex portion of the envelope is reached.

[21] Weinstein's theorem. See Pauling and Wilson, reference 12. A sufficient condition for the validity of the theorem is $2H_1<E_0+E_s$, where φ_s is the lowest excited state not orthogonal to Ψ_0.

that is, approximate the true spectrum of the Hamiltonian by a continuous one. This greatly facilitates all considerations. The distribution function ρ_η gives a description of the manner in which the various correct eigenfunctions combine into Ψ_0.[21a] A simple form for ρ_η,

$$\rho_\eta=(\eta-\eta_0)^{k/2}\exp\left[-(\eta-\eta_0)^p/2\beta^p\right] \qquad (k>-1,\ p>0,\ \beta>0) \quad (12b)$$

is an exponential distribution with a single peak, whose location is regulated by k, width by β, slope by p. With this ρ_η one finds

$$H_n=N^{-1}\int_{\eta_0}^{\infty}\rho_\eta^2\eta^n d\eta=\eta_0^n+\binom{n}{1}\eta_0^{n-1}\beta\frac{\Gamma((k+2)/p)}{\Gamma((k+1)/p)}+\binom{n}{2}\eta_0^{n-2}\beta^2\frac{\Gamma((k+3)/p)}{\Gamma((k+1)/p)}+\cdots. \quad (13)$$

In general the important contributions to Ψ_0 will come from various regions in η, and the correct ρ_η may be written as a sum $\rho=a_1\rho_1+a_2\rho_2+\cdots$ of expressions of type (12b). Relations of type (13) connect the parameters in ρ. By suitably adjusting them, η_0 can be varied. Naturally, there must be sufficient parameters to avoid contradictions. The questions arise: (1) To what η_0 will a reasonable assumed ρ lead? (2) How unreasonably must ρ be assumed in order to obtain η_0 for oxygen as low as -270 or even less? The question whether arbitrarily small η_0 can be obtained is an important one. This is certainly possible when only H_1 is known, $\eta_0\to-\infty$ as $\beta\to\infty$ in the expression for H_1 given by (13). Whether this is still possible when H_1, H_2, H_3, or more H_i are given, has in general not been investigated, but it seems that the present procedure should yield some information. Weinstein's theorem suggests that there must be some limitations. In the present paper the case for which H_1, H_2, H_3 are given is considered. ρ is taken in the form (12b), which is a good approximation if Ψ_0 is close to a true eigenfunction of H.[22] Under these assumptions there actually exists a lower bound for η_0. One also finds that the slightly more general, and by assuming the lowest state discrete, slightly more correct five-parameter Ansatz

$$\Psi_0=(1+\lambda^2N)^{-\frac{1}{2}}\left[\varphi_0+\lambda\int_{\eta_0}^{\infty}\rho_\eta\varphi_\eta d\eta\right] \qquad (\lambda^2>0) \quad (14)$$

leading to the biquadratic equation

$$(F_2-1)(\eta_0-H_1)^4-(3-2F_2)D_3(\eta_0-H_1)^2+D_3(\eta_0-H_1)+F_2D_3^2=0 \quad (15)$$

(F_2 is given in Eq. (16)), does not go beyond the limits imposed by Eq. (17). The lowest η_0 is obtained when $\lambda=\infty$, i.e. when Eq. (14) reduces to Eq. (12a).

Expression (12b) is specifically adapted to the case when the first three H_i are known. They permit determination of β, k, p as functions of η_0. Eq. (13) leads to the relations

$$\begin{aligned}&R_1(\eta_0)=F_1(p,k),\\&R_2(\eta_0)=F_2(p,k),\end{aligned} \qquad (16a)$$

$$\left(R_n(\eta)\equiv K_{n+1}(\eta)K_n^{-2}(\eta)K_{n-1}(\eta),\right.$$

$$F_n(p,k)\equiv\Gamma\left(\frac{k+n+2}{p}\right)\times\left[\Gamma\left(\frac{k+n+1}{p}\right)\right]^{-2}\Gamma\left(\frac{k+n}{p}\right)\Bigg)$$

connecting p and k, β is given by

$$\beta=\frac{\Gamma[(k+1)/p]}{\Gamma[(k+2)/p]}K_1(\eta_0). \qquad (16b)$$

For practical calculations it is simpler to fix a definite value for p instead of η_0. Plot η and R_1 *vs.* $\Delta(\eta)=R_1-R_2$, and on the same graph plot k and F_1 *vs.* $\delta(k)=F_1-F_2$. The ordinate through the intersection of F_1 and R_1 cuts η and k in points corresponding to the selected p. $\delta(k)$ is always positive. $\Delta(\eta)$ is a monotonically decreasing function of $-\eta$ for $\eta\leqslant\eta_{\lim}$ (defined by Eq. (17)).

[21a] The distribution function ρ should not be confused with the force ratio $\rho=-A/72$ considered in earlier sections of this paper.

[22] If Ψ_0 is an eigenfunction, say φ_ν, then Eq. (12a) with $\rho_\eta=\delta(\eta-\eta_\nu)$ is exact. Such a δ function can be arbitrarily well approximated by expressions of type (12b).

Consequently the root η_{lim} of

$$\Delta(\eta)\equiv R_1(\eta)-R_2(\eta)=0 \tag{17}$$

forms a lower bound for η_0. As this limiting case is approached $k\to\infty$, $p\to 0$, $\beta\to 0$.[23]

Appendix II. Matrix Elements[24]

(a) The fundamental formula (22)

In this section formulas will be developed for the matrix elements of operators[25]

$$V=\sum_{i_1}'\cdots\sum_{i_m}'V(i_1,\cdots,i_m) \tag{18}$$

referred to wave functions of the type $\Psi_{\alpha\beta}=V_\alpha V_\beta\Psi_0$, $\Psi_{\gamma\delta}=V_\gamma V_\delta\Psi_0$, where $V_\alpha,\cdots,V_\delta$ are certain operators, and Ψ_0 is the Hartree-Fock determinant

$$\Psi_0=\frac{1}{(n!)^{\frac{1}{2}}}\begin{vmatrix}\psi_1(1) & \cdots & \psi_1(n)\\ \cdot & & \cdot\\ \cdot & & \cdot\\ \psi_n(1) & \cdots & \psi_n(n)\end{vmatrix} \tag{19}$$

constructed from single particle wave functions $\psi_1,\psi_2,\cdots,\psi_n$. These are assumed to be mutually orthogonal,

$$\int\psi_i^*(1)\psi_k(1)dT_1=N_i\delta_{ik}. \tag{20}$$

dT is a four-dimensional volume element, including spin coordinates. For V_{00} one finds[26]

$$V_{00}\equiv(0|\sum_{i_1}'\cdots\sum_{i_m}'V(i_1,\cdots,i_m)|0)\equiv\int\Psi_0^*V\Psi_0dT_{1\cdots n}$$

$$=N\int\cdots\int\mathbf{V}(1,2,\cdots,m)\begin{vmatrix}\sum_\iota\psi_\iota'^*(1)\psi_\iota'(1) & \cdots & \sum_\iota\psi_\iota'^*(1)\psi_\iota'(m)\\ \cdot & & \cdot\\ \cdot & & \cdot\\ \sum_\mu\psi_\mu'^*(m)\psi_\mu'(1) & \cdots & \sum_\mu\psi_\mu'^*(m)\psi_\mu'(m)\end{vmatrix}dT_{1\cdots m}. \tag{21}$$

$\mathbf{V}$ denotes the operator V operating on the arguments of unstarred ψ_ι only, and $N=N_1N_2\cdots N_n$. The matrix elements $V_{\alpha\beta;\,\gamma\delta}$ are then obtained by replacing $\mathbf{V}$ in the integrand by $\mathbf{V}_\beta^\dagger\mathbf{V}_\alpha^\dagger\mathbf{V}\mathbf{V}_\gamma\mathbf{V}_\delta$. $\mathbf{V}_\alpha^\dagger$ denotes the Hermitian conjugate of V_α operating on $\mathbf{V}_\beta^\dagger$ which precedes it, and on the arguments of the starred ψ_ι^*.

In order to simplify Eq. (21) the wave functions ψ_ι are assumed in the form of a space function u_i multiplied by one of the four spin functions η_k. Multiplying out the determinant and performing the spin summation, on the assumption that V does not involve a spin operation, and that all occupied space orbits are fully occupied one obtains[27]

$$V_{00}=N\int\cdots\int\mathbf{V}(1,2,\cdots,m)\mathfrak{D}^{(m)}d\tau_{1\cdots m}, \tag{22a}$$

where $d\tau$ is a three-dimensional volume element,

$$\begin{aligned}
\mathfrak{D}^0&=1\\
\mathfrak{D}^{\mathrm{I}}&=(1)\\
\mathfrak{D}^{\mathrm{II}}&=(1)(2)-\tfrac{1}{4}|12|^2\\
\mathfrak{D}^{\mathrm{III}}&=(1)(2)(3)-\tfrac{1}{4}(1)|23|^2-\tfrac{1}{4}(2)|13|^2\\
&\quad-\tfrac{1}{4}(3)|12|^2+\tfrac{1}{16}(122331)+\tfrac{1}{16}(133221)\\
&\cdots\cdots\cdots

The following abbreviations are used:

$$\begin{gathered}\sum_j u_j'^*(2)u_j'(3)\equiv(23),\\ (122331)\equiv(12)(23)(31),\\ |12|^2\equiv(1221),\\ (1)\equiv(11).\end{gathered}\tag{23}$$

(122331) is called a three-index cycle, $|12|^2(3)$ a two-cycle (product of two cycles).

(b) Examples

1. Ordinary exchange operators:—The exchange operator P_{12} exchanges indices 1 and 2 in $\mathfrak{D}$, the operator $\mathbf{P}_{12}$ exchanges them in the even positions, $\mathbf{P}_{12}^{\dagger}$ in the odd positions. Abbreviated expressions must be written out in full before applying the operators:

$$P_{12}(1)|23|^2=(2)|13|^2,$$

$$\mathbf{P}_{12}^{\dagger}(1)|23|^2=\mathbf{P}_{12}^{\dagger}(11)(23)(32)=(21)(13)(32)=(133221),$$

$$\mathbf{P}_{12}(1)|23|^2=\mathbf{P}_{12}(11)(23)(32)=(122331).$$

It is thus seen that for individual terms one may have $\mathbf{P}_{12}(\ )\neq\mathbf{P}_{12}^{\dagger}(\ )$, but one finds $\mathbf{P}_{12}\mathfrak{D}=\mathbf{P}_{12}^{\dagger}\mathfrak{D}$. The term $(122331)|45|^2(6)$ of $\mathfrak{D}^{\mathrm{VI}}$ has the coefficient 4^{3-6} and the sign $(-1)^{6-3}$. One can write $4^3=2^3\cdot 2^3$. One of the factors 2^3 arises from the ordinary spin summation[28]

$$\sum_{s_1}^{\sigma}\cdots\sum_{s_6}^{\sigma}\langle 122331\rangle^{\sigma}\langle 4554\rangle^{\sigma}\langle 66\rangle^{\sigma},$$

the other from the corresponding isotopic spin summation. The superscripts σ denote that these expressions are now restricted to ordinary spins. They will be omitted if there is no danger of misunderstanding. This shows at once how to proceed when spin exchange operators are present.

2. Spin exchange operators:—The following is an example: Use the abbreviation[28]

$$[\ ]\equiv\langle 122331\rangle^{\sigma}\langle 4554\rangle^{\sigma}\langle 66\rangle^{\sigma}.$$

Since

$$\mathbf{Q}^{\sigma}{}_{1346}[\ ]=\langle 14455661\rangle^{\sigma}\langle 2332\rangle^{\sigma},$$

on summing over the spin coordinates one finds

$$\sum_{s_1}^{\sigma}\cdots\sum_{s_6}^{\sigma}[\ ]=2^3,\quad \sum_{s_1}^{\sigma}\cdots\sum_{s_6}^{\sigma}\varrho^{\sigma}{}_{1346}[\ ]=2^2.$$

This result is denoted by writing

$$\mathbf{Q}^{\sigma}{}_{1346}\frac{2^3\cdot 2^3}{4^6}(122331)|45|^2(6)=\frac{2^2\cdot 2^3}{4^6}(122331)|45|^2(6).$$

The general rule is: if $f(\mathbf{P})$ changes an n-cycle into an m-cycle, the corresponding $f(\mathbf{Q}^{\sigma})$ leaves the cycle structure unchanged but changes the factor 2^n into 2^m. The isotopic spin operator $\mathbf{Q}^{\tau}$ is treated in a similar way. With this interpretation spin exchange operators can be applied in Eq. (22) even though the spin functions have already been eliminated.

3. Differential operators:—(a) Since $\nabla(ab)=(\nabla a)b+a(\nabla b)$, one can write

$$\begin{gathered}\nabla_2(2)=\nabla_2(2,2)=\tfrac{1}{2}\nabla_2(2,2)=\tfrac{1}{2}\nabla_2(2),\\ \nabla_2|12|^2=\tfrac{1}{2}\nabla_2|12|^2,\\ \nabla_2[(122331)+(133221)]=\tfrac{1}{2}\nabla_2[(122331)+(133221)].\end{gathered}\tag{24a}$$

(But $\nabla_2(122331)\neq\tfrac{1}{2}\nabla_2(122331)$.) (b)

$$\Delta_2(12)=\Delta_2(12),\quad \Delta_2(21)=0,\quad \Delta_2(2)=[\Delta_2(a,2)]_{a=2}.\tag{24b}$$

4. Special cases:—(a) One finds that $\mathfrak{D}^{\mathrm{VI}}$ consists of one six-cycle, 15 five-cycles, 85 four-cycles, 225 three-cycles, 274 two-cycles, and 120 one-cycles, a total of 6! terms. These figures can be checked in the following way: consider

$$(0|\sum_{i_1}'\cdots\sum_{i_6}'V(i_1,\cdots,i_6)|0)\quad\text{for } V(i_1,\cdots,i_6)=1,\quad N=1.$$

$V_{00}=n(n-1)\cdots(n-5)$. This result must also be obtained from $\int\cdots\int\mathbf{V}(123456)\mathfrak{D}^{\mathrm{VI}}d\tau_{1\cdots 6}$. For simplicity consider oxygen ($n=16$). For this case $\int(123\cdots l1)d\tau_{1\cdots l}=4^{l+1}$, and therefore

$$\int\mathfrak{D}^{\mathrm{VI}}d\tau_{1\cdots 6}=4^6\left[4^6-\frac{15\times 4^5}{4}+\frac{85\times 4^4}{4^2}-\frac{225\times 4^3}{4^3}+\frac{274\times 4^2}{4^4}-\frac{120\times 4}{4^5}\right]=\frac{16!}{10!},\ \text{q.e.d.}$$

(b) For $m=0$ Eq. (21) reduces to $1_{00}=N$, for

[28] For notation see Appendix IV.

$m=n$ to the single term

$$(0|V(1,2,\cdots,n)|0)=N\int\psi_1'^*\cdots\psi_n'^*\mathbf{V}\Psi_0'dT_{1-n} \quad (25)$$

for $m>n$ it vanishes.

5. The density function for oxygen:—For oxygen take

$$\begin{aligned}u_1(i)=\cdots=u_4(i)&=S(x_iy_iz_i)\\&=(2\alpha\sigma/\pi)^{\frac{1}{4}}\exp(-\tau r_i^2),\\ u_{13}(i)=\cdots=u_{16}(i)&=z_iP(x_iy_iz_i)\\&=z_i(4\alpha\sigma)^{\frac{1}{2}}(2\alpha\sigma/\pi)^{\frac{1}{4}}\exp(-\tau r_i^2),\end{aligned} \quad (26a)$$

$$N_S=\int S^*(1)S(1)d\tau_1=(\alpha\sigma/\tau)^{\frac{1}{4}},$$

$$N_P=\int z^2P^*Pd\tau=(\alpha\sigma/\tau)^{5/2},\quad N=N_S^4N_P^{12}. \quad (26b)$$

Naturally the integration over τ refers to the space coordinates, not to the parameter τ. Actually $\tau\equiv\alpha\sigma$, and so the normalization constants reduce to unity. It is preferable to write τ in the exponent instead of $\alpha\sigma$, because some matrix elements can be obtained by differentiation with respect to τ and replacing τ afterwards by $\alpha\sigma$. In terms of the functions (26)

$$\begin{aligned}\tfrac{1}{4}(12)&=S^*(1)S(2)+\mathbf{r}_1\cdot\mathbf{r}_2P^*(1)P(2)\\&=(2\alpha\sigma/\pi)^{\frac{1}{4}}[1+4\alpha\sigma\mathbf{r}_1\cdot\mathbf{r}_2]\\&\quad\times\exp(-\tau(r_1^2+r_2^2)).\end{aligned} \quad (27)$$

For example, in

$$\int J(r_{13})J^2(r_{23})(3)|12|^2d\tau_{1-3}=4^2\int J(r_{13})J^2(r_{23})$$
$$\times[S^6+(3x_3^2+6x_1x_2)S^4P^2+(6x_1x_2x_3^2+12x_1x_2y_3^2$$
$$+3x_1^2x_2^2+6x_1y_1x_2y_2)S^2P^4+(3x_1^2x_2^2x_3^2$$
$$+6x_1^2x_3^2y_3^2+12x_1y_1x_2y_2x_3^2+6x_1y_1x_2y_2z_3^2)P^6]d\tau_{123}$$

the exponential dependence of the integrand is given by

$$\exp\{-\alpha[r_{13}^2+2r_{23}^2+2\sigma(r_1^2+r_2^2+r_3^2)]\}.$$

The substitution

$$\mathbf{r}_1=\mathbf{R}_1+\frac{\mathbf{R}_2}{2\sigma+1},\quad \mathbf{r}_2=\mathbf{R}_2+\frac{\mathbf{R}_3}{\sigma+1},\quad \mathbf{r}_3=\mathbf{R}_3,$$

permits separation of the variables. A typical term

$$C_2^{\mathrm{III}}\equiv\int J(r_{13})J^2(r_{23})x_1y_1x_2y_2S^2P^4d\tau_{123}$$

thus becomes

$$[A^3(2\alpha\sigma/\pi)^{9/2}(4\alpha\sigma)^2]\int\exp\left\{-\alpha\left[(2\sigma+1)R_1^2\right.\right.$$
$$\left.\left.+2(\sigma+1)R_2^2+2\sigma\left(1+\frac{3\sigma+2}{(2\sigma+1)(\sigma+1)}\right)R_3^2\right]\right\}$$
$$\times\left[\frac{X_3^2Y_3^2}{(2\sigma+1)^2(\sigma+1)^2}+\cdots\right]dT_{123}$$

and can be written in the form

$$[\ ]\int\exp\{\ \}\left[\frac{R_3^4}{15(2\sigma+1)^2(\sigma+1)^2}\right](4\pi)^3$$
$$\times R_1^2R_2^2R_3^2dR_1dR_2dR_3$$

which now permits immediate integration. The result is

$$C_2^{\mathrm{III}}=A^3\frac{2^{\frac{1}{2}}\sigma^3}{[2(\sigma+1)^2+2\sigma+1]^{7/2}}.$$

For many indices the decomposition into a linearly independent set of such integrals, even to a greater extent than their evaluation, becomes overwhelmingly laborious. In the case of oxygen evaluation of H_3 necessitated the calculation of several thousand such terms.

6. Matrix elements of $T_{\mathrm{c.g.}}$:—Substitute $T_{\mathrm{c.g.}}=-(1/2n)\Delta_{\mathrm{c.g.}}$ into formula (25), introduce relative and c.g. coordinates, $z=z_{\mathrm{rel}}+z_{\mathrm{c.g.}}$, and write Ψ_0 in the form determinant $\times\exp\{-\tau[\sum r_{\mathrm{rel}}^2+nr_{\mathrm{c.g.}}^2]\}$. One finds[29]

$$\Delta_{\mathrm{c.g.}}\Psi_0=(-6\tau n+4\tau^2n^2r_{\mathrm{c.g.}}^2)\Psi_0. \quad (28)$$

Integration yields $(T_{\mathrm{c.g.}})_{00}=\frac{3}{2}\alpha\sigma$, and more generally, since $T_{\mathrm{c.g.}}$ commutes with $J(r_{ij})$, $(T_{\mathrm{c.g.}})_{ij}=\frac{3}{2}\alpha\sigma 1_{ij}$.

[29] The case of oxygen is considered but the method is also applicable in other cases. See Bethe and Rose, Phys. Rev. **51**, 283 (1937).

(c) Matrix components of H_1, H_2, H_3

Determination of H_n requires the evaluation of expressions of the type

$$W_{MT}=\int \Psi_M W\Psi_T=\int \Psi_0{}^* M^\dagger WT\Psi_0.$$

The expressions for the matrix elements listed below which do not involve the operator T are general. The same holds true for T_{WW}, T_{MW}, T_{MM}. These matrix elements have been calculated by decomposing them into sums of type (22). The other matrix elements involving T imply the use of functions of type (26). With these functions, the observation[30]

$$\begin{aligned} T\Psi_0&=[(3s+5p)\tau-2\tau^2\textstyle\sum r_i{}^2]\Psi_0=\Gamma\Psi_0, \\ \Gamma(\tau)&=(3s+5p)\tau+2\tau^2 d/d\tau \end{aligned} \qquad (29)$$

permits a much simpler method of evaluation than the use of formula (22). A matrix element given in the form $\Gamma_a\Gamma_b{}^2 NV_{kl}$ will be evaluated in the following way: first, perform the operation $\Gamma(\tau_a)[\Gamma(\tau_b)]^2$; second, replace in the result $\tau_a{}^i\tau_b{}^j$ by τ^{i+j}, $2^{i+j}(d^i/d\tau_a{}^i)(d^j/d\tau_b{}^j)$ by $d^{i+j}/d\tau^{i+j}$; third, apply this new operator on NV_{kl} where N is given by formula (26b); fourth, replace τ by $\alpha\sigma$. This simplified calculation is possible in all those cases where T can be applied directly on Ψ_0, e.g. in $\int\Psi_0{}^* WMT\Psi_0$. Expressions of type $\int\Psi_0{}^* WTM\Psi_0$ lead to

$$\int\Psi_0{}^* WMT\Psi_0+\int\Psi_0{}^* W(TM-MT)\Psi_0,$$

i.e. the sum of a term obtainable by differentiation and a commutator term. This permits the determination of T_{WW}, T_{MW}, T_{MM} by calculating W_{WT}, W_{MT}, M_{MT}, and adding merely the "grad" integrals indicated in the former. The labor thus saved is enormous, but this simplification was noticed too late to make extensive use of it in the present calculations.[31]

Formulae (30)

$$V_{ij}=V_{ji}\quad (V=1, W, M, T),$$

$$1_{OO}=1,$$

$$1_{WO}=W_{OO}=\tfrac{1}{2}\int J(r_{12})\mathfrak{D}^{II}d\tau_{12},$$

$$1_{MO}=M_{OO}=\tfrac{1}{2}\int J(r_{12})\mathbf{P}_{12}\mathfrak{D}^{II}d\tau_{12},$$

$$1_{WW}=W_{WO}=\tfrac{1}{4}\int J(12)J(34)\mathfrak{D}^{IV}dt_{1-4}+\int J(13)J(23)\mathfrak{D}^{III}d\tau_{1-3}+\tfrac{1}{2}\int J^2(12)\mathfrak{D}^{II}d\tau_{12},$$

$$1_{MW}=W_{MO}=M_{WO}=\tfrac{1}{4}\int J(12)J(34)\mathbf{P}_{12}\mathfrak{D}^{IV}d\tau_{1-4}$$
$$+\int J(13)J(23)\mathbf{P}_{12}\mathfrak{D}^{III}d\tau_{1-3}+\tfrac{1}{2}\int J^2(12)\mathbf{P}_{12}\mathfrak{D}^{II}d\tau_{12},$$

$$1_{MM}=M_{MO}=\tfrac{1}{4}\int J(12)J(34)\mathbf{P}_{12}\mathbf{P}_{34}\mathfrak{D}^{IV}d\tau_{1-4}+\int J(13)J(23)\mathbf{P}_{123}\mathfrak{D}^{III}d\tau_{1-3}+\tfrac{1}{2}\int J^2(12)D^{II}d\tau_{12},$$

$$W_{WW}=\tfrac{1}{8}\int J(12)J(34)J(56)\mathfrak{D}^{VI}+\tfrac{3}{2}\int J(12)J(35)J(45)\mathfrak{D}^{V}+3\int J(12)J(23)J(34)\mathfrak{D}^{IV}$$
$$+\int J(12)J(13)J(14)\mathfrak{D}^{IV}+\tfrac{3}{4}\int J(12)J^2(34)\mathfrak{D}^{IV}+3\int J(13)J^2(23)\mathfrak{D}^{III}$$
$$+\int J(12)J(23)J(31)\mathfrak{D}^{III}+\tfrac{1}{2}\int J^3(12)\mathfrak{D}^{II},$$

$$W_{MW}=M_{WW}=\tfrac{1}{8}\int J(12)J(34)J(56)\mathbf{P}_{12}\mathfrak{D}^{VI}+\int J(12)J(35)J(45)(\tfrac{1}{2}\mathbf{P}_{12}+\mathbf{P}_{35})\mathfrak{D}^{V}$$
$$+\int J(12)J(23)J(34)(2\mathbf{P}_{12}+\mathbf{P}_{23})\mathfrak{D}^{IV}+\int J(12)J(13)J(14)\mathbf{P}_{12}\mathfrak{D}^{IV}$$
$$+\int J(12)J^2(34)(\tfrac{1}{4}\mathbf{P}_{12}+\tfrac{1}{2}\mathbf{P}_{34})\mathfrak{D}^{IV}+\int J(13)J^2(23)(\mathbf{P}_{13}+2\mathbf{P}_{23})\mathfrak{D}^{III}$$
$$+\int J(12)J(23)J(31)\mathbf{P}_{12}\mathfrak{D}^{III}+\tfrac{1}{2}\int J^3(12)\mathbf{P}_{12}\mathfrak{D}^{II},$$

[30] s gives the number of s particles, p the number of p particles in the nucleus.

[31] However some of the checking was done by the simpler method. It is to be considered very satisfactory that the matrix elements evaluated by the two independent methods agree to nine figures. Most of the matrix elements were calculated to ten figures.

$$W_{MM}=M_{MW}=\tfrac{1}{6}\int J(12)J(34)J(56)\mathbf{P}_{12}\mathbf{P}_{34}\mathfrak{D}^{VI}+\int J(12)J(35)J(45)(\tfrac{1}{2}\mathbf{P}_{345}+\mathbf{P}_{12}\mathbf{P}_{35})\mathfrak{D}^{V}$$
$$+\int J(12)J(23)J(34)(\mathbf{P}_{123}+\mathbf{P}_{132}+\mathbf{P}_{12}\mathbf{P}_{34})\mathfrak{D}^{IV}+\int J(12)J(13)J(14)\mathbf{P}_{123}\mathfrak{D}^{IV}$$
$$+\int J(12)J^2(34)(\tfrac{1}{4}+\tfrac{1}{2}\mathbf{P}_{12}\mathbf{P}_{34})\mathfrak{D}^{IV}+\int J(13)J^2(23)(1+\mathbf{P}_{123}+\mathbf{P}_{132})\mathfrak{D}^{III}$$
$$+\int J(12)J(23)J(31)\mathbf{P}_{123}\mathfrak{D}^{III}+\tfrac{1}{2}\int J^3(12)\mathfrak{D}^{II},$$

$$M_{MM}=\tfrac{1}{6}\int J(12)J(34)J(56)\mathbf{P}_{12}\mathbf{P}_{34}\mathbf{P}_{56}\mathfrak{D}^{VI}+\tfrac{3}{2}\int J(12)J(35)J(45)\mathbf{P}_{12}\mathbf{P}_{345}\mathfrak{D}^{V}$$
$$+\int J(12)J(23)J(34)(\mathbf{P}_{1234}+\mathbf{P}_{1243}+\mathbf{P}_{1342})\mathfrak{D}^{IV}+\int J(12)J(13)J(14)\mathbf{P}_{1234}\mathfrak{D}^{IV}$$
$$+\tfrac{3}{4}\int J(12)J^2(34)\mathbf{P}_{12}\mathfrak{D}^{IV}+\int J(13)J^2(23)(\mathbf{P}_{12}+2\mathbf{P}_{13})\mathfrak{D}^{III}$$
$$+\int J(12)J(23)J(31)\mathbf{P}_{12}\mathfrak{D}^{III}+\tfrac{1}{2}\int J^3(12)\mathbf{P}_{12}\mathfrak{D}^{II},$$

$$1_{TO}=T_{OO}=\Gamma_b N1_{OO},\qquad T_{WT}=\Gamma_b{}^2NW_{OO},$$
$$1_{TT}=T_{TO}=\Gamma_a\Gamma_b N1_{OO},\qquad T_{MT}=\Gamma_b{}^2NM_{OO},$$
$$T_{TT}=\Gamma_a\Gamma_b{}^2N1_{OO},$$
$$W_{WT}=\Gamma_b NW_{WO},$$
$$T_{WO}=W_{TO}=\Gamma_b NW_{OO},\qquad W_{MT}=M_{WT}=\Gamma_b NW_{MO},$$
$$T_{MO}=M_{TO}=\Gamma_b NM_{OO},\qquad M_{MT}=\Gamma_b NM_{MO},$$
$$W_{TT}=\Gamma_a\Gamma_b NW_{OO},$$
$$M_{TT}=\Gamma_a\Gamma_b NM_{OO},$$

$$-2T_{WW}=\tfrac{1}{6}\int J(12)J(34)\Delta_5\mathfrak{D}^{V}d\tau_{1-5}+\int J(12)J(34)\Delta_4\mathfrak{D}^{IV}d\tau_{1-4}+\int J(13)J(23)\Delta_4\mathfrak{D}^{IV}d\tau_{1-4}$$
$$+\int[J(13)J(23)(2\Delta_1+\Delta_3)-\nabla_3 J(13)\cdot\nabla_3 J(23)]\mathfrak{D}^{III}d\tau_{1-3}$$
$$+\tfrac{1}{2}\int J^2(12)\Delta_3\mathfrak{D}^{III}d\tau_{1-3}+\int[J^2(12)\Delta_1-\{\nabla_1 J(12)\}^2]\mathfrak{D}^{II}d\tau_{12},$$

$$-2T_{MW}=\tfrac{1}{6}\int J(12)J(34)\Delta_5\mathbf{P}_{12}\mathfrak{D}^{V}d\tau_{1-5}+\int J(12)J(34)\Delta_4\tfrac{1}{2}(\mathbf{P}_{12}+\mathbf{P}_{34})\mathfrak{D}^{IV}d\tau_{1-4}$$
$$+\int J(13)J(23)\Delta_4\mathbf{P}_{12}\mathfrak{D}^{IV}d\tau_{1-4}+\int[J(13)J(23)(2\Delta_1+\Delta_3)-\nabla_3 J(13)\cdot\nabla_3 J(23)]$$
$$\times\tfrac{1}{2}(\mathbf{P}_{13}+\mathbf{P}_{23})\mathfrak{D}^{III}d\tau_{1-3}+\tfrac{1}{2}\int J^2(12)\Delta_3\mathbf{P}_{12}\mathfrak{D}^{III}d\tau_{1-3}+\int[J^2(12)\Delta_1-\{\nabla_1 J(12)\}^2]\mathbf{P}_{12}\mathfrak{D}^{II}d\tau_{12},$$

$$-2T_{MM}=\tfrac{1}{4}\int J(12)J(34)\Delta_5\mathbf{P}_{12}\mathbf{P}_{34}\mathfrak{D}^{V}d\tau_{1-5}+\int J(12)J(34)\Delta_4\mathbf{P}_{12}\mathbf{P}_{34}\mathfrak{D}^{IV}d\tau_{1-4}$$
$$+\int J(13)J(23)\Delta_4\mathbf{P}_{123}\mathfrak{D}^{IV}d\tau_{1-4}+\int[J(13)J(23)(2\Delta_1+\Delta_3)-\nabla_3 J(13)\cdot\nabla_3 J(23)]$$
$$\times\tfrac{1}{2}(\mathbf{P}_{123}+\mathbf{P}_{132})\mathfrak{D}^{III}d\tau_{1-3}+\tfrac{15}{16}\int J(23)\nabla_1 J(13)[\nabla_1(133221)-\nabla_1(122331)]d\tau_{1-3}$$
$$+\tfrac{1}{2}\int J^2(12)\Delta_3\mathfrak{D}^{III}d\tau_{1-3}+\int[J^2(12)\Delta_1-\{\nabla_1 J(12)\}^2]\mathfrak{D}^{II}d\tau_{12}.$$

A very convenient check is available for these expressions. Consider for example $-2T_{MM}$. Replace Δ_i by 1, $J(r_{ik})$ by 1. It is seen from expression (31) that $-2T_{MM}$ must reduce to $\frac{1}{4}n[n(n-1)]^2$. By example 4a, $-2T_{MM}$ becomes

$$\tfrac{1}{4}n(n-1)(n-2)(n-3)(n-4)+2n(n-1)(n-2)(n-3)+\tfrac{7}{2}n(n-1)(n-2)+n(n-1),$$

the required result.

The derivation of the formula for T_{MM} illustrates the method by which expressions (30) were obtained:

$$-2T_{MM}=\tfrac{1}{4}(0|\sum_{\alpha\neq\beta}\sum J(\alpha\beta)\mathbf{P}_{\alpha\beta}{}^{\dagger}\sum_{i}\Delta_i\sum_{\gamma\neq\delta}\sum J(\gamma\delta)\mathbf{P}_{\gamma\delta}|0) \tag{31}$$

$$=\tfrac{1}{4}\int J(12)\mathbf{P}_{12}{}^{\dagger}(\sum_{1}^{3}\Delta_i)J(34)\mathbf{P}_{34}\mathfrak{D}+\int J(13)\mathbf{P}_{13}{}^{\dagger}(\sum_{1}^{4}\Delta_i)J(23)\mathbf{P}_{23}\mathfrak{D}$$

$$+\tfrac{1}{2}\int J(12)\mathbf{P}_{12}{}^{\dagger}(\sum_{1}^{3}\Delta_i)J(12)\mathbf{P}_{12}\mathfrak{D}.$$

It will suffice to evaluate the terms $\sum_{1}^{3}$ in the middle expression of the right-hand side. Write $\mathbf{P}_{13}{}^{\dagger}\mathbf{P}_{23}\mathfrak{D}^{\mathrm{III}}=\mathbf{P}_{123}\mathfrak{D}^{\mathrm{III}}$ in the form

$$\tfrac{1}{2}(\mathbf{P}_{123}+\mathbf{P}_{132})\mathfrak{D}^{\mathrm{III}}+\tfrac{15}{32}[(122331)-(133221)]$$

and abbreviate this expression by $\mathbf{P}\mathfrak{D}+\frac{15}{32}R$. Then

$$\int J(13)\Delta_1 J(23)\mathbf{P}\mathfrak{D}=\int J(13)J(23)\Delta_1\mathbf{P}\mathfrak{D},$$

$$\int J(13)\Delta_2 J(23)\mathbf{P}\mathfrak{D}=\int J(13)[\Delta_2 J(23)]\mathbf{P}\mathfrak{D}+2\int J(13)\nabla_2 J(23)\cdot\nabla_2\mathbf{P}\mathfrak{D}+\int J(13)J(23)\Delta_2\mathbf{P}\mathfrak{D}$$

$$=\int J(13)J(23)\Delta_2\mathbf{P}\mathfrak{D}$$

(by formula (24a) and by Green's theorem),

$$\int J(13)\Delta_3 J(23)\mathbf{P}\mathfrak{D}=\int[J(13)J(23)\Delta_3-\nabla_3 J(13)\cdot\nabla_3 J(23)]\mathbf{P}\mathfrak{D},$$

$$\int J(13)(\Delta_1+\Delta_2)J(23)\tfrac{15}{32}R=\tfrac{15}{16}\int J(23)\nabla_1 J(13)\cdot[\nabla_1(133221)-\nabla_1(122331)]d\tau_{123},$$

$$\int J(13)\Delta_3 J(23)\tfrac{15}{32}R=0, \qquad \text{q.e.d.}$$

Appendix III

Derivation of formula (21)

It is sufficient to establish Eq. (21) for the two-index operator, $V=\sum_{i\neq k}\sum V(ik)$.

$$(A)\equiv(0|\,V(ik)\,|0)=\int(1/n!)^{\frac{1}{2}}\sum_{\nu}(-1)^{\nu}P_\nu\psi_1^*(1)\cdots\psi_n^*(n)\,V(ik)\,(1/n!)^{\frac{1}{2}}\sum_{\mu}(-1)^{\mu}P_\mu\psi_1(1)\cdots\psi_n(n)dT_{1-n}$$

$$=(1/n!)\sum_{\nu}\sum_{\mu}(-1)^{\nu+\mu}\int P_\nu\psi_1^*(1)P_\mu\psi_1(1)dT_1\cdots$$

$$\times\Big[\int\int P_\nu\psi_i^*(i)P_\nu\psi_k^*(k)\,V(ik)P_\mu\psi_i(i)P_\mu\psi_k(k)dT_{ik}\Big]\cdots\int P_\nu\psi_n^*(n)P_\mu\psi_n(n)dT_n,$$

where $\sum_{\nu}(-1)^{\nu}P_{\nu}$ effects all $n!$ permutations in the subscripts, and the sign, $+$, $-$ is taken according to whether the permutation is even or odd, respectively. For nonvanishing terms one must have

$$P_\nu\psi_j = P_\mu\psi_j \text{ for all } j \text{ except } j=i \text{ or } j=k. \text{ For}$$

$$\begin{matrix} P_\nu\psi_i^* = \psi_\iota^* \\ P_\nu\psi_k^* = \psi_\kappa^* \end{matrix} \text{ one must have either } \begin{matrix} P_\mu\psi_i = \psi_\iota \\ P_\mu\psi_k = \psi_\kappa \end{matrix} \text{ or } \begin{matrix} P_\mu\psi_i = \psi_\kappa \\ P_\mu\psi_k = \psi_\iota \end{matrix}.$$

The latter is obtained from the former by a transposition (odd permutation). Thus expression (A) becomes

$$(A) = (1/n!)\sum_{\nu} N_1 N_2 \cdots \left[\int\int \psi_\iota^*(i)\psi_\kappa^*(k)\, V(ik)\, \{\psi_\iota(i)\psi_\kappa(k) - \psi_\iota(k)\psi_\kappa(i)\}\, dT_{ik}\right] \cdots N_n$$

$$= (1/n!)N\sum_{\nu}\int\int \psi_\iota'^*(1)\psi_\kappa'^*(2)\, V(12) \begin{vmatrix} \psi_\iota'(1) & \psi_\iota'(2) \\ \psi_\kappa'(1) & \psi_\kappa'(2) \end{vmatrix} dT_{12},$$

and since there are $(n-2)!$ permutations which give $\psi_\iota^* = P_\nu\psi_i^*$ and $\psi_\kappa^* = P_\nu\psi_k^*$ one can write $\sum_{\nu} = (n-2)!\sum_{\iota\neq\kappa}\sum$. But the determinant vanishes for $\iota=\kappa$, so the condition $\iota\neq\kappa$ can be dropped and one obtains

$$(0|\, V(ik)\,|0) = \frac{N}{n(n-1)}\int\int \mathbf{V}(12) \begin{vmatrix} \sum_\iota \psi_\iota'^*(1)\psi_\iota'(1) & \sum_\iota \psi_\iota'^*(1)\psi_\iota'(2) \\ \sum_\kappa \psi_\kappa'^*(2)\psi_\kappa'(1) & \sum_\kappa \psi_\kappa'^*(2)\psi_\kappa'(2) \end{vmatrix} dT_{12},$$

from which Eq. (21) follows at once by observing that there are $n(n-1)$ $i\neq k$ combinations.

Appendix IV

Derivation of formula (22)

Use the abbreviations

$$\psi_\iota(13) \equiv \psi_\iota'^*(1)\psi_\iota'(3), \quad u_\iota(13) \equiv u_\iota'^*(1)u_\iota'(3),$$

$$\langle 133221\rangle \equiv [\eta_1(S_1)\eta_1(S_2) + \eta_2(S_1)\eta_2(S_2) + \eta_3(S_1)\eta_3(S_2) + \eta_4(S_1)\eta_4(S_2)]$$
$$\cdot [\eta_1(S_2)\eta_1(S_2) + + +] \cdot [\eta_1(S_2)\eta_1(S_1) + + +].$$

Obviously,

$$\sum_{S_1}\sum_{S_2}\sum_{S_3}\langle 133221\rangle = \sum_{S_1}\sum_{S_2}\sum_{S_3}[\eta_1^2(S_1)\eta_1^2(S_2)\eta_1^2(S_3) + \eta_2^2(S_1)\eta_2^2(S_2)\eta_2^2(S_3) + \eta_3^2(S_1)\eta_3^2(S_2)\eta_3^2(S_3)$$
$$+ \eta_4^2(S_1)\eta_4^2(S_2)\eta_4^2(S_3) + \text{terms involving cross products of } \eta_\iota],$$

and this expression reduces by orthogonality and completeness relations to

$$\sum_{S_1}\sum_{S_2}\sum_{S_3}\langle 133221\rangle = 4,$$

and in general one obtains

$$\sum_{S_1}\sum_{S_2}\cdots\sum_{S_n}\langle 1223\cdots n1\rangle = 4 \qquad (=2 \text{ for the case of two spin functions}).$$

In establishing Eq. (22) it is sufficient to consider a typical product to which expansion of the

determinant and spin summation lead for the case of $m=4$:

$$(B)\equiv\sum_{S_1}\sum_{S_2}\sum_{S_3}\sum_{S_4}\sum_{\iota}\psi_{\iota}(13)\sum_{\varkappa}\psi_{\varkappa}(32)\sum_{\lambda}\psi_{\lambda}(21)\sum_{\mu}\psi_{\mu}(44).$$

This expression must reduce to

$$4^{-2}(133221)(4).$$

But, if S denotes the summation over all separated space orbits (each separate orbit contributes one term, $S=\sum_{\iota/4}$) expression (B) becomes

$$(B)=\sum_{S_1}\cdots\sum_{S_4}S\cdots S u_{\iota}(13)u_{\varkappa}(32)u_{\lambda}(21)u_{\mu}(44)\langle 133221\rangle\langle 44\rangle$$

$$=4^{-4}\sum_{S_1}\cdots\sum_{S_4}\sum_{\iota}\cdots\sum_{\mu}=4^{2-4}(133221)(4),\quad \text{q.e.d.}$$

The exponent of 4 in the numerator gives the number of cycles, the one in the denominator the number of indices.

JANUARY 1, 1939 PHYSICAL REVIEW VOLUME 55

Dissipative Acoustic Reflection Coefficients in Gases by Ultrasonic Interferometry

R. S. ALLEMAN
Rowland Physical Laboratory, The Johns Hopkins University, Baltimore, Maryland

(Received August 8, 1938)

Reflection coefficients for ultrasonic waves in gases, much lower than allowed by the dynamical theory of sound, first evaluated for a single frequency by J. C. Hubbard, and found by R. W. Curtis to have a frequency dependence, are satisfactorily explained by the new heat conduction theory of acoustic reflection developed by K. F. Herzfeld. This paper presents a modification of the theory of the acoustic resonator interferometer so as to include dissipative losses by emission and reflection at the source as well as losses by reflection at the reflector. The analysis of previously obtained and new data for CO_2, air, and He shows excellent agreement with Herzfeld's theory in all cases showing minimum losses. The requirements for securing such data, including the plane parallelism of source and reflector and modes of vibration of the source have been studied by optical, electrical and acoustical methods. The parallelism requirement is most rigorous and of a higher order of magnitude than for velocity determinations. Slight departures result in apparent losses of great magnitude. This requirement is best fulfilled by adjustment for maximum acoustic reaction, or peak height, while the interferometer is in actual operation. The sensitivity of the interferometer is greatly increased by blocking out unused radiation by reflecting plates at a quarter wave-length distance from the source.

INTRODUCTION

THE study of acoustic resonator interferometry, by Hubbard,[1] resulting in experimental evaluations of the fraction, γ^2, of normal incident ultrasonic energy which is reflected from a plane solid boundary, gave values which indicated a reflection loss of several percent—approximately 7 percent—in the case of dry air at 597 kc. He used a steel or brass reflector, for which the loss predicted by the usual calculation[2] for the vibrational energy transmitted to the reflector should be about 0.04 percent—nearly 200 times smaller than the value deduced from

[1] J. C. Hubbard, Phys. Rev. **38**, 1011 (1931); **41**, 523 (1932); **46**, 525 (1934).

[2] I. B. Crandall, *Theory of Vibrating Systems and Sound* (D. Van Nostrand Company), pp. 92 ff.

experiment. Then, it was suggested that resonant effects might easily account for such high losses, but subsequent measurements by Curtis[3] indicated systematically lower reflection coefficients at higher frequencies and thus higher losses.

Following the work of Curtis, K. F. Herzfeld[4] made theoretical calculations in an attempt to explain the experimental results on the basis of heat conduction into the solid boundary from the higher temperatures of compressions, and out of the boundary during the rarefactions. The result was the introduction into the theory of reflection of a highly damped, slowly moving wave, called "temperature wave," in the gas. This wave, being out of phase with the incident and reflected waves, reduces the amplitude and changes the phase of the wave at reflection, thereby giving rise to a considerable energy loss of a dissipative nature. Reflection losses thus predicted depend not only on the particular gas, but also upon the square root of the frequency of the sound wave. Numerical calculations showed that these considerations accounted in some cases for half, in many cases for much less than half the losses deduced from measurements with the acoustic interferometer. In the theory of the interferometer, according to the usual boundary conditions, a coefficient of reflection had been assigned to the reflector, but not to the source.

It has, therefore, been the object of the studies presented here to investigate the experimental and theoretical bases of acoustic resonator interferometry, in an attempt to find a satisfactory explanation for the wide discrepancies between theoretical and experimental values of reflection coefficients. In the first part is presented a revision of the acoustical analysis of the interferometer, as required by Herzfeld's new theory of sound reflection, after which experimental requirements and investigations are discussed.

Acoustical Analysis of Interferometer with Dissipative Reflection Coefficients

The acoustical analysis of Hubbard's resonator interferometer consists of finding expressions for equilibrium values of excess pressure, caused by multiply reflected waves, between a source, S,

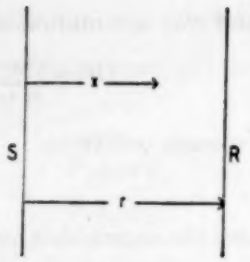

Fig. 1. Scheme of interferometer with source S, reflector R, and fluid column of length r.

and a solid plane reflector, R, parallel to the source, Fig. 1. Such expressions are to be written in terms of: the motion of the source, $\dot{\xi}_{x=0}=\dot{\xi}_0 e^{i\omega t}$; the attenuation coefficient, α, such that $d\dot{\xi}_x/\dot{\xi}_x=-\alpha dx$; coefficients of sound reflection, γ; velocity, v, frequency, $\nu=\omega/2\pi$, and gas density, ρ; and the coordinates x and r. In the notation used here, $\dot{\xi}_{x=x}=\dot{\xi}_x e^{i\omega t}$ is the particle velocity at the point x, and at the time t, in which $\dot{\xi}_x$ is the complex amplitude of particle velocity, and includes the phase of the motion with respect to that of the source, at $x=0$.

Characteristics of the reflection process, and thus of the reflection coefficients, are obtained from Herzfeld's new analysis of sound reflection, namely: (1) heat conduction effects, dissipative processes, reduce the accelerating force possessed by a gas wave near a solid boundary; (2) all solids act as infinitely good conductors as compared with the gas; (3) the amplitude reflection coefficient, γ, is a complex fraction defined by $\gamma^2\equiv\gamma^* e^{-2i\varphi}\equiv e^{-\beta^*}e^{-2i\varphi}$, which expresses a phase change upon reflection, with respect to the incident wave; and (4), continuity of velocity at a boundary is preserved by a highly damped, slow velocity wave, called "temperature wave," which is set up in the gas near the reflector.

The relative order of magnitudes of the losses caused by this dissipative reflection coefficient, γ, and the usual nondissipative loss, caused by $\gamma_0=(v_1\rho_1-v_2\rho_2)/(v_1\rho_1+v_2\rho_2)$, are such, it has been assumed in what follows, that the latter is negligible, and that accordingly the reflector is stationary insofar as it effects the pressure variations at the source.

By applying the same type of analysis as used by Herzfeld in obtaining the reduction in amplitude of a wave on reflection, it may be shown that the wave emitted by a source also suffers

[3] R. W. Curtis, Phys. Rev. 46, 811 (1934).
[4] K. F. Herzfeld, Phys. Rev. 53, 899 (1938).

a reduction in amplitude and phase as it leaves the source. The result is, within the same limits of approximation used by him, that the amplitude of motion, ξ_0, of the source produces a regular wave of amplitude $\gamma'\xi_0$, and a temperature wave of amplitude $(1-\gamma')\xi_0$, in which γ' is related to the γ previously defined and calculated by Herzfeld, by the equation

$$\gamma' = \tfrac{1}{2}(1+\gamma) \tag{1}$$

or approximately, $\gamma' = \gamma^{\frac{1}{2}}$. This equation, and the previous definitions allow one to write down the necessary expressions for particle velocities near the source, in terms of direct and reflected waves of both types: temperature waves of velocity v_2, and ordinary waves of velocity v.

At a point x, near the source, one need not consider temperature waves proceeding from the reflector, since they are so quickly removed by absorption. (The absorption coefficient, α_2, of these temperature waves, as calculated by Herzfeld, is, for $\nu = 10^6$, in air, about 7×10^3.) Accordingly, if $\xi_x(+)$, $\xi_x(-)$, and $\xi_x(T+)$, represent respectively the sum of amplitudes of forward, backward, and forward temperature waves at x, near the source, it follows that

$$\xi_x(+) = \xi_0\gamma' e^{-(\alpha+i\omega/v)x}\sum,$$

$$\xi_x(-) = -\xi_0\gamma'\gamma e^{-(\alpha+i\omega/v)(2r-x)}\sum,$$

and

$$\xi_x(T+) = \xi_0 e^{-(\alpha_2+i\omega/v_2)x} \times\{(1-\gamma')+(1-\gamma)\gamma'\gamma e^{-(\alpha+i\omega/v)2r}\sum\},$$

in which $\sum$ stands for the sum

$$\sum = \sum_{m=0}^{m=\infty}[\gamma^2 e^{-(\alpha+i\omega/v)2r}]^m = [1-\gamma^* e^{-2r\alpha-i\delta}]^{-1},$$

where the phase angle, δ, is given by

$$\delta = 2r\omega/v + 2\varphi. \tag{2}$$

At $x=0$, or the source, the expressions above reduce to

$$\xi_0(+) = \xi_0\gamma'[1-\gamma^* e^{-(2r\alpha+i\delta)}]^{-1}, \tag{3}$$

$$\xi_0(-) = -\xi_0(\gamma'/\gamma)\gamma^* e^{-(2r\alpha+i\delta)} \times[1-\gamma^* e^{-(2r\alpha+i\delta)}]^{-1}, \tag{4}$$

and

$$\xi_0(T+) = \xi_0 - \xi_0(+) - \xi_0(-). \tag{5}$$

The latter equation expresses the fact of continuity of velocity at the source.

For convenience in calculating the pressure on the source, Eqs. (3), (4) and (5) may be written as:

$$\xi_0(+) = \xi(+)[1-\epsilon(+)], \tag{6}$$

where $\xi(+) = \xi_0\sum$ and $\epsilon(+) = (1-\gamma')$;

$$\xi_0(-) = -\xi(-)[1-\epsilon(-)], \tag{7}$$

where $\xi(-) = \xi_0(\sum -1)$, and $\epsilon(-) = (1-\gamma'/\gamma)$;

and $$\xi_0(T+) = \xi(+)\epsilon(+) - \xi(-)\epsilon(-). \tag{8}$$

Thus, the excess pressure, $p_{x=0} = p_0 e^{i\omega t}$, at the source, is calculated by

$$p_0 = \rho v\{\xi_0(+) - \xi_0(-) + (v_2/v)\xi_0(T+)\}, \tag{9}$$

or

$$p_0 = \rho v\{\xi(+)+\xi(-)\} - \rho v\{\epsilon(+)\xi(+)+\epsilon(-)\xi(-)\} + \rho v(v_2/v)\{\xi(+)\epsilon(+)-\xi(-)\epsilon(-)\}.$$

The principal contribution to p_0 will come from the first term; the second, is of the order $1-\gamma'$ compared with the first; and the third, the contribution of the temperature waves, is of still higher order in $1-\gamma$, on account of the small velocity, $v_2 \sim v(1-\gamma^*)$, of these temperature waves.

When the values for $\epsilon(+)$ and $\epsilon(-)$ are placed in (9), and the pressure of the temperature waves neglected, p_0 becomes,

$$p_0 = \rho v[\xi(+)+\xi(-)] - \rho v(1-\gamma')[\xi(+)+\xi(-)] + \rho v[(1/\gamma)-1]\gamma'\xi(-). \tag{10}$$

This complex expression can be rationalized into the form

$$p_0 = \rho v\xi_0 P_0 + \rho v\omega\xi_0 Q_0, \tag{11}$$

in which $P_0 = P+\Delta P$, and $Q_0 = Q+\Delta Q$, where

$$P = [\sinh(2r\alpha+\beta^*)]/[\cosh(2r\alpha+\beta^*)-\cos\delta], \tag{12}$$

$$Q = \sin\delta/[\cosh(2r\alpha+\beta^*)-\cos\delta];$$

and

$$\Delta P = (\tfrac{1}{2})(1-\gamma^{*\frac{1}{2}})[Q\sin\varphi - 1], \tag{13}$$

$$\Delta Q = (\tfrac{1}{2})\sin\varphi[1-P(1-\gamma^{*\frac{1}{2}})].$$

Since γ is a complex quantity of amplitude near unity and of phase $\varphi \doteq (1-\gamma^*)/2 \doteq \beta^*/2$, the

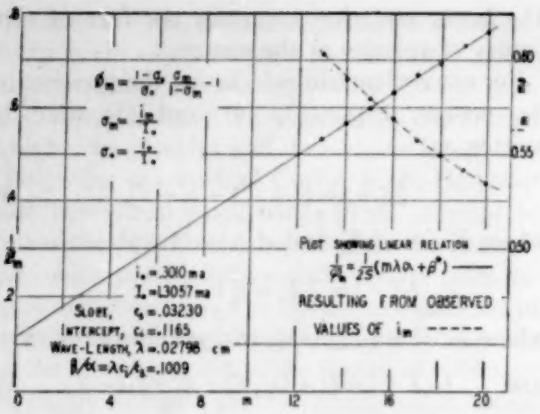

FIG. 2. Typical set of interferometer data, from which the ratio of reflection and absorption constants is calculated.

following approximations were used to obtain (13): $(\gamma^*)^{-\frac{1}{2}}-(\gamma^*)^{\frac{1}{2}}=2(1-\gamma^{*\frac{1}{2}})$, $(\gamma^*)^{-\frac{1}{2}}+(\gamma^*)^{\frac{1}{2}}=2$, $\cos\varphi=1$, and $\sin\varphi\doteq 1-(\gamma^*)^{\frac{1}{2}}\doteq\varphi$.

The functions P_0 and Q_0 have thus been written in terms of P and Q, because of the simplicity of calculation of these latter functions, and because of the relative magnitudes of ΔP and ΔQ compared with P and Q respectively. ΔP and ΔQ introduce slight dissymmetries into P_0 and Q_0, but the magnitude to which they effect interferometric current readings is small compared to the usual precision of measurements and subsequent approximations made in their analysis.

Therefore, to a good approximation for interferometer measurements, one can put $P_0=P$, and $Q_0=Q$ and write, for the excess pressure on the source,

$$p_{x=0}=\rho v\xi_{x=0}P+\rho v\omega\xi_{x=0}Q, \qquad (11')$$

wherein $\xi_{x=0}$ and $\xi_{x=0}$ are the velocity and displacement, respectively, of the source. P and Q can be given the useful forms

$$\begin{aligned} P&=\sinh\chi/[\cosh\chi-\cos\delta],\\ Q&=\sin\delta/[\cosh\chi-\cos\delta], \end{aligned} \qquad (12')$$

in which $\delta=[(r+\Delta r)/(\lambda/2)-m]2\pi$, $\Delta r/\lambda=\varphi/2\pi$, $\chi=2r\alpha+\beta^*$, and $\lambda=2\pi v/\omega$. Here, m is the nearest whole number of half-wave-lengths included in the distance r, between the reflector and source.

Hubbard has given the general character of the functions P and Q as r is varied, and has shown that at points for $\delta=0$, they take on critical values which yield to analysis. Thus at $\delta=0$, $Q_m=0$, $\chi_m=m\lambda\alpha+\beta^*-2\Delta r\alpha$ and

$$\begin{aligned} P_m&=1/\tanh(\chi_m/2) \qquad (14)\\ &\doteq 2/\chi_m, \end{aligned}$$

or $$1/P_m\doteq(m\lambda\alpha+\beta^*-2\Delta r\alpha)/2.$$

These values of P_m, for $\delta=0$, are maximum values and occur at half-wave-length separations; although the effect of the phase change, φ, occurring at the source and reflector, is to shorten the distance r necessary to make $\delta=0$, it does not alter the validity of the half-wave-length separations of P_m.

Hubbard has shown that interferometric current measurements, are capable of yielding experimental determinations of ultrasonic reflection and absorption coefficients by making use of equations analogous to (12) and (14). Thus, the function Φ_m, of current measurements, defined by

$$\Phi_m=[\{\sigma_m/(1-\sigma_m)\}\{(1-\sigma_0)/\sigma_0\}-1] \qquad (15)$$

was shown to be related to the values P_m by $\Phi_m=SP_m$ in which S is a constant of the interferometer unit. Accordingly, a linear relation should exist between observed values of m and $1/\Phi_m$ in the following form:

$$1/\Phi_m=\beta^*(m\lambda\alpha/\beta^*+1)/2S, \qquad (16)$$

in which the term $2\Delta r\alpha$ has been neglected in comparison with β^* in using Eq. (14).

Figure 2 shows a typical set of data and the corresponding plot of $1/\Phi_m$ against m, and illustrates the validity of their linear relationship. An electrical interpretation of Φ_m is the number of times the equivalent resistance of the interferometer unit, for $r=m\lambda/2$, has increased over its minimum value at $r=\lambda/4$. From the slope, $C_s=\beta^*\lambda(\alpha/\beta^*)/2S$, and intercept, $C_i=\beta^*/2S$, of the $1/\Phi_m$, m plot, the ratio $\beta^*/\alpha=\lambda C_i/C_s$ of the reflection and absorption constants is determined, provided the wavelength, λ, of the sound waves has been simultaneously observed. The remainder of the analysis to determine α and β^* separately from the peak structure, is outlined in Hubbard's original paper.

A comparison between this case of dissipative reflection losses, and that of nondissipaitve coefficients, first considered by Hubbard,[1] shows

that amplitude reflection coefficients as determined on the latter basis are actually intensity coefficients when interpreted on the dissipative basis. For, the term $\alpha\lambda C_i/C_s$ actually represents the exponential power in the intensity coefficient $\gamma^*=e^{-\beta^*}$, rather than the power in the former amplitude coefficient $\gamma=e^{-\beta}$.

Experimental Evidence for the New Theory of Sound Reflection

In the previous section it has been shown that one can easily convert previously determined values of reflection losses, assumed nondissipative, into losses interpreted on a dissipative basis. This has been done for previous measurements of Hubbard[1] and Curtis[3] as well as for some measurements of the author, for three gases; and the results compared with the theoretical frequency dependence as calculated by Herzfeld.[4] Table I presents nine such comparisons, in which the theoretical values have been determined from the following equations, taken from the original manuscript of Herzfeld's paper, showing how the square of the amplitude reflection coefficient γ^*, should depend upon the frequency $\nu=\omega/2\pi$. For air, $1-\gamma^*=4.4\times10^{-5}\sqrt{\nu}$; for CO_2, $1-\gamma^*=2.8\times10^{-5}\sqrt{\nu}$; and for helium, $1-\gamma^*=9.5\times10^{-5}\sqrt{\nu}(1-5\times10^{-5}\sqrt{\nu})$.

The experimental results given in Table I, also plotted on logarithmic scales in Fig. 3, by no means represent all values which have been recorded, but have been selected as *lower limiting values* of experimental determinations which, as a group, are in good agreement with the theoretical predictions. Numerous other determinations, all of which give much higher values of $1-\gamma^*$, are probably the result of improper alignment in the interferometer unit, as indicated in the following paragraphs. It is of interest to note that the first published result of Hubbard, when interpreted in terms of emissive and reflective losses at the source as well as losses at the reflector, for air at 597 kc, agrees perfectly with theory; and also of interest is the good agreement one obtains when reflection losses are high, and thus more easily measured, as for helium, as contrasted with the case of CO_2 in which reflection losses are small and measurements, because of high absorption, are exceedingly difficult.

Table I. *Theoretical and experimental reflection losses in air, helium and carbon dioxide.*

Gas	Frequency (kc/sec.)	$1-\gamma^*$ (exp.)	$1-\gamma^*$ (theo.)
Air	597	0.034*	0.034
"	1237	0.051†	0.049
CO_2	189	0.015‡	0.0122
"	597	0.0148*	0.0216
He	252	0.048‡	0.046
"	792	0.089†	0.081
"	1001	0.085‡	0.092
"	1192	0.101†	0.097
"	1976	0.118†	0.124

* Hubbard, reference 1. † Author. ‡ Curtis, reference 3.

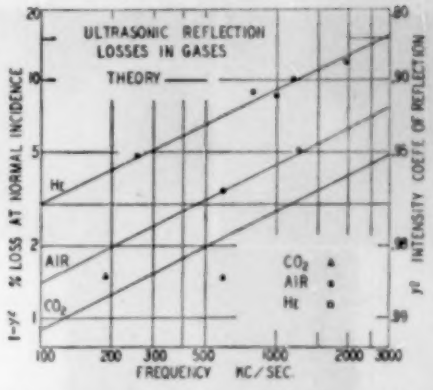

Fig. 3. Logarithmic plot of experimental and theoretical values of reflection coefficients, showing the frequency dependence, and degree of agreement of experimental values with theory (full curve).

Experimental Requirements and Adjustments in Ultrasonic Interferometry with Gases

As pointed out above, the lower values of $1-\gamma^*$ previously obtained are in good accord with Herzfeld's theory. However, the experimental requirements for obtaining limiting values are extremely rigorous, and small departures from such requirements result in great exaggeration of the values of the losses as calculated from experimental data. Therefore, in these last paragraphs some of the difficulties and requirements which must be met in working with the interferometer are presented.

The basic assumption and requirement in acoustic interferometry is that one works with plane, normal, sinusoidal waves between the source, a piezoelectric quartz plate in this case,

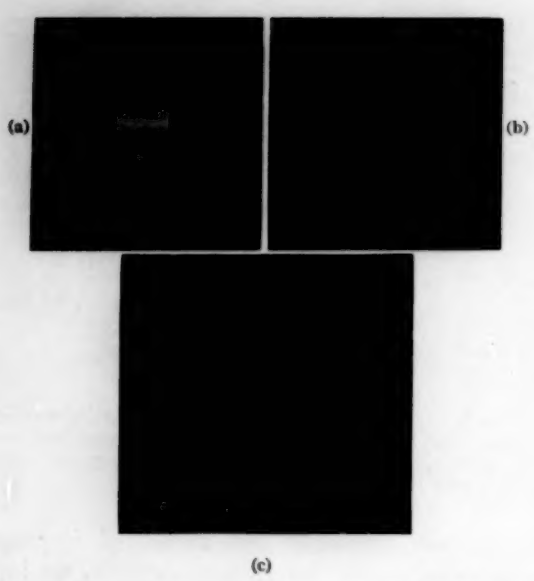

FIG. 4. *Schlieren* pictures of ultrasonic radiation fields in air. (a) and (b) are two different modes of the same crystal. (c) shows the standing wave structure of such disturbances.

and the reflector, with both source and reflector being plane and parallel to each other. The more nearly the mode of vibration of the source resembles a simple piston-like motion, the more nearly will the waves be plane. Thus the selection of a proper source involves finding a suitable mode of vibration. Two methods for investigating this point have been used: *schlieren* photographs have been made of the sound field, by using apparatus similar to that described by Taylor and Waldram.[5] Typical pictures indicating the type of acoustic disturbances created by certain quartz crystals are shown in Fig. 4; (a) and (b) are pictures of two different modes of the same 600-kc crystal, in which the mode (a) is more suitable for interferometric work than is (b). Fig. 4(c) is a typical picture of ultrasonic standing waves, obtained by allowing light from both sides of the central image in the diffraction pattern to form the image. (a) and (b) do not show standing waves, according to the Abbe theorem, since the diffraction pattern in such cases consists principally of only one first-order diffraction band.

The second method employed for the study of the mode of vibration is illustrated in Fig. 5. Here typical current peaks of acoustic reaction have been plotted for two conditions: (a) reflector parallel to source, and (b) reflector inclined at about 10′ of arc. Each secondary peak in the latter case is associated with a resonance position of the reflector with reference to an active region on the surface of the source, while the relative separation of the secondary peaks is indicative of the relative distribution of active regions of the source. The peak structure caused by nonparallelism is thus dependent upon the individual crystal used as well as its particular mode of vibration.

The evaluation of absorption and reflection coefficients being dependent upon measurement of peak width is thus seen to require a much higher degree of parallelism of source and reflector than that necessary for velocity measurements, since peculiarities of peak structure resulting from nonparallelism are repeated with only minor progressive changes over a considerable number of half-wave-length intervals. The necessary degree of parallelism is best

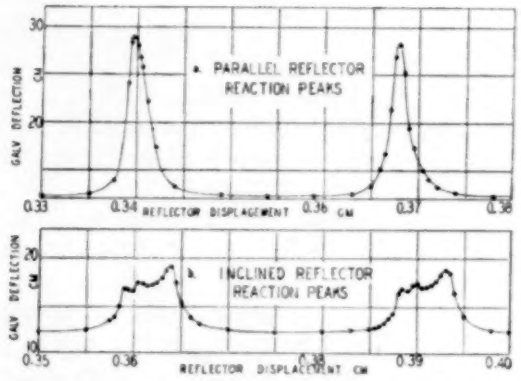

FIG. 5. The structure of reaction peaks depends greatly upon the alignment of the source and reflector. Adjustment for parallelism is critical for maximum height and minimum half-width.

attained while the interferometer is in actual operation, first by adjustment for decreasing the separation between principal and secondary peaks, finally by adjustment for absolute maximum of peak height. When this is attained the peaks have the appearance shown in Fig. 5(a). In the opinion of the author, lack of this adjustment, although only in a minor degree, is the most logical explanation of the abnormally high values of reflection losses obtained in the larger

[5] H. G. Taylor and J. M. Waldram, J. Sci. Inst. 10, 378 (1933).

number of experiments so far recorded. Particular attention should in future be given to the design of the interferometer with reference to the maintenance of this adjustment over considerable variations of distance.

As an extra precaution, increasing the sensitivity of adjustment for maximum peak height, and also increasing the precision of the determination of peak width, it is desirable to mount the source so as to secure lowest decrement or equivalent resistance. By backing the unused face of the quartz resonator with a solid plane cover placed at approximately an odd quarter wave-length, the equivalent minimum resistance of the interferometer is considerably reduced, as illustrated in Fig. 6. Here, two crevasses are plotted for two different boundary conditions: (1) odd quarter wave-length backing, and (2) open to bell jar covering. The deeper crevasse corresponds to the smaller resistance. This procedure should be followed in all work with the acoustic interferometer for gases, particularly if the gas is of high acoustic absorption, as is the case with CO_2.

Conclusion

The acoustic interferometer has been by far the most precise means available for determining ultrasonic velocity and absorption in gases. Herzfeld's theory of reflection of sound has now made possible the allocation of losses to both source and reflector so that excellent agreement is now obtained between the theoretical and experimental values of the reflection coefficients. It should be pointed out that nothing in this analysis affects the usual procedure in deriving values for acoustic velocity; the revised analysis affects the derivation of absorption coefficients only to the second order. Since dissipative reflection losses at ultrasonic frequencies are of a higher order of magnitude than losses by reflection as ordinarily calculated, the reflector may be considered as stationary insofar as it affects the pressure on the source.

Investigations of the experimental requirements in the design and operation of the interferometer have shown not only that a nearly piston-like mode of vibration of the source must be sought, but that acoustic parallelism, obtained by adjustment while the interferometer is in operation for maximum acoustic reaction or peak height, must for the evaluation of absorption and reflection coefficients be realized to a much higher order of precision than that required for simple velocity measurements.

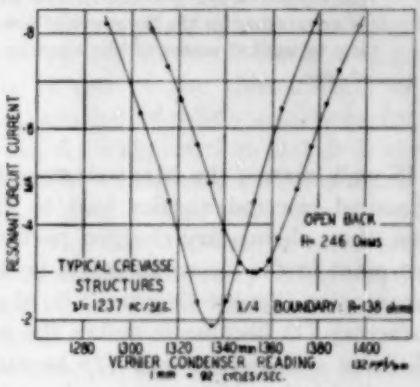

FIG. 6. Characteristic crevasse phenomena of quartz resonators. Height of minimum indicates the magnitude of the equivalent resistance. Blocking unwanted acoustic radiation by a backing plate on one side at $\lambda/4$ reduced the equivalent resistance from 246 to 138 ohms.

The author wishes to express his appreciation to Professor J. C. Hubbard for directing this research, to Professor K. F. Herzfeld for use of the manuscript of his paper, and to Mr. Lambert D. Johnson of Evansville, Indiana, for financial support in this work.

A Field Theory of Elementary Particles

N. ROSEN
*Physics Institute, Academy of Science, Kiev, Ukrainian Soviet Socialist Republic**

(Received October 6, 1938)

Previous attempts at constructing a classical field theory of the electron are reviewed and it is shown that hitherto it has not been possible to combine the two conditions: gauge-invariance and freedom from singularities. It is pointed out that this can be done by the introduction of new matter functions similar to the wave functions of quantum theory. A simple possibility of this type is considered and is found to lead to equations admitting electron-like solutions. The electron turns out to have a negative mass (but perhaps this difficulty will disappear when the equations are quantized). The theory, although classical, offers in principle a possibility of accounting for the Sommerfeld fine-structure constant. There are also solutions corresponding to excited states of the electron and to heavier particles, including particles with zero charge.

AS IS well known, the Maxwell equations of classical electrodynamics lead to the description of an elementary charged particle as a singular point in the electromagnetic field. Such a representation ("point-electron") is, of course, unsatisfactory (1) because it makes the particle have infinite self-energy, and (2) because the presence of the singularity means that the field equations are not valid at the point in question, so that it is necessary to have equations of motion for the charge in addition to the equations for the field.

In order to overcome these difficulties, Mie[1] proposed a modification of the Maxwell equations which would admit a solution for an electron as a charge, free from singularities, occupying a finite volume. However, there were serious objections to this theory and it was abandoned for a time.

When quantum electrodynamics was developed, it was found that the equations of the new theory, obtained by quantizing the classical equations, failed to get rid of the difficulties of the older theory in connection with the point-electron. It was therefore natural to conclude that one ought to try to remove these difficulties from the classical theory before going over to the quantum theory. This led Born and Infeld[2] to propose a nonlinear system of equations of electrodynamics to replace the Maxwell equations The new equations have a solution for the electron with the field everywhere finite and with finite self-energy. However the field in this case still contains a singularity and hence it is still necessary to supplement the equations for the field with equations of motion for the electron.[3] Efforts at modifying this theory have been only partially successful.

One must therefore conclude that the problem of the existence of the electron in the classical theory has not yet been satisfactorily solved. In the present paper is described another attempt at a solution to this problem.

I. The Equations of Maxwell, Mie, and Born and Infeld

The Maxwell equations can be written in tensor notation

$$F^{\mu\nu};_{\nu}=0, \tag{1}$$

where the electromagnetic field tensor $F^{\mu\nu}$ is derived from a potential vector φ_μ:

$$F_{\mu\nu}=(\partial\varphi_\nu/\partial x_\mu)-(\partial\varphi_\mu/\partial x_\nu) \tag{2}$$

and (;) denotes covariant differentiation.

Equations (1) can be obtained from a variational principle. If we define the Lagrangian

$$L_f=-F_{\mu\nu}F^{\mu\nu}/8\pi, \tag{3}$$

* Now at the Massachusetts Institute of Technology, Cambridge, Mass.

[1] G. Mie, Ann. d. Physik **37**, 511 (1912); **39**, 1 (1912); **40**, 1 (1913).

[2] Born and Infeld, Proc. Roy. Soc. **A144**, 425 (1934); **147**, 522 (1934); **150**, 141 (1935).

[3] J. Frenkel, Proc. Roy. Soc. Lond. **A146**, 933 (1934); E. Feenberg, Phys. Rev. **47**, 148 (1935).

then the condition

$$\delta \int L_f(-g)^{\frac{1}{2}} d\tau = 0 \quad (d\tau = dx_1 dx_2 dx_3 dx_4) \quad (4)$$

leads to the Maxwell equations, provided the components of the potential are given infinitesimal variations, arbitrary except for the restriction that they vanish on the boundary of the (four-dimensional) region of integration.

A characteristic of the Eqs. (1) and the Lagrangian (3) is that they depend on the potential φ_μ only through the field tensor $F_{\mu\nu}$ and not directly. This has the well-known consequence that a gauge-transformation, whereby the potential φ_μ is replaced by

$$\varphi_\mu' = \varphi_\mu + \partial\lambda/\partial x_\mu \quad (5)$$

with λ an arbitrary function of the coordinates, does not change the function L_f or the form of Eqs. (1), since the field tensor remains unchanged. That is to say, the theory is gauge-invariant.

For deriving other systems of equations in place of those of Maxwell, the variational principle provides a convenient starting point. Thus, one can choose a scalar function of the field variables, L, and by taking as the law for the field

$$\delta \int L(-g)^{\frac{1}{2}} d\tau = 0, \quad (6)$$

where the potentials are varied as in the case of (4), one obtains a set of equations. If the equations are written in the form

$$F^{\mu\nu}{}_{;\nu} = 4\pi s^\mu, \quad (7)$$

the vector s^μ, depending on the field variables, can be considered as the charge-current density vector, in the sense of the Lorentz electron theory. If one can find a static spherically-symmetric solution of Eqs. (7), free from singularities, such that the charge is confined to a small volume, the solution might be considered as representing an electron at rest in the absence of an external field.

The question arises as to what form one is to choose for the function L. To agree with experiment the function L in the case of weak fields must go over into the Maxwell function L_f. But this in itself is, of course, far from sufficient to determine the function.

If L is allowed to depend explicitly on the potential φ_μ in addition to its dependence on $F_{\mu\nu}$, then in general L and hence the field equations must change under a gauge-transformation (5). However, it is believed that only the field $F_{\mu\nu}$ has physical significance and not the potential, so that the transformation (5), which does not change the field, should not bring about any essential changes in the predictions of the theory.

In Mie's theory of the electron L depends directly on φ_μ, and the resulting lack of gauge-invariance is one of the chief defects of the theory. A solution of Mie's equations for the electron might be expected to change if the external potential were changed by a constant, although from the physical point of view such a change of potential appears to have no significance. A further difficulty in Mie's theory is the lack of a criterion for the choice of the Lagrangian L.

To satisfy the requirement of gauge-invariance, Born and Infeld assume from the very beginning that L depends only on the field tensor and not explicitly on the potential. However, this too has its difficulties, as can be seen from the following discussion.

Let us assume that L is a function only of $F_{\mu\nu}$. Then Eq. (4) can be written in the form

$$\int D^{\mu\nu} \delta F_{\mu\nu} (-g)^{\frac{1}{2}} d\tau = 0, \quad (4a)$$

where $D^{\mu\nu}$ is an antisymmetric tensor defined by

$$D^{\mu\nu} = -4\pi \frac{\partial L}{\partial F_{\mu\nu}}. \quad (8)$$

It follows that

$$\int D^{\mu\nu} \delta F_{\mu\nu} (-g)^{\frac{1}{2}} d\tau = 2 \int D^{\mu\nu} \delta \frac{\partial \varphi_\mu}{\partial x_\nu} (-g)^{\frac{1}{2}} d\tau,$$

$$= -2 \int D^{\mu\nu}{}_{;\nu} \delta\varphi_\mu (-g)^{\frac{1}{2}} d\tau, \quad (9)$$

after integrating by parts and discarding the (vanishing) surface integral. For the integral (9) to vanish with $\delta\varphi_\mu$ arbitrary, one must have

$$D^{\mu\nu}{}_{;\nu} = 0, \quad (10)$$

which represents the set of field equations and is therefore equivalent to (7).

In view of the antisymmetry of $D^{\mu\nu}$, one can rewrite (10) in the form

$$\frac{\partial}{\partial x_\nu}[D^{\mu\nu}(-g)^{\frac{1}{2}}]=0, \tag{11}$$

that is, as the vanishing of an ordinary divergence. In the case of a static spherically-symmetric solution, expressed in polar coordinates, this reduces to the single relationship:

$$d(r^2D_r)/dr=0, \tag{12}$$

where D_r is the radial component of the three-dimensional vector $\mathbf{D}=(D^{41}, D^{42}, D^{43})$. The solution of (12) is

$$D_r=e/r^2, \tag{13}$$

where e is a constant of integration. If L has been chosen so that for weak fields the equations go over into those of Maxwell, then by comparing (8) and (3) one sees that for large values of r (13) goes over into

$$E_r=e/r^2,$$

where E_r is the radial component of the three-dimensional electric field vector $\mathbf{E}=(F^{41}, F^{42}, F^{43})$. From this it is clear that e in (13) is the charge of the electron and therefore cannot be put equal to zero. Consequently D_r is infinite for $r=0$. If D_r is a well-behaved function of E_r, as defined by Eq. (8), this makes E_r infinite for $r=0$ and one has a singular point.[4]

To avoid this difficulty one can try choosing L such that D_r as a function of E_r becomes infinite for some finite value E_0 of the latter. In this case, at the origin $r=0$ where D_r becomes infinite, E_r takes on this value E_0, the limiting value of the field, and thus remains finite. This is the situation in the theory of Born and Infeld. At first sight it appears that the singularity has been avoided, but a closer inspection shows that the vector $\mathbf{E}$ has a discontinuity in direction at the origin, which is therefore still a singular point. In consequence the field equations do not completely determine the motion of the electron and additional conditions have to be added.

[4] For the preceding argument I am indebted to Professor A. Einstein.

Hoffmann and Infeld[5] discuss this difficulty and proceed to remedy it. In order to avoid the discontinuity in $\mathbf{E}$ at the origin it is necessary to make $E_r=0$ there; that is, one must choose a Lagrangian such that $E_r=0$ for $D_r=\infty$. But this also leads to a difficulty, for at large distances from the origin both E_r and D_r must tend to zero, and thus we have the situation that D_r as a function of E_r must be double-valued: for $E_r=0$, $D_r=0$ and $D_r=\infty$. This means that the Lagrangian L must be a double-valued function of the field $F_{\mu\nu}$. That is essentially the case with the function proposed by Hoffmann and Infeld. One can give it the appearance of single-valuedness by writing it as a function of both $F_{\mu\nu}$ and $D_{\mu\nu}$, but the tensor components $D_{\mu\nu}$ cannot be considered as independent physical variables since, as we have seen from (13), they have singularities. In general, a theory with a double-valued action function does not seem satisfactory; in particular, the derivatives of the latter with respect to the field will have a singularity on the surface where the two values join. Incidentally, Hoffmann and Infeld obtain for E_r an *even function* of r in the static spherically-symmetric case, and this might also be interpreted to mean that there is a singularity at $r=0$ (in the higher derivatives).

Thus one must conclude that choosing L to depend only on $F_{\mu\nu}$ as has been done in the more recent papers, is unsatisfactory.

II. Proposed Lagrangian

From the preceding it appears that, in a classical field theory of the type considered here, on the one hand it is necessary for the Lagrangian function to depend explicitly on the potentials to avoid singularities, and on the other hand the theory ought to be gauge-invariant. The question arises as to how one can reconcile these two requirements with each other. One way of doing this that suggests itself is to choose L an explicit function of the potentials, but to introduce, in addition to the potentials, new variables which will make L gauge-invariant.

A familiar example of this situation is the Lagrangian function from which the Schrödinger wave equation is derived. In this case, the

[5] Hoffmann and Infeld, Phys. Rev. **51**, 765 (1937).

Lagrangian depends on the potential and on the wave function. Under a gauge transformation both the potential and the wave function transform in such a way as to leave the Lagrangian invariant.

In accordance with this point of view we take

$$L=L_f+L_m, \tag{14}$$

where L_f is given by Eq. (3) and describes the electromagnetic field, while L_m is a function of the potentials and of the new variables (maintaining gauge-invariance) and can be considered as describing matter.

The simplest nontrivial possibility is to introduce as additional variable (in analogy to the example mentioned) a scalar function ψ such that when φ_μ is transformed according to (5), ψ is transformed to

$$\psi'=\psi e^{i\epsilon\lambda}, \tag{15}$$

where ϵ is a (real) constant of the dimensions (charge)$^{-1}$. From ψ and φ_μ one can form two simple invariants suitable for use in the variational principle:[6] $\psi\psi^*$ and $\chi^\mu\chi_\mu{}^*$, where

$$\chi_\mu=\partial\psi/\partial x_\mu-i\epsilon\varphi_\mu\psi. \tag{16}$$

One can take for L_m a linear combination of these scalars with arbitrary numerical coefficients. One of the coefficients can be absorbed by the function ψ, so that there is left only one arbitrary constant. The signs of the terms, however, cannot be changed by any transformation of ψ. It is therefore necessary to consider all possible combinations of signs of the two terms in L_m. It turns out that of the four possibilities only one combination allows "electron" solutions.

Let us restrict ourselves hereafter to the case of special relativity and let us take the metric in the form

$$ds^2=-dx_1{}^2-dx_2{}^2-dx_3{}^2+dx_4{}^2 \tag{17}$$

with $\quad x_1=x, \quad x_2=y, \quad x_3=z, \quad x_4=t$

(the unit of time is chosen so that the velocity of light is equal to unity). Then the proper linear combination for L_m is given by

$$L_m=-\chi^\mu\chi_\mu{}^*+\sigma^2\psi\psi^*, \tag{18}$$

where σ is a real constant of the dimensions (length)$^{-1}$. The complete Lagrangian is then

$$L=-F_{\mu\nu}F^{\mu\nu}/8\pi-\chi^\mu\chi_\mu{}^*+\sigma^2\psi\psi^*, \tag{19}$$

where $\quad (\varphi^1, \varphi^2, \varphi^3, \varphi^4)=(A_1, A_2, A_3, \varphi),$

$$(F_{12}, F_{23}, F_{31}, F_{14}, F_{24}, F_{34})=(H_3, H_1, H_2, E_1, E_2, E_3).$$

If one takes, as the law for the field, Eq. (6) where φ_μ and ψ are varied independently, one obtains the following system of differential equations

$$\chi^\nu{}_{;\nu}-i\epsilon\varphi_\nu\chi^\nu+\sigma^2\psi=0, \tag{20}$$

and

$$F^{\mu\nu}{}_{;\nu}=4\pi s^\mu, \tag{21}$$

with

$$s^\mu=\tfrac{1}{2}i\epsilon(\psi^*\chi^\mu-\psi\chi^{\mu*}). \tag{22}$$

The connection with the usual notation is given by

$$(s^1, s^2, s^3, s^4)=(j_1, j_2, j_3, \rho),$$

so that

$$\rho=\frac{i\epsilon}{2}\left(\psi^*\frac{\partial\psi}{\partial t}-\psi\frac{\partial\psi^*}{\partial t}\right)+\epsilon^2\varphi\psi\psi^*. \tag{23}$$

Equation (20) written in terms of ψ has practically the same form as the Gordon-Klein relativistic wave equation in quantum mechanics. An essential difference, however, is that in the Gordon-Klein equation the potentials which occur are those of the "outer" field, i.e., they do not include the field due to the charge and current determined by ψ, whereas in the present equation the potentials include the latter field as well. The result is that here the system of Eqs. (20) and (21) is nonlinear in ψ, which therefore may not be normalized arbitrarily as is done in wave mechanics. Furthermore the constants occurring in (20) will have values different from the corresponding ones in the Gordon-Klein equation.

The constants ϵ and σ in the present case are dimensional constants and hence their values cannot be predicted from the theory since these depend on the system of units used. They must be chosen so as to agree with experiment, that is,

[6] There are, of course, other invariants. If we accept only terms of the second or lower order of differentiation and bilinear in ψ and ψ^* there remains $F_{\mu\nu}F^{\mu\nu}\psi\psi^*$. Since this is the product of two invariants already present, it was considered as being of a more complicated type and was discarded. It could be added with another arbitrary constant.

give the correct values for the charge and mass of the electron. One can predict in advance their orders of magnitude:

$$e\sim 1/e, \quad \sigma\sim 1/a=mc^2/e^2,$$

where e, m, and a are the charge, mass and "radius" of the electron, respectively.

From the Lagrangian L one can calculate the energy-impulse density tensor $T_{\mu\nu}$ by means of the relation

$$T_{\mu\nu}=\partial L/\partial g_{\mu\nu}-\tfrac{1}{2}g_{\mu\nu}L. \tag{24}$$

One finds

$$T_{\mu\nu}=(T_{\mu\nu})_f+(T_{\mu\nu})_m, \tag{25}$$

where

$$(T_{\mu\nu})_f=(g_{\mu\nu}F_{\alpha\beta}F^{\alpha\beta}-2F_{\mu\alpha}F_{\nu}{}^{\alpha})/16\pi, \tag{26}$$

$$(T_{\mu\nu})_m=\tfrac{1}{2}[g_{\mu\nu}(\chi^{\alpha}\chi_{\alpha}{}^{*}-\sigma^2\psi\psi^{*}) -\chi_{\mu}\chi_{\nu}{}^{*}-\chi_{\mu}{}^{*}\chi_{\nu}]. \tag{27}$$

The energy density is given by T_{44}. From (26) and (27) one finds, using the values of the metric-tensor components in (17), that

$$(T_{44})_f=\frac{1}{16\pi}\sum_{\alpha,\beta}F_{\alpha\beta}F_{\alpha\beta}, \tag{28}$$

$$(T_{44})_m=-\tfrac{1}{2}(\sum_{\alpha}\chi_{\alpha}\chi_{\alpha}{}^{*}+\sigma^2\psi\psi^{*}), \tag{29}$$

from which it follows that

$$(T_{44})_f\geqslant 0, \quad (T_{44})_m\leq 0,$$

so that the sign of T_{44} is not definite. It appears that this is closely connected with the existence of discrete charges. Thus, one can reverse the sign of L_m and in that way make T_{44} positive definite, but one then finds that there are no electron-like solutions of the resulting field equations. We shall have occasion later on to return to this question.

The tensor $T_{\mu\nu}$, on the basis of the field equations, satisfies the divergence equation

$$\partial T^{\mu\nu}/\partial x_{\nu}=0. \tag{30}$$

From this it follows that if there exists a solution, for which the energy is localized in a finite volume (or tends rapidly enough to zero at infinity), then one can define an energy-impulse vector[7]

$$P^{\mu}=\int T^{\mu 4}dv \tag{31}$$

(where the integral is taken over all three-space), such that

$$dP^{\mu}/dt=0. \tag{32}$$

The energy is given by

$$W=P^{4}=\int T^{44}dv=\int T_{44}dv. \tag{33}$$

If one integrates (30) over a finite three-dimensional volume V bounded by a surface S one gets

$$\frac{d}{dt}\int_V T^{\mu 4}dv=-\int_S T^{\mu n}df, \tag{34}$$

where df is a surface element and the index n denotes the component in the direction of the outward normal to the surface. One can apply this to the case of a solution corresponding to a particle moving slowly in a weak, slowly-varying, external field. One takes the surface S in the form of a sphere with center at the particle and radius large compared to the particle radius, so that on the surface one can neglect $(T^{\mu\nu})_m$ and take $(T^{\mu\nu})_f$ corresponding to the external field + the electromagnetic field of the particle (considered as a point charge). One can then show that (34) gives the equations of motion of the particle corresponding to the action of the Lorentz force.

III. Spherically-Symmetric Case

We now investigate the spherically-symmetric static solution of the field equations. A static solution means one in which the electromagnetic field, and hence the charge distribution, does not change with time. For this it is sufficient for ψ to be of the form:

$$\psi=\theta e^{-i\kappa\mu t}, \tag{35}$$

where θ is a function of (x, y, z) and μ an arbitrary constant. Furthermore, from the condition of spherical symmetry it follows that

$$s_1=s_2=s_3=0 \quad s_4=\rho(r), \tag{36a}$$

where r is the distance from the origin of coordinates. One can also take

$$\varphi_1=\varphi_2=\varphi_3=0 \quad \varphi_4=\phi(r) \tag{36b}$$

and, on the basis of (36a), one can assume θ to

[7] Cf. H. Weyl, *Raum, Zeit Materie* (Berlin, 1923), p. 204.

be real, without loss of generality. One then has that

$$\rho=\epsilon^2(\phi+\mu)\theta^2. \tag{37}$$

With these simplifications the field equations (20) and (21) take on the form

$$\nabla^2\theta+[\epsilon^2(\phi+\mu)^2-\sigma^2]\theta=0, \tag{38}$$

$$\nabla^2\phi+4\pi\epsilon^2(\phi+\mu)\theta^2=0. \tag{39}$$

The boundary conditions for a particle solution are

$$r=0: \quad d\theta/dr=d\phi/dr=0, \tag{40a}$$

$$r\to\infty: \quad \theta\to 0, \quad \phi\sim\text{const.}/r. \tag{40b}$$

The conditions (40a) are necessary in order that there be no discontinuities in the gradients of θ and ϕ at the origin.

It is convenient to introduce dimensionless variables by means of the substitution

$$\theta=\sigma y/\epsilon(4\pi)^{\frac{1}{2}}, \quad \phi+\mu=\sigma z/\epsilon, \quad r=x/\sigma. \tag{41}$$

The equations then become

$$d^2(xy)/dx^2=x(1-z^2)y, \tag{42}$$

$$d^2(xz)/dx^2=-xy^2z. \tag{43}$$

If one makes a further change of variables

$$xy=\eta, \quad xz=\zeta \tag{41a}$$

one gets for the equations

$$\eta''=(1-\zeta^2/x^2)\eta, \tag{44}$$

$$\zeta''=-\eta^2\zeta/x^2, \tag{45}$$

where primes denote differentiation with respect to x. The boundary conditions now become

$$\eta(0)=\zeta(0)=\eta(\infty)=0, \tag{46a}$$

$$(\zeta/x)_\infty=\epsilon\mu/\sigma(\equiv\beta). \tag{46b}$$

But since μ is not known, (46b) is really not a condition but an equation which determines μ (or β) after a solution has been found.

If one has obtained a solution of the field equations, corresponding to a particle, the charge of the latter e is connected with the constant ϵ by the relation

$$e=4\pi\int_0^\infty \rho r^2dr=\alpha/\epsilon, \tag{47}$$

where

$$\alpha=\int_0^\infty y^2zx^2dx. \tag{48}$$

For the energy density one finds

$$T_{44}=\frac{1}{8\pi}\left(\frac{d\phi}{dr}\right)^2-\tfrac{1}{2}\epsilon^2(\phi+\mu)^2\theta^2-\tfrac{1}{2}\left(\frac{d\theta}{dr}\right)^2-\tfrac{1}{2}\sigma^2\theta^2.$$

The total energy is then given by

$$W=4\pi\int_0^\infty T_{44}r^2dr.$$

Integrating by parts and making use of the field equations, one obtains

$$W=-\sigma w/2\epsilon^2, \tag{49}$$

where

$$w=\alpha\beta+\gamma, \tag{50a}$$

and

$$\gamma=\int_0^\infty y^2z^2x^2dx. \tag{50b}$$

IV. Electron Solution

The field equations, in the form (44) and (45), for example, can be integrated starting from $x=0$. If one takes $\eta(0)=\zeta(0)=0$, the solution is determined by the parameters

$$\eta'(0)=y(0)=a, \quad \zeta'(0)=z(0)=b. \tag{51}$$

In order for the solution to have the proper behavior at infinity one must choose suitable values for these parameters. It is seen from Eq. (44) that, for a solution representing a particle, η must fall off exponentially at large distances. This will be the case if $z^2<1$ at infinity, i.e., if $\beta^2<1$. It can be easily shown that to obtain a solution of this type it is necessary to have $b^2>1$. In the region where $z^2>1$, η will have an oscillatory behavior.

If one has found a solution for which η has the proper behavior at infinity, then it follows from Eq. (45) that z or ζ will also behave properly at large distances and one has there

$$z\sim\alpha/x+\beta, \quad \zeta\sim\alpha+\beta x. \tag{52}$$

This means that, if the value of β is not prescribed, the parameters a and b of (51) have to be chosen so as to satisfy the boundary conditions at infinity for only one function, η. In general this can be done by choosing one of the parameters arbitrarily and then suitably determining the other.

The simplest solution is one for which both θ and ϕ are without nodes in the finite part of space. It is reasonable to expect that this might describe the simplest known charged particle, the electron (or, if one changes the signs of ϕ and μ, the positron). Hence this solution was investigated in some detail by means of numerical integration.

As has been pointed out, one can obtain solutions of this type for a finite range of values of one of the parameters a and b if one determines the other accordingly. In other words there exists a one-parameter family of solutions of the nodeless type. For fixed values of the constants ϵ and σ these solutions differ from one another with respect to charge and energy. The question then arises: if this type of solution describes an electron, how is one to account for the fact that all ordinary electrons have the same charge and mass? To be sure, the charge and mass of a single isolated particle are conserved; but if several particles interact what is to prevent one of them from acquiring part of the charge and mass of another?

A possible explanation appears to be that, of the family of solutions, there is one solution for which the energy is a *minimum;* and that this represents the normal state of the isolated electron. Calculations were therefore carried out to determine whether there exists a minimum for the energy. Several values of a were taken and in each case b was determined by trial so as to give a solution of the desired type. For each solution the quantity w was calculated according to (50a). It was found that w has a maximum. The position of the latter has not been determined very accurately but is in the neighborhood of $a=1.6$ ($b=2.19$, $\alpha=1.91$, $\beta=0.015$), where it has the value 2.83.

From (49) it follows that the mass of such an electron is *negative*. This accounts for the stability of the electron (since energy would have to be added to it in order to explode it), but unfortunately it is in disagreement with our knowledge about the electron. However, it must be borne in mind that one is dealing here with a classical theory. Before comparing with experiment, one must find the quantum generalization. This should be of such a form that the equations will agree with the Dirac equations for the electron in the approximation in which one neglects the finite radius of the electron and considers it as a point charge. Now the Dirac equations give essentially the same solutions (with a different numbering) for a negative as for a positive mass. If one considers states corresponding to *positive energy*, the Dirac electron with negative mass is indistinguishable in its behavior from one with its mass positive. It may therefore be that in the quantum generalization of the present equations the difficulty with the sign of the mass will disappear.

In the neighborhood of $a=1.6$ it is found that β, as given by (46b) passes through zero. It may be that the minimum of the energy is located at the point where $\beta=0$. If this is *not* the case, there arises an interesting possibility. In this case the electron has both energy and frequency, and one can define for the ratio a constant

$$h'=|W/\nu|. \tag{53}$$

If one makes use of Eqs. (35), (46b), (47), (49) and (50a) and takes the customary unit for time, this relation can be written in the form

$$\alpha'\equiv 2\pi e^2/h'c=|2\alpha^2\beta/(\alpha\beta+\gamma)|.$$

Calculations of α' were attempted, but it was difficult to obtain any great accuracy. It was found that $\alpha'\lesssim 0.04$, It may be that it has the value 1/137 of the Sommerfeld fine-structure constant. Should this turn out to be the case, it would mean that there is a much closer relationship between the quantum theory and the classical theory than has hitherto been supposed. Even in the classical theory there would be associated with a moving electron something like a de Broglie wave.

It is to be noted that the electron here is similar in its structure to the "wave packet" electron considered during the early period of quantum mechanics. However one would expect that the mutual interaction between various parts of the electron considered here prevents it from spreading in the course of time (as occurs in wave mechanics) at least in the case of weak fields. To be sure, in strong fields the present electron will flow apart. Thus one sees that even a classical theory can explain why electrons, *as particles*, cannot be nuclear constituents.

V. Other Solutions

Besides the simple solution already considered there are also more complicated solutions. Among these are solutions for which θ is of the same form as in the previous case whereas z has a number of nodes. Such solutions correspond to particles in which the charge distribution consists of concentric layers alternating in sign. One would expect that a particle of this type, compared with the simple particle considered in the previous section having the same charge, will have a considerably greater mass, since the quantity γ, which essentially determines the energy, depends on z^2 and thus adds for the various layers, whereas their charges tend to cancel each other. It may be that such solutions are associated with heavy particles. In this connection it is worth pointing out that among these solutions there will also be some for which the net charge of the particle vanishes.

Then there are also solutions for which θ has nodes. It may be that these correspond to internal excited states of elementary particles (heavy electrons?).

VI. Conclusions

In the present paper is suggested a possibility for a classical theory of elementary particles. It has a shortcoming in that it leads to a negative mass for the electron. However it may be that this difficulty will be removed in the process of going over from the classical to the quantum theory. At any rate one has here for the first time a theory leading to equations which are gauge-invariant and at the same time give solutions which are free from singularities, in fact, which are analytic functions.

There appears to be a possibility of deriving the Sommerfeld fine-structure constant from the theory considered here in spite of the fact that it is a classical theory. Should this turn out to be an actuality, it would have an important bearing on the problem of the foundations of the quantum theory. If it is found that the numerical value obtained for the constant is not correct, it does not necessarily mean that the general idea considered here must be abandoned. The particular Lagrangian (19), which was used to derive the field equations, is only one—the simplest—of a number of possibilities. Perhaps some other one should have been chosen.

In conclusion, the writer wishes to express his deep indebtedness to Professor A. Einstein for many interesting discussions on the subject of field theories. He would also like to thank Mr. M. Feingold for assistance with the numerical calculations.

LETTERS TO THE EDITOR

Prompt publication of brief reports of important discoveries in physics may be secured by addressing them to this department. Closing dates for this department are, for the first issue of the month, the eighteenth of the preceding month, for the second issue, the third of the month. Because of the late closing dates for the section no proof can be shown to authors. The Board of Editors does not hold itself responsible for the opinions expressed by the correspondents.

Communications should not in general exceed 600 words in length.

On the Change of Magnetic Properties of the Single Crystal of Nickel Due to Temperature

Recently Williams[1] has published in this journal the results of his observation on the magnetization curve of the single crystals of silicon steel. He used samples in the form of a hollow parallelogram, the sides of which coincide with the principal crystallographic directions. The results agree fairly well with those expected by Kondorsky's theory[2] of initial susceptibility of ferromagnetic crystals. Now by the same method as that of Williams, we have measured the magnetic properties of the single crystal of nickel at various temperatures. We prepared a nickel single crystal in the form of a hollow parallelogram, the sides of which lie in the direction [111]. The description of our sample and the main results of observation are as follows.

The dimensions of the sides of the ring are 8.0 by 18.6 mm and the cross-sectional area of each side is 1.96×1.89 mm². The magnetizing coil is wound on each side in one layer (the constant of coil, $4\pi n$ is 289), and the search coil of 50 turns is wound on one of its sides. The initial magnetizing curve as well as the hysteresis curve are measured by the ballistic method; the main results of observation are summarized in Fig. 1. In Fig. 1, we can find the coercive force H_c, residual magnetization I_r and the hysteresis loss E in the temperature range from the boiling point of nitrogen to the Curie point of nickel. For the sake of reference the intensity of magnetization I_{15} produced by the magnetizing field of 15 oersteds is also shown in the same figure. Generally speaking, nickel single crystal is, with respect to magnetic properties, much "harder" than that of iron single crystal. As the figure shows, residual magnetism, coercive force and hysteresis loss attain each a maximum at 100°C. During the fall of temperature those values decrease gradually and the coercive force reaches a value 0.7 oersted at the boiling point of nitrogen. The existence of such a low value of coercive force is very interesting if we remember that the coercive force at ordinary temperature is 2.4 oersteds.

In summary, it is to be concluded that the magnetic characters of single crystal of nickel are greatly affected by temperature.

T. Okamura
T. Hirone

The Research Institute for
Iron, Steel and Other Metals,
Tôhoku Imperial University,
Sendai, Japan,
November 25, 1938.

[1] H. J. Williams, Phys. Rev. **52**, 747, 1004 (1937).
[2] E. Kondorsky, Phys. Rev. **53**, 319 (1938).

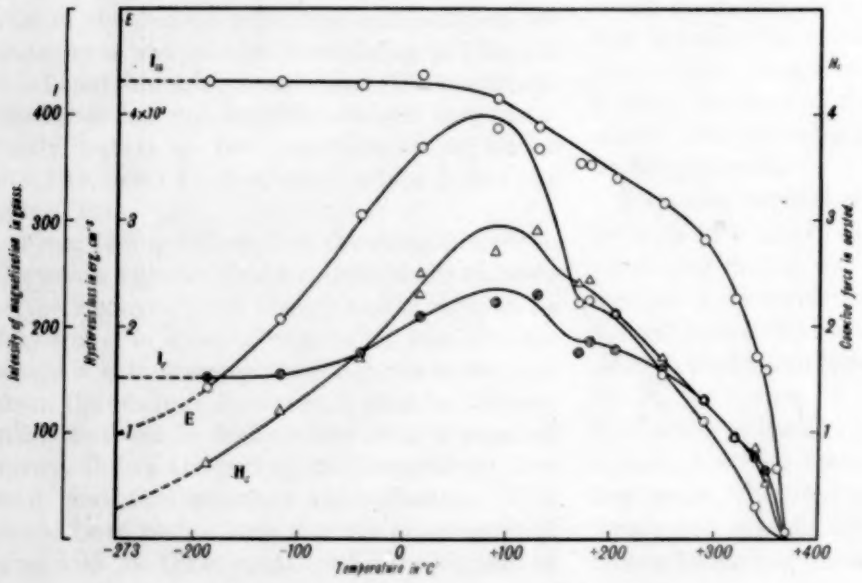

FIG. 1. Magnetic properties of a nickel single crystal.

Energy Production in Stars

In several recent papers,[1-3] the present author has been quoted for investigations on the nuclear reactions responsible for the energy production in stars. As the publication of this work which was carried out last spring has been unduly delayed, it seems worth while to publish a short account of the principal results.

The most important source of stellar energy appears to be the reaction cycle:

$$\begin{aligned} &C^{12}+H^1=N^{13}\ (a),\ N^{13}=C^{13}+\epsilon^+\ (b)\\ &C^{13}+H^1=N^{14}\ (c)\\ &N^{14}+H^1=O^{15}\ (d),\ O^{15}=N^{15}+\epsilon^+\ (e)\\ &N^{15}+H^1=C^{12}+He^4\ (f). \end{aligned} \qquad (1)$$

In this cycle, four protons are combined into one α-particle (plus two positrons which will be annihilated by two electrons). The carbon and nitrogen isotopes serve as catalysts for this combination. There are no alternative reactions between protons and the nuclei $C^{12}C^{13}N^{14}$; with N^{15}, there is the alternative process

$$N^{15}+H^1=O^{16},$$

but this radiative capture may be expected to be about 10,000 times less probable than the particle reaction (f). Thus practically no carbon and nitrogen will be consumed and the energy production will continue until all protons in the star are used up. At the present rate of energy production, the hydrogen content of the sun (35 percent by weight[4]) would suffice for 3.5×10^{10} years.

The reaction cycle (1) is preferred before all other nuclear reactions. Any element *lighter* than carbon, when reacting with protons, is destroyed permanently and will not be replaced. E.g., Be^9 would react in the following way:

$$\begin{aligned} &Be^9+H^1=Li^6+He^4\\ &Li^6+H^1=Be^7\\ &Be^7+\epsilon^-=Li^7\\ &Li^7+H^1=2He^4. \end{aligned}$$

Therefore, even if the star contained an appreciable amount of Li, Be or B when it was first formed, these elements would have been consumed in the early history of the star. This agrees with the extremely low abundance of these elements (if any) in the present stars. These considerations apply also to the heavy hydrogen isotopes H^2 and H^3.

The only abundant and very light elements are H^1 and He^4. Of these, He^4 will not react with protons at all because Li^5 is unstable, and the reaction between two protons, while possible, is rather slow[5] and will therefore be much less important[6] in ordinary stars than the cycle (1).

Elements heavier than nitrogen may be left out of consideration entirely because they will react more slowly with protons than carbon and nitrogen, even at temperatures much higher than those prevailing in stars. For the same reason, reactions between α-particles and other nuclei are of no importance.

To test the theory, we have calculated (Table I) the energy production in the sun for several nuclear reactions, making the following assumptions:

(1) The temperature at the center of the sun is 2×10^7 degrees. This value follows from the integration of the Eddington equations with any reasonable "star model."[4] The "point source model" with a convective core which is a very good approximation to reality gives 2.03×10^7 degrees.[7] The same calculation gives 50.2 for the density at the center of the sun. The central temperature is probably correct to within 10 percent.

(2) The concentration of hydrogen is assumed to be 35 percent by weight, that of the other reacting element 10 percent. In the reaction chain (1), the concentration of N^{14} was assumed to be 10 percent.

(3) The ratio of the average energy production to the production at the center was calculated[7] from the temperature-density dependence of the nuclear reaction and the temperature-density distribution in the star.

TABLE I. *Energy production in the sun for several nuclear reactions.*

REACTION	AVERAGE ENERGY PRODUCTION ϵ(erg/g sec.)
$H^1+H^1=H^2+\epsilon^++f$.*	0.2
$H^2+H^1=He^3$	3×10^{16}
$Li^7+H^1=2He^4$	4×10^{14}
$B^{10}+H^1=C^{11}+f$.	3×10^8
$B^{11}+H^1=3He^4$	10^{10}
$N^{14}+H^1=O^{15}+f$.	3
$O^{16}+H^1=F^{17}+f$.	10^{-4}

* "$+f$." means that the energy production in the reactions following the one listed, is included. E.g. the figure for the $N^{14}+H^1$ includes the complete chain (1).

It is evident from Table I that only the nitrogen reaction gives agreement with the observed energy production of 2 ergs/g sec. All the reactions with lighter elements would give energy productions which are too large by many orders of magnitude if they were abundant enough, whereas the next heavier element, O^{16}, already gives more than 10,000 times too small a value. In view of the extremely strong dependence on the atomic number, the agreement of the nitrogen-carbon cycle with observation is excellent.

The nitrogen-carbon reactions also explain correctly the dependence of mass on luminosity for main sequence stars. In this connection, the strong dependence of the reaction rate on temperature ($\sim T^{18}$) is important, because massive stars have much greater luminosities with only slightly higher central temperatures (e.g., Y Cygni has $T=3.2\times10^7$ and $\epsilon=1200$ ergs/g sec.).

With the assumed reaction chain, there will be no appreciable change in the abundance of elements heavier than helium during the evolution of the star but only a transmutation of hydrogen into helium. This result which is more general than the reaction chain (1) is in contrast to the commonly accepted "Aufbauhypothese."

A detailed account of these investigations will be published soon.

H. A. BETHE

Cornell University,
Ithaca, New York,
December 15, 1938.

[1] C. F. v. Weizsaecker, Physik. Zeits. **39**, 639 (1938).
[2] J. Oppenheimer and R. Serber, Phys. Rev. **54**, 540 (1938).
[3] G. Gamow, Phys. Rev. (in print).
[4] B. Strömgren, Ergebn. d. Exak. Naturwiss. **16** (1937).
[5] H. Bethe and C. Critchfield, Phys. Rev. **54**, 248 (1938).
[6] Only for very cool stars (red dwarfs) the H+H reaction may become important.
[7] The author is indebted to Mr. Marshak for these calculations.

The Difference in the Absorption of Cosmic Rays in Air and Water and the Instability of the Barytron

Ehmert[1] and Auger, Ehrenfest, Freon and Fournier[2] have found that the intensity of the cosmic radiation depends not only upon the quantity of a given kind of matter traversed by the rays, but that it is a function of the distribution of that matter as well, the denser matter appearing to absorb the rays less. As an interpretation of these results Kulenkampf and Euler and Heisenberg[3] have pointed out that the instability of the barytron, predicted by Yukawa,[4] should give rise to a lower intensity when the time required for the secondary barytrons produced in the upper atmosphere to reach the apparatus is greater. The mean life predicted by Yukawa for the barytron at rest is $\tau_0=0.5\times10^{-6}$ sec., and because of the relativity transformation the stability appears to increase in proportion to the energy for energies large compared with the rest energy μc^2. A recent comparison of the cosmic-ray intensities and zenith angle distributions at two elevations by Ehrenfest and Freon[5] enabled these authors to compute a rest life of the order of 4×10^{-6} sec., or about ten times that predicted by Yukawa.

W. F. G. Swann has recently had erected at the Bartol Laboratory a cylindrical water tower three meters in diameter and 8.9 meters deep, with a room beneath for experimentation. He has generously placed this at our disposal for a similar investigation in which we have had the advantage of making all measurements under favorable laboratory conditions at a single location. In these experiments the counting rate of a quadruple coincidence counter train of large area but small angular aperture was recorded, first when it was directed vertically upwards through the 8.9 meters of water and the equivalent 10 meters of atmosphere, and then when it was inclined at the zenith angle $\zeta=\sec.^{-1}(1.89)=58°$. Lead plates for eliminating the soft component were stacked between counters to a thickness of 17 cm and 38 cm, respectively, in two independent experiments. In both instances the counting rates in the inclined position were less than those in the vertical; if j_ζ and j_v designate the respective intensities the experiments gave

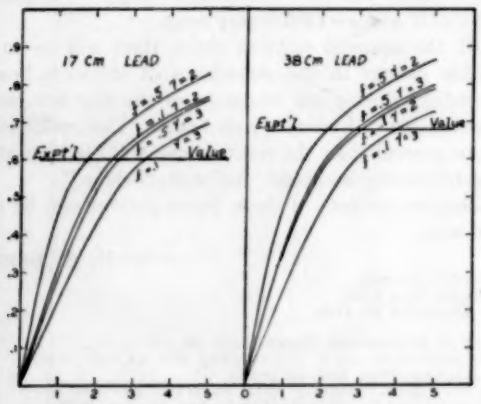

FIG. 1. Ordinates: calculated values of j_ζ/j_v. Abscissae: the rest life τ_0 in microseconds.

$$j_\zeta/j_v=0.60\pm0.02 \text{ with 17 cm lead}$$
$$\text{or} \quad =0.68\pm0.02 \text{ with 38 cm lead.}$$

In order to evaluate the mean life of the barytron from these data we have used two types of calculation, both of which involve assumptions which must be regarded as more or less arbitrary in the present state of our knowledge. Barytrons incident at zenith angle ζ are assumed to have originated as secondaries at an atmospheric depth $h=fH\cos\zeta$ where H is the depth of the homogeneous atmosphere ($=8\times10^5$ cm) and f is a fraction of the order of 1/10; the actual height above sea level, corresponding to this depth, is $x=H\log(\sec.\zeta/f)$. The mean life of barytrons of energy $\epsilon\mu c^2$ is $\tau_0\epsilon$, and if a ray loses energy by ionization at the constant rate $i\mu c^2$ per cm in normal air, the probability of a ray of initial energy $\epsilon\mu c^2$ reaching sea level without disintegrating is given by

$$P(\epsilon,\zeta)=\exp-[(H\sec.\zeta/c\tau_0\epsilon)\times\log(\epsilon/ifH-1)/(\epsilon/iH\sec.\zeta-1)]. \quad (1)$$

In the first calculation we let $j(\epsilon)d\epsilon$ represent the number of barytrons per cm² per sec. per unit solid angle whose initial energies lie between $\epsilon\mu c^2$ and $(\epsilon+d\epsilon)\mu c^2$, a function which may be supposed independent of the direction, so that the number of rays of these initial energies which reach sea level in the vertical direction is $j(\epsilon)P(\epsilon,0)$. The experiments of Ehmert[1] and Wilson[6] show the latter function to be of the form $A/(\epsilon-iH(1-f))^\gamma$ where $2<\gamma<3$. If $\alpha\mu c^2$ is the energy required to penetrate the lead shield, the intensity in the vertical direction under 8.9 meters of water and the atmosphere may be expressed by

$$j_v=\int_{iH(1.89-f)+\alpha}^{\infty}j(\epsilon)P(\epsilon,0)d\epsilon$$
$$=A/(\gamma-1)(\alpha+0.89iH)^{\gamma-1}, \quad (2)$$

whereas that in the inclined position is given by

$$j_\zeta=\int_{iH(\sec.\zeta-f)+\alpha}^{\infty}j(\epsilon)P(\epsilon,\zeta)d\epsilon. \quad (3)$$

We have chosen as a value of the rest mass of the barytron one-tenth of the proton mass, and with the rate of loss of energy by ionization proportional to the inverse square of the velocity we find $\alpha=3.6$ for 17 cm lead, 6.4 for 38 cm lead, and $iH=20$. The values of j_ζ/j_v calculated for various values of τ_0, for the cases where $f=0.1$ and 0.5 and $\gamma=2$ and 3, are shown in Fig. 1. Agreement with our measured values occurs for values of τ_0 between 2 and 4×10^{-6} sec.

The second calculation is concerned with the disintegrations of rays whose energies lie within the narrow band of energies which penetrate the 17-cm lead absorber, but fail to pass through the 38-cm shield; this calculation is independent of the energy distribution and applies to only those rays whose initial energy is given by

$$\epsilon_1=iH(1.89-f)+\bar{\alpha},$$

where $\bar{\alpha}$ is the average of the minimum energies for penetration of the two thicknesses of lead. In this calculation τ_0 is obtained from the equation

$$\eta=\frac{j_v(17)-j_v(38)}{j_\zeta(17)-j_\zeta(38)}=P(\epsilon_1,0)/P(\epsilon_1,\zeta). \quad (4)$$

The order of runs in these experiments was not arranged to give an accurate value of η, but we can give $\eta=0.40$ as a preliminary value from which we calculate $\tau_0=2.6\times10^{-6}$ sec. with $f=1/10$ or $=2.4\times10^{-6}$ sec. with $f=0.5$. The result is insensitive to the choice of f.

We wish to acknowledge helpful discussions with Dr. C. G. Montgomery and to state that the Carnegie Institution of Washington contributed to the support of the experiments.

THOMAS H. JOHNSON
MARTIN A. POMERANTZ

The Bartol Research Foundation of the Franklin Institute,
Philadelphia, Pennsylvania,
December 8, 1938.

[1] A. Ehmert, Zeits. f. Physik **106**, 751 (1937).
[2] P. Auger, P. Ehrenfest, A. Freon and A. Fournier, Comptes rendus **204**, 257 (1937).
[3] H. Euler and W. Heisenberg, Ergeb. d. Exakt. Naturwiss. (1938).
[4] H. Yukawa, Proc. Phys.-Math. Soc. Japan **17**, 48 (1935); See also H. J. Bhabha, Nature **141**, 117 (1938).
[5] P. Ehrenfest and A. Freon, Comptes rendus **207**, 853 (1938).
[6] V. Wilson, Phys. Rev. **53**, 337 (1938).

Ferromagnetism of Semi-Conductors

A theory of ferromagnetism of semi-conductors has been proposed on the basis of Wilson's model of semi-conductors[1] and Slater's model of ferromagnetic substances[2] in which ferromagnetism appears in crystals having very large exchange integrals.

The outline of our theory is as follows: We assume that in semi-conductors there are two near energy bands, and at absolute zero temperature the lower band in which a very large exchange integral exists between two electrons is entirely filled up, while the higher band in which the exchange integral is small is entirely empty.

In a suitable temperature range several electrons are excited to the higher band, and thereby make positive holes in the lower band. Then ferromagnetism can appear.

The number of positive holes $2n$ at $T°$K is

$$2n=2\varphi_1(T)\nu\exp(-\Delta B/2kT),$$

where $\varphi_1(T)$ is a function related with the shape of the lower (magnetic) band, ν is the total number of ferromagnetic atoms in the crystal, and ΔB is the width of the forbidden region.

Then the magnetic moment M_s of one mole of the crystal is given by the following formulae:

$$M_s=M_\infty\exp(-\Delta B/2kT)\tanh(\alpha+M_s\theta/M_\infty T),$$
$$M_\infty=2\mu L\varphi_1(T),$$
$$\alpha=\mu H/kT,$$
$$\theta=J\varphi_1(T)/k,$$

where L is the number of atoms of one mole, k the Boltzmann's constant, J the exchange integral in the free atom, H the magnetic field, μ the Bohr magneton and T the temperature on absolute scale.

If we assume $\varphi_1(T)$ is a constant b, and the magnetic field is weak, we can calculate M_s numerically as the function of absolute temperature for the different values of γ, where $\gamma=\frac{1}{2}\Delta B/Jb$.

Ferromagnetism can not appear in every temperature when $\gamma>1/e$.

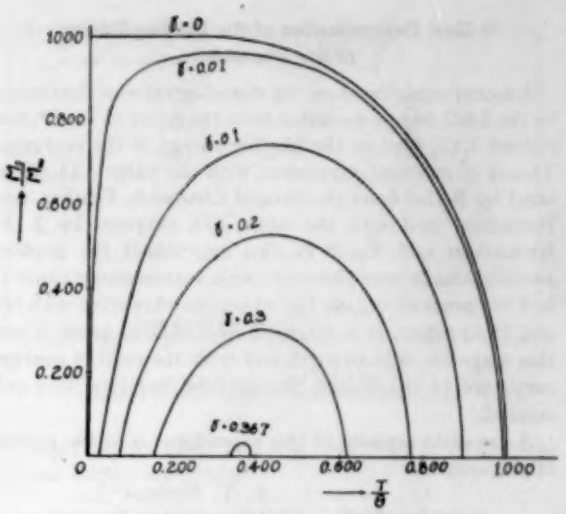

FIG. 1. Ferromagnetism of semi-conductors.

The results are different from those calculated by the ordinary Weiss-Heisenberg theory.

Our results are illustrated in Fig. 1. It is specially interesting to note that at very low temperature ferromagnetism vanishes.

This result will be useful for the interpretation of experimental facts on magnetite,[3] pyrrhotite[4] and chromium sulphide.[5] Further experiment which is necessary for the verification of our theory is now in progress.

The detailed account of the above theory will be published at a later date.

SYÔHEI MIYAHARA

The Research Institute for
Iron, Steel and Other Metals,
Tôhoku Imperial University,
Sendai, Japan,
November 25, 1938.

[1] Wilson, Proc. Roy. Soc., London **A133**,458 (1931); **134**, 277 (1931).
[2] Slater, Phys. Rev. **49**, 537 (1936); **49**, 931 (1936).
[3] Weiss and Forrer, Ann. d. Phys. **12**, 279 (1929); Okamura, Sci. Rep. Tôhoku Imp. Univ. **21**, 231 (1932).
[4] Ziegler, thesis, Zurich, 1915.
[5] Haraldsen and Neuber, Zeits. f. anorg. allgem. Chemie **234**, 337 (1937).

Mesotron as the Name of the New Particle

After reading Professor Bohr's address at the British Association last September in which he tentatively suggested the name "yucon" for the newly discovered particle, I wrote to him incidently mentioning the fact than Anderson and Neddermeyer had suggested the name "mesotron" (intermediate particle) as the most appropriate name. I have just received Bohr's reply to this letter in which he says:

"I take pleasure in telling you that every one at a small conference on cosmic-ray problems, including Auger, Blackett, Fermi, Heisenberg, and Rossi, which we have just held in Copenhagen, was in complete agreement with Anderson's proposal of the name 'mesotron' for the penetrating cosmic-ray particles."

ROBERT A. MILLIKAN

California Institute of Technology,
Pasadena, California,
December 7, 1938.

A New Determination of the Binding Energy of the Deuteron

A recent experiment on the distintegration of deuterium by the 2.623 Mev γ-radiation from the decay of Th C'', has yielded 2.17_4 Mev as the binding energy of the deuteron. This is in excellent agreement with the value 2.17 calculated by Bethe[1] from the data of Chadwick, Feather, and Bretscher,[2] and with the value 2.18 obtained by J. R. Richardson and Emo.[3] In this experiment the product protons' tracks were observed (with a stereoscopic camera) in a low pressure (12 cm Hg) cloud chamber filled with H^2_2 and H^2_2O vapor, in a magnetic field of 3762 gauss. From this magnetic field strength and from the radii of average curvature of the tracks, the protons' energies were calculated.

A complete account of this experiment is in the process of preparation.

F. T. Rogers, Jr.,
Marguerite M. Rogers

The Rice Institute,
Houston, Texas,
December 10, 1938.

[1] H. Bethe, Phys. Rev. **53**, 313 (1938).
[2] J. Chadwick, N. Feather, and E. Bretscher, Proc. Roy. Soc. **A163**, 366 (1938).
[3] J. R. Richardson and L. Emo, Phys. Rev. **53**, 234 (1938).

The Neutron-Proton Scattering Cross Section*

The scattering of thermal neutrons in paraffin has been extensively investigated.[1] The results of such experiments, however, do not yield directly the cross section for the scattering of slow neutrons by free protons, for, as Fermi has indicated,[2] the protons in the paraffin may be considered free only if the neutron energy, E, is large compared with $h\nu$, the energy of the lowest vibrational level of the paraffin molecule. Since this condition is not realized for thermal neutrons ($E\sim0.026$ ev; $h\nu\sim0.3$ ev) the free proton cross section may be inferred from the thermal neutron cross section only by means of a theoretical calculation of the effect of chemical binding. In view of the inaccuracies necessarily attendant upon this calculation, a direct measurement of the neutron-proton scattering cross section, a quantity of great importance in the investigation of nuclear forces, seems highly desirable.

The existence of resonance levels in the region of $1-10$ ev affords a convenient method of employing neutrons which satisfy the condition $E \gg h\nu$. An ideal experiment on the scattering of resonance neutrons would be one which utilizes an initial beam homogeneous in energy, and a detector sensitive only to neutrons of that energy. The fact that a neutron upon suffering a collision in the hydrogenous scatterer would undergo an energy loss and escape detection obviates the necessity of correcting for scattering into the detector. In practice this homogeneous beam may be approximately realized by utilizing those neutrons which are strongly absorbed in a resonance filter, thus introducing an energy in homogeneity of the order of the resonance width. That contribution to the activity of a detector of the same material which arises from scattered neutrons will then be limited to those which have been deviated through such small angles that the associated energy loss is insufficient to remove them from the resonance region.

An experiment of the above type has been performed with filter and detector films of Rh of 0.1 g/cm^2. As a source of neutrons we used a Rn-Be bulb of 600–300 mC in a cylinder of paraffin. A boron carbide diaphragm with an aperture 5 cm in diameter served to define the effective source of the neutron beam. Both source and detector were shielded with Cd to elimipate any effect of thermal neutrons. The detector, 45 cm^2 in area, was placed 30 cm from the source with the detector placed midway between source and detector. Each detector consisted of four rectangles of nickel sheet coated with Rh powder mixed with a small amount of Zapon lacquer as a binder. The four segments were jointed so that irradiations could be made with the detector spread out, while the activity could be measured with the detector folded so as to enclose a Geiger-Mueller counter.

From our data we conclude the mean free path of Rh resonance neutrons in paraffin to be 0.56 cm. This corresponds to a cross section of 20×10^{-24} cm^2, if we take the value of the carbon cross section[3] to be 4.8×10^{-24} cm^2. The probable error as calculated from the data is about five percent. However, in view of the approximations made in correcting the transmissions for scattering into the detector, we consider the above result to be good to about ten percent.

The experiments on the neutron scattering in ortho- and parahydrogen[4] permit an independent determination of the neutron-proton scattering cross section which is in substantial agreement with the value obtained in these measurements.

Since the scattering cross section obtained by direct measurement is considerably larger than the value of 14×10^{-24} cm^2 deduced from the thermal neutron cross section,[5] nuclear quantities calculated from the singlet scattering cross section will be altered appreciably. Two instances are: the increase in the magnitude of the singlet neutron-proton interaction, thereby affecting the comparison with the singlet proton-proton interaction; and, numerically more significant, the effect on the calculated cross section for slow neutron capture by protons, which increases approximately in the same ratio as the scattering cross section. A more detailed discussion of these experiments and their consequences will be presented in a forthcoming publication.

Victor W. Cohen
H. H. Goldsmith
Julian Schwinger

Columbia University,
New York, New York,
December 2, 1938.

* Publication assisted by the Ernest Kempton Adams Fund for Physical Research.
[1] M. Goldhaber and G. H. Briggs, Proc. Roy. Soc. **162**, 127 (1937); S. Frisch, H. v. Halban, H. Koch, Kgl. Dansk. Vid. Selsk. **15**, 10 (1938); H. Carroll and J. Dunning, Phys. Rev. **54**, 541 (1938).
[2] E. Fermi, Ric. Sci. **7**, 13 (1936).
[3] M. Goldhaber and G. H. Briggs, Proc. Roy. Soc. **162**, 127 (1937); J. Whittaker and O. Beyer, unpublished.
[4] F. G. Brickwedde, J. C. Dunning, H. J. Hoge and J. H. Manley, Phys. Rev. **54**, 266 (1938).
[5] H. Bethe, Rev. Mod. Phys. **9**, 69 (1937).

The Resonance Absorption of Slow Neutrons in Indium*

It is known that In^{115} exhibits a strong absorption for neutrons of about two ev energy giving rise to two β-active periods of 13 sec. and 54 min. In order to investigate the nature of the level responsible for this absorption we have determined the self-absorption curve for thicknesses of indium up to 1.3 g/cm² using the 54-min. activity of a thin (0.08 g/cm²) indium foil indicator.

Before it is possible to determine the neutron absorption coefficient at resonance ($n\sigma_0/\rho$ cm²/g) from such a curve, it is necessary to know the β-ray absorption of the indicator. We have observed the electronic absorption curve for this case to be exponential over the detector thickness used. The coefficient is 20 cm²/g. With this value and the same type of analysis as applied to rhodium,[1] the neutron absorption curve has been calculated for various values of $n\sigma_0/\rho$. We find that any value $n\sigma_0/\rho \gtrsim 100$ cm²/g gives a satisfactory fit. This indicates a cross section $\sigma_0 \gtrsim 20{,}000 \times 10^{-24}$ cm².

From the results it is evident that present data do not provide enough sensitivity for determining a unique value of σ_0; hence the neutron and radiation widths cannot be determined. Additional observations and calculations are now in progress.

J. H. Manley

Department of Physics,
University of Illinois,
Urbana, Illinois.

H. H. Goldsmith
Julian Schwinger

Department of Physics,
Columbia University,
New York, New York,
December 5, 1938.

* Publication assisted by the Ernest Kempton Adams Fund for Physical Research of Columbia University.

[1] J. H. Manley, H. H. Goldsmith and J. Schwinger, in this issue.

A Precise Measurement of the Mass Difference $_4Be^9 - _4Be^8$; The Stability of $_4Be^9$

The energy of the deuterons from the reaction $_4Be^9(p,d)_4Be^8$ has been measured with the electrostatic analyzer previously described.[1] Our most reliable curves have been taken at proton energies of 258 and 262 Kev; *A* and *C* of Fig. 1 are curves of this type. *C* shows the alpha-particle limit at 1.412 Mev from the concomitant reaction $_4Be^9(p,\alpha)_3Li^6$ and the surprisingly sharp deuteron limit at 0.628 Mev. Curve *A* is a separate investigation of the immediate region around the deuteron limit. The results of three determinations of the upper limit of the deuteron energy (thick target) shows that Q_3 for the deuteron reaction is 0.557 Mev.

Curve *B*, at 351 Kev, shows both limits close together. *X* shows the expected location of the deuteron limit obtained by conservation of energy and momentum from the limit as it appears at 262 Kev in curve *C*. The shift of the limits identifies the upper one as representing the alpha-particles; that of the lower limit agrees with the assumption of deuterons. The hump at the low energy end of *B* represents scattered protons from the target.

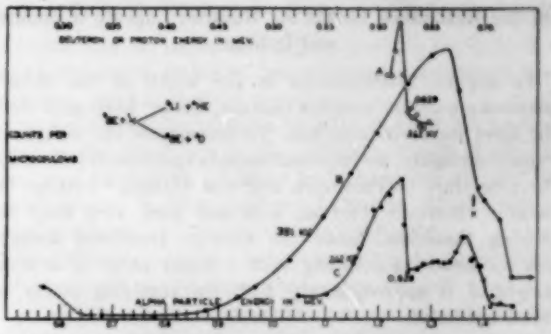

FIG. 1. The energy spectrum of particles from a thick target of beryllium under proton bombardment.

Using $D = 2.01473 \pm 2$ and $H = 1.00813 \pm 2$ after Livingston and Bethe,[2] we obtain

$$_4Be^9 - _4Be^8 = {}_1D^2 - {}_1H^1 + Q_3 = 1.00720 \pm 0.00003.$$

From their neutron mass, 1.00897 ± 6, the binding energy of the odd neutron in $_4Be^9$ is 1.65 ± 0.05 Mev, which should be the threshold for photodisintegration of $_4Be^9$.

The stability of $_4Be^8$ may now be expressed entirely in terms of measured reaction energies and the mass spectroscopic value of the difference

$$2\,{}_1H^2 - {}_2He^4 = K = 0.02561 \pm 0.00004.^3$$

Using the values Q_1 of $_4Be^9(d,\alpha)_3Li^7$ and Q_2 of $_3Li^7(p,\alpha)_2He^4$ which have been measured with an accuracy comparable to our work, we obtain

$$_4Be^8 - 2\,{}_2He^4 = Q_1 + Q_2 - Q_3 - K = 0.00033 \pm 0.00006$$

with $Q_1 = 6.95$ Mev,[4] $Q_2 = 17.13$ Mev.[5] Thus $_4Be^8$ is stable with respect to two alpha-particles by 0.31 ± 0.06 Mev. The fact that the deuteron limit is sharp in our curves shows that the deuteron in this reaction recoils from a single nucleus of $_4Be^8$.

Using the above *Q* values in connection with the atomic weights of hydrogen, deuterium, and helium, and Q_4 of $_4Be^9(p,\alpha)_3Li^6$ as 2.152 ± 0.04 Mev,[1] we can write

$$_4Be^8 = Q_1 + Q_2 - Q_3 - K + 2\,{}_2He^4 = 8.00739$$
$$_4Be^9 = Q_1 + Q_2 - {}_1D^2 + 3\,{}_2He^4 - {}_1H^1 = 9.01459$$
$$_3Li^6 = Q_1 + Q_2 - Q_4 + 2\,{}_2He^4 - {}_1D^2 = 6.01655.$$

A more detailed report of our experiments will be submitted to the *Physical Review* in the near future.

Samuel K. Allison
Elizabeth R. Graves
Lester S. Skaggs
Nicholas M. Smith, Jr.

Ryerson Physical Laboratory,
University of Chicago,
Chicago, Illinois,
November 30, 1938.

[1] S. K. Allison, L. S. Skaggs and N. M. Smith, Phys. Rev. 54, 171 (1938).
[2] M. L. Livingston and H. Bethe, Rev. Mod. Phys. 9, 246 (1937).
[3] K. T. Bainbridge and E. D. Jordan, Phys. Rev. 51, 384 (1937).
[4] J. H. Williams, R. O. Haxby, and W. G. Shepherd, Phys. Rev. 52, 1031 (1937).
[5] M. L. E. Oliphant, A. E. Kempton, and Lord Rutherford, Proc. Roy. Soc. 149, 406 (1935) corrected by M. L. Livingston and H. Bethe, reference 2.

On the Resonance Levels for Neutron Capture of Iodine and Indium

To explain discrepancies in the width of the iodine resonance level for neutron capture, Bethe[1] suggested that the level might be multiple. To investigate the situation more thoroughly, we have performed experiments following the procedure of Preiswerk and von Halban.[2] Instead of paraffin, however, carbon, iron and lead were used as slowing materials. Since the average fractional energy loss for neutrons colliding with a heavy atom of atomic weight A is approximately $2/A$, the resolving power is much increased.

In Figs. 1 and 2 the apparent transmissions are plotted against the thickness of slowing substances interposed between absorber and detector. The conditions under which the various curves were obtained are indicated in the figures. The iodine detectors contained 0.04 g/cm² I, the absorbers 0.077 g/cm² I (curves a) and 0.16 g/cm² I (curves b).

In general, the iodine curves show a gradual rise upon which, in the case of carbon and iron, several minima are superimposed. The rise is caused by the slowing of neutrons of slightly more than resonance energy into the resonance region. Minima occur at those thicknesses which slow down neutrons of one resonance level into the region of a lower level.

To make certain that the minima are not caused by accidental effects, experiments were performed under conditions identical with the ones of Fig. 1a, except that the iodine absorbers and detectors were replaced by 0.008 g/cm² of indium. The curve, Fig. 1c, so obtained, is smooth.

To evaluate the results, the average number N of collisions made by a neutron was computed from the known scattering coefficients,[3] the fractional energy loss being taken as $(1-2/A)^N$. For thin layers, $N \leqq 1$, this approximation is invalid, and the appropriate energy loss was obtained from the energy distribution of the slowed neutrons.

It is found that the spacings corresponding to the first two carbon minima and the last two iron minima are equal. The relative spacings $\Delta E/E$ (ΔE the spacing, E the average resonance energy) are approximately: 0.05, 0.09, 0.15, 0.26, 0.34, and 0.46. The maximum value of $\Delta E/E$ obtained with lead is 0.04. These six minima can be explained by assuming at least four levels for iodine.

From the initial slope of the curves, the average width of the levels can be estimated. If the half-width Γ of the level is not $\ll 2E/A$, some of the neutrons, slowed into the resonance region (thus causing the rising curve), are absorbed, so that the flattening of the absorption band requires a greater thickness of slowing material. Values for the average width of the levels have been computed from the theoretical expression for the shape of a resonance level, the energy distribution after one or two collisions, and the absorption due to the flattened level. Because of large geometrical corrections, the result is not too reliable.

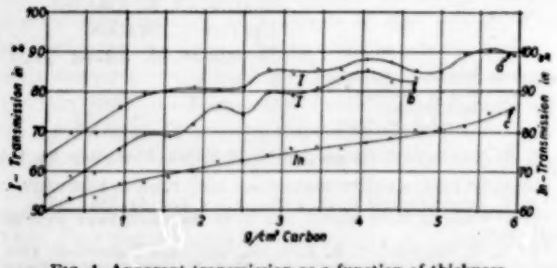

FIG. 1. Apparent transmission as a function of thickness of slowing substance between absorber and detector.

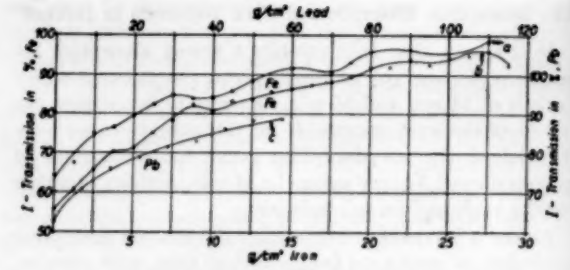

FIG. 2. Apparent transmission as a function of thickness of slowing substance between absorber and detector.

The curve, Fig. 1a, is in agreement with the assumption $\Gamma/E \ll 2/A$. From Fig. 2a an upper limit $\Gamma/E < 0.012$ was found. Fig. 2c gives $\Gamma/E = 0.005 \pm 0.002$.

This value may be compared with an average width obtained from the absorption coefficients ($K_{res} = 5$ cm²/g for iodine[4]), namely, $\Gamma/E = 0.008$ for $E = 140$ ev,[1, 5] or 0.012 for $E = 30$ ev.[4, 6] We have compared the activabilities of iodine and of rhodium, finding for iodine $\Gamma/E = 0.0045$ or 0.011, using for rhodium[1] $\Gamma/E = 0.054$ or 0.13, respectively.

Measurements of self-absorption of iodine at room and at liquid-air temperatures showed no evidence of Doppler broadening, giving $\Gamma/E > 0.003$.

From Fig. 1c, the relative width $\Gamma/E = 0.1 \pm 0.05$ is found for indium. From the absorption coefficients, $\Gamma/E = 0.08$. In separate experiments, we measured the coefficient for self-absorption of indium as 50 ± 10 cm²/g.

Fuller details and additional data will appear shortly. The authors wish to express their gratitude to Professor E. O. Salant for his helpful support and steady interest in the work.

New York University,
Washington Square College,
New York, New York,
December 3, 1938.

J. HORNBOSTEL
F. A. VALENTE

[1] H. A. Bethe, Rev. Mod. Phys. **9**, 134–147 (1937).
[2] H. v. Halban, P. Preiswerk, J. de phys. et rad. **8**, 29 (1937).
[3] M. Goldhaber, G. H. Briggs, Proc. Roy. Soc. **162**, 127 (1937). A. C. G. Mitchell *et al.*, Phys. Rev. **50**, 133 (1936); **52**, 283 (1937).
[4] O. Frisch, Kgl. Danske Vidensk. Selskab. Math. Phys. Medd. **14**, 12 (1937).
[5] H. H. Goldsmith, F. Rasetti, Phys. Rev. **50**, 328 (1936).
[6] F. Norling, R. Fleischmann, Zeits. f. Physik **108**, 483 (1938).

The Scattering of the D–D Neutrons

Recently, we measured the atomic scattering cross section of 21 elements for D–D neutrons,[1] and found that it varies in a complicated manner with the atomic number. In the new series of experiments we extended the measurement to 37 elements. The high accuracy could now be obtained by measuring the neutron intensity by means of

an ionization chamber filled with methane at 20 atmospheres pressure connected to a quadrant electrometer. The ionization current was usually about 10^4 times the natural leakage current. The ionization chamber was of cylindrical form 8 cm in effective length and 6 cm in effective diameter. The absorbers were mostly of cylindrical form 6 cm in

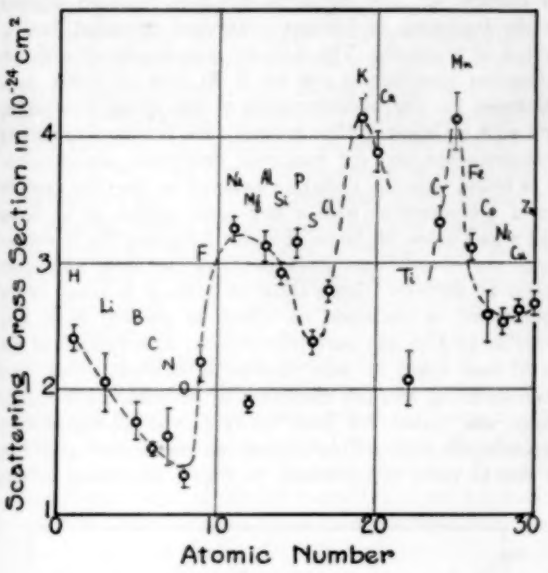

FIG. 1. Scattering cross section for D−D neutrons for elements of low atomic number.

diameter. The distance of the center of the chamber from the deuterium target was 40 cm, where the wall effect was about 10 percent of the total ionization current. The accelerating voltage was about 300 kv and the neutrons emitted at right angle to the deuteron beam were used. The energy of the neutron is therefore 2.4 Mev. The results for the elements of low atomic number are shown in Fig. 1. As will be seen the cross section is by no means a monotonic increasing function of the atomic number. It is an interesting problem to study, if the points are distributed quite irregularly or if they lie along a certain smooth curve. Though it is difficult to draw a definite conclusion, it will be interesting to note that, if we exclude a few elements, the points seem to lie along a smooth curve indicated in the figure by a dotted line. A similar trend is seen even in the region of high atomic number.

The results seem to be very important in connection with the theory of interaction of the neutron with the atomic nucleus. The discussions will be given later when the experiments with neutron source of different energy spectrum, now going on, will be finished.

SEISHI KIKUCHI
HIROO AOKI

Osaka Imperial University,
Osaka, Japan,
November 15, 1938.

[1] Seishi Kikuchi and Hiroo Aoki, Scientific Papers of I. P. C. R. **34**, 864 (1938).

A New Periodic Orbit in the Field of a Magnetic Dipole

In his classical paper on periodic orbits in the field of a magnetic dipole, Störmer[1] has exhibited examples of the following types of periodic orbits:

(a) Orbits intersecting the equator at right angles and reaching the boundary of the forbidden region $Q=0$. To this type belong the principal periodic orbits studied by Lemaitre and Vallarta and by Lemaitre, which play a fundamental role in the theory of cosmic rays.

(b) Orbits intersecting the equator at right angles more than once and not reaching the boundary $Q=0$.

(c) Orbits not intersecting the equator at right angles and reaching the boundary $Q=0$.

It does not appear that among the known examples of type *c* an orbit has ever been found having one or more loops. In the course of an investigation of reentrant orbits,[2] carried out in the spring of 1937 by means of Bush's differential analyzer,[3] the writer accidentally discovered an example of such an orbit. This is exhibited in Fig. 1.

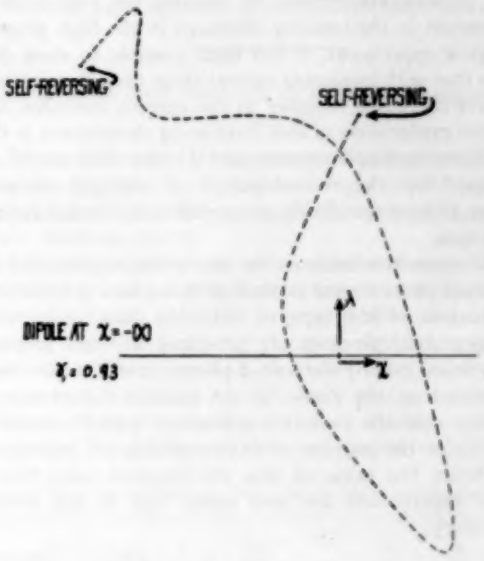

FIG. 1.

In the $x\lambda$-plane[4] the coordinates of the two points of reversal of this interesting orbit, as given directly by Bush's machine, are: $x=-0.547$, $\lambda=0.608$; $x=0.041$, $\lambda=0.510$. The intersections with the equator are at $x=-0.103$ and $x=0.167$, and the corresponding angles $-72.5°$ and $-75.0°$. The equatorial inclinations are thus seen to be nearly equal.

R. ALBAGLI HUTNER

Massachusetts Institute of Technology,
Cambridge, Massachusetts,
December 5, 1938.

[1] C. Störmer, Zeits. f. Astrophys. **1**, 237 (1930).
[2] E. J. Schremp, Phys. Rev. **54**, 153 (1938).
[3] V. Bush, J. Frank. Inst. **212**, 447 (1931).
[4] For the necessary definitions see, for instance, G. Lemaitre and M. S. Vallarta, Phys. Rev. **49**, 719 (1936).

The Dellinger Phenomenon

In his review[1] of the problem of sudden disturbances of the ionosphere, J. H. Dellinger suggests that the source of the sudden ionization changes must be of a character distinct from the source of ionization in the E, F, and F_2 layers since the disturbance has to come through these layers. The level at which the effect is produced is one where the density is great enough to insure numerous collisions of moving ions and rapid recombination of the ions. Recent observations of the new high pressure nitrogen afterglow, in which the $^2P-{}^4S$ nitrogen line and the Vegard-Kaplan bands are very strong, have shown the presence in the spectrum of the afterglow of the Goldstein-Kaplan bands and of a number of new bands, the most prominent of which is at 3246A. Weaker than the other features of the afterglow spectrum, but definitely present, are the first-negative or auroral bands of N_2^+. An examination of some old high pressure discharge spectra in pure nitrogen shows the N_2^+ bands, the Goldstein-Kaplan bands, and the new 3246 bands, thus clearly pointing to this combination of band spectra as having some physical connection. By varying the magnitude of the current in the exciting discharge in the high pressure afterglow experiment, it has been possible to show definitely that with increasing current these three "connected" features decreased together as the current increases. One possible explanation of this interesting observation is that the Goldstein-Kaplan system and the new 3246 system are produced by the recombination of nitrogen molecule ions or at least are closely connected with the behavior of these ions.

The connection between the above observations and the Dellinger phenomenon is that we have here a laboratory observation of the type of radiation that occurs when nitrogen molecule ions are produced at high pressure. Since this is exactly the sort of phenomenon that Dellinger postulated as the cause of the sudden disturbance, it suggests that the radiation associated with it should be studied for the purpose of understanding the mechanism and hence the cause of this phenomenon more clearly. These experiments are now under way in the writer's laboratory.

JOSEPH KAPLAN

Departments of Physics and Astronomy,
University of California at Los Angeles,
Los Angeles, California,
December 7, 1938.

[1] J. H. Dellinger, J. App. Phys. 8, 732 (1937).

Radioactive Isotopes of Element 43

In a previous paper[1] we have reported the results of activity measurements of a molybdenum target which had been bombarded with deuterons of the Berkeley cyclotron. It has been shown that the activity must be ascribed to radioactive isotopes of element 43[2] and it is mainly owing to low energy electrons; a component of the radiation was found to be due to electrons having a half-value thickness of about 1.4 mg/cm² Al absorber and a half-value period of 90 days. Besides it was observed that there were also some other components of higher energy but it was rather difficult to identify them on account of the small activity of our sample.

With a new molybdenum target which has been bombarded in the cyclotron and kindly sent to Palermo by Professor E. O. Lawrence, it has been also possible to study the harder γ-components of the radiation emitted by element 43. The measurements here reported started at the beginning of January, 1938 and extended over a period of 9 months. The activity was measured with an ionization chamber closed by 2 Al foils of 0.001 mm thickness for the measurements of the decay constants, and with a Geiger-Müller counter tube for the absorption measurements and for magnetic deflection experiments. It is found that the radiation emitted by the Mo sample has a γ-component with a half-value period of 62 days and a half-value thickness of about 2.5 g/cm² Al. Furthermore the absorption curves in Al of the total radiation taken at different times show that there is some other component of radiation on which at present it is not possible to give any sure information. Absorption curves in Al were taken for nine months at different times, and corresponding to each thickness of Al absorber a decay curve was drawn. All these decay curves are apparently exponentials although really resulting from the composition of two or more exponentials. In Fig. 1 the values of the

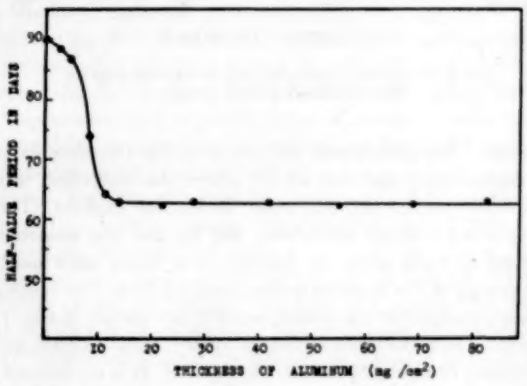

FIG. 1. Half-value period of the radiation emitted by element 43 as a function of the Al absorbing thickness.

total radiation half-lives are plotted as a function of the Al absorbing thickness. It is then seen that at the beginning of the curve, where the strong soft electron component of the radiation is predominant, the half-value period is 90 days, while at about 12 mg/cm² and for all the greater absorbing thicknesses measured (up to 600 mg/cm² Al) the half-value period has the constant value of 62 days.

We thank Professor E. O. Lawrence for the gift of the active molybdenum and Professor E. Segrè for his interest in this work.

B. N. CACCIAPUOTI

Royal University,
Palermo, Italy,
December 14, 1938.

[1] B. N. Cacciapuoti, E. Segrè, Phys. Rev. 52, 1253 (1937).
[2] C. Perrier, E. Segrè, J. Chem. Phys. 5, 712 (1937); Lincei Rend. 25, 723 (1937); 27, 579 (1938).

Comment on a Paper by W. E. Bowls, "Second Townsend Coefficient"

The discussion of the possible ionization of mercury by metastable nitrogen molecules calls for some comment even at this late date. Unfortunately, my attention was attracted to this paper[1] only recently, and yet I feel that these remarks may help others in future considerations involving metastable nitrogen molecules.

The energy of the metastable $A^3\Sigma$ level of nitrogen has now been definitely established at 6.14 volts, and the commonly quoted 8.2-volt value should not be used. The value of 9.77 volts, as given by Saha and Mathur, is undoubtedly their value for the energy that can be transferred by active nitrogen. Now the fact that the energy of the metastable state is less than the 10.39 volts required for the ionization of mercury should not deter anyone from supposing that active nitrogen can ionize mercury vapor. The 10.4- and the 9.77-volt values for the energy that can be transferred in active nitrogen are obtained from experiments on the Lewis-Rayleigh afterglow, and it is now well established that strong afterglows possessing auroral and night-sky spectra can be produced. At the present time the writer is observing a high pressure afterglow of quite long duration which is bluish-white in color because of the N_2^+ and second positive bands in the blue-violet and blue-green. The energy required for the excitation of the auroral N_2^+ bands is 18.65 volts for the zero vibrational level and a little higher than this for the higher vibrational levels. It is safe to say therefore that the energy transferred in the auroral afterglow is greater than 19 volts, i.e., almost twice the ionization potential of mercury.

It seems proper to remark that the 15.50-volt value for the ionization potential of N_2 has now been obtained by Worley and Jenkins, and this value should be used instead of the 16.7-volt value quoted by Bowls.

JOSEPH KAPLAN

University of California at Los Angeles,
Los Angeles, California,
December 7, 1938.

[1] W. E. Bowls, Phys. Rev. **53**, 298 (1938).
[2] J. Kaplan, Phys. Rev. **54**, 176 (1938).
[3] R. E. Worley and F. A. Jenkins, Phys. Rev. **54**, 305 (1938).

Elastic Scattering of Fast β-Particles by Atomic Nuclei

In continuation of previous work,[1] the elastic scattering of β-particles in the energy range 0.7–1.2 Mev by iodine nuclei has been examined with a cloud chamber. The preliminary results show that the scattering is from one-half to one-third of that predicted by Mott's theory. Our collected data are given in the following Table I.

TABLE I. *Values of the ratio R of the calculated to the observed elastic scattering in the angular range 20° to 180° for β-particles in the energy range 0.7 to 1.2 Mev.*

ELEMENT	ATOMIC NUMBER Z	R
N	7	1.1
I	53	2.5
Hg	80	7.0

We have not been able to account for the results by a straightforward modification of the potential field and it seems unlikely that any small adjustment of existing theory will explain the discrepancy. It is possible that the anomalous elastic scattering process is closely connected with the processes of inelastic scattering and pair production, both of which are anomalous. Since the problem may also be closely connected with β-disintegration, it may well be one of nuclear type in which the motion of the particle can no longer be considered as taking place in the general potential field of the remainder of the system. Finally the anomalous behavior may set in suddenly at a particular energy, as is certainly the case with pair production. This energy consideration alone might be sufficient to account for the normal behavior of the K electron since the energy of the latter, even in the heaviest elements, is much smaller than that with which we are concerned.

F. C. CHAMPION
A. BARBER

King's College,
University of London,
London, England,
November 17, 1938.

[1] A. Barber and F. C. Champion, Proc. Roy. Soc. **A933**, 159 (1938).

Absorption of Slow Neutrons of Different Energies by B, Co and Mn

We have measured the absorption of neutrons of different energies by various substances, using a Ra-Be source in paraffin and the usual Geiger-Müller tube and scale-of-eight counting system.

With boron absorbers, our geometrical conditions in experiments with C and D neutrons were nearly those of a parallel beam; three thicknesses of absorbing material ranging from 0.02 to 0.1 g/cm² were used. At these energies with other absorbers and at higher energies, measurements were made with, usually, only two absorber thicknesses. Absorption coefficients were evaluated by the method of Frisch.[1] Some of the results are shown in Table I.

TABLE I. *Absorption coefficients, in cm²/g, of* B, Mn *and* Co *with different detectors.*

ELEMENT	C (Rh)	D (Rh 44″)	Ag 22″	I 25′	Br 18′	Ag 2.3′	Mn 150′
B	30.0	5.35	2.46	0.97	0.82	≃0.2	
Mn	0.14	0.015	<0.003	0.02	0.04	<0.003	0.80
Co	0.32	0.09	0.03	0.04			

The boron absorption coefficients agree, in general, with those already reported by other workers.[2] Our value for the D neutrons is, however, somewhat higher, giving 0.94 v for the resonance level of Rh. For I neutrons, our value agrees with those of Frisch and of Norling and Fleischmann, and we confirm the latter in placing the Br level at a somewhat higher energy than the I level.

The coefficient of self-absorption for Mn, determined with a thin detector and a thin absorber, is unusually low. It is seen that the Mn resonance band extends well into the region of the I and Br resonance energies. The ratio of the Mn absorption coefficients for C and D neutrons is 9,

whereas the same ratio for boron is 5.6, suggesting a resonance level for Mn in the thermal region also.

The fact that the absorption by Co of I neutrons is greater than that of Ag neutrons, shows the presence of a resonance band for Co in the region of the I energy level.

These and other results will appear in more detail.

E. O. SALANT
W. J. HORVATH
H. I. ZAGOR

New York University,
Washington Square College,
Washington Square, New York,
December 3, 1938.

[1] O. R. Frisch, Kgl. Danske Vidensk. Selskab. Math. Phys. Medd. **14**, 12 (1937).
[2] J. R. Dunning, G. B. Pegram, G. A. Fink and A. C. G. Mitchell, Phys. Rev. **48**, 265 (1935); H. H. Goldsmith and F. Rasetti, Phys. Rev. **50**, 328 (1936); F. Norling and R. Fleischmann, Zeits. f. Physik **108**, 483 (1928).

A Remark on the Latitude Effect of Cosmic Rays

New measurements of the cosmic-ray latitude effect[1] show that the latitude, where the effect begins, remains the same in the whole atmosphere. This behavior denotes that the existence of a "critical latitude" is produced, not by atmospheric absorption,[2] but by absence, in the incident radiation, of rather slow rays;[3] they either are deflected by the sun's magnetic field or do not exist at all in the primary spectrum. We wish to call attention to a consequence of this conception, which possibly may permit us to decide, if the hard component, considered here alone, is primary in origin, or secondary—as recently suggested by some authors.[4]

If the component is a secondary one, its latitude effect accompanies that of the primaries and the critical latitude will be the same at *all* depths.

But if the hard rays are themselves primaries, the constancy of the critical latitude is limited to depths $x < E_{\min}/s$ only, where s is the specific ionization and $E_{\min}$ the threshold value of the energy spectrum. Only rays of energies higher than $E_{\min}$ are able to reach to depths $x > E_{\min}/s$ since the maximum range of an ionizing ray of energy E is always $R = E/s$, whatever may be the kind of its energy loss. Therefore, with increasing depth the critical latitude will shift to lower values, nearer the equator, exactly as is shown by the absorption theory. It can be calculated by the well-known equation $E_\lambda = sx$, where E_λ is the threshold energy imposed for incoming rays by the earth's magnetic field. Such a shift was observed by Clay[5] for rays which had penetrated more than one atmosphere. If his result could be confirmed definitively, it would prove a primary origin for the hard component.

B. GROSS

Instituto Nacional de Technologia
do Ministerio do Trabalho,
Rio de Janeiro, Brazil,
November 19, 1938.

[1] M. Cosyns, Nature **137**, 616 (1936); A. H. Compton, Phys. Rev. **43**, 387 (1933); H. Carmichael, E. Dymond, Nature **141**, 910 (1938); T. H. Johnson, Phys. Rev. **54**, 151 (1938).
[2] J. Clay, Proc. Roy. Soc. Acad. Amsterdam **33**, 711 (1930); **35**, 1282 (1932).
[3] L. Janossy, Zeits. f. Physik **104**, 430 (1937); B. Gross, Zeits. f. Physik **105**, 334 (1937); M. S. Vallarta, Nature **139**, 839 (1937).
[4] J. S. Bowen, R. A. Millikan, H. V. Neher, Phys. Rev. **46**, 641 (1934); **52**, 80 (1937); **53**, 217 (1938); H. Euler, Naturwiss. **26**, 382 (1938); H. J. Bhabha, Proc. Roy. Soc. London, **A164**, 257 (1938).
[5] J. Clay, Physica **2**, 299 (1935).